UNIVERSITY OF OXFORD

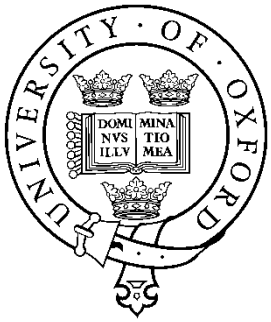

PATERNAL AGE EFFECT MUTATIONS IN GERM CELL DEVELOPMENT: PATHOLOGICAL CORRELATES IN NORMAL TESTIS AND TESTICULAR TUMOURS

JASMINE LIM
GREEN TEMPLETON COLLEGE

THESIS SUBMITTED FOR THE DEGREE OF DOCTOR OF PHILOSOPHY

Trinity Term 2011

Supervisor: Prof. A. O. M. Wilkie
Weatherall Institute of Molecular Medicine
John Radcliffe Hospital
Headington, Oxford
United Kingdom

PREFACE

Declaration of originality

This dissertation is the result of research undertaken between October 2007 and November 2010 (3 years and 2 months) mainly at the Weatherall Institute of Molecular Medicine in Oxford. Experiments involving spermatocytic seminoma, intratubular spermatocytic seminoma and fetal tissues were conducted by myself at the University Department of Growth and Reproduction, Copenhagen University Hospital (Rigshospitalet), Copenhagen, Denmark in collaboration with Dr Ewa Rajpert-De Meyts from 17th August 2009 until 3rd October 2009. The following part of my thesis was not my own work:

i. Immunohistochemical scoring of Ki67 in a panel of spermatocytic seminoma (Table 5.5 in Chapter 5) and intratubular spermatocytic seminoma samples (Table 5.6 in Chapter 5) were carried out by Dr Katherine A Ewen from University Department of Growth and Reproduction, Copenhagen University Hospital (Rigshospitalet), Copenhagen, Denmark.

Jasmine Lim

DPhil in Clinical Laboratory Sciences candidate

Green Templeton College

University of Oxford

ABSTRACT

Paternal age effect mutations in germ cell development: pathological correlates in normal testis and testicular tumours

A thesis submitted for the degree of D.Phil, by Jasmine Lim
Green Templeton College, Oxford
Trinity Term 2011

Pathogenic gain-of-function mutations associated with increased paternal age, albeit harmful to embryonic development, are paradoxically enriched in the normal testis. Evidence from previous studies indicates that these so-called paternal age-effect mutations confer a proliferative advantage to the spermatogonia in which they arise, leading to clonal expansion within the normal testis over time. Recently, spermatocytic seminoma (SS; a rare testicular germ cell tumour that occurs mainly in older men) has emerged as a key link between the processes of somatic and germline mutation (Goriely *et al*, *Nat Genet*. 41:1247-52, 2009), suggesting that the proposed clonal expansion events can in some cases lead to testicular tumourigenesis.

In this thesis, I have used immunohistochemistry to seek evidence for putative clones of cells in the normal adult testis. To address this, a screening approach was developed using markers chosen from analysis of normal testicular tissues and SS. The ontogeny of OCT2 and SSX expression in human testis, from embryonic development to adulthood, identified distinct subpopulations of spermatogonia at different maturation stages. Together, these data reveal the potential of OCT2 as a novel marker of A_{dark} spermatogonia (human reserve spermatogonial stem cells). In parallel with these observations, two distinct types of SS characterised by differential OCT2 and SSX immunoexpression were identified, providing new evidence for heterogeneity of this tumour.

This work provided the backdrop to the detailed immunohistochemical study of normal adult testis by characterising in serial sections the expression of five spermatogonial markers, MAGEA4, SSX, FGFR3, OCT2 and SAGE1, and a proliferation marker, Ki67. Independent sections were screened with predetermined criteria set to identify unusual positively-stained cellular clusters within the seminiferous tubules. Several antigenic combinations previously described in SS were observed in a subset of these clones, suggesting differing genetic origins and a possible link with early events of testicular tumourigenesis. The size (minimum number of cells) of each clonal event was estimated and its correlation with the staining pattern of the molecular markers was investigated.

In summary, the data presented in this thesis convincingly identify for the first time the previously hypothesised clonal events in the testis using immunohistochemical markers. My research will pave the way for future work involving genetic analysis of microdissected cells from these putative clones, aimed at identifying the underlying mutational events thought to be present.

ACKNOWLEDGMENTS

This study was conducted at the Institute of Molecular Medicine, John Radcliffe Hospital, Oxford as well as in the University Department of Growth and Reproduction, Copenhagen University Hospital (Rigshospitalet), Copenhagen, Denmark; it was funded by a Malaysian Ministry of Higher Education Fellowship.

First and foremost, my heartfelt gratitude must go to my supervisor Prof. Andrew Wilkie whose guidance, advice and encouragement from the initial to the final level of my D.Phil enabled me to develop an understanding of the subject. I am also thankful to Dr. Anne Goriely for her untiring effort, commitment and support particularly in the day-to-day practical supervision.

I would like to extend my gratitude to Dr. Gareth Turner for his unfailing support and large number of clinicians as well as nurses who have aided in the collection of these samples. I am grateful to Dr. Ewa Rajpert De-Meyts for the close collaborations especially in the study on spermatocytic seminoma and all the associates in Copenhagen University Hospital (Rigshospitalet), Denmark for sample preparations, immunohistochemical study and NanoZoomer virtual microscopic work. A big thank you also goes to all the patients who agreed to participate in this study

I am indebted to everyone working in the Wilkie Lab for making my D.Phil experience an enjoyable and memorable one; it has been a real pleasure working in such a friendly and enthusiastic environment. I would like to thank every former and current member of the group for their invaluable help and advice; my thanks go to Steve Twigg, Christian Babbs, Indira Taylor, Elena Bochukova, Dagan Jenkins, Geoffrey Maher, Vikram Sharma and Aimee Fenwick.

My gratitude also goes to Russell Leek and Graham Steers for DotSlide virtual microscopic work and Kevin Clarke for help with automated sequencing.

Finally, from the bottom of my heart, a huge thank you to my friends including Angela Green, Chern Ein Oon and Sook Teng Vun for the wonderful experience in Oxford as well as my family and my partner for their continuing love and support. Oxford just wouldn’t have been the same without you.

Thank you so much once again for all the people who have made this study a success.

CONTENTS

FIGURES

Chapter 1

Chapter 2

Chapter 3

Chapter 4

Chapter 5

Chapter 6

Chapter 7

TABLES

Chapter 1

Chapter 2

Chapter 4

Chapter 5

Chapter 6

Chapter

ABBREVIATIONS

bp	base pair
DNA	deoxyribonucleic acid
EDTA	ethylenediaminetetraacetic acid
g	relative centrifugal force expressed in units of gravity
h	hour
H_2O	water
Ig	immunoglobulin
kb	kilobase
M	molar
Mb	megabase
$MgCl_2$	magnesium chloride
Min	minute
ml	mililitre
mM	milimolar
mRNA	messenger RNA
ng	nanogram
nm	nanometer
OD	optical density
TBS	tris buffered saline
PCR	polymerase chain reaction
pg	picogram
RNA	ribonucleic acid
RPM	revolutions per minute
RT-PCR	reverse transcriptase polymerase chain reaction
S	second
Taq	*Thermus aquaticus*
TBE	tris-borate-EDTA
TBS	tris-buffered saline
Tris	2-amino-2-(hydroxymethyl)-1,3-propanediol
μg	microgram
μl	microlitre
μM	micromolar
U	units
UV	ultra violet
V	volts
W	watt

ABBREVIATIONS

bp	base pair
DNA	deoxyribonucleic acid
EDTA	ethylenediaminetetraacetic acid
g	relative centrifugal force expressed in units of gravity
h	hour
H_2O	water
Ig	immunoglobulin
kb	kilobase
M	molar
Mb	megabase
$MgCl_2$	magnesium chloride
Min	minute
ml	mililitre
mM	milimolar
mRNA	messenger RNA
ng	nanogram
nm	nanometer
OD	optical density
TBS	tris buffered saline
PCR	polymerase chain reaction
pg	picogram
RNA	ribonucleic acid
RPM	revolutions per minute
RT-PCR	reverse transcriptase polymerase chain reaction
S	second
Taq	*Thermus aquaticus*
TBE	tris-borate-EDTA
TBS	tris-buffered saline
Tris	2-amino-2-(hydroxymethyl)-1,3-propanediol
μg	microgram
μl	microlitre
μM	micromolar
U	units
UV	ultra violet
V	volts
W	watt

CHAPTER 1

INTRODUCTION

Chapter 1: Introduction

An understanding of mutation is arguably the most fundamental challenge in the field of genetics as it is the engine both of evolution and of all genetically determined disease. A change in a DNA sequence, termed mutation, can occur within a gene or at chromosomal level, usually leading to the alteration of the structure, function or expression level of protein(s). The primary site of mutations is divided into two categories: the germline and the soma. Germline mutations are defined by the presence of DNA alterations in the germ cells (sperm and egg) that becomes incorporated into every cell in the body and can be inherited from a parent. Genetic lesions arising in a germ cell or the fertilised egg are known as *de novo* mutations and manifest as an affected child without family history of the disorder. Somatic mutations, on the other hand, are acquired after conception and occur in any individual cells in the body except the germ cells. This type of mutation cannot be passed on to the offspring.

The work in this thesis addresses a particular mutational phenomenon termed paternal age-effect (PAE) mutation. Over the past decade, evidence has accumulated that a subset of congenital malformations are caused by *de novo* mutations associated with near-exclusive paternal origin and advanced paternal age. These pathogenic mutations are proposed to arise by random replication errors but then accumulate, driven by a selective advantage mechanism during pre-meiotic cell divisions in spermatogenesis. It has been suggested that PAE mutations confer a proliferative advantage to the spermatogonia in which they arise, leading to clonal expansion within the normal testis over time.

The ultimate goal of this thesis is to visualise and understand these early mutational events leading to the formation of putative clones in the normal adult testis and their potential contribution to testicular tumourigenesis. Therefore, the initial introductory segments of this study will focus on PAE mutations as well as their association with human

disease, normal adult spermatogenesis and testicular tumour development. Note that mutation here generally refers to point mutation which involves a change in a single nucleotide of a gene.

1.1 Germline mutation rates

As the fundamental basis of all genetic variation, it is important to investigate the rate of mutations underlying human genetic disease for understanding the relevant biological scenarios. There have been many previous attempts to quantify the mutation rates and attaining accuracy in the measurements still remains a major challenge. Among the reasons for this challenge are the low level of mutation rate per nucleotide, the influence of genetic background, mutagenic environmental and physiological factors on the mutation frequency, the measurement method which is determined by the kind of mutations studied, the nature of mutation itself as a random event and its frequency dependence on selection and evolution (as reviewed in Kondrashov and Kondrashov, 2010).

With the accumulation of sequence data on mutant alleles, Kondrashov (2003) estimated the rate of *de novo* mutations directly at 20 different loci which cause Mendelian diseases in humans. In this phenotypic mutation screening, loci bearing loss of function mutation implicated in clear-cut phenotypes were chosen and their mutation rates were established at least within a factor of 2-3. Alternatively, Nachman and Crowell (2000) applied an indirect approach to estimating the mutation rate per nucleotide in humans. Based on earlier evidence showing that the neutral mutation rate is equal to the rate of evolution (Kimura, 1968), the author assessed the mutation rate by comparing the sequences of orthologous pseudogenes in human and chimpanzee. The level of transitions (change from a purine nucleotide to another purine, A ↔ G or a pyrimidine nucleotide to another pyrimidine, T ↔ C) and transversions (substitution of a purine with a pyrimidine or vice versa) were estimated and compared at CpG and non-CpG sites in both studies. Notably,

CpG sites are mutation hotspots particularly for transition because of the substitution of 5-methylcytosine into thymidine via methylation-mediated deamination (Cooper and Krawczak, 1993).

The mutation rate from both studies, estimated per nucleotide per generation, are summarised in Table 1.1. Together, the occurrence of transitions was consistently more frequent than transversions and the mutation levels were higher at CpG dinucleotides compared to non-CpG sites. The frequency of transitions and transversions are 14.9-17 fold and 2.8-8 fold more prevalent at CpG dinucleotides than at non-CpG sites, respectively. Collectively, evidence from both studies indicated that spontaneous germ line point mutations (transitions and transversions) in humans were estimated at average rates of 4-160 x 10^{-9} per nucleotide per generation.

Table 1.1: The estimated rate of spontaneous point mutations in human.

Mutation type	Data source and mutation rates	
	Kondrashov (2003)	**Nachman and Crowell (2000)**
Transition at CpG	1.1 x 10^{-7}	1.6 x 10^{-7}
Transversion at CpG	1.1 x 10^{-8}	4.4 x 10^{-8}
Transition at non-CpG	7.4 x 10^{-9}	1.2 x 10^{-8}
Transversion at non-CpG	3.9 x 10^{-9}	5.5 x 10^{-9}

Recently, the first direct study of new mutations in the human germline, acquired from the whole-genome sequencing of a family quartet, estimated that the human diploid genome contains ~70 *de novo* mutations (Roach, *et al.*, 2010). Analysis from this study revealed that the observed ratio of transitions to transversions was in line with the previous predictions of 3.6 and 2.2 for CpG and non-CpG sites, respectively (Nachman and Crowell, 2000). Furthermore, Conrad et al (2011) have recently documented a direct comparison of male and female germline mutation rates from the complete genome sequences of two families, each comprising a single child and the parents. Interestingly, 92% (45/49) of new mutations in one family arose from the paternal germline whilst in the other family, 64% (22/35) of germline *de novo* mutations were of maternal origin. Impressive as these works

are, the age of the parents at the birth of each child was not available for either study. Nevertheless, the parental origin of each mutation (which was not mentioned in the Roach study) could be investigated using physically linked single nucleotide polymorphisms, SNPs (Moloney, *et al.*, 1996).

1.2 Sex differences in mutation rate

The first evidence for a paternal bias in mutation rate came from Haldane (1947) based on his studies on X-linked haemophilia. He hypothesised that if the mutation rates were equal between both sexes, 2/3 of affected males would inherit the disease gene from their carrier mothers and 1/3 would represent new mutations. However, he deduced that nearly all the affected males had heterozygous, carrier mothers, suggesting that the mutation must have arisen during earlier generations such as from the maternal grandfather. Although this early finding was difficult to prove owing to the heterogeneity of haemophilia and the lack of technology in heterozygote detection, subsequent work from other groups has further supported his conclusion (Crow and Denniston, 1985).

Using a direct estimation approach, the magnitude of α, which is the ratio of the number of mutations of paternal origin to that of maternal origin, was measured to determine the extent of parental bias in the origin of human mutations. This parental origin discrepancy can be well illustrated by germinal retinoblastoma. In this childhood malignancy, the first affected child in the family who acquires a new disease allele of tumour suppressor *RB1* gene from an unaffected parent will only develop retinoblastoma if a somatic mutation involving the normal allele of *RB1* is acquired in the retinal cells. Previous studies showed that 85% of the germinal mutation in retinoblastoma was paternal in origin; giving an α value of 5.67. In contrast, the somatic rate for the second hit mutation was about the same in both sexes (Dryja, *et al.*, 1997). The male germline mutation bias has also been observed in a number of autosomal dominant disorders using a similar approach (Hurst and Ellegren,

1998) (Table 1.2 and 1.3). However, the estimate of α is highly variable and the direct method has been criticised as most of the point mutations are located at a few specific sites with unusually high rates of mutation (Li, *et al.*, 2002). For instance, infinite values of α were observed in achondroplasia and Apert syndrome, which are caused by specific point mutations exclusively of paternal origin, no female-derived mutations being identified in either of the samples (Table 1.2); whilst in neurofibromatosis type 2 and von Hippel-Lindau syndrome, both paternal and maternal origins were observed yielding a value of α close to unity (Table 1.3).

Alternatively, the molecular evolutionary approach is an indirect method for providing evidence of the elevated mutation rate in the male germline. This method is normally performed by investigating known homologous sequences on the X and Y chromosome located outside the pseudoautosomal region, and comparing these with orthologues in another species to estimate the rate of synonymous mutations on the X and Y chromosomes. The Y chromosome is exclusively present in males whilst the X chromosome is found in both sexes. One would expect the evolutionary rate of a neutral locus on the Y chromosome will be higher compared to the X chromosome if point mutation is a more frequent event in the males. The evolutionary analysis using a pair of homologous non-functional Y-linked and X-linked sequences from human and apes demonstrated that the Y chromosome does evolve approximately five times more rapidly (Makova and Li, 2002). However, one may argue that the α value calculated from Y chromosome mutation is overrepresented owing to the intrinsic reduced mutation rate on the X chromosome. It has been proposed that natural selection will favour a higher fidelity of replication on the X chromosome because deleterious recessive mutations might be subjected to purifying selection on a hemizygous chromosome (McVean and Hurst, 1997). This hypothesis was rejected based on evidence obtained from molecular evolutionary analysis of the *CHD*

Table 1.2: Autosomal dominant disorders involving a single gene and exhibiting paternal age-effect mutations[a]

Gene symbol	Gene name	Mutation: DNA & amino acid substitution	Clinical disorder	Paternal origin	Maternal origin	α	Average paternal age (years)	Average increase in paternal age (years)	References
FGFR2	Fibroblast growth factor receptor 2	755C>G (S252W) 758C>G (P253R)	Apert syndrome	75	0	∞	33.6 (Hansen, 2006) 32.6 (Hansen, 2006) average: 33.2	2.9 1.7 average: 2.53	(Moloney, et al., 1996; Hansen, 2006)
FGFR2		Various	Crouzon/Pfeiffer syndrome	39	0	∞	34.5	4.1	(Glaser, *et al.*, 2000)
FGFR3	Fibroblast growth factor receptor 3	1138G>A, 1138G>C (both G380R)	Achondroplasia	40	0	∞	35.9		(Wilkin, *et al.*, 1998)
FGFR3		749C>G (P250R)	Muenke syndrome	10	0	∞	35.1	4.1	(Rannan-Eliya, *et al.*, 2004)
HRAS	Harvey rat sarcoma viral oncogene homolog	34G>A (G12S), 35G>C (G12A), 37G>T (G13C), 38G>A (G13D)	Costello syndrome	38	2	19	37.2 (Sol-Church, *et al.*, 2006), 38.0 (Zampino, *et al.*, 2007), 36.2 (Schulz, *et al.*, 2008) Average: 37.1	5.1 (4-7)	(Sol-Church, *et al.*, 2006; Sovik, *et al.*, 2007; Zampino, *et al.*, 2007; Schulz, *et al.*, 2008)
PTPN11	Protein tyrosine phosphatase, non-receptor type 11	922A>G (N308D) and others	Noonan syndrome	14	0	∞	35.6		(Tartaglia, *et al.*, 2004)
RET	Ret proto-oncogene	Various	Multiple endocrine neoplasia type 2A	11	0	∞	39.3		(Mulligan, *et al.*, 1994; Wohllk, *et al.*, 1996; Schuffenecker, *et al.*, 1997)
RET		2753T>C (M918T)	Multiple endocrine neoplasia type 2B	24	1	24	33.0		(Carlson, *et al.*, 1994; Kitamura, *et al.*, 1995)

[a]Criteria for inclusion were ≥10 cases informative for parental origin, with a male/female mutation ratio >10 and increased paternal age at birth (≥2 years or average paternal age ≥33 years)

- Adapted from Goriely *et al* (2009).

Table 1.3: Autosomal dominant disorders for which mutations are predominantly of paternal origin, but without obvious paternal age-effect.

Gene symbol	Gene name	Mutation: DNA & amino acid substitution	Clinical disorder	Paternal origin	Maternal origin	α	Average paternal age (years)	References
GFAP	Glial fibrillary acidic protein	715C>T (R239C) and others	Alexander disease	18	4	4.5	32.0	(Li, *et al.*, 2006)
KJN11	Potassium inwardly-rectifying channel, subfamily J, member 11	602G>A (R201H) and others	Neonatal diabetes mellitus	10	5	2	31.1	(Edghill, *et al.*, 2007)
NF1	Neurofibromatosis 1	Indirect testing	Neurofibromatosis type 1	[a]22	[a]2	11	29.8 (Jadayel, et al., 1990)	(Jadayel, et al., 1990; Stephens, et al., 1992)
NF2	Neurofibromatosis 2	Various	Neurofibromatosis type 2	13	10	1.3	31.2 (Evans, *et al.*, 1992)	(Evans, *et al.*, 1992; Kluwe, et al., 2000)
SALL1	Sal-like 1 (Drosophila)	826C>T (R276X) and others	Townes-Brocks syndrome	5	2	2.5	29.1	(Bohm, *et al.*, 2006)
SCN1A	Sodium channel, voltage-gated, type I, alpha subunit	Various	Dravet syndrome	25	8	3.1	33.3	(Heron, *et al.*, 2010)
VHL	von Hippel-Lindau tumour suppressor	Various	von Hippel-Lindau syndrome	4	3	1.3	30.7	(Richards, *et al.*, 1995)

[a]The paternal origin is estimated based on statistical analysis without knowing the type of mutations which probably are point mutations or small deletions.

(chromodomain helicase DNA binding protein) gene on the Z and W sex chromosomes in birds. A male-biased mutation ratio ($\alpha = 6.5$; range 2.8-10.2) was observed although males are homogametic (ZZ) and females are heterogametic (ZW) in birds (Ellegren and Fridolfsson, 1997).

How can we explain the higher average point mutation rate in the male germline compared to the female germline? The most obvious explanation would be the large discrepancy in the number of germ cell divisions. In humans, oogenesis begins during fetal life and all the oocytes are formed by the 5^{th} month of development, with only two further cell divisions required to produce an egg cell. Therefore, the number of successive cell divisions from a zygote to an ovum constantly remains as 24 in which 22 mitotic cell divisions are completed before birth and two during meiosis after puberty, giving a total of 23 chromosome replications. In contrast, spermatogenesis occurs throughout male reproductive life. Thirty cell divisions occur prior to puberty and at sexual maturity, each spermatogonial stem cell undergoes a cell division every 16 days for a total of 23 cycles per year. This is subsequently followed by four mitotic and two meiotic divisions before a sperm is produced.

The consequence of these dynamics is that the number of cell divisions required to produce a sperm in males is age-dependent. This means that sperm produced by man at the age of 40 would have undergone up to 610 cell divisions and chromosome replications, which is approximately 4 times more compared to a man of age 20 (Crow, 2006) (Box 1.1). In the context of mutation, if mutations are related to replication and accumulate progressively with the number of replications, one would expect a higher mutation rate in male germ line attributable to advanced paternal age. This theory was first proposed by Penrose (1955) as the ‘copy-error hypothesis’ to explain the increased paternal age observed in achondroplasia (short-limbed dwarfism).

There are an estimated 30 divisions before puberty and then one stem / progenitor cell division every 16 days, or 23 per year. Before sperm formation, there are four mitotic and two meiotic divisions (one chromosome replication).

A = age

N_A = number of germline chromosome replications by age A

N_p = the number of germline chromosome replications at puberty

A_p = the age at puberty = 15 years

Hence: $N_A = N_p + 23(A-A_p) + 4 + 1 = 35 + 23(A-15)$

The result of this calculation is presented in the table.

Age	Chromosome replications
15	35
20	150
30	380
40	610
50	840

Box 1.1: An estimation of the number of male germ cell divisions. The number of cell divisions preceding the production of the mature sperm has been calculated by Vogel and Rathenberg (1975), and Drost and Lee (1995).

1.3 Paternal age-effect in paternally originating mutations

As described in Section 1.2, *de novo* point mutations are proposed to arise from the multiple chromosome replications during spermatogenesis and the level of these genetic lesions increases with the age of men. A paternal age-effect has been described in some, but not other genetic conditions resulting from mutations of paternal origin (Tables 1.2 and 1.3). Apert syndrome, a congenital disorder caused by two distinct mutations encoded by the *FGFR2* gene, is one of the classical examples of a paternal age-effect disorder (Risch, et al., 1987). In 1996, Moloney *et al* demonstrated the exclusive paternal origin (male-to-female ratio: ∞) of this disorder using an amplification refractory mutation system (ARMS) approach; this method was based on an allele-specific amplification of sequence variants lying close to the mutation site to distinguish the parental alleles in the affected child. Together with a more recent study, a paternal age-effect of +2.53 years (n = 75) was observed in Apert syndrome (Moloney, et al., 1996; Hansen, 2006). The average paternal age in other particular disorders including Crouzon/Pfeiffer syndrome, achondroplasia, Muenke syndrome, Noonan syndrome, multiple endocrine neoplasia (MEN) type 2A and 2B are ≥33 years, significantly older than the population mean (~30 years) (summarised in Table 1.2). Moreover, *HRAS* mutations described in Costello syndrome arise from fathers of patients

who average 37.1 years in age, representing an increase in paternal age of 5.1 years compared to the matched normal population (n = 40) (Hennekam, 2003; Sol-Church, *et al.*, 2006; Sovik, *et al.*, 2007; Zampino, *et al.*, 2007; Schulz, *et al.*, 2008).

In contrast to the above examples, it is important to note that many other paternally-derived point mutations do not show any significant paternal age-effect. Examples include germline retinoblastoma (Dryja, *et al.*, 1989; Kato, *et al.*, 1994) and Wilm's tumour mutations (Olson, *et al.*, 1993) and other autosomal dominant disorders with a bias towards paternal mutations (Table 1.3); the average paternal age at birth is ~ 4.7 years younger than those described in Table 1.2. Hence the phenomena of paternal bias in the origin of new mutations, and paternal age-effect, can be clearly separated; many disorders show a variable bias in favour of paternally originating mutations, but little or no paternal age-effect (Table 1.3). A more limited number of genes show more extreme paternal bias in parental origin, and a strong paternal age-effect (Table 1.2). This latter group is discussed further in the next section.

1.4 Identification of five paternal age-effect genes – *FGFR2, FGFR3, RET, PTPN11& HRAS*

Evidence from section 1.2 and 1.3 collectively demonstrates the presence of a subset of autosomal dominant disorders with both very high α and a significant paternal age-effect (as shown in Table 1.2), suggesting a distinct origin of these mutations which preferentially occur during spermatogenesis. These specific heterogeneous point mutations were identified in the *FGFR2*, *FGFR3*, *RET*, *PTPN11* and *HRAS* genes, all of which encode components of the RAS-MAPK pathway (discussed in detail in Section 1.5).

A paradigmatic example is provided by a study on 57 cases of Apert syndrome (characterised by craniosynostosis and syndactyly), which showed that all *de novo* mutations were paternal and caused by one or other of two specific nucleotide substitutions, both C→G

tranversions, at sites 755 and 758 of the coding sequence in the *FGFR2* gene (Moloney, *et al.*, 1996). Based on the live birth prevalence of 1 in 70,000, the level of Apert mutations are estimated at 9.4 x 10^{-6} and 4.8 x 10^{-6} for the 755C>G and 758C>G transversions respectively in sperm (Hansen, 2006). A high mutation rate of 7.6 x 10^{-6} in male germline was also revealed in Muenke syndrome which is caused by a 749C>G transversion in the *FGFR3* gene (Rannan-Eliya, et al., 2004). Likewise, *FGFR3* 1138G>A or C mutations that both result in a specific amino acid substitution (G380R) are responsible for more than 97% of achondroplasia, corresponding to estimated mutation levels of 1.1-5.6 x 10^{-5} in sperm (Bellus, *et al.*, 1995a; Wilkin, et al., 1998). Together, the data suggest that the levels of these heterozygous *de novo* base substitutions are remarkably elevated compared to the average rates (Table 1.1, Section 1.1).

In summary, the apparent germline rates of these causative point mutations are 100-1000 fold higher than expected, and they arise nearly exclusively from the healthy fathers (male to female ratio, $\alpha > 10{:}1$) who tend to be 2-6 years older than the population mean. Genetic lesions consisting of these collective properties are termed *paternal age-effect mutations* (Goriely, et al., 2009). These mutations are described in greater detail in the next section.

1.5 Structure, function and mutation spectrum in each of the paternal age-effect genes

1.5.1 *FGFRs*

FGFRs share a similar structure composed of three extracellular immunoglobulin-like domains (D1-D3), a hydrophobic transmembrane (TM) region and a cytoplasmic split tyrosine kinase (TK) domain containing the catalytic protein kinase core (Johnson and Williams, 1993). In addition, a conserved positively charged region that serves as a heparin sulphate proteoglycan (HSPG) binding site (Schlessinger, *et al.*, 2000) and an acidic box consisting of seven to eight acidic residues are located within the D2 domain, and the linker

region between D1 and D2, respectively (Figure 1.1A). An alternative mRNA splicing event involving exons IIIb and IIIc (encoding the second half of the D3 domain) in *FGFR2* and *FGFR3* results in the formation of FGFR IIIb and FGFR IIIc isoforms respectively (Figure 1.1B). The expression of these variants is tissue-specific, whereby IIIb isoforms are mainly expressed in epithelium while IIIc isoforms are mostly present in mesenchymal cells (Miki, *et al.*, 1992; Orr-Urtreger, *et al.*, 1993; Chellaiah, *et al.*, 1994; Naski and Ornitz, 1998). The IIIb and IIIc isoforms differ in ligand-binding specificity; for instance, FGFR2b (the IIIb isoform of *FGFR2*) binds fibroblast growth factors (FGFs) 3, 7, 10 and 22 whilst FGFR2c (the corresponding IIIc isoform) binds FGFs 2, 4, 6, 8 and 9 but not FGF7 and 10 (Johnson and Williams, 1993; Ornitz, *et al.*, 1996; Ibrahimi, *et al.*, 2004). The interaction between epithelial FGFR2b receptor with ligands present predominantly in the mesenchymal cells, and vice versa, demonstrates a tight regulation of signalling activity between the epithelium and mesenchyme in human development.

FGFRs and their FGF ligands control a diverse array of biological processes during embryonic development by regulating mesencyhmal-epithelial communication events such as mesoderm patterning and organogenesis (Kimelman and Kirschner, 1987; De Moerlooze, *et al.*, 2000). In the adult organism, both FGFRs and FGFs continue to regulate tissue homeostasis but are also involved in angiogenesis, wound healing and tissue repair. FGFRs are activated upon binding to FGF ligands in the presence of HSPG which leads to receptor dimerisation and intermolecular transphosphorylation of the tyrosine kinase domains. Notably, HSPG is a low affinity receptor and does not transmit any biological signal. Nevertheless, it acts as an accessory molecule in recruiting FGFs to the cell surface, increasing their localised concentration as well as cooperating with FGFs to promote and stabilise FGFR interaction. Phosphorylated tyrosine residues serve as docking sites for

adaptor proteins and signal effectors, leading to the initiation and activation of multiple intracellular downstream signalling pathways (as further described in Section 1.6).

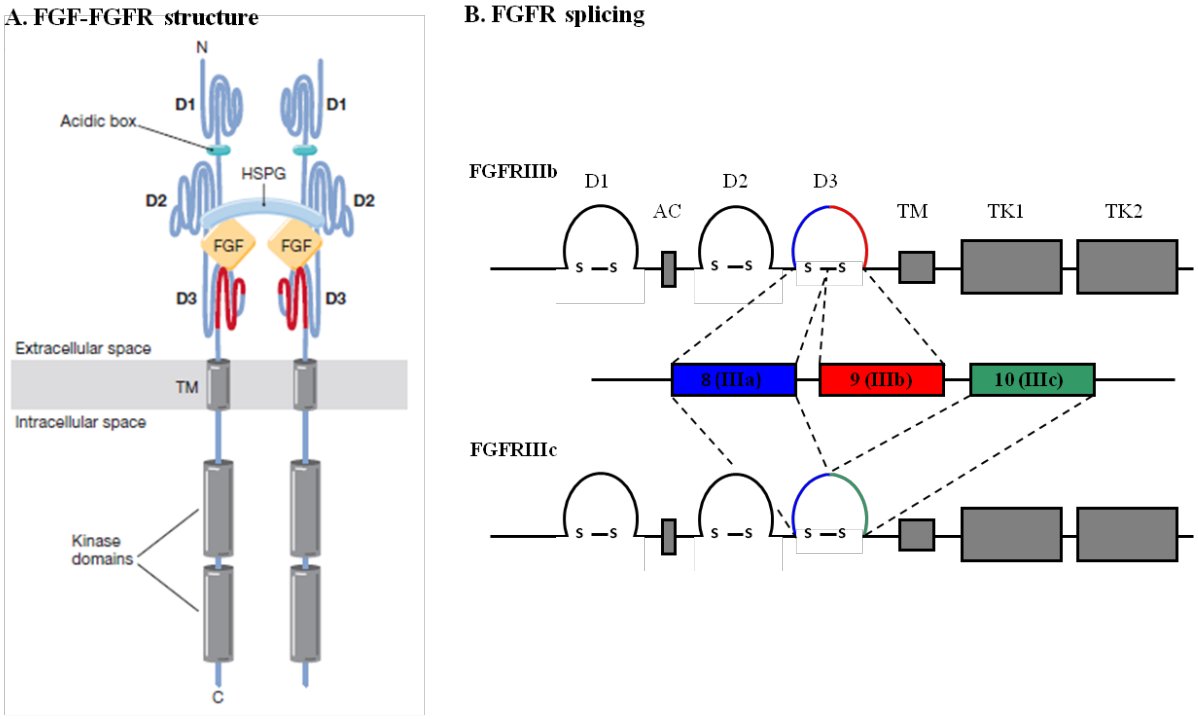

Figure 1.1: FGFR structure. The basic structure of the FGF and FGFR complex is composed of two receptors, two ligands and a HSPG chain as shown in A. The receptor consists of three immunoglobulin-like domains (D1, D2 and D3) in the extracellular space, interspersed by an acidic box (AC), a transmembrane domain (TM) and a split tyrosine kinase domain (TK). Alternative splicing occurs in the D3 domain (red colour, A) where the first half of D3 is encoded by an invariant exon 8 (IIIa) and the second half is spliced to either exon 9 (IIIb) or exon 10 (IIIc), resulting in two different FGFR IIIb and IIIc isoforms (B) (Adapted from Johnson and Williams, 1993; Grosso, *et al.*, 2008).

The importance of FGFR signalling in skeletal development was initially demonstrated in 1994 when point mutations (1138G>A or C, both encoding Gly380Arg) of the *FGFR3* gene were identified in all 39 unrelated individuals diagnosed with achondroplasia (Rousseau, *et al.*, 1994; Shiang, *et al.*, 1994). Since then, a spectrum of FGFR mutations has been demonstrated in around twenty dominantly inherited human genetic disorders, as described below. An unusually high absolute mutation level at specific residues is observed in several of these disorders. These highly recurrent mutations in FGFR include

FGFR3 1138G>A or C (G380R) in achondroplasia, *FGFR3* 749C>G (P250R) in Muenke syndrome as well as *FGFR2* 755C>G (S252W) and *FGFR2* 758C>G (P253R) in Apert syndrome. A striking regional distribution of mutations between *FGFR2* and *FGFR3* is also observed, in which IgIIIa/IgIIIc mutations are more abundant in *FGFR2* compared to *FGFR3* mutations that are more common in the TM and TK regions (Wilkie, 2005). The following subsections will further illustrate the *FGFR2* and *FGFR3* genetic lesions in relation to paternal age-effect mutations.

The abnormal phenotypes observed in genetically engineered mice with specific disruptions in *Fgfr* genes support their potential roles in skeletal development. For example, early embryonic death at day 10.5 was reported in *Fgfr2*$^{-/-}$ mice along with the absence of limb buds (Xu, *et al.*, 1998). Subsequent study in conditional *Fgfr2* knockout mice revealed several skeletal malformations such as skeletal dwarfism and decreased bone density as a result of the disruption of Fgfr2 signalling in the chondrocyte and osteoblast lineages (Yu, *et al.*, 2003). In contrast, *Fgfr3*$^{-/-}$ mice were viable but with inner ear defects and severe skeletal overgrowth with enhanced and prolonged endochondral bone growth. This abnormal growth is accompanied by expansion of proliferating and hypertrophic chondrocytes within the cartilaginous growth plate (Deng, *et al.*, 1996).

1.5.1.1 ***FGFR2***

A wide range of missense mutations present in the IgIIIa and IgIIIc domains of *FGFR2*, account for the majority of Crouzon (Reardon, *et al.*, 1994) and Pfeiffer (Schell, *et al.*, 1995) syndromes (Figure 1.2). Despite the similar craniosynostosis features (caused by premature ossification and fusion of the developing cranial sutures), these clinical disorders are distinguished by different degrees of limb abnormalities, ranging from normal hands and feet in Crouzon syndrome to broad thumbs and big toes in Pfeiffer syndrome. In contrast, Apert syndrome is characterised by craniosynostosis and severe syndactyly (cutaneous and

bony fusion of the digits); it is caused by two specific mutations in the *FGFR2* gene (Figure 1.2). The genetic basis of this disorder was first elucidated by Wilkie *et al* (1995) in which heterozygous base substitutions 755C>G (Ser252Trp) or 758C>G (Pro253Arg) in the linker between IgII and IgIII domains were responsible for all 40 unrelated Apert syndrome cases studied. To date, ~ 98% Apert syndrome cases are due to these transversion mutations. Still, in some independent cases, patients were identified with either a heterozygous 755_756CG>TT or TC (Ser252Phe) double nucleotide substitution (Oldridge, *et al.*, 1997; Lajeunie, *et al.*, 1999; Goriely, et al., 2005), partial or complete insertions of *Alu*-elements (214-368 bp) within or near exon IIIc of *FGFR2*, or a 1.93-kb intragenic deletion including exon IIIc (Oldridge, *et al.*, 1999; Bochukova, *et al.*, 2009). Although the vast majority of new cases of paternal age-effect syndromes arise as *de novo* mutations from the paternal germline, maternal somatic mosaicism was molecularly proven in a single case of Crouzon syndrome (Goriely, *et al.*, 2010). The *FGFR2* 1007A>G (Asp336Gly) heterozygous mutation identified in the affected child was found to have originated from the mother, who appeared clinically normal and was mosaic for this substitution in her peripheral blood DNA; highighting that different mechanisms such as high-level parental mosaicism can occasionally cause apparent *de novo* mutations even in classical paternal age-effect syndromes.

Interestingly, somatic mutations identical to *FGFR2* paternal age-effect mutations have recently been identified in several tumours (Figure 1.2). According to the Catalogue of Somatic Mutations in Cancer database (www.sanger.ac.uk/perl/genetics/CGP/cosmic) (COSMIC), 11% of the endometrial carcinoma harboured a point mutation in the *FGFR2* gene, amongst which the *FGFR2* S252W Apert mutation was the most common amino acid substitution, followed by N549K single amino acid change and the P253R Apert mutation (Pollock, *et al.*, 2007; Dutt, *et al.*, 2008). Further evidence has been found in gastric carcinoma and lung carcinoma, where a S267P Crouzon mutation causing constitutive

homodimerisation of the receptor (Anderson, *et al.*, 1998) and a W290C mutation previously studied in Pfeiffer patients were identified respectively (Jang, *et al.*, 2001; Davies, *et al.*, 2005). Together, these observations suggest that somatically arising *FGFR2* mutations identical to germline paternal age-effect mutations are oncogenic in a subset of tissue environments.

The gain-of-function properties arising from missense mutations in *FGFR*2 are attributable to two broad molecular mechanisms, depending on whether or not the ligand is required to be present. For instance, the extracellular Ig-like domain mutations described in most of the craniosynostosis syndromes are associated with gain or loss of a cysteine residue, which normally forms an intramolecular disulphide bridge with a second cysteine amino acid in the IgIII domain of *FGFR2*. In the ligand-independent event, the unpaired cysteine amino acid in the extracellular domains from two mutant receptors is linked with an intermolecular disulphide bond, fixing the FGFR molecules in a dimerised state. This mechanism is supported by the functional analysis on *Xenopus* (Neilson and Friesel, 1995; 1996). The microinjection of *Xenopus* blastomeres and oocytes with mRNA bearing analogous *FGFR2* Cys278Phe and Cys342Tyr mutations to those described in humans resulted in mesoderm induction in animal pole explants driven by FGF-independent signalling. Further analysis revealed that in the absence of ligand binding activity, increased tyrosine phosphorylation was observed following the formation of a disulphide-linked homodimer between the mutant receptors. Interestingly, the structure of the FGF/FGFR complexes demonstrated that non-cysteine mutations e.g. Tyr340His located within the IgIII domain constitutively activates the receptor by destabilizing the IgIII domain to prevent the normal intramolecular disulphide bond forming within the receptor monomer and thus allowing the creation of an intermolecular disulphide bridge with a neighbouring receptor (Robertson, *et al.*, 1998).

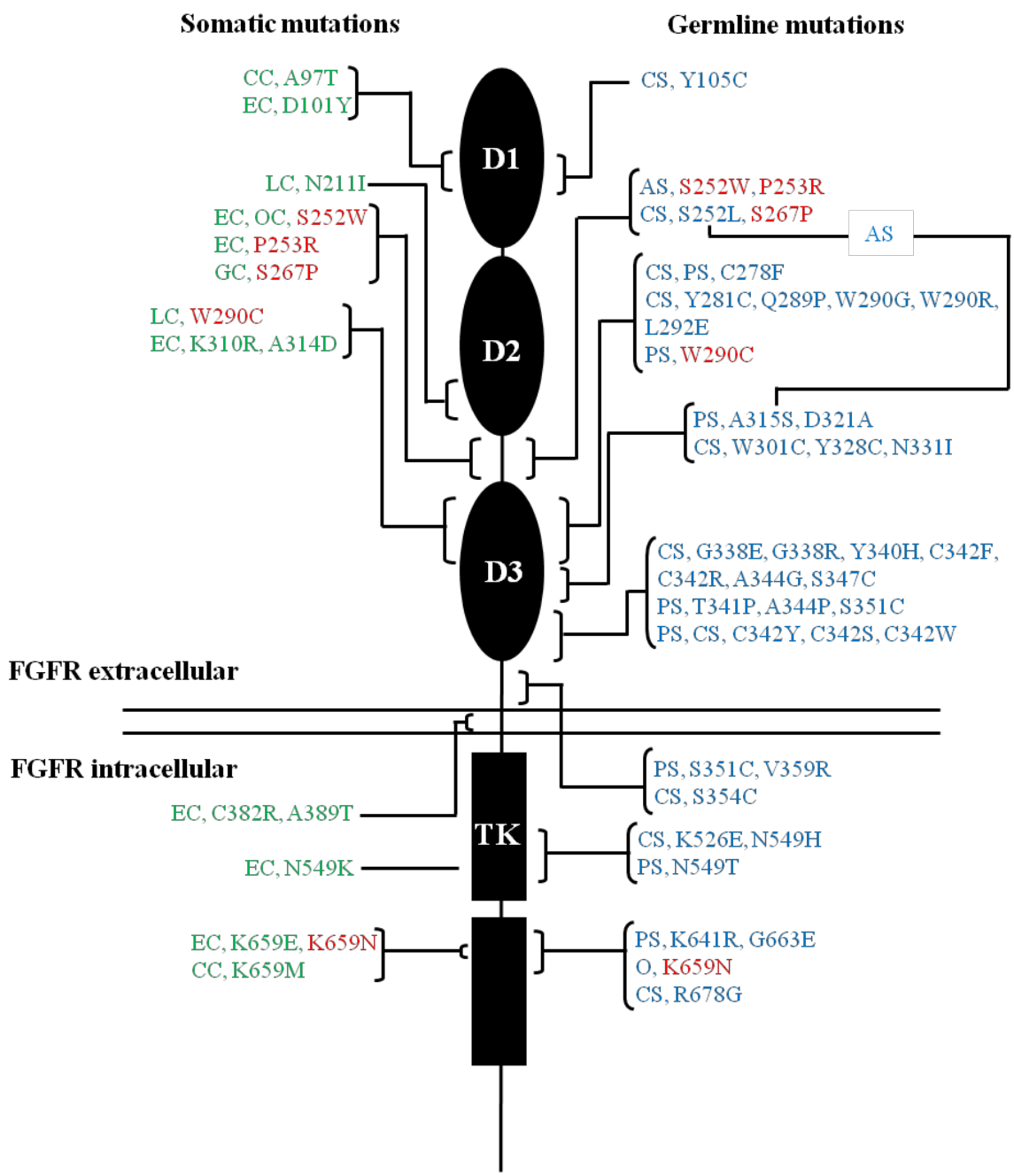

Figure 1.2: The distribution of *FGFR2* germline and somatic mutations in humans. Mutations in germline are in blue, soma in green or both in red. Abbreviations indicate Apert syndrome (AS), Crouzon syndrome (CS), Pfeiffer syndrome (PS), cervical carcinoma (CC), endometrial carcinoma (EC), gastric carcinoma (GC), lung carcinoma (LC), other unclassified craniosynostosis (O) and ovarian carcinoma (OC). The line connecting S252L and A315S indicates a double mutation found in patients with Apert syndrome-like syndactyly, without craniosynostosis (Adapted from COSMIC, Kan, *et al*., 2002 and Ornitz, 2005).

For activating *FGFR2* missense Apert mutations which localised at the adjacent highly conserved Ser252 and Pro253 codons, it was first suggested that Ser252Trp substitution enhances the affinity of FGFR2c-FGF2 binding due to a conformational change within the linker region which reduces the ligand dissociation rate (Anderson, *et al.*, 1998). Biochemical analysis further uncovered a violation driven by the Apert Ser252Trp mutation of the canonical rules of epithelial-mesenchymal signalling restriction. The mutant FGFR2c isoform derived from the mesenchymal cells was abnormally activated in response to mesenchymally expressed ligands FGF7 or FGF10 whilst, mutant epithelial splice form of FGFR2 (FGFR2b) was atypically susceptible to activation by FGF2, FGF6 and FGF9 ligands expressed in the epithelial cells (Yu, *et al.*, 2000). The precise mechanism of these gain-of-function ligand-dependent mutations become evident only after the first crystal structure of FGF-FGFR was described. Crystallographic analysis of the Apert mutant (either S252W or P253R) FGFR2c in complex with FGF2 revealed that these mutations increase the affinity of receptor-ligand binding. For instance, FGFR2c Ser252Trp mutant receptor makes an additional contact with the N-terminus of the FGF2 ligand whereas in the Pro253Arg FGFR2c-FGF complexes, three additional hydrogen bonds are created between the guanidinium group of the mutant Arg253 residue and the β-trefoil core region of FGF2 (Figure 1.3). In addition, binding analysis demonstrated that the increased ligand binding affinity resulting from the Apert mutation is sufficient to alter FGFR2c-ligand binding specificity and allow the illegitimate binding of FGF10 with the receptor (Ibrahimi, *et al.*, 2001; 2004).

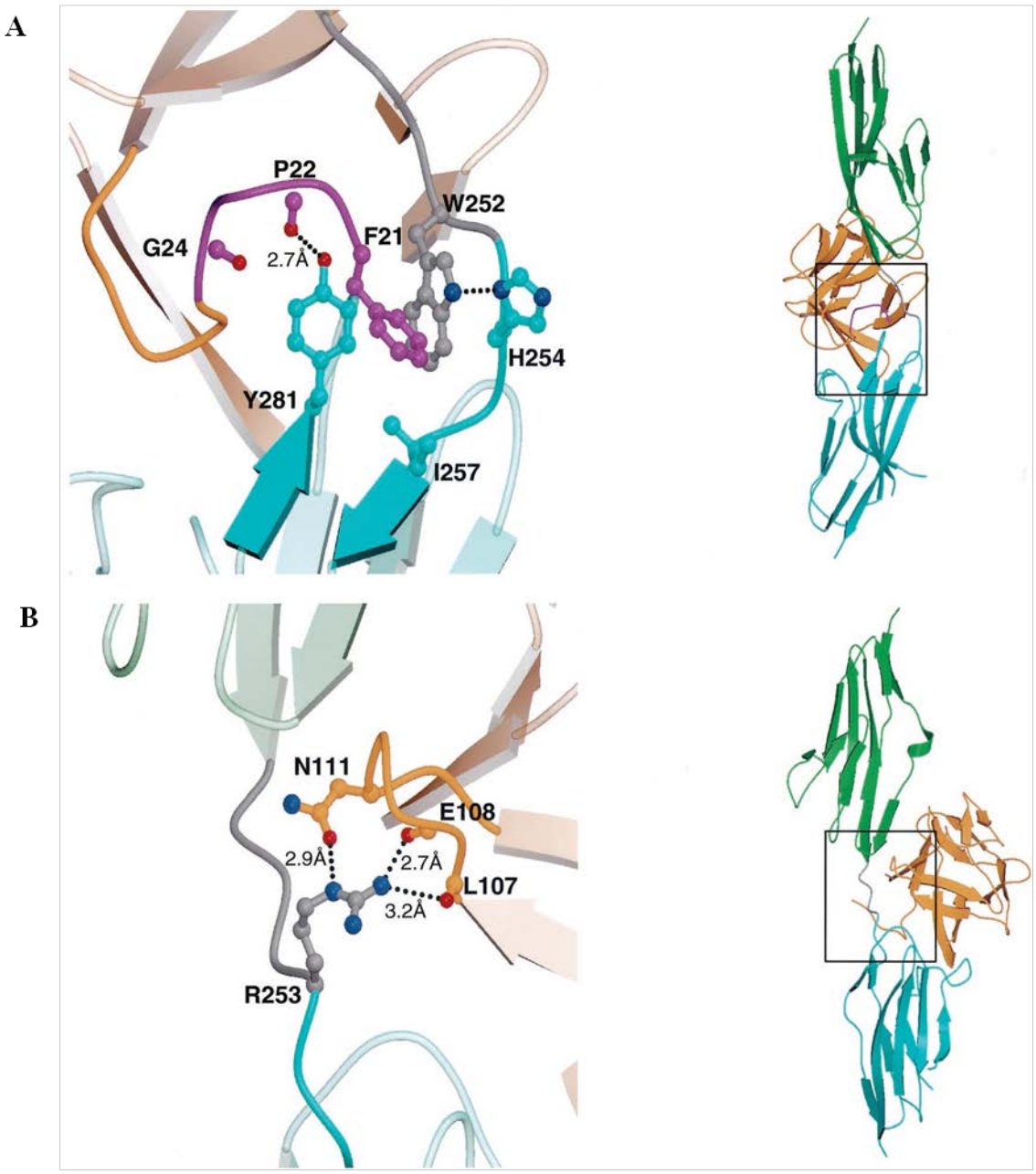

Figure 1.3: Gain-of-function interactions between the Apert syndrome FGFR2 mutants and FGF2. A. Additional hydrophobic contact between Phe21 in the N-terminus of FGF2 and the Ser252Trp mutant FGFR2. **B.** Hydrogen bonds between FGF2 and Arg-253 of the Pro253Arg mutant FGFR2. D2 and D3 of FGFR2 are shown in green and cyan, respectively. The short linker that connects D2 and D3 is coloured grey. FGF2 is shown in orange. In addition, the FGF2 N-terminal region (Phe21-Pro-Pro-Gly24), which is ordered only in the Ser252Trp mutant FGFR2–FGF2 structure, is coloured purple. Oxygen atoms are red, nitrogen atoms blue, and carbon atoms have the same colouring as the molecules to which they belong. Dotted lines represent hydrogen bonds. The hydrogen-bonding distances are indicated. (Right) Views of whole structure in the exact orientation as in the detailed views are shown, and the region of interest is boxed (Adapted from Ibrahimi, et al., 2001).

1.5.1.2 ***FGFR3***

Activating *FGFR3* heterozygous mutations were identified in a spectrum of human short limb dwarfism syndromes including achondroplasia (ACH), hypochondroplasia (HCH), severe achondroplasia with developmental delay and acanthosis nigricans (SADDAN), and thanatophoric dysplasia (TD) I and II (Figure 1.4). ACH is the most common autosomal dominant form of skeletal dwarfism, and mutation at codon 380 leading to a Gly → Arg amino acid change within the TM region (Rousseau, et al., 1994; Shiang, et al., 1994) is responsible for ~99% of the cases studied (Wilkie, 2005). Other rare causes of ACH are Gly346Glu and Gly375Cys (Nishimura, *et al.*, 1995; Superti-Furga, *et al.*, 1995). Radiological analysis revealed a similar but milder form of ACH, known as HCH, characterized by mild short stature. About 42% of HCH cases studied arise from the base substitution 1620C>A or G (both encoding Asn540Lys) located within the TK domain of *FGFR3* (Bellus, *et al.*, 1995b).

TDI (the most common form of severe skeletal dwarfism) is generally distinguished by curved, short femurs and the absence of cloverleaf skull. TDI is caused by several different mutations in *FGFR3*. Mutations to Cys at residues 248 (caused by 742C>T transition) and 373 (caused by 1118A>G single base substitution) in the protein represent 56% and 22% of all the TDI cases studied respectively, whilst 12% of the cases are caused by a stop codon mutation giving rise to the translation of an additional 141 amino acids at the C-terminus of the protein (Rousseau, *et al.*, 1995; Tavormina, et al., 1995; Wilkie, 2005). It is notable that TD resembles the clinical phenotype of homozygous ACH (Stanescu, *et al.*, 1990). Compared to TDI, TDII is a severe form of skeletal dysplasia leading to lethality in the perinatal period caused by a *FGFR3* 1948A>G (Lys650Glu) substitution in the second TK domain of *FGFR3* (Tavormina, *et al.*, 1995). The phenotype of TDII includes straight thigh bones and a distinct severe cloverleaf skull deformity.

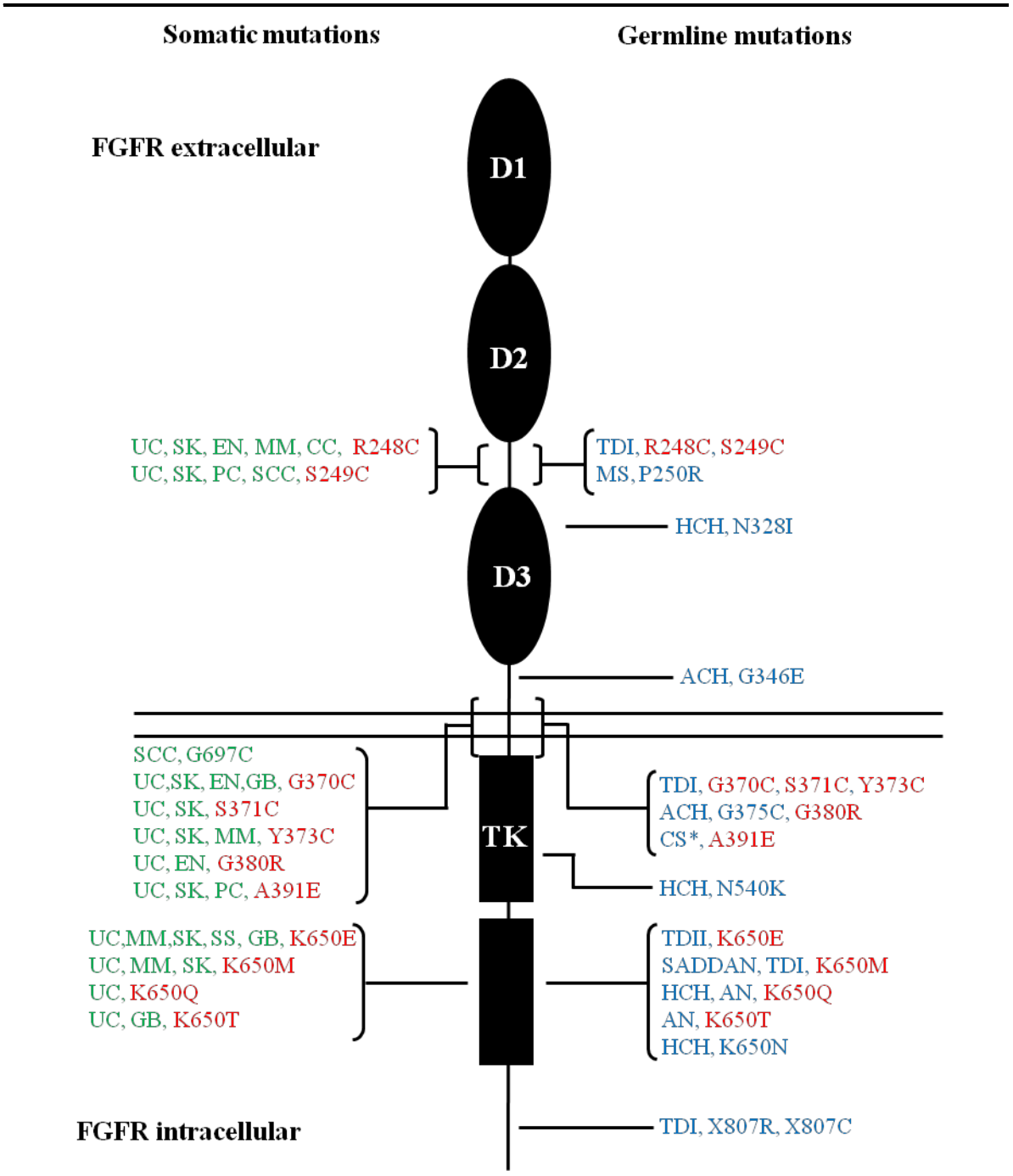

Figure 1.4: The distribution of *FGFR3* germline and somatic mutations in humans. Mutations in germline are in blue, soma in green or both in red. Abbreviations indicate achondroplasia (ACH), acanthosis nigricans (AN), Crouzon syndrome with acanthosis nigricans (CS*), hypochondroplasia (HCH), Muenke syndrome (MS), severe achondroplasia with developmental delay and acanthosis nigricans (SADDAN), cervical carcinoma (CC), epidermal naevus (EN), glioblastoma (GB), multiple myeloma (MM), prostate carcinoma (PC), squamous cell carcinoma (SCC), seborrhoeic keratoses (SK), spermatocytic seminoma (SS) and urothelial carcinoma (UC) (Adapted from COSMIC and Ornitz, 2005).

The aetiology of SADDAN is a lysine to methionine substitution in the TK region of *FGFR3* and accounts for 100% of cases studied (Bellus, *et al.*, 1999; Tavormina, *et al.*, 1999). The clinical features of SADDAN patients include shorter limbs, developmental delay, reverse bowing of the fibula and tibia, and acanthosis nigricans (a dermatological abnormality characterised by hyperkeratosis and hyperpigmentation). Allelic mutations at Lys650 codon in *FGFR3* give rise to congenital disorders with a wide range of clinical severity. For example, different missense *FGFR3* mutations are responsible for acanthosis nigricans, HCH (the mildest form of skeletal dwarfism), SADDAN and TDII (the lethal form of skeletal dysplasia) when threonine, glutamine / asparagine, methionine and glutamic acid are the corresponding amino acids substituted.

Two specific mutations in *FGFR3* are associated with phenotypes characterised by craniosynostosis rather than bone dysplasia. These are *FGFR3* Pro250Arg, which causes ~99% of Muenke syndrome (presenting with coronal craniosynostosis as well as mild limb malformations and hearing loss observed in some cases; Muenke, *et al.*, 1997), and *FGFR3* A391E which causes a subset of Crouzon syndrome associated with the development of acanthosis nigricans (Schweitzer, *et al.*, 2001).

In the soma, analogous *FGFR3* mutations were identified in several tumours including urothelial carcinoma, multiple myeloma and seborrhoeic keratoses (Figure 1.4). In urothelial carcinoma (previously known as transitional cell carcinoma), activating *FGFR3* mutations were identified in up to 46% of all cases, S249C and Y373C mutations previously identified in TDI responsible for the majority according to the COSMIC database. A spectrum of *FGFR3* point mutations (including R248C, S249C, G370C, S371C, Y373C, G380R, A391E, K650E and K650M) associated with paternal age-effect clinical disorders have also been identified in benign skin tumours (seborrhoeic keratoses and epidermal naevi) (Hafner, *et al.*, 2006; 2007a; 2007b; 2008). Similar amino acid substitutions were also

reported in multiple myeloma, an uncommon kind of bone marrow cancer that affects antibody producing plasma cells (Chesi, *et al.*, 1997; 2001; Sibley, *et al.*, 2002; Soverini, *et al.*, 2002).

A number of missense mutation-specific mechanisms resulting in activation of FGFR3 signalling have been proposed. In the extracellular region, amino acid substitutions to cysteine promote the formation of intermolecular disulphide bonds between receptors, leading to ligand-independent dimerisation and constitutive activation of the downstream pathways, as previously described for Crouzon / Pfeiffer FGFR2 mutations (Section 1.5.1.1) (Naski, *et al.*, 1996; Adar, *et al.*, 2002). The G380R ACH mutation in the transmembrane region increases the phosphorylation of FGFR3 in both the absence of ligand and at low ligand concentration. It has been proposed that an alteration of the mutant unliganded dimer structure makes it easier to phosphorylate tyrosines 647 and 648 (He, *et al.*, 2010). Activating mutations within the activation loop of the intracellular kinase domain promote ligand-independent autophosphorylation. This has been attributed to disruption of an autoinhibitory 'molecular brake' mechanism mediated by triad of component residues in the kinase hinge region. In the unphosphorylated mutants, the molecular brakes are disengaged directly or indirectly from the kinase domain, leading to a constitutively activated state (Chen, *et al.*, 2007). Besides this, biochemical analysis has shown that the elevated level of autophosphorylation activation caused by different amino acid substitutions in the tyrosine kinase domain is linked with the clinical severity. For instance, FGFR3 TDII (K650E) and SADDAN (K650M) mutations demonstrated a higher degree of tyrosine kinase activity compared with FGFR3 K650N/Q causing HCH (Bellus, *et al.*, 2000).

In addition to the relatively easily explained structure / function relationships of different mutations, there are more unpredictable consequences of these FGFR3 mutations at a cellular level. For example, the FGFR3 TDII (K650E) and SADDAN (K650M) mutations

increase the stability of mutant protein through the abrogation of lysosomal degradation targeting by c-Cbl-mediated ubiquitination. It has been proposed that activated Sprouty 2 may delay the turnover of phosphorylated receptor by sequestering c-Cbl away from FGFR3. As a consequence, the upregulated intrinsic kinase activity exaggerates the normal inhibitory FGFR3 signals on chondrocyte proliferation and differentiation in the skeletal growth plate, resulting in reduced bone growth (Cho, *et al.*, 2004; Guo, *et al.*, 2008). Other findings have suggested that highly activated SADDAN and TDII mutants disrupt the biosynthesis of the receptor monomers and their transport to the cell surface. In transient expression assays, the incompletely glycosylated receptors are trapped within endoplasmic reticulum and prematurely activates extracellular regulated kinase (ERK) signalling through an FRS2α- and PLCγ-independent pathway (Figure 1.5A), which is then suppressed by Sprouty 4 and results in apoptosis. By contrast, in the stable cells lines where both immature and mature fully glycosylated TDII and SADDAN receptors are identified, the canonical FRS2α/Grb2/Ras-dependent and Sprouty 4-independent ERK1/2 signalling cascade is triggered by the mature FGFR3 from cell surface in the absence of ligand (Figure 1.5B) (Lievens and Liboi, 2003; Lievens, *et al.*, 2004; 2006; 2009).

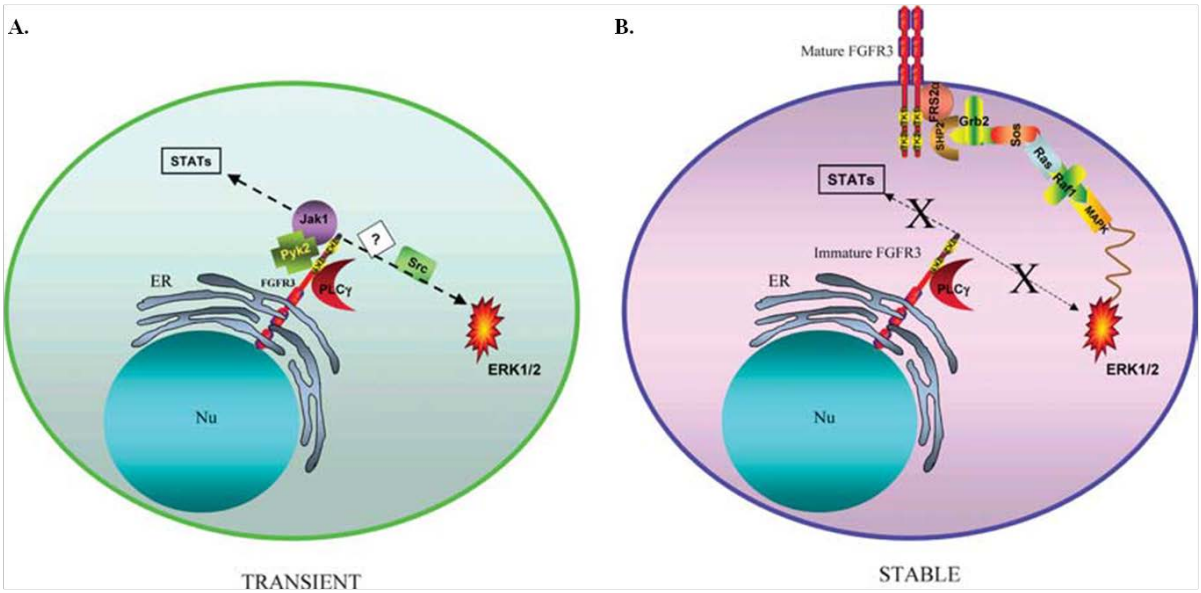

Figure 1.5: Cartoon model describing signalling by FGFR3 mutants. (A) The highly activated SADDAN and TDII mutants are trapped in the endoplasmic reticulum (ER) in their immature phosphorylated forms in transient transfection. Mutants FGFR3 recruit PLC$_\gamma$, Pyk2 and JAK1. The Erk1/2 activation occurs through a Src family member through an FRS2α and PLC$_\gamma$-independent pathway. (B) Both immature and mature phosphorylated FGFR3 are present in the ER and cell surface, respectively. The mature receptors signal from the cell surface in the absence of ligand through the canonical FRS2α-dependent pathway, ending in Erk1/2 activation. Erk1/2 and STAT1 are not activated from the ER (Adapted from Lievens, et al., 2006).

1.5.2 ***RET***

The *RET* proto-oncogene encodes a receptor tyrosine kinase comprising an extracellular ligand-binding region (which contains four cadherin-like (CL) repeats and a highly conserved cysteine-rich domain, CRD), a transmembrane region and a cytoplasmic tyrosine kinase (TK) region (Figure 1.6). Notably, the cysteine-rich domain is crucial for the tertiary structure and dimerisation through disulphide bond formation. Alternative splicing results in two significant RET isoforms, RET 9 and RET51, that vary in the length of the carboxy 3' terminal region (Figure 1.6) (Myers, *et al.*, 1995). The ligands of the RET receptor are derived from the glial-derived neurotrophic factor (GDNF) family comprising GDNF, neuturin, artemin and persephin. To activate RET signalling, the receptor requires a ligand

and a GDNF-family receptor α (GFRα) protein to form a tripartite cell-surface complex. GFRα receptors are glycosylphosphatidylinositol-anchored coreceptors without a transmembrane or intracellular domain. There are four GFRα receptors which differ in ligand binding specificity; GDNF preferentially binds with GFRα1 whilst neuturin, artemin and persephin associate with GFRα2, GFRα3 and GFRα4, respectively.

It has been suggested that lipid raft on the plasma membrane are essential for RET signalling by interacting with the activating complex via two different mechanisms. GFRα receptors are generally present in lipid rafts and after ligand binding, RET is incorporated into the raft where it dimerises and interacts with specific docking proteins that trigger signalling cascades. Phosphorylated RET can then drift away from the lipid rafts and it is degraded or internalised. Alternatively, the GDNF-family ligands bind to the soluble form of GFRα (sGFRα) before binding with two inactive RET monomers. As the GDNF-sGFRα-RET complex is outside the lipid raft, the activated RET is then relocalised to the lipid raft (Phay and Shah, 2010). Dimerisation of RET receptors results in autophosphorylation of intracellular tyrosine residues, providing the docking sites for various adaptor proteins including fibroblast growth factor receptor substrate 2 (FRS2), protein kinase Cα (PKCα) as well as Src homology and collagen (SHC) that are mediators of MAPK, phosphoinositide 3-kinase (PI3K)/AKT and c-Jun N-terminal kinase (JNK) pathways.

Heterogeneous single base substitution in the *RET* gene causes multiple endocrine neoplasia type 2A (MEN2A) and type 2B (MEN2B). MEN2 is an autosomal dominant genetic disorder characterised by predisposition to endocrine tumours, primarily medullary thyroid carcinoma (MTC), a tumour arises from calcitonin-producing thyroid C-cells, and pheochromocytoma (PCC), a neuroendocrine tumour derived from the medulla of adrenal gland. In MEN2A, the tumours tend to be less aggressive than in MEN2B, and parathyroid hyperplasia is observed in MEN2A patients only. Patients with MEN2B, in addition, develop

skeletal abnormalities, mucosal neuromas and a Marfanoid habitus. RET point mutations in MEN2A reside virtually exclusively in the extracellular cysteine-rich domain which includes codons 609, 611, 618, 620 and 634; of which missense mutations at Cys634 account for nearly 85% of the MEN2A cases and all possible amino acid substitutions arising from a single base change to the codon (to glycine, pheynylalanine, proline, serine, tryptophan and tyrosine) have been described (Mulligan, et al., 1994; Wohllk, et al., 1996; Schuffenecker, et al., 1997) (Figure 1.6). In the case of MEN2B, strikingly, a *de novo RET* 2753T>C transition (encoding Met918Thr within the tyrosine kinase domain) originating from the unaffected father is the underlying molecular cause of most cases (Carlson, et al., 1994). Additionally, there are individual cases of MEN2B patients with RET A883F mutation, which are associated with a less aggressive form of MTC compared to those bearing the common *RET* M918T amino acid change (Jasim, *et al.*, 2011) (Figure 1.6).

Alterations of the RET protooncogene involving gain-of-function mutations which result in aberrant RET activation are oncogenic events in the thyroid gland. For instance, MTC is closely associated with the MEN2A and MEN2B disorders; the penetrance of developing into this malignancy is nearly 100%. A subgroup of MEN2A and MEN2B patients are also genetically predisposed to developing into PCC. In parallel with these clinical observations, somatic mutations analogous to the MEN2A and MEN2B germline lesions, which cluster in the extracellular cysteine rich region and cytoplasmic tyrosine kinase domain respectively, were isolated in MTC and PCC tumours (COSMIC) (Figure 1.10). Mutation to threonine at residue 918 in the protein is the most prevalent variant in the human tumourigenesis particularly in MTC where ~ 95% of the mutational events were observed (COSMIC), suggesting that M918T confers more strongly activating gain-of-function effects than mutations within the cysteine-rich domain.

Amino acid substitutions at the cysteine residues located at the extracellular domain of the cysteine rich region introduce a ligand-independent oncogenic activation. The mutation affects the paired cysteine bonds and leads to the formation of an intermolecular disulphide bridge between the unpaired cysteines of two RET mutant proteins, causing constitutive RET activation by covalent dimerisation (Drosten and Putzer, 2006). This mechanism is analogous to that described for specific mutations in *FGFR2* (Section 1.5.1.1) and *FGFR3* (Section 1.5.1.2). In contrast, MEN2B mutations cause a conformational shift in the intracellular tyrosine kinase domain and high level of transforming activity (particularly for M918T and A883F), leading to the activation of the RET receptor in its monomeric state (Santoro, *et al.*, 1995; Iwashita, *et al.*, 1996; 1999). In addition to aberrant kinase activity, changes in the intramolecular interactions were evident in RET receptor bearing M918T mutation and potentially causing a reduction in conformational rigidity (Gujral, *et al.*, 2006). During the inactivated state, the wild type RET monomers are in a closed 'autoinhibited' conformation to inhibit the interaction between the activation loop and the substrate-binding pocket. This rigid conformation, which is maintained by the tight intramolecular interactions, is energetically stable (high melting temperature). By contrast, the inactive state of mutant RET has a lower melting temperature, suggesting a relatively less conformationally stable kinase with a partially open overall structure. In the activated state, the melting temperature of both wild type and mutant RET receptor was much lower, in line with the thermodynamic effects of the release of autoinhibition for a more open conformation. Collectively, these observations suggest that mutant RET has a more flexible protein conformation resulting from the partial loss of autoinhibition – again, analogous to "kinase brake" mechanism in FGFR tyrosine kinase domain.

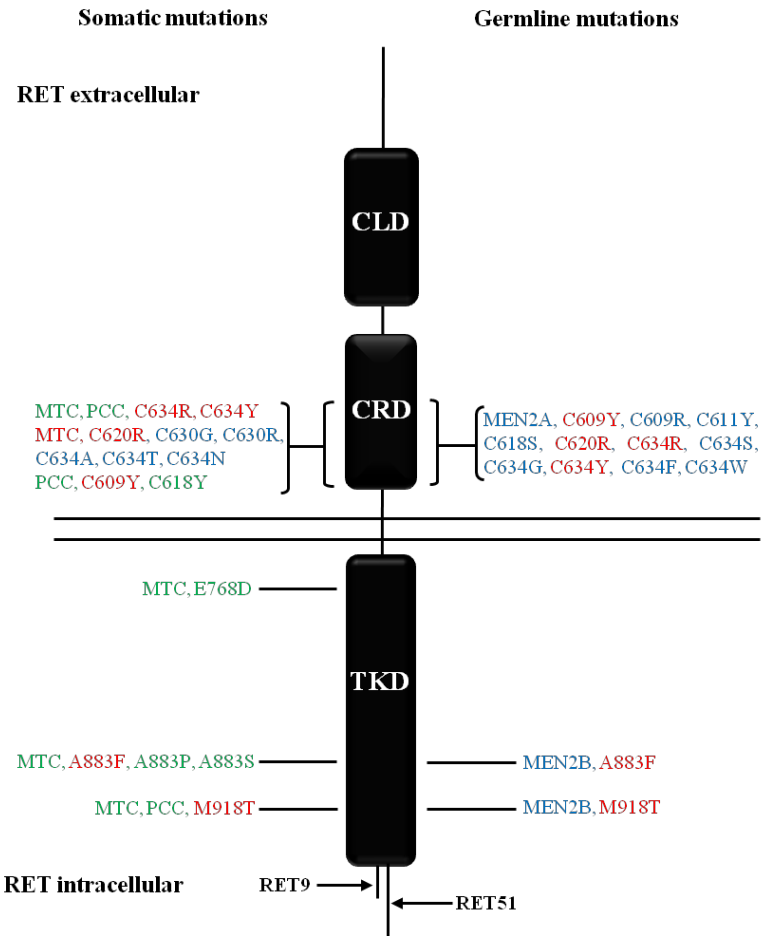

Figure 1.6: Schematic RET protein structure showing distribution of germline and somatic mutations in humans. RET protein is structured with a extracellular region consisting of cadherin-like domain (CLD) and cysteine-rich domain (CRD), a transmembrane region as well as a tyrosine kinase domain (TKD). Mutations in germline are in blue, soma in green or both in red. Abbreviations indicate multiple endocrine neoplasia type 2A (MEN2A), multiple endocrine neoplasia type 2B (MEN2B), medullary thyroid cancer (MTC) and pheochromocytoma (PCC) (COSMIC, Mulligan, et al., 1994; Wohllk, et al., 1996; Schuffenecker, et al., 1997).

1.5.3 ***PTPN11***

The *PTPN11* gene belongs to a structurally diverse family of protein tyrosine phosphatases (PTP), which are broadly categorised into receptor-like forms and non-receptor forms (Andersen, *et al.*, 2001). It encodes a non-transmembrane (non-receptor) PTP known as SHP2 protein, constituting a PTP domain linked to SH2 (Src-homology 2) domains that are crucial for mediating protein-protein interaction (Figure 1.7). The catalytic PTP domain

consists of approximately 280 residues including a highly conserved active region with a cysteine amino acid that is required for catalytic activity.

SHP2 serves as a mediator of activated tyrosine kinases regulating signal transduction events in cell proliferation, adhesion and migration. In the inactive state, SHP2 is regulated by an autoinhibitory mechanism in which the N-terminal SH2-domain binds with the PTP domain blocking the interaction of potential substrates with the active site. To function, the inhibitory interaction of the N-terminal SH2 domain and PTP domain is resolved to enable SHP2 to be employed to specific targets such as surface-receptor signalling complexes. This event may occur either through direct recruitment of SH2 domains to the tyrosine phosphorylation binding site of the surface receptor or through scaffolding adaptor proteins, including insulin-receptor substrate 1 (IRS1), FGFR substrate 2 (FRS2), growth factor receptor-bound protein 2 (GRB2)-associated binding protein 1 (GAB1) or GAB2 (Feng, 1999; Neel, *et al.*, 2003) (Figure 1.8a).

In the germline, *de novo* autosomal activating *PTPN11* mutations have emerged as the cause of approximately 50% of Noonan syndrome (Tartaglia, *et al.*, 2001). Noonan syndrome is a dominant developmental disorder defined by short stature, facial dysmorphism, skeletal abnormalities, cardiac defects and learning disabilities. Cardiovascular abnormalities mainly pulmonary stenosis or hypertrophic cardiomyopathy are observed in up to 85% of the Noonan patients whilst, a predisposition to haematological disorders, primarily juvenile myelomonocytic leukaemia (JMML) is also associated (Tartaglia and Gelb, 2005). The germline point mutations are predominantly identified in codons located at the N-terminal SH2 domain and PTP domain (Figure 1.7); of which the heterozygous *PTPN11* 922A>G transition (N308D) is the most common single base substitution (Tartaglia, et al., 2004). A study by Tartaglia et al (2004) of 14 informative cases showed that all were of paternal origin and associated with advanced paternal age (Table 1.2).

Furthermore, somatic *PTPN11* mutations occur primarily in haematological disorders including acute lymphoblastic leukaemia (ALL), acute myeloid leukaemia (AML), chronic myelomonocytic leukaemia (CML), juvenile myelomonocytic leukaemia (JMML) and myelodysplastic syndrome (MDS) (COSMIC) (Figure 1.7). There are also few cases of lung carcinoma, neuroblastoma, ovarian serous carcinoma and rhabdomyosarcoma which were found harbouring *PTPN11* point mutations (COSMIC) (Figure 1.7). Notably, genetic lesions in *PTPN11* occur in a mutually exclusive fashion with mutations of other genes in the RAS-ERK pathway in these haematological disorders, indicating that activation of the RAS-ERK signalling cascade is the core function conferred by transforming mutations of SHP2 (Ostman, *et al.*, 2006).

Investigations of the pathogenesis of SHP2 mutations show that the amino acid substitutions confer gain-of-function properties to the mutant proteins, resulting to varying degrees in the alteration of phosphatase activity, the affinity of the SH2 domain for phosphotyrosyl ligands, or substrate specificities. For instance, elevated basal activation was observed in a SHP2 mutant in which oncogenic leukaemia-associated D61Y and E76K showed a higher basal catalytic activity than that of the most common mutant found in Noonan syndrome N308D (Tartaglia, *et al.*, 2003; Fragale, *et al.*, 2004). These observations suggest that the oncogenicity of the mutant proteins is correlated with the extent of basal phosphatase activity. Increased ligand affinity and changes in substrate selectivity were also indicated in mutants bearing activating *PTPN11* lesions located at the SH2 domain and PTP domain respectively (Keilhack, *et al.*, 2005) . It has been proposed that oncogenic mutations in SHP2 clustered at the interface of the N-terminal SH2 domain impair the inhibitory binding of the N-terminal SH2 domain to the catalytic domain, leading to constitutive activation of the corresponding signalling pathway (Figure 1.8b).

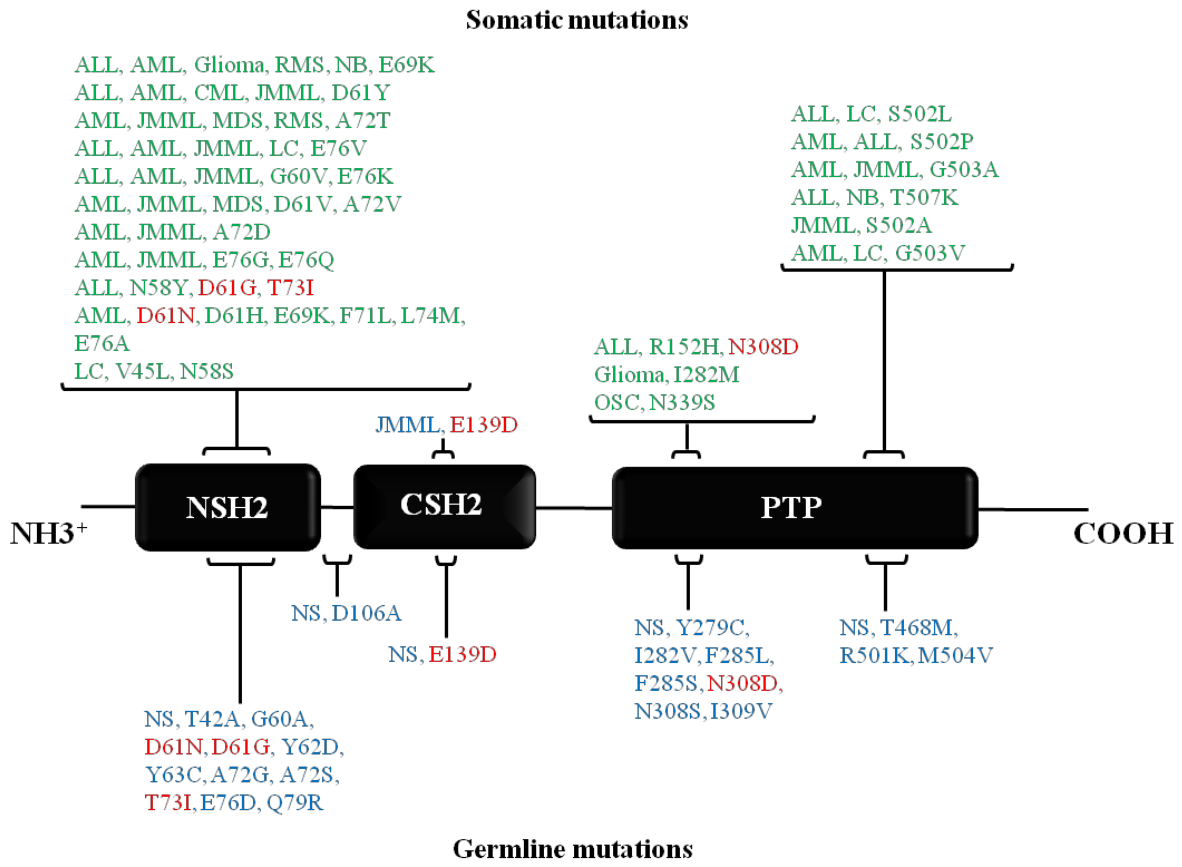

Figure 1.7: Schematic PTPN11 protein structure showing distribution of germline and somatic mutations in humans. PTPN11 consists of a protein tyrosine phosphatase (PTP) domain as well as two tandem Src-homology 2 (SH2) domains towards N-terminus. Mutations in germline are in blue, soma in green or both in red. Abbreviations indicate Noonan syndrome (NS), acute lymphoblastic leukaemia (ALL), acute myeloid leukaemia (AML), chronic myelomonocytic leukaemia (CML), juvenile myelomonocytic leukaemia (JMML), lung carcinoma (LC), myelodysplastic syndrome (MDS), neuroblastoma (NB), ovarian serous carcinoma (OSC) and rhabdomyosarcoma (RMS). (COSMIC, Tartaglia, et al., 2001; 2002; 2004; Tartaglia and Gelb, 2005)

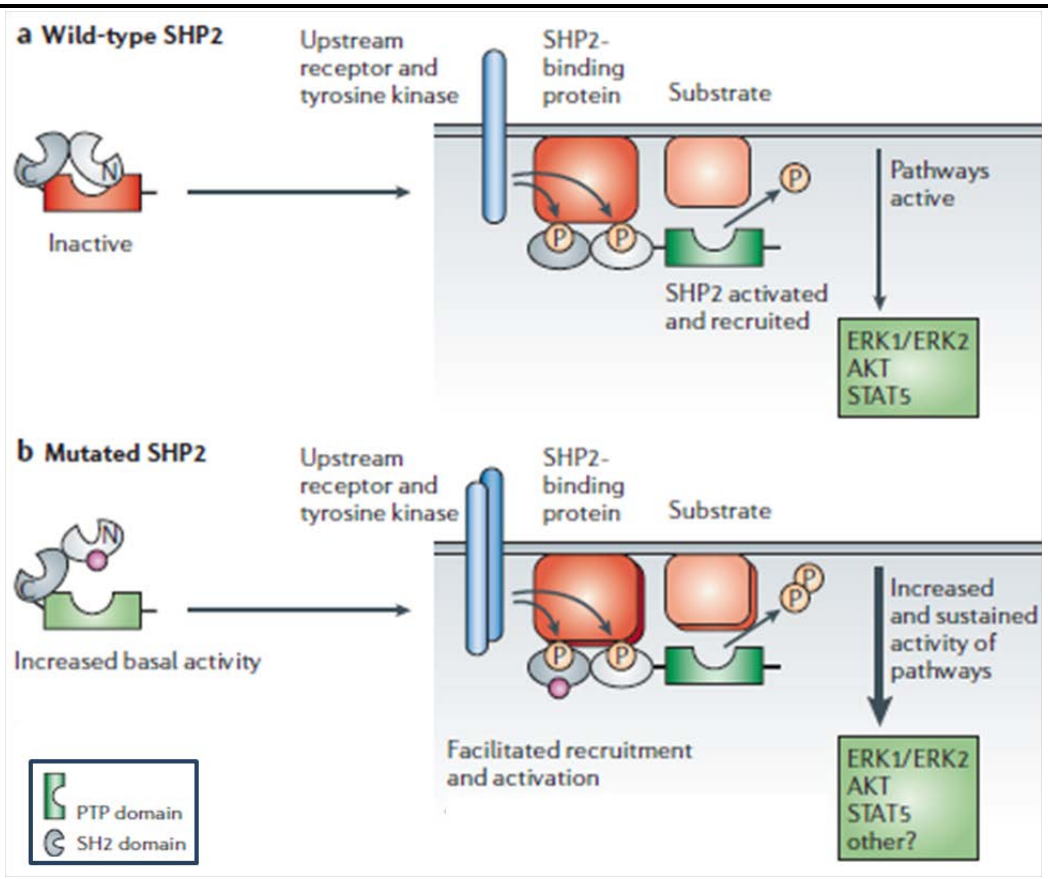

Figure 1.8: Mechanism of SHP2-mediated signal transduction and the effect of SHP2 mutations in leukaemia.

a. In the absence of upstream stimulation, SHP2 is kept in a low-activity state by interaction of the N-terminal SH2 domain with the protein-tyrosine phosphatase (PTP) domain. Activation of surface receptors, and subsequent tyrosine phosphorylation of binding sites for the SHP2 SH2 domains, in receptor-tyrosine kinases (RTKs) or scaffolding adapter proteins such as growth factor receptor-bound protein 2 (GRB2)-associated binding protein 2 (GAB2), leads to recruitment of SHP2. Occupation of the N-terminal SH2 domain results in conformational shift and resolves the inhibitory interaction of the N-terminal SH2 domain and the PTP domain. Activated SHP2 dephosphorylates substrates that, directly or indirectly, have an inhibitory role for signalling toward extracellular signal-regulated kinase 1 (ERK1)/ERK2, AKT or signal transducer and activator of transcription 5 (STAT 5). These include binding sites for negative regulators of the RAS-pathway such as RAS-GTPase-activating protein (RASGAP) or C-terminal SRC kinase (CSK). This leads to release of the corresponding pathways from inhibition.

b. Leukaemia-associated mutations in PTPN11 inhibit the interaction of the SHP2 N-terminal SH2 domain with PTP domain, leading to increased basal activity and increased affinity of the N-terminal SH2 domain for phosphotyrosine ligands. Activation of upstream receptors, and recruitment of SHP2, is also mandatory to initiate signalling by mutant SHP2. The changes in SHP2 structure caused by mutations facilitate activation and therefore increase sensitivity for the corresponding ligands of upstream receptors. Activation of downstream signalling presumably occurs by similar mechanisms as those of wild-type SHP2, but to supra-physiological levels and in a more sustained manner (Adapted from Ostman, et al., 2006).

1.5.4 ***HRAS***

RAS proteins are small GTPases that cycle between inactive guanosine diphosphate (GDP)-bound and active guanosine triphosphate (GTP)-bound conformations (Boguski and McCormick, 1993; Donovan, *et al.*, 2002). There are four highly homologous proteins in this family consisting of HRAS, NRAS, KRAS4A and KRAS4B proteins, encoded by three RAS genes. KRAS4A and KRAS4B are the results of an alternate splicing of *KRAS* transcripts at the C terminus. In terms of the structure, *HRAS* contains a highly conserved G domain (amino acids 1-165) and a hypervariable region (amino acids 166-189) at the N-terminal and the C-terminal ends respectively (Figure 1.9). The C terminus of HRAS protein is farnesylated at a CAAX motif (C = cysteine; A = aliphatic and X = any amino acid) and there are two upstream cysteine palmitoylation sites which serve as a second membrane binding signal.

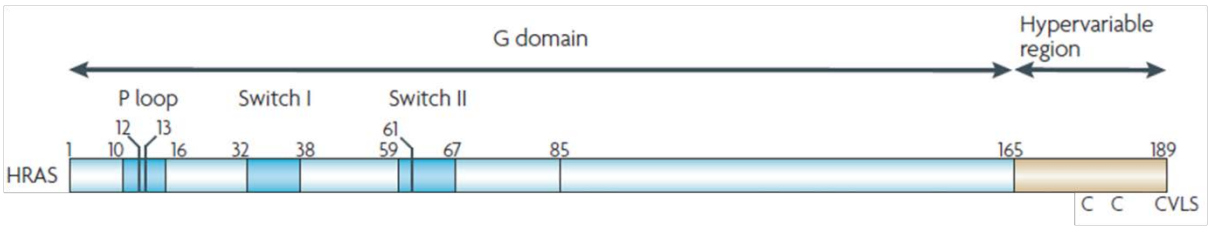

Figure 1.9: The structure of HRAS. The first 85 residues specify binding to GDP and GTP in which the P loop (phosphate binding loop) binds the γ-phosphate of GTP, and switch I and II regulates binding to HRAS regulators and effectors. The C-terminal hypervariable domain specifies membrane localisation through post-translational modifications that include the farnesylation on the C-terminal CVLS and palmitoylation of key cysteines (C). Germline and somatic HRAS mutations leading to amino acid changes were identified at codon 12, 13 or 61 (Adapted from Schubbert, et al., 2007).

Working as molecular switches, RAS proteins regulate cellular proliferation, differentiation and survival by integrating signals from activated receptors to downstream effector pathways. In the basal state, RAS is held in an inactive RAS-GDP complex and spontaneous dissociation of GDP from this complex may occur occasionally. As the cellular

levels of GTP are usually higher than GDP (~10-fold), RAS generally rebinds with GTP which in turn stimulates a conformational change in RAS and increases its affinity for effectors to activate the downstream signalling pathways. However, the RAS-GTP signalling is sufficiently terminated by an intrinsic hydrolysis activity where RAS hydrolyses the terminal phosphate of GTP at a slow rate (approximately once per hour) (Gibbs, *et al.*, 1984; John, *et al.*, 1988; Neal, *et al.*, 1988). In response to receptor-ligand binding, RAS are activated by recruiting the guanine nucleotide-exchange factors (GNEFs) SOS (son of sevenless) 1 & 2 and a family of guanine nucleotide-releasing proteins (GRPs) to facilitate nucleotide change (GDP → GTP) on RAS. It has been suggested that SOS1 opens up the nucleotide-binding site through the insertion of an α helix causing displacement of switches I and II in Ras, which consequently disrupts nucleotide binding. Previous studies also demonstrated that SOS1 contains an allosteric RAS-GTP binding site that stimulates binding of RAS-GDP to the catalytic site and thus amplifies RAS activation (Boriack-Sjodin, *et al.*, 1998; Margarit, *et al.*, 2003). RAS-GTP signalling is terminated by hydrolysis to RAS-GDP, a negative regulation catalysed by the GTPase-activating proteins (GAPs) (including p120GAP and neurofibromin) which markedly accelerate the intrinsic GTPase activity.

Recently, the impact of increased paternal age was observed in Costello syndrome originating from *de novo* germline mutations in *HRAS* at codons Gly12 and Gly13 (Sol-Church, et al., 2006; Sovik, et al., 2007; Zampino, et al., 2007; Schulz, et al., 2008). Costello syndrome is a rare congenital condition characterised by distinctive facial appearance, cardiovascular abnormalities, skin and musculoskeletal defects, mental retardation and tumour predisposition (Hennekam, 2003; Aoki, *et al.*, 2005). The most common causative mutation in Costello syndrome is an *HRAS* 34G>A transition resulting in G12S substitution whilst other mutations include G12A, G13C and G13D; all of which located at the P loop of the G domain (Table 1.4). In addition, germline mutations that encode G12C, G12D and

G12V HRAS amino acid changes were identified in Costello syndrome patients with severe clinical outcome and death in early infancy (Lo, *et al.*, 2008; Kuniba, *et al.*, 2009).

Table 1.4: The mutation spectrum of *HRAS* in the germline and soma.

Nucleotide change	Amino acid change	Germline mutations (phenotype)	Somatic mutations (cell type involved)
34G>A	G12S	Costello syndrome	Bladder, bone, cervix, large intestine, penis, prostate, salivary gland, skin, soft tissue, thyroid, upper aerodigestive tract.
34G>T	G12C	Costello syndrome	Bladder, lung, skin, thyroid, upper aerodigestive tract.
34G>C	G12R		Large intestine, pituitary, salivary gland, skin, thyroid, upper aerodigestive tract.
35G>C	G12A	Costello syndrome	Bone, thyroid.
35G>T	G12V	Costello syndrome with early lethality	Bladder, cervix, oesophagus, pituitary, prostate, salivary gland, skin, soft tissue, stomach, thyroid, upper aerodigestive tract.
35G>A	G12D	Costello syndrome	Bladder, breast, salivary gland, skin, soft tissue, thyroid, upper aerodigestive tract.
37G>T	G13C	Costello syndrome	Bladder, upper aerodigestive tract.
37G>A	G13S		Bone, lung, soft tissue, upper aerodigestive tract.
37G>C	G13R		Adrenal gland, bladder, prostate, salivary gland, skin, soft tissue, upper aerodigestive tract.
38G>A	G13D	Costello syndrome	Haematopoietic and lymphoid tissue, skin, upper aerodigestive tract.
38G>T	G13V		Bladder, thymus, upper aerodigestive tract.
181C>A	Q61K		Bladder, kidney, skin, soft tissue, testis, thyroid, upper aerodigestive tract.
181C>G	Q61E		Cervix.
182A>G	Q61R		Bladder, cervix, haematopoietic and lymphoid tissue, prostate, salivary gland, skin, testis, thyroid, upper aerodigestive tract.
182A>T	Q61L		Bladder, lung, oesophagus, penis, prostate, skin, thyroid, upper aerodigestive tract.
182A>C	Q61P		Thyroid, upper aerodigestive tract.
183G>C	Q61H		Endometrium, haematopoietic and lymphoid tissue, prostate, skin, thyroid, upper aerodigestive tract.

Somatic gain-of-function mutations in *HRAS*, which was the very first human oncogene described (Chang, *et al.*, 1982), have been associated with the development of many tumours in humans over the past decades (Malumbres and Barbacid, 2003; Downward, 2006). These oncogenic mutations are predominantly clustered at codons Gly12, Gly13 and Gln61 and have been identified in malignancies including urothelial carcinoma, skin tumours and thyroid neoplasms; of which some occur as germline mutations in Costello syndrome (COSMIC, Table 1.4). The *HRAS* mutation spectra highlight several points. Firstly, G12V is

identified as the most frequently isolated cancer-associated substitution, which is remarkably different from the mutation spectrum in the germline with the most prevalent mutation being G12S. Secondly, exclusive occurrence of Gln61 substitutions to arginine, leucine, lysine and histidine is described in tumours only but not in the germline, potentially suggesting a different phenotype or even embryonic lethality of these point mutations. Thirdly, mutually exclusive genetic events involving *HRAS* are detected in some tumours. For example, *FGFR3* and *HRAS* mutations are present in 55% and 10% urothelial carcinoma studied respectively. None of the mutation positive cases harboured both *FGFR3* and *HRAS* oncogenic lesions simultaneously (Jebar, *et al.*, 2005), which suggests that they encode components of the same signalling cascade, activation of only one of which is required for aberrant signalling.

With the introduction of these genetic alterations, intrinsic biochemical and functional properties of the encoded *HRAS* protein are disrupted resulting in aberrant cellular proliferation, signalling and survival. Biological data suggest that any amino acid change at Gly12 (except to proline) confers varying transformation potential to the encoded mutant protein. For example, G12V has more potent transforming ability compared to G12S which accounts for most of the Costello syndrome (Seeburg, *et al.*, 1984). Furthermore, it has been shown that the cancer-associated mutations perturb the intrinsic GTPase activity and cause resistance to GAPs, which gives rise to the accumulation of mutant RAS proteins in the active, GTP-bound conformation (Trahey and McCormick, 1987). Structural analysis of the complex between RAS and the catalytic domain of p120GAP uncovers an important arginine amino acid (arginine 789 in p120GAP, known as the arginine finger) that interacts with the phosphate-binding loop (P-loop) of RAS. This interaction potentially stabilises a high energy transition state during the RAS-GTP hydrolysis reaction. Amino acid substitutions at codon Gly12 affect the GTP-GDP transition state owing to the steric clash of side chains with the catalytic arginine and the side chain of glutamine 61 (Scheffzek, *et al.*, 1997). It has also been

reported that glutamine 61 is important for GTP hydrolysis and any amino acid substitution at this codon except glutamic acid blocks hydrolysis (Der, *et al.*, 1986), promoting the constitutive autoactivation (gain-of-function) of RAS signalling.

1.6 Receptor tyrosine kinase-Ras signalling and downstream pathways

The receptor tyrosine kinases (RTKs) are a large and diverse family of cell surface receptors consisting of an extracellular ligand-binding site, a single hydrophobic transmembrane region and a cytoplasmic domain that includes a catalytic region for tyrosine kinase activity. FGFR2, FGFR3 and RET are examples of RTKs described previously in Section 1.5.1, 1.5.1.1, 1.5.1.2 and 1.5.2. These RTKs dimerise in response to ligand binding, resulting in a conformational change in receptor structure that mediates the intracellular kinase domain activation by intermolecular transphosphorylation of tyrosine kinase domains. The phosphotyrosine amino acids in activated receptor serve as the docking sites for adaptor proteins, which thereby activate multiple signalling cascades.

The activated RTKs interact with RAS via SOS1 and GRB2 (growth factor receptor bound protein 2) adaptor molecules. The SH2 domain in GRB2 recognises the sequence C-terminal of the phosphotyrosine residue on RTKs and anchors to the membrane spanning proteins whilst the SOS1 molecule is bound to the two GRB2 SH3 domains. SOS1 and other exchange factors facilitate the conversion from inactive RAS-GDP into active RAS-GTP by stimulating guanine nucleotide dissociation from RAS (as mentioned in Section 1.5.4). Some RTKs interact with GRB2 through the PTB (phosphotyrosine-binding) domain of SHC (SH2-containing protein) which docks to the amino acids upstream of phosphotyrosine and is later phosphorylated by its host RTKs creating a GRB2 binding site. Likewise, SHP2 serves the similar adaptor role as SHC in mediating the activation of RAS signalling (Figure 1.10). In FGFR signalling, FGFR substrate 2 (FRS2) is a key adaptor molecule which binds to the juxtamembrane region of FGFRs via its PTB domains. Tyrosine phosphorylated FRS2α (one

of the two members of FRS family) can recruit GRB2/SOS1 complexes directly or indirectly through SHP2 (Section 1.5.3) in response to FGF-stimulation (Eswarakumar, *et al.*, 2005).

Active RAS-GTP mediates signalling networks involving in cellular proliferation, survival and differentiation by interacting and activating distinct groups of effectors (Repasky, *et al.*, 2004; Mitin, *et al.*, 2005) (summarised in Figure 1.11). The RAF-MEK-ERK pathway is the best elucidated RAS downstream signalling cascade (Repasky, et al., 2004). Three *RAF* genes encode the serine/theorine kinases ARAF, BRAF and RAF1 that integrate the upstream input signals and are responsible for the phosphorylation of MEK which later phosphorylates ERK. ERK kinases regulate a large number of downstream molecules, both nuclear and cytosolic. For instance, phospho-ERK1/2 is suggested to dimerise and translocate to the nucleus where multiple transcription factors such as c-MYC, c-FOS and members of the ETS family (Khokhlatchev, *et al.*, 1998) are then phosphorylated. Evidence from previous studies showed that the expression of proteins that control cell-cycle progression such as cyclin D1 was attributable to ERK1/2 activation. Notably, cyclin D1 expression enables the cell to progress through the G1 phase of the cell cycle. Inhibition of the RAS signal cascade perturb the expression of cyclin D1, suggesting the role of cyclin D1 in governing cell proliferation (Roovers and Assoian, 2000).

Furthermore, phosphatidylinositol 3 kinases (PI3K) are heterodimers comprising a regulatory subunit (p85) and a catalytic subunit (p110). RAS proteins especially HRAS are able to activate the signal transduction of PI3K-AKT pathway by direct interaction with p110α encoded by *PI3KCA* (Rodriguez-Viciana, *et al.*, 1994; Yan, *et al.*, 1998; Pacold, *et al.*, 2000; Li, *et al.*, 2004). The binding of RAS-GTP with PI3K phosphorylates phosphatidylinositol-4,5-biphosphate (PIP2) and generates phosphatidylinositol-3,4,5-triphosphate (PIP3). AKT is then translocated to the plasma membrane where it is phosphorylated by 3-phosphoinositide-dependent protein kinase 1 (PDK1) (Bader, *et al.*,

2005). AKT is a kinase for regulating PI3K-dependent cell survival responses and therefore overexpression of AKT exerts an anti-apoptotic effect in many cell types, leading to a resistance or delay of cell death (Fresno Vara, *et al.*, 2004). AKT promotes cell survival directly through phosphorylation and inactivation of pro-apoptotic proteins including BAD which controls the release of cytochrome c from mitochondria (Datta, *et al.*, 1997; del Peso, *et al.*, 1997). Alternatively, AKT indirectly governs the apoptotic machinery by phosphorylating the forkhead family of transcription factors (such as FKHR, AFX and FKHRL1) which thereby inhibits transcription of pro-apoptotic genes (*FASLG*, *IGFBP1* and *BCL2L11*) (Datta, *et al.*, 1999; Nicholson and Anderson, 2002).

RAS-GTP can interact with a family of exchange factors for the RAL small GTPases comprising of RALGDS, RALGDS-like gene (RGL) and RGL2 (Wolthuis and Bos, 1999). RAL is stimulated by these exchange factors which in turn participate in the activation of phospholipase D (PLD). The RAL effector acts as a regulator of vesicle trafficking which in turn regulates cell proliferation, cell fate and cell signalling (Kops, *et al.*, 1999; Goi, *et al.*, 2000; Henry, *et al.*, 2000; Chien and White, 2003; Agapova, *et al.*, 2004; Essers, *et al.*, 2004; Balakireva, *et al.*, 2006). Additionally, the RALDGS pathway is responsible, together with AKT, for the inhibition of the forkhead transcription factors of the FOX family which trigger G1 cell cycle arrest through upregulation of the cyclin-dependent kinase inhibitor KIP1 and apoptosis via the expression of pro-apoptotic genes (De Ruiter, *et al.*, 2001).

There are several other RAS effectors pathways which have important roles in regulating cellular responses. Activated RAS interacts with RAC exchange factor tumour invasion and metastasis inducing protein 1 (TIAM1) and results in the increased levels of RAC. Alternatively, RAC (a RHO family protein) can be activated via a PI3K-dependent pathway leading to subsequent actin cystoskeleton organization (Lambert, *et al.*, 2002; Malliri, *et al.*, 2002). Phospholipase Cε contains two RAS association regions and a RAS-

GEF domain which initiate the hydrolysis of PIP2 to diacylglycerol and inositol-1,4,5-triphosphate, leading to the activation of PKC kinase and calcium signalling (Shibatohge, *et al.*, 1998; Kelley, *et al.*, 2001; Song, *et al.*, 2001).

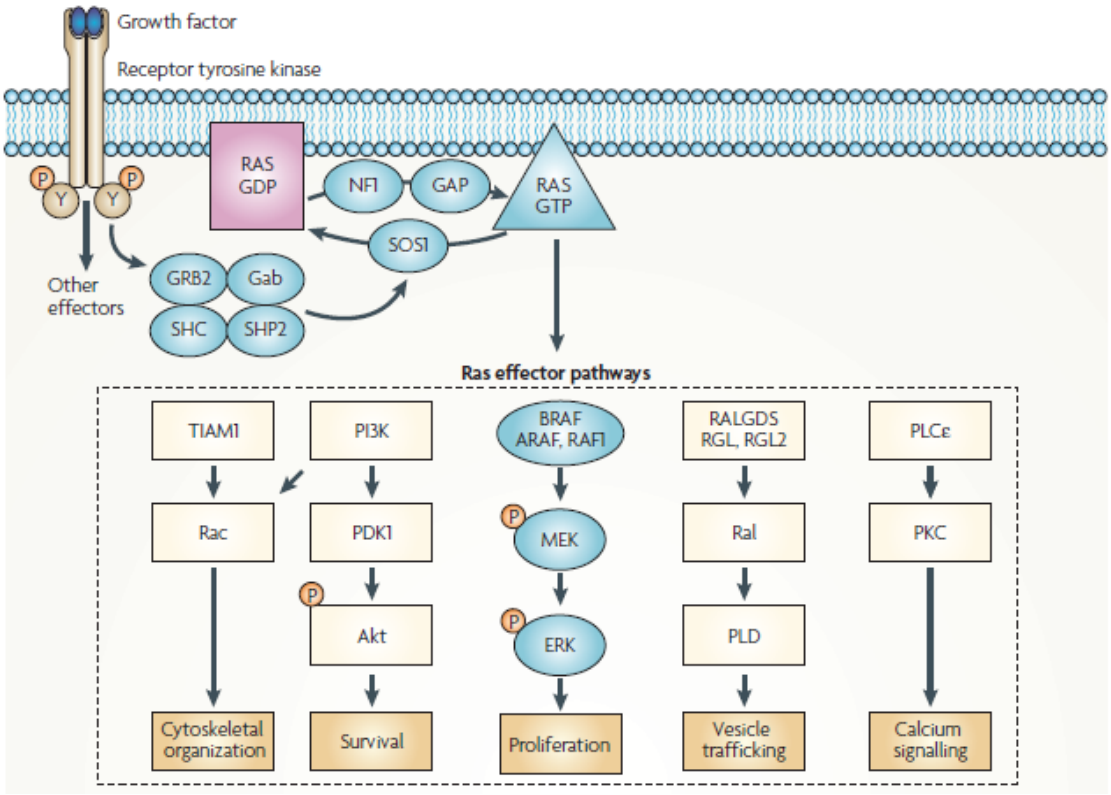

Figure 1.10: The RAS signalling pathway. Abbreviations indicate v-akt murine thymoma viral oncogene homolog 1(AKT1; also known as AKT), v-raf murine sarcoma 3611 viral oncogene homolog (ARAF), v-raf murine sarcoma viral oncogene homolog B1 (BRAF), extracellular signal-regulated kinase (ERK), GRB2-associated binding (Gab), GTPase-activating protein (GAP), growth-factor-receptor bound protein 2 (GRB2), mitogen-activated and extracellular-signal regulated kinase kinase (MEK), neurofibromin (NF1), 3-phosphoinositide-dependent protein kinase 1 (PDK1), phosphatidylinositol 3-kinase (PI3K), phospholipase Cε (PLCε), phospholipase D (PLD), protein kinase C (PKC), RAS-related Rac (Rac), RAS-related Ral (Ral; also known as RALA, v-ral simian leukaemia viral oncogene homolog A), ral guanine nucleotide dissociation stimulator (RALGDS), v-raf murine leukaemia viral oncogene homolog 1 (RAF1), RAS-guanosine diphosphate (RAS-GDP), RAS-guanosine triphosphate (RAS-GTP), ral guanine nucleotide dissociation stimulator-like 1 (RGL; also known as RGL1), ral guanine nucleotide dissociation stimulator-like 2 (RGL2), SH2-containinig protein (SHC), Src homology 2- containing tyrosine phosphatase (SHP2; also known as *PTPN11*), son of sevenless homolog 1 (SOS1), tumour invasion and metastasis inducing protein 1 (TIAM1) (Adapted from Schubbert, et al., 2007).

1.7 FGFR mutations in human sperm: reflecting the paternal age-effect

The exclusive paternal origin and paternal age-effect previously described in several congenital disorders (Section 1.3; Table 1.2), indicated that the associated point mutations occur predominantly in the spermatogonial cells, which continuously divide throughout a male's life time. Methods have been developed by several groups to directly measure these base substitutions in sperm; one would expect that the increased number of mutations in sperm with donor age would reflect the age-dependent prevalence of these disorders, regardless of which mechanism had generated the mutations. With reference to the observed birth prevalence, the expected mutation levels in sperm would still fall in the 10^{-4} - 10^{-6} range, pushing current molecular detection technologies to the limit. The earliest investigations of paternal age-effect mutations in sperm were performed on *FGFR3* and *FGFR2* mutations occurring in ACH (Section 1.5.1.2) and Apert syndrome (Section 1.5.1.1), respectively.

In 2002, Tiemann-Boege *et al* (2002) examined the level of *FGFR3* 1138G>A ACH mutation in the sperm of healthy male donors (n = 118) aged between 18 and 80 years; these men did not have a child with ACH. The authors employed an approach which involved a combination of primer-mismatch PCR amplification and restriction digest (to isolate mutant *FGFR3* alleles), followed by allele-specific quantitative amplification of the mutant sequence. To measure the amount of 1138G>A mutations, sperm DNA was compared with standards containing a constant amount of blood cell DNA mixed with varying numbers of genomes from a human cell line homozygous for the 1138G>A mutation. Each sperm DNA sample (1 µg) was subjected to 5-14 independent measurements distributed among 3-6 experiments. The frequency of mutant sperm appeared stable between the ages of 18 and 40, and the ages of 55 and 80 years (Figure 1.11B). However, an approximately 2-fold increase in mutation frequency was detected in the age group between 40 and 55 years; neither a linear nor an exponential model of mutation accumulation was able to fit the findings satisfactorily.

In comparison to the observed birth data for ACH (Risch, et al., 1987), the magnitude of the increase in mutation frequency with age was inadequate to explain the paternal age-effect observed in ACH.

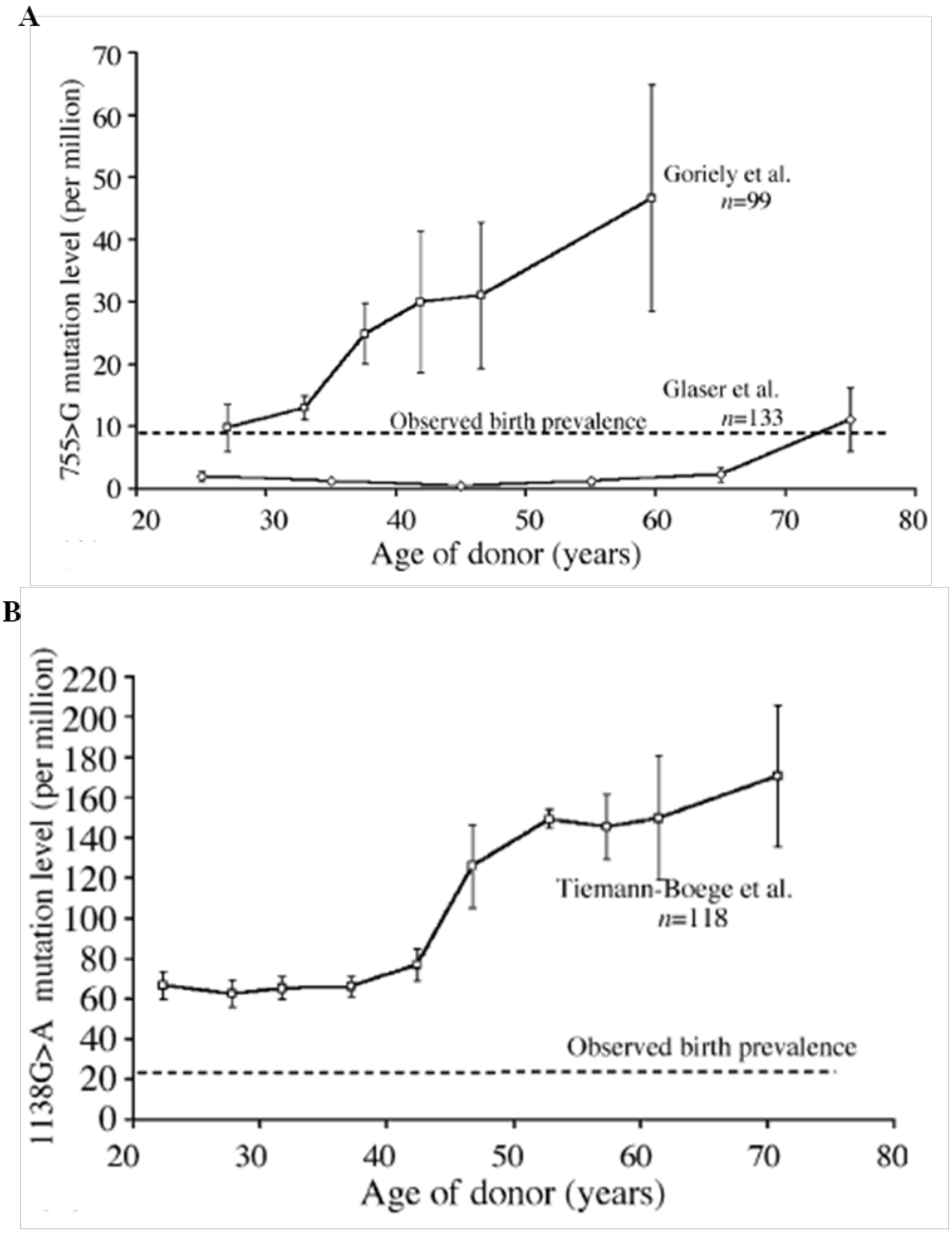

Figure 1.11: Comparison of experimentally determined mutation data from human sperm in relation to donor age. **A** 755C>G mutation in *FGFR2* (Glaser, *et al.*, 2003; Goriely, *et al.*, 2003). **B** 1138G>A mutation in *FGFR3* (Tiemann-Boege, et al., 2002). The values shown are for mean mutation level ± standard error of the mean, calculated in 5-year age bins (note the difference in scale between A and B). The expected prevalence of each mutation is represented by the dashed line (Adapted from Wilkie, 2005).

A similar conclusion was reached by another group which studied both the 755C>G and 758C>G *FGFR2* Apert transversions in sperm (Glaser, *et al.*, 2003). The samples were collected from 133 men who had not fathered a child with Apert syndrome, ranging in age from 21 to 80 years and screened using a one-step allele-specific PCR method; in which a peptide nucleic acid was used to mask the wild type allele and amplification was attempted specifically from mutant allele as a template. Every sperm sample consisting of 0.15 µg was independently analysed 7-16 times and compared to standards prepared from a series of dilutions of genomic DNA from an affected patient heterozygous for each mutation mixed with human genomic DNA. The authors demonstrated a highest increase in Apert mutation frequency in men aged > 60 years (Figure 1.11A) ; however, in the context of the age relationship with the mutation frequency (when considering the 755C>G and 758C>G mutations both independently and combined), it was again insufficient to account for the paternal age-effect compared with the observed birth data for Apert syndrome (Risch, et al., 1987).

In contrast, a third study conducted by Goriely *et al* (2003) obtained strikingly different results from the previous two studies and successfully demonstrated the increase of *FGFR2* 755C>G point mutations in sperm with age, consistent with the paternal age-effect associated with Apert syndrome. Goriely *et al* screened the level of 755C>G transversion in sperm sampled from 99 healthy men (aged 23.8-73 years), without a family history of Apert syndrome using two rounds of restriction digest selection and PCR amplification, followed by Pyrosequencing. Three aliquots of each sample containing 10 µg of DNA were spiked with known concentrations of genomic DNA from a patient heterozygous for a novel triple nucleotide substitution to determine the absolute mutation levels. The 755C>G mutation was detected at high levels (maximum of 1.6×10^{-4}) and showed a positive correlation with donor

age that closely mirrored the raw estimates of the relative birth rate of Apert syndrome at different paternal ages (Figure 1.11A).

Taken together, the distinctive discrepancies in the relationship between the absolute mutation levels and donor age amongst these studies were most likely attributed to methodological variations (as discussed in Wilkie, 2005). For instance, each assay employed a different amount of DNA and number of replicates to measure the mutation level in individual specimens, as detailed above. These were equivalent to a maximum number of ~ 4.0, 0.7 and 8.6 million haploid genomes examined for Tiemann-Boege *et al*, Glaser *et al* and Goriely *et al*, respectively. The measurement unit used by Glaser *et al* (0.15 µg; ~ 43000 haploid genomes) was too small, which restricted them from identifying rare mutations in individual assays and led them to underestimate the mutation levels (Figure 1.11A). In addition, the lowest detectable mutation level in the Tiemann-Boege *et al* study was about 1 in 26,000; any individual with a lower reading was scored at this background level, which probably led to artefactually inflated mutation levels in younger men, thus obscuring the paternal age-effect. Conversely, with a larger measurement unit, Goriely *et al* were able to measure a mutation level of 10^{-5} with 2-fold accuracy which then allowed accurate estimation of the mutation levels even in the youngest age groups. Intriguingly, the mutation levels in sperm of fathers of Apert patients all fell within the range of normal values, suggesting that these Apert fathers were sampled from the normal population, and that their chance of fathering another affected child would be very low.

1.7.1 Explaining the elevated mutation rate: evidence for selection

An extension of the study done by Goriely *et al* (2003) was used to explain the high absolute level of *FGFR2* 755C>G mutation found in sperm. The authors explored the occurrence of the 755C>G Apert mutation on the two *FGFR2* alleles in normal heterozygous men by determining their phase in relation to a common upstream intronic single nucleotide

polymorphism (SNP) (-112G/A). The ratio of mutations present on each of the two alleles was estimated and related to the absolute level of mutation. Intriguingly, the 755C>G mutation was found often to predominate on one or other allele even in individuals with high levels of this substitution. However, no bias was evident in favour of preferential mutation accumulation on one of the alleles across the population as a whole (Figure 1.12A). The authors also measured the level of 755C>T transitions (encoding Ser252Leu), which is expected to be the more frequent mutation at a CpG dinucelotide and was previously related with a normal or mild Crouzon syndrome (as described in Figure 1.2). The mutation level was high (although the average level was 1.66-fold lower than 755C>G) and positively correlated with donor age. In terms of the mutation distribution between two alleles around the -112G/A polymorphism, it was markedly less skewed (Figure 1.12B).

The observation that the more prevalent 755C>G mutation showed greater skewing than the less prevalent C>T mutation could not be explained by any neutral model of mutation accumulation through many independent replications errors during spermatogenesis (see Section 1.2), but indicated that the two mutations must be subject to different strengths of positive selection. Goriely *et al* concluded that the 755C>G substitution arises less frequently but confers a greater selective advantage compared with the 755C>T mutation which occurs more frequently, conferring a weaker selective advantage. Positive selection driven by the infrequent gain-of-function mutations explains several other elements of their data, including the high absolute levels of specific mutations in particular tissues (sperm but not blood), the observed higher levels of C>G mutations at position 755 despite the expected higher level of C>T transition at methylated cytosines, the greater variation in C>G mutation frequency between individuals and the detection of multiple mutations in *cis* to C>T (observed both in patients and sperm), explained by sequential selection events (Oldridge, et al., 1997; Lajeunie, et al., 1999; Wilkie, *et al.*, 2002; Goriely, et al., 2003; 2005).

Additionally, subsequent studies by an other group (Qin, *et al.*, 2007; Choi, *et al.*, 2008; Yoon, *et al.*, 2009), which measured *FGFR2* 755C>G and 758C>G Apert mutations by a completely different method known as Bi-PAP-A (Bi-directional pyrophosphorolysis-activated polymerisation allele-specific amplification), obtained values for the 755C>G substitution that were indistinguishable from the Goriely *et al* (2003) study.

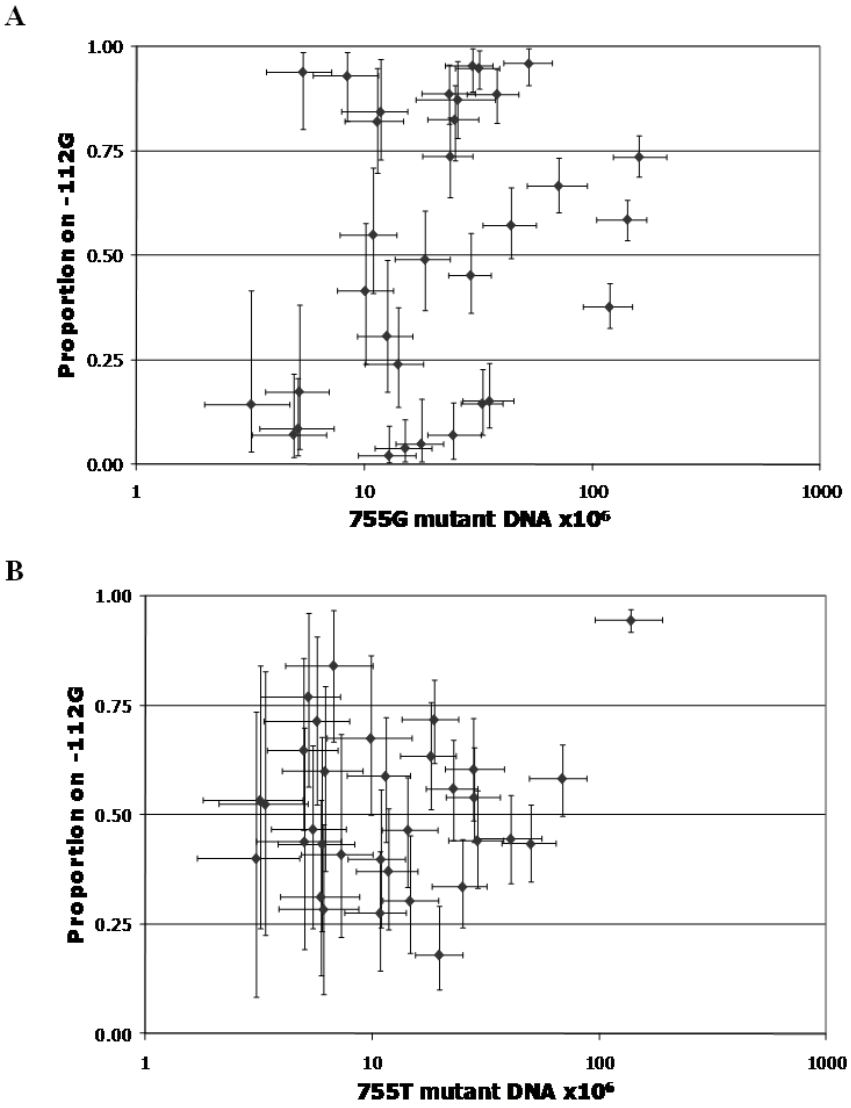

Figure 1.12: The distribution of 755C single base substitutions in sperm between *FGFR2* alleles. The ratio of C>G (**A**) and C>T (**B**) mutations on the G allele in sperm of -112GA heterozygotes, plotted against the estimated level of the corresponding mutation; the levels of both substitutions in all individuals were above 3 x 10^6 (n = 33) (Adapted from Goriely, et al., 2003).

A more recent investigation has sought further evidence of selection by analysing the prevalence of 9 potential *FGFR3* point mutations at codon 650 (Section 1.5.1.2) (Goriely, et al., 2009). A total of 78 sperm samples and 8 blood samples collected from healthy donors were included in this study. Every DNA sample was prepared into three aliquots (each containing 10 µg), two of which were spiked with a different quantity of diluted genomic DNA heterozygous for the *FGFR3* 1948A>C transversion as an internal standard to quantify the absolute mutation levels. Samples were treated with two rounds of restriction digest selection and PCR amplification using primers including unique 4-nucleotide tags to identify individual samples. All the amplified products were subsequently pooled together for a given spike level to assemble three independent libraries prior to massively parallel sequencing. The level of *FGFR3* 1948A>G causing TDII (Section 1.5.1.2) was usually greater (maximum of 2.1×10^{-4}) in the sperm compared to other 8 possible base substitutions at the K650 codon and positively correlated with donor age. This genetic lesion was most prevalent in 66/78 samples and responsible for 73% of total mutations in these samples whilst the 1948A>C transversion causing familial acanthosis nigricans (Section 1.5.1.2) was the most prevalent mutation in 8/78 samples and contributed 17% of total mutations in sperm. The 1948A>T (K650M) and 1950G>C/T (K650N) each accounted for > 1% of the total mutation levels whereas all three other base substitutions encoding synonymous, conservative or stop codon changes were >1000-fold less prevalent than 1948A>G. The discrepancy of different mutation frequencies at the codon Lys650 observed in this study suggests differential selection of cells harbouring mutant proteins with different degree of gain-of-function properties that correspond with the severity of the clinical phenotype (as described in Section 1.5.1.2).

1.8 Paternal age-effect mutations and testicular tumourigenesis

1.8.1 Normal human spermatogenesis

To understand the pathological basis of paternal age-effect mutations, one has to explore the events that occur in human spermatogenesis. Spermatogenesis is an ongoing life-long process that begins in fetal development when proliferating primordial germ cells (PGCs) in the fetal testis migrate to the genital ridges and become enclosed within testicular cords by the 8^{th} weeks of gestation (wg) (Wartenberg, 1981). The PGCs differentiate into a heterogeneous population of fetal germ cells consisting of gonocytes, intermediate germ cells and prespermatogonia (Fukuda, *et al.*, 1975). Gonocytes are a population of single, round cells located at the centre of the lumen-less seminiferous cords which later migrate to the basement membrane to adopt a spermatogonial feature; this relocation process is important for their differentiation and the nonmigrating gonocytes are subjected to apoptosis (Tres and Kierszenbaum, 2005). The majority of the cells during the first trimester (7-9 wg) are categorised as gonocytes whilst three distinct populations of gonocytes, intermediate cells (normally occurring in pairs) and prespermatogonia were identified within the same seminiferous cord in the second trimester (14-19 wg). By the end of second trimester (from 18 wg onwards), the number of prespermatogonia increased and became the most predominant germ cells in the fetal testes. These prespermatogonia (infantile spermatogonia) acquire competence of development into haploid gametes only after puberty. Mature post-pubertal spermatogonia, located at the basal membrane of the seminiferous tubules, comprise a heterogeneous population of germ cells. These can be classified according to their morphologies and correspond to three main maturation stages: A_{dark} spermatogonia, which are considered to represent the reserve stem cell population; highly proliferating A_{pale} spermatogonia; and more mature B spermatogonia that give rise to pre-leptotene primary spermatocytes, which enter meiosis and lead to the formation of haploid spermatids.

Morphologically, A_{dark} spermatogonia have a spherical or ovoid nucleus consisting of deeply stained dust-like chromatin, and characterised by the presence of a vacuole-like cavity in the nucleus (Figure 1.13-1). A_{pale} spermatogonia have an ovoid nucleus containing pale, finely granulated chromatin (Figure 1.13-1&2), whilst a spherical nucleus showing a lightly stained granulated chromatin is observed in B spermatogonia (Figure 1.13-2). Based on the ratio of different cells in the seminiferous epithelium (A_{dark}: A_{pale}: B: Primary spermatocytes = 1: 1: 2: 4), Clermont proposed that each A_{dark} spermatogonium undergoes an asymmetrical mitotic division yielding a daughter stem cell (self-renewing) and an A_{pale} spermatogonium which differentiates into B spermatogonia and is eventually lost as sperm (Clermont, 1966a; b) (Figure 1.14A). The number of cell divisions that have occurred prior to the production of sperm varies amongst men, depending on their age as described earlier in Section 1.2.

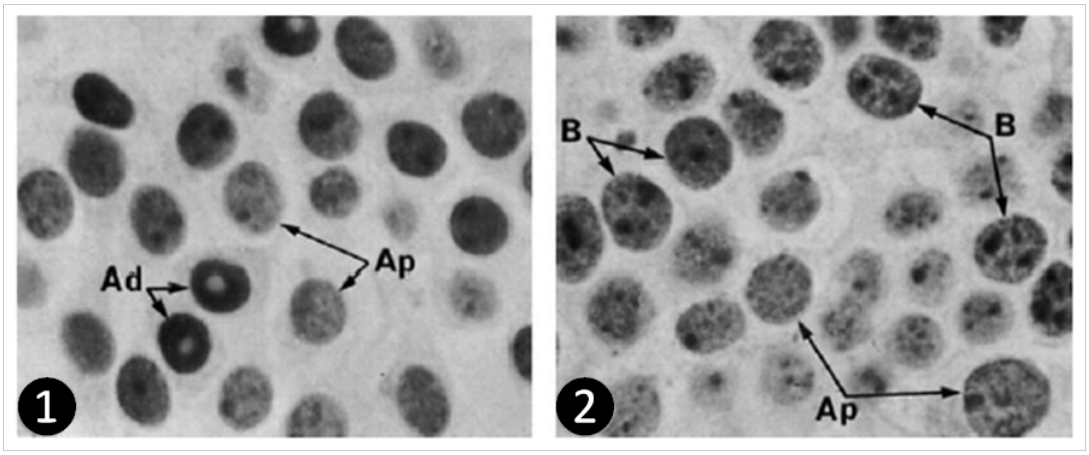

Figure 1.13: The morphology of three types of spermatogonia. Abbreviations indicate A_{dark} spermatogonia (Ad), A_{pale} spermatogonia (Ap) and B spermatogonia (B) (Adapted from Clermont, 1966a).

By contrast, the spermatogonial proliferation / differentiation in mouse spermatogenesis is defined by the incomplete cell division that results in the daughter cells remaining interconnected via intercellular bridges (de Rooij and Russell, 2000). The heterogeneity of spermatogonia in mouse is better characterised compared to human. The

isolated A_{single} or A_s spermatogonia are recognised as the most primitive cells and give rise to pairs, followed by chains from 4 to 16 cells, which are known as A_{paired} (A_{pr}) and $A_{aligned}$ (A_{al}) spermatogonia, respectively. These A_s, A_{pr} and A_{al} spermatogonia are collectively called the undifferentiated spermatogonia (Huckins, 1971). A_{al} spermatogonia are able to differentiate into a series of differentiating spermatogonia consisting of A_1, A_2, A_3, A_4, In (intermediate) and B spermatogonia. After undergoing around 10 successive mitotic divisions, B spermatogonia enter meiosis to produce primary spermatocytes, secondary spermatocytes and eventually spermatids (Figure 1.14B). Evidence from previous studies proposed that A_s spermatogonia (without intercellular bridges) serves as the stem cells that divide either into a new A_s stem cell or divide into A_{pr} spermatogonia (with intercellular bridges), committing to differentiation and irreversibly losing stem cell capacity (Huckins, 1971; Oakberg, 1971). This classical 'A_s model' which suggested stem cell as long-lived cells that rarely turnover was recently questioned by other studies demonstrating a stochastic self-renewal model of mouse spermatogenesis (Nakagawa, *et al.*, 2007; Klein, *et al.*, 2010). Results showed that each stem cell (undifferentiated spermatogonium) is equipotent in coordinating a continuous self-renewing process that occurs on average every 2 weeks; these cells are equally likely either to multiply to replace the neighbouring stem cells or be lost irrespective of its clonal history, maintaining the constant number of stem cells.

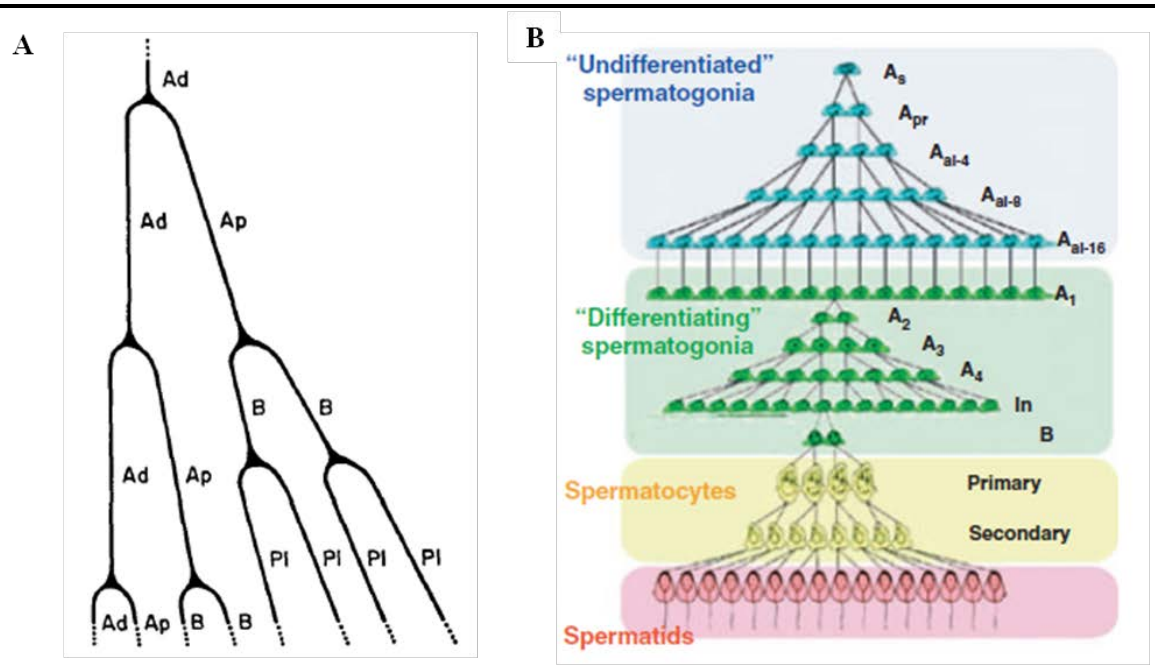

Figure 1.14: Diagram illustrating the development of the spermatogonia in human (A) and in mouse (B). The divisions of cells are represented by the junction of three lines in A and B. Abbreviations indicate A_{dark} spermatogonia (Ad), A_{pale} spermatogonia (Ap), A_{single} spermatogonia (A_s), A_{paired} spermatogonia (A_{pr}), $A_{aligned}$ spermatogonia (A_{al}), B spermatogonia (B), Intermediate spermatogonia (In) and preleptone primary spermatocytes (Pl) (Adapted from Clermont, 1966a; Yoshida, 2010).

Furthermore, the spermatogonial population is supported by specialised microenvironments termed niches that provide the extrinsic stimuli that are essential for stem cell maintenance (Spradling, *et al.*, 2001; Scadden, 2006). Stem cell niches are provided by the somatic cells including Sertoli cells that reside around spermatogonial stem cells (SSCs), peritubular myoid cell and interstitial Leydig cells. Yoshida *et al* (2007) observed that A_s spermatogonia (SSCs) as well as A_p and A_{al} spermatogonia (progeny cells of SSCs) were preferably confined in the areas of seminiferous tubules adjacent to interstitial tissue (e.g. Leydig cells), suggesting the stem cell niche in mouse is associated with the presence of interstitial cells. Stem cells residing near the niche are proposed to undergo self renewal whereas those in a cellular environment away from the niche will differentiate. Recent evidence from mice suggests that impaired function of the niche microenviroment partly

accounts for the age-related decreases in fertility, rather than deterioration of SSCs' capabilities to undergo self-renewal and differentiation (Ryu, *et al.*, 2006; Zhang, *et al.*, 2006).

Sertoli cells are the major contributor to the niche as these cells produce growth factors that trigger self-renewal (GDNF; Section 1.5.2 & FGF2; Section 1.5.1) and differentiation (activin A, BMP4, bone morphogenetic protein 4 and SCF, stem cell factor) (as reviewed in de Rooij, 2009). GDNF is one the ligands of RET receptor (Section 1.5.2) that serves as an important niche factor in regulating SSC self-renewal. Spermatogenesis in heterozygous *Gdnf*$^{+/-}$ knockout mice was disrupted owing to SSC depletion; whilst overexpression of Gdnf resulted in the accumulation of undifferentiated spermatogonia (Meng, *et al.*, 2000). Likewise, abnormalities in germ cell maturation were observed in *Ret* hypomorphic mice and manifested during the first wave of spermatogenesis (Jain, *et al.*, 2004). Evidence from recent work showed that Gfrα1 (the co-receptor of RET receptor; Section 1.5.3) and Ret proteins were present in a subpopulation of gonocytes at birth and confined to SSCs during normal spermatogenesis. Notably, undifferentiated spermatogonia expressing Plzf (a well-characterised transcriptional repressor identified in SSCs and crucial for SSC self renewal) (Buaas, *et al.*, 2004; Costoya, *et al.*, 2004), Ret and Gfrα1 were defined as SSCs. Severe depletion of SSCs as a result of the perturbation of SSC proliferation and inability of SSCs to maintain an undifferentiated state was evident in mutant mouse testes with Gdnf, Grfα1 and Ret deficiency, further supporting the requirement of the GDNF-mediated RET/GFRα1 receptor complex in activating spermatogonial self-renewal (Naughton, *et al.*, 2006).

In addition, FGF2 is required in the media of SSC cultures to enhance their long-term self-renewing expansion in combination with GDNF; however, a similar result could not be obtained with FGF2 alone (Kubota, *et al.*, 2004). FGF2 has been demonstrated as a survival

factor for Sertoli cells and a mitogenic factor for gonocytes (Van Dissel-Emiliani, *et al.*, 1996). The immunoreactivity of FGF2 was detected in Sertoli cells, Leydig cells and gonocytes/spermatogonia (Mullaney and Skinner, 1992; Han, *et al.*, 1993; Koike and Noumura, 1995). FGFR2 and FGFR3 (Section 1.5.1.1 and 1.5.1.2) are the receptors of FGF2 ligand. The expression of two different isoforms (IIIb, IIIc) of *Fgfr2* (Section 1.5.1) was observed in rat spermatogonial stem cell lines, where one line exhibited exclusive expression of *Fgfr2c*, whilst in the other *Fgfr2b* was seen to predominate (Goriely, et al., 2005). These observations suggest that differential expression of each receptor splice form may indicate different stages of spermatogenesis. Fgfr2 was immunolocalised to spermatocytes and spermatids of immature and adult mouse testes, in addition to its expression in immature adult-like Leydig cells (Cancilla and Risbridger, 1998), suggesting the potential involvement of this receptor in supporting spermatogonial division.

1.8.2 A link of clonal expansion in the testis with paternal age-effect mutations

The idea of selective advantage leading to clonal expansion is an important element in evolutionary theory. It is acknowledged that some malignancies acquire a 'mutator phenotype' which results in increased mutation susceptibility and tumour growth. However, using a mathematical models of tumour growth, Tomlinson *et al* (1996) showed that it is not essential to invoke an increased mutation rate to explain cancer. Instead, selection of advantageous mutations with a normal intrinsic mutation rate can account for the development of sporadic tumours associated with clonal expansion. This is analogous to the properties of paternal age-effect mutations in the cellular context of the testis. These rare activating point mutations, albeit detrimental to embryonic development, confer selective advantage to the spermatogonia in which they arise (see section 1.7.1) and these mutant spermatogonial cells are proposed to become progressively enriched in the testis over time, resulting in clonal expansion. It has been postulated that a premeiotic (spermatogonial)

positive selection as low as 0.002 per cell generation in the germline is adequate to account for the clinical observations of congenital syndromes caused by paternal age-effect mutation (Crow, 2006). Occasional symmetric cell divisions of spermatogonia harbouring pathogenic point mutations are important to increase the number of cell exponentially over the course of time, forming clones within the normal testis. This is because there will be no net change to the number of spermatogonia when mutations were introduced if these cells are only undergoing asymmetrical divisions at the stem cell stages (Crow, 2006).

Following the earlier studies of sperm described in Section 1.7.1, putative *FGFR2* 755C>G and 758C>G mutant clones have been identified in the testis (Qin, *et al.*, 2007; Choi, *et al.*, 2008). The authors obtained the frozen cadaveric testes from both older and younger men where each testis was dissected into ~200 pieces and the level of Apert mutations was measured in every piece using BiPAP-A (Section 1.7.1), followed by quantitative PCR. For each older case (men aged 45, 54 and 62 years), a localised distribution of these mutations was observed in the testes, in which 95% of the mutations were clustered in just 5% of the testis; the mutation level within these small regions (given the absolute mutation levels found) was 10^3 to 10^4 times higher than the remaining ones. In contrast, there were either no clusters, or clusters with much lower mutation frequencies, observed in samples from the younger men (aged 19 and 23 years) (Figure 1.15). The localised distribution of these genetic lesions in the normal testis further revealed that occasional symmetrical divisions, which occurred at an average inferred rate of one in every 100 divisions or approximately once in every 4 years, were sufficient to explain the observed mutation frequencies (10^{-4} – 10^{-5}), which is concurrent with the results published by Goriely *et al*. (2003) (Section 1.7). In other words, fewer than 1% of symmetrical cell divisions are required for the enrichment of paternal age-effect mutations up to 1000-fold in the testis (Crow, 2006; Qin, et al., 2007; Goriely and Wilkie, 2010). A further study involving analysis

of *FGFR3* 1138G>A transition causing achondroplasia (Section 1.5.1.2) in testicular biopsies identified a marked increase to 2.08 x 10^{-3} of the mutation frequency after the age of 70 years; of which the highest mutation rate of 1.5 x 10^{-2} was studied in the testis cells from a 95 year old subject (Dakouane Giudicelli, *et al.*, 2008). In short, these findings are in parallel with the proposed selective advantage mechanism caused by paternal age-effect mutations.

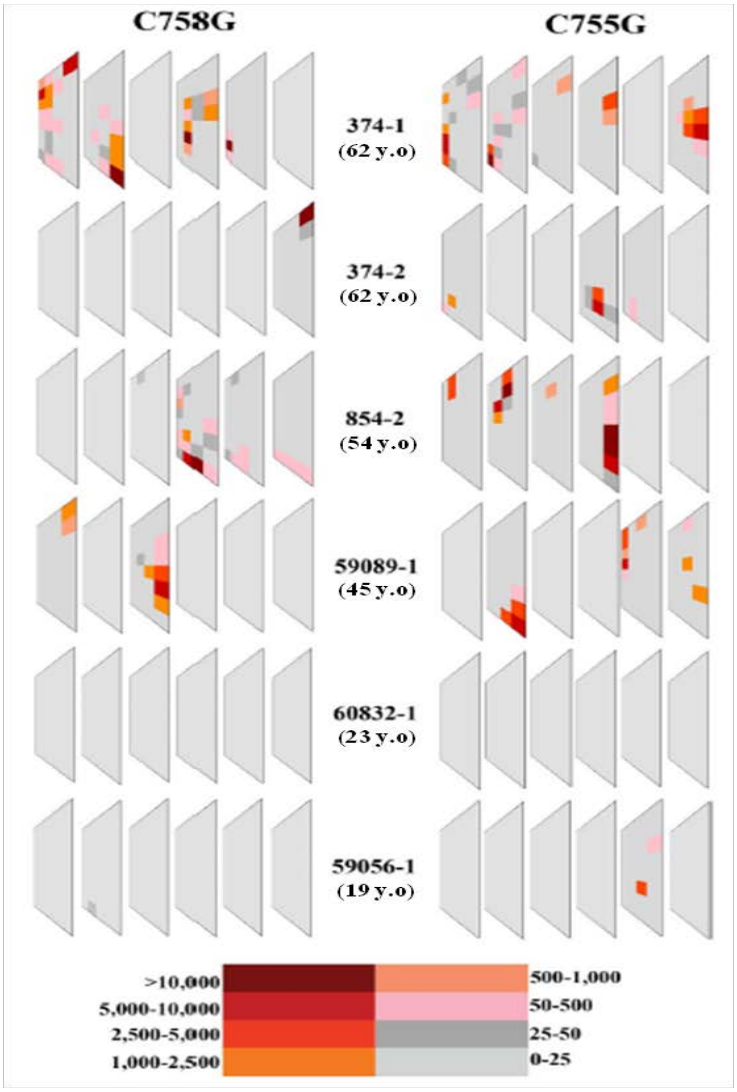

Figure 1.15: Distribution of *FGFR2* Apert missense mutations in dissected human testes. Each of the testes was studied for 758C>G (left column) and 755>G (right column) transitions. The donor/testis identification number as well as his age locates between the data for each mutation type. Each testis is demonstrated as six slices where each of these is further divided into 32 pieces. The colour code represents the number of mutant molecules per million genomes. Note that the first two testes are from the same donor whilst the rest are donated by different individuals. Abbreviation indicates years old (y.o) (Adapted from Choi, et al., 2008).

1.8.3 Spermatocytic seminoma: a pathological correlate of paternal age-effect mutations

In general, testicular germ cell tumours (except spermatocytic seminoma) are believed to be derived from a precursor condition, called carcinoma in situ (CIS) testis or intratubular germ cell neoplasia, unclassified (IGCNU), considered to be derived from developmentally arrested gonocytes. These tumours are found mainly in young patients, aged from 25-35 years old (Skakkebaek, *et al.*, 1987; Oosterhuis and Looijenga, 2005; Rajpert-de Meyts and Hoei-Hansen, 2007; Sonne, *et al.*, 2009). Earlier attempts to identify mutations of *FGFR2* or *FGFR3* in common testicular germ cell tumours (seminomas and non-seminomas) yielded negative results (Hansen, *et al.*, 2005; Bignell, *et al.*, 2006); subsequently the focus of study shifted to a different testicular tumour, termed spermatocytic seminoma (SS). SS is a rare tumour type, first distinguished from other types of germ cell tumours that occur in adolescents and young men by Masson (1946). SS presents in men with a late mean age of diagnosis; ~54-59 years in most studies (Eble, 1994; Carriere, *et al.*, 2007; Goriely, et al., 2009). SS is occasionally diagnosed in men in their thirties or early forties, suggesting that the real age of onset of this benign tumour may sometimes be younger than generally believed.

SS is a slow-growing neoplasm that metastasises exceedingly rarely and has a characteristic cytomorphology with the presence of nuclei of three different sizes (Eble, 1994; Woodward, et al., 2004). It is considered to have an early stage of progression in tumourigenesis, the so-called intratubular spermatocytic seminoma (ISS) where abnormal cells accumulate inside the tubules with partially preserved spermatogenesis (Muller, *et al.*, 1987). This stage should not be confused with CIS/IGCNU which has a completely different appearance and pathogenesis. Identification of ISS alone – without the presence of a tumour – is extremely rare (Eble, 1994) because this lesion is asymptomatic and is not associated

with infertility or testicular dysgenesis. Instead, in some SS cases, ISS can be observed adjacent to the invasive tumour. However, it is not clear whether the ISS tubules in the vicinity of the tumour represent the preinvasive stage of SS or rather a Pagetoid spread of invasive tumour within surrounding tubules. It has been widely agreed that SS differs from other types of testicular germ cell tumour (TGCT); however, the pathogenesis has long been unclear and it was postulated that an amplification of the *DMRT1* locus on chromosome 9 could be involved (Looijenga, *et al.*, 2006). The identity of the progenitor cells of SS has been suggested to be derived from an adult germ cell lineage that lacks any residual embryonic traits – either the spermatogonia (Rajpert-De Meyts, *et al.*, 2003) or primary spermatocytes (Looijenga, *et al.*, 2006).

Rajpert-De Meyts *et al* (2003) observed the expression of spermatogonial markers including MAGEA4 (melanoma antigen family A, 4), CHK2 (indicator of mitotic germ cells), and neurone-specific enolase proteins in spermatocytic seminoma; in addition to the absence of $p19^{INK4d}$ (protein involved in the transition from mitotic to meiotic division in germ cells) as well as TRA-1-60 and placental-like alkaline phosphatase (both are markers known for germ cell tumours of young adult). These findings supported the proposed origin of spermatocytic seminoma from premeiotic spermatogonia that has lost embryonic traits but has not yet passed the meiotic checkpoint. In contrast, the mRNA expression profile revealed the significant presence of genes known to be specifically expressed during meiosis prophase I in spermatocytic seminoma (Looijenga, et al., 2006). These include cancer testis antigen containing *CTCFL* (CCCTC-binding factor (zinc finger protein)-like) and *SYCP1* (synaptonemal complex protein 1) as well as other genes consisting of *TCFL5* (transcription factor-like 5 - basic helix-loop-helix), *CLGN* (calmegin; a chaperone interacting with TCFL5) (Siep, *et al.*, 2004) and *LDHC* (lactate dehydrogenase C; a germ cell lineage-specific variant) (Markert, *et al.*, 1998); these data, in contrast to the conclusion of Rajpert De-Meyts (2003),

thereby suggested that spermatocytic seminoma may derive from primary spermatocytes of the adult testis that have at least entered the prophase of meiosis I.

Together, the above observations suggested that spermatocytic seminoma might be a type of testicular tumour that was more relevant to the proposed origins of paternal age-effect mutations compared to others. Accordingly, a mutational analysis was undertaken of known hotspots in 17 candidate genes in 30 SS cases. These included fibroblast growth factor receptor genes (*FGFR1*, *FGFR2*, *FGFR3*), genes mutated in syndromes exhibiting a strong paternal age-effect (*RET*; Section 1.5.2, *PTPN11;* Section 1.5.3, *HRAS*; Section 1.5.4), genes involved in the signalling cascades (MAPK and PI3K; Section 1.6) in which pathogenic activating mutations have been documented (*AKT1*, *BRAF*, *KRAS*, *MAP2K1*, *MAP2K2*, *NRAS*, *PIK3CA*, *SOS1*) and genes for which oncogenic mutations are commonly found in tumours (bladder, thyroid and endometrial malignancies) where paternal age-effect mutations have also been reported (*CTNNB1*, *EGFR*, *KIT*). The results revealed the presence of analogous paternal age-effect mutations in 7 (~ 23%) of the cases. Heterozygous mutation in *FGFR3* (1948A>G transition, encoding Lys650Glu) (Section 1.5.1.2) was evident in two different tumours, whilst five tumours (all *FGFR3* mutation negative cases) were identified with *HRAS* homozygous mutations at codon Gln60, two of which were 181C>A (Gln61Lys) transversions (Section 1.5.2) and three were 182A>G (Gln61Arg) transitions (Section 1.5.2). These mutations were absent in adjacent histopathologically normal seminiferous tubules in six available cases.

Interestingly, the oncogenic mutation-positive SS occurred in a subset of relatively older men (average age 74.9 years, compared with 57.6 years for the mutation-negative samples). Upregulation of FGFR3 and HRAS proteins determined by immunohistochemistry was observed either independently or collectively in 70% of the tumours; the presence of FGFR3 and HRAS was mutually exclusive in most tumours although no simple correlation

was identified with the mutation background of the tumours. pERK protein (Section 1.6) was present in 56% of the tumours (Goriely, et al., 2009). Collectively, these findings suggested that with activation of the ERK signal transduction pathway involving mutation or upregulation of FGFR3 and / or HRAS, mutant spermatogonia become progressively enriched in the testis over time through a selective proliferation, leading to clonal expansion which results in the formation of SS tumours in some extreme cases. These observations provide a unified theory for the origins of paternal age-effect mutations and SS, and support a premeiotic origin for SS as proposed by Rajpert De-Meyts (2003).

1.8.4 Mouse models for the effects of paternal age-effect mutations in the testis

In 2007, Nakagawa *et al* (2007) described for the first time the presence of a second population termed 'potential stem cells' in the mouse spermatogonial stem cell system, in addition to the actual self-renewing stem cells. 'Potential stem cells' are defined as the immediate progeny of the actual stem cells which may still preserve their stem cell potential while undergoing differentiation with high probability, regardless of cell type (Potten and Loeffler, 1990). The authors first set up a study to observe the distribution of undifferentiated spermatogonia during normal spermatogenesis for a period of 3 months using *Ngn3/Cre*ER^{TM}; CAG-CAT-Z transgenic mice. Under the tamoxifen-inducible *Cre* recombinase (*Cre*ER^{TM})-*Lox*P system, the transiently activated CreER^{TM} deletes the *CAT* gene which thereby induce the expression of *LacZ* under the CAG promoter after pulsing with tamoxifen. Of note, Ngn3 (neurogenin3) protein was defined in a small subset of undifferentiated spermatogonia, and this mouse model is useful in studying the fate of Ngn3+ spermatogonial cells (Yoshida, *et al.*, 2004; 2006). Results from this attempt showed that the undifferentiated spermatogonia were found predominantly clustered in the inner layer of the seminiferous tubules and the majority of them differentiated into mature spermatozoa which were thereby released and hence lost from the seminiferous tubules (Nakagawa, et al., 2007).

Interestingly, there was a small subset of undifferentiated spermatogonial clusters that persisted in the seminiferous tubules and contained all stages of spermatogenic cells, indicating that these cells were able to generate differentiating cells whilst retaining their own populations. These characteristics are compatible with the definition of 'actual stem cells' as proposed (Potten and Loeffler, 1990).

To determine the natural history of these 'potential stem cells' during the course of spermatogenesis and whether these would be recruited during the loss of 'actual stem cells', a second attempt was initiated to observe the active spermatogenesis over times up to 14 months (Figures 1.16) (Nakagawa, et al., 2007). The number of persistent clusters as described previously (within 3 months) declined by 14 months, suggesting that the actual stem cells may have died or gradually lost their ability to self renew and committed into the differentiation lineages. In contrast, the remaining clusters were rather prominent and extended in length although the total length of the 'actual stem cells' clusters in the testis remained statistically unaffected, suggesting that the loss of actual stem cells was compensated by the expansion of the surviving cells in order to maintain the overall spermatogenesis.

Analysis on older mice further revealed that the enlargement of the remaining clusters became more evident with age; this observation was attributed to the coordinated self-renewal of stem cells in a stochastic manner during steady-state mouse spermatogenesis as demonstrated in a recent reanalysis of the original data (Klein, et al., 2010). The ongoing loss of stem cells clones due to normal aging is compensated by the expansion of progeny cells from the neighbouring stem cells clones which occurs on average every two weeks, regardless of the clonal history. Findings from these studies may be a relevant model for the increase of sperm harbouring some genetic lesions including *FGFR2* Apert and *FGFR3*

achondroplasia mutations that are related with older age (Section 1.3). Nakagawa *et al* (2007) suggested that

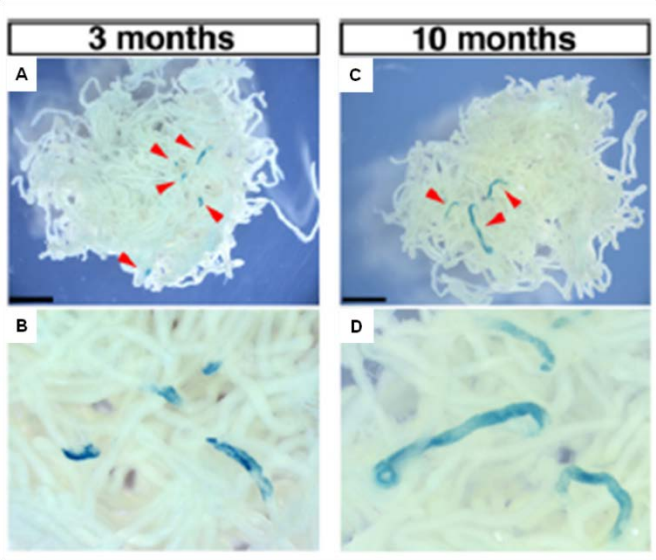

Figure 1.16: Clusters of labelled cells after prolonged period of time. (A-D) Whole-mount X-gal staining of seminiferous epithelium (A & C) 3 and (C & D) 10 months after pulse. (B) and (D) are high power view of (A) and (C), respectively. Arrowheads indicate the persistent clusters of LacZ-positive cells (Adapated from Nakagawa, et al., 2007).

'potential stem cells' carrying beneficial heritable traits are very likely to become the new actual stem cells and expand gradually in the normal testis through multiple divisions. In a related example, normal spermatogenesis was preserved in a Klinefelter syndrome patient (non-mosaic 47,XXY karyotype; normally characterised by eunuchoid body proportions, gynaecomastia, small firm testes and azoospermia) heterozygous for the *FGFR3* 1138G>A ACH mutation (Section 1.5.1.2), suggesting that the gain-of-function Gly380Arg mutation has maintained the self-renewal machinery that is usually lost in the seminiferous tubules of individuals with Klinefelter syndrome. These observations provide a plausible biological mechanism whereby spermatogonia carrying constitutively activating paternal age-effect mutations have a proliferative advantage compared to their wild type spermatogonial

neighbours, leading to clonal expansion of mutant cells within the normal testis (Goriely, et al., 2003; 2005; 2009).

A further mouse model that is relevant to SS and supports a premeiotic origin for this tumour and central role of Hras, was described by Lee *et al* (2009). These authors transfected DNA encoding the *Hras* G12V mutation into murine SSCs in culture, and performed both biochemical assays and germ cell transplantation to assess the consequences. The biochemical findings are reviewed in the next section 1.8.5. Histological analyses of testes after transplantation identified the presence of a subpopulation of germ cell colonies with irregular shape within the seminiferous tubules. Further analysis revealed that these abnormal colonies were seminomatous tumours containing round cells with little cytoplasm that expressed placental alkaline phosphatase (PLAP – a marker of seminoma; Manivel, *et al.*, 1987); the tumour invaded into the adjacent interstitial tissue but no distant metastasis or lymphocytic infiltration were associated with these tumours, whilst normal spermatogenesis still occurred in other parts of the recipient testis (Lee, et al., 2009).

1.8.5 Abnormal RAS signalling in the proposed spermatogonial proliferation

All the best-documented paternal age-effect mutations containing *FGFR2*, *FGFR3*, *RET*, *PTPN11* and *HRAS* (Section 1.5) encode key components of a signalling cascade consisting of tyrosine kinase receptors signalling to RAS (Section 1.6). These activating gain-of-function point mutations confer a selective advantage to the spermatogonia in which they arise (Section 1.7.1), leading to clonal expansion over a course of time in the normal adult testis (Section 1.8.2). Data from previous functional studies suggest the potential involvement of two RAS downstream effector pathways (Figure 1.10) – MAPK and PI3K/AKT in driving this proposed spermatogonial proliferation and / or differential survival, which are presented in the following subsections.

1.8.5.1 Evidence favouring the MAPK pathway

Missense mutations in genes encoding components of the RAS-MAPK pathway have been found in various human genetic diseases. Most notably, heterozygous mutations of *BRAF, MAP2K1* and *MAP2K2* occur in cardio-facio-cutaneous syndrome, a disorder with overlapping clinical features to Costello and Noonan syndromes caused by mutations in *HRAS* and *PTPN11* respectively (Schubbert, et al., 2007). Further *in vivo* studies showed that abnormal phenotypes of mice harbouring *Fgfr2* and *Ptptn11* missense mutations were restored upon inactivation of the MAPK pathway (Shukla, *et al.*, 2007; Krenz, *et al.*, 2008). For instance, a marked reversal of the craniosynostosis normally present in newborn mice with Apert-like syndrome was described when the pregnant female *Fgfr2*$^{\text{Neo-S252W/+}}$ mutant mice were treated with a drug (U0126) that inhibits ERK1/2 phosphorylation by binding to MEK1 and MEK2, the kinases that lie immediately upstream in the RAS-MAPK pathway (Shukla, *et al.*, 2007). Moreover, recent work demonstrated a significant decrease of the initially abnormal endocardial size in the Noonan mouse model carrying an endothelial lineage-specific expression of *Ptpn11* Gln79Arg amino acid change (Schollen, *et al.*, 2003), when these mice were crossed with homozygous ERK1 mice (Krenz, et al., 2008). Consistent with this observation, upregulation of ERK2 activity was described in a COS-7 cell line expressing an activating Noonan mutation (*PTPN11* 922A>G transition encoding N308D) (Section 1.5.3), in response to epidermal growth factor stimulation (Tartaglia, et al., 2003).

These results illustrate the pathogenic role of the constitutive ERK1/2 hyperactivation in both Apert syndrome and Noonan syndrome, resulting from the gain-of-function missense mutations in *FGFR2* and *PTPN11* genes. The activation of this signalling cascade by spermatogonia bearing the analogous paternal age-effect mutations may lead to the enrichment of these mutant cells in the normal adult testis, forming localised clusters of cells which potentially contribute to the oncogenesis of testicular tumour in some cases (Section

1.8.3). For instance, the overexpression of phospho-ERK (the downstream effector of MAPK pathway) was observed in 56% of the spermatocytic seminoma cases studied (Goriely, et al., 2009) (Section 1.8.3). In the context of normal spermatogenesis, evidence from the study by He *et al* (2008) supports the importance of Ras-ERK1/2 signalling cascade in promoting the proliferation of mouse spermatogonial stem cells. Upon GDNF stimulation, the number of BrdU (Bromodeoxyuridine; a marker for detecting proliferating cells) positive cells was accelerated in the mouse spermatogonial stem/progenitor cells line (C18-4), in addition to the presence of active GTP-RAS and increased phosphorylation of ERK1/2. However, GDNF-regulated proliferation of mouse spermatogonial stem cells was abrogated after the ERK1/2 phosphorylation was blocked by pretreatment with MEK1 inhibitor (PD98059). These observations were partly supported by another group in which the growth of HRAS G12V activated-germline stem cells was partially affected when a MEK inhibitor was introduced (Lee, et al., 2009). Together, these indicate the potential involvement of RAS-MAPK cascade in spermatogonial proliferation and testicular tumourigenesis.

1.8.5.2 Evidence favouring the PI3K/AKT pathway

The PI3K-AKT pathway is one of the downstream signalling cascades upon the activation of receptor tyrosine kinase-RAS signalling complex (Section 1.6). Lee *et al* (2007) studied the self-renewal mechanism using in vitro cultured mouse spermatogonial stem cells (germline stem or GS cells). The participation of PI3K-Akt pathway in the self-renewal process of GS cells was observed by adding LY294002 (a PI3K-specific inhibitor) to the GS cell culture. The growth of these cells was markedly inhibited and persisted after 6 days of culture; GS cell proliferation was restored in response to the withdrawal of LY294002. To determine the functional involvement of Akt in self-renewal, the GS cells were transfected with a conditionally active form of Akt encoded by a plasmid expressing myristoylated (myr)-Akt-Mer protein. In the presence of 4-hydroxy-tamoxifen (the Mer ligand), Akt-

transfected GS cells costimulated by FGF2 were able to proliferate and rescued the apoptosis of SSCs in the absence of GDNF. Analysis from the spermatogonial transplantation assay also illustrated the colonization and differentiation of these Akt-GS cells in the recipient testis, confirming the stem cell capacity retained in these GS cells (Lee, et al., 2007).

Recently, further *in vitro* studies were undertaken to investigate the role of *Ras* proto-oncogene in signalling pathway mediating murine GS cell self renewal (Lee, *et al.*, 2009; see also Section 1.8.4). Transfected Ras was activated in GS cell culture upon epidermal growth factor (EGF), FGF2 or GDNF stimulation; this was inhibited by PP2, a Src inhibitor previously described to be involved in SSC and spermatogonial proliferation (Braydich-Stolle, *et al.*, 2007; Oatley and Brinster, 2008). With the introduction of *Hras*-N17 (encoding a dominant-negative HRAS), the proliferation of Akt-GS cells was disrupted suggesting that HRAS is necessary for SSC proliferation. This was further confirmed with the identification of germ cell colonies in recipient testis transplanted with *Hras* G12V-GS cells. As in the previous study by Lee et al (2007), abrogation of cell proliferation was noted with the addition of LY294002, as well as Akt inhibitor IV. Collectively, Lee et al (2009) concluded that murine SSC self-renewal is regulated by activation of the Ras-PI3k-Akt signalling cascade; activation of Mek may enhance the biological activity of Akt and facilitate the cell proliferation induced by Hras (Section 1.8.5.1).

1.9 Aims of the thesis

All the findings presented above provide a clear precedent for the involvement of paternal age-effect mutations in congenital disorders (Section 1.3), human spermatogenesis (Section 1.8.2) and testicular tumour development (Section 1.8.3). However, all previous works to identify clonal events in the testis had involved DNA analysis, which by definition destroys the architecture of the normal testis (Section 1.8.2). Hence, the main aim of this thesis was to identify these events using immunohistochemistry. To do so, I first undertook a

systematic search of the Human Protein Atlas database (www.proteinatalas.org) and previous literature to choose a preferred set of candidate markers (Chapter 3), the optimisation of which in normal testis sections yielded additional information on normal spermatogenesis (Section 1.8.1) that is described in Chapter 4. This was followed by using spermatocytic seminoma (Section 1.8.3) as a model system to identify altered patterns of marker expression; owing to parallels with spermatocytic seminoma, a preliminary study of urothelial bladder carcinoma was also performed (Chapter 5). Finally, with the establishment of a robust panel of markers, I have successfully identified likely clonal events in normal testis by immunohistochemistry (Chapter 6).

CHAPTER 2

MATERIALS AND METHODS

Chapter 2: Materials and Methods

2.1 Ethics approval

Permission for the anonymous analysis of all human tissue was granted from the Oxfordshire Research Ethics Committee A (code: C03.076; 'Receptor tyrosine kinases and germ cell development: detection of mutations in normal testis, testicular tumours and sperm') and Regional Committee for Medical Research Ethics in Denmark.

2.2 Sourcing of samples

Controls containing both tonsillar tissue and normal adult testes with preserved complete spermatogenesis and without germ cell tumours (obtained following orchidectomy for hernia repair or benign Leydig cell tumour) (Chapter 3) as well as all the formalin-fixed, paraffin-embedded urothelial carcinoma (UC) samples from bladder (Chapter 5) were obtained from the archives of the Department of Cellular Pathology, John Radcliffe Hospital, University of Oxford. These samples were stored at room temperature prior to DNA extraction and immunohistochemical staining.

Fetal testicular tissues (Chapter 4), spermatocytic seminoma (SS) and intratubular spermatocytic seminoma (ISS) tumour samples (Chapter 5) were acquired in collaboration with Dr. Ewa Rajpert De-Meyts (ERDM) from University Department of Growth and Reproduction, Copenhagen University Hospital (Rigshospitalet), Copenhagen, Denmark. Twenty three samples of morphologically normal fetal testicular tissue collected from induced or spontaneous abortion or autopsy of stillbirths ranging from 16^{th} – 42^{nd} weeks of gestation (wg) and without known chromosome or genetic disease, and five samples of infantile and prepubertal testicular tissues (age 2 months – 4.5 years) were also included (Table 2.1). The tissue examination and determination of the fetal age were performed by an experienced pathologist (Dr. Niels Graem from Department of Pathology, Copenhagen University Hospital (Rigshospitalet), Copenhagen, Denmark) as described in detail in

previous research using similar samples (Jorgensen, *et al.*, 1995; Rajpert-De Meyts, *et al.*, 2004).

Table 2.1: Number of testicular tissues at different stages of development.

Tissue type	Age	Number of samples
Fetal testes	16th wg	1
	17th wg	1
	18th wg	2
	20th wg	3
	21st wg	3
	22nd wg	1
	24th wg	4
	25th wg	1
	27th wg	1
	31st wg	1
	33rd wg	1
	39th wg	1
	41st wg	2
	42nd wg	1
Infantile and prepubertal testes	2 months	1
	3 months	1
	4 months	1
	1 year 11 months	1
	4 ½ years	1

The SS samples were collected from the archives of several departments of pathology in Denmark and Sweden. Tumour samples were fixed in 4% buffered formaldehyde and embedded in paraffin. For each SS, representative tumour tissue was identified by Dr. Grete Krag Jacobsen, the pathologist from Department of Pathology, Copenhagen University Hospital (Rigshospitalet), Copenhagen, Denmark and used for the preparation of tumour tissue microarrays (TMAs). The TMAs included 36 SS samples, including one with ISS (mean age 63.8 years; range 34-89) and control tissues. The latter consisted of five adult testes (morphologically normal tubules in vicinity of SS), three embryonal carcinoma, one case each of classical seminoma and high mitotic rate seminoma, as well as one sample each of B-cell lymphoma, normal prostate, lung, and epididymis. Each specimen contained a single core of tumour tissue in the TMAs except two SS samples which were sampled twice.

After TMAs were constructed, three other ISS located adjacent to previously identified SS were also obtained. A control additional to those included in the TMAs was a B-cell lymphoma from an adult testis. Experiments involving the TMAs and fetal tissues were conducted and examined by J. Lim in the ERDM's laboratory in Copenhagen, Denmark.

For studies in Chapter 6, normal adult testes were ascertained via the urology ward at the Churchill Hospital, Oxford Radcliffe Hospitals NHS Trust, Oxford, UK, according to guidelines approved by the Oxfordshire Research Ethics Committee A (code: C03.076). A letter inviting participation in the study, along with an information sheet and consent form, was given to patients who were diagnosed with prostate cancer and would be undergoing orchidectomy. Following consent, samples were collected directly from the surgical ward and stored in an ice box at ≈ 0 °C prior to tissue preparation which is discussed in detail in sections 7.2.1 and 7.2.2. All of the tissue processing procedures involved in the preparation of formalin-fixed paraffin embedded tissue were performed by staff in the histology laboratory of the Cellular Pathology Unit, John Radcliffe Hospital, University of Oxford. In addition, a normal testis removed due to an incarcerated left inguinal hernia was included into the study. The sample was retrieved from the archive of the Department of Cellular Pathology, John Radcliffe Hospital, University of Oxford through an application process to Oxford Centre for Histopathology Research (OCHRe).

2.3 Reagents

All chemicals, unless stated otherwise, were obtained from Sigma-Aldrich or VWR International Limited. Restriction enzymes were from New England Biolabs or Fermentas, while oligonucleotides were ordered through either Sigma-Aldrich (Sigma-Genosys) or Eurogentec Ltd. All oligonucleotides employed, along with their nucleotide sequences, are available in Table 2.2.

Table 2.2: PCR Primers

Gene	Exon	Codon queried	Forward amplification primer (5'→3')	Reverse amplification primer (5'→3')
FGFR3	7	R248, S249	CGGCAGTGGCGGTGGTGGTG	AGCACCGCCGTCTGGTTGGC
FGFR3	10 (IIIb)	G372, S373, Y375	CCTCAACGCCCATGTCTTTGC	GGGAGCCCAGGCCTTTCTTG
FGFR3	15	K650	GTGATGAAGATCGCAGACTTCGGGCTG	GCCAGGCGTCCTACTGGCATGA
HRAS	2	G12, G13	GTGGGGCAGGAGACCCTGTAGGAGGAC	CAGGCTCACCTCTATAGTGGGGTCG
HRAS	3	Q61	GGAAGCAGGTGGTCATTGATGGGGAG or AGACGTGCCTGTTGGACATACTGGATACCGCCG	ACAGGAAGCCCTCCCCGGTGCG

2.4 Primary antibodies

Antibodies are immunoglobulin (Ig) proteins consisting of two identical heavy chains and light chains. The class of the molecule is determined by the heavy chains, which carry different antigenic and structural properties. All the primary antibodies utilised in these studies were of the IgG class, predominantly found in the hyper-immunised host. These proteins were either in monoclonal or polyclonal form, where the latter bind to various epitopes on the antigen against which they were raised, compared with the former that have a specific antigenic site. With their higher homogeneity, monoclonal antibodies are advantageous over the polyclonal ones because of their higher specificity. The optimal concentration of an antibody is defined as its highest dilution resulting in maximum specific staining, with the least interference from background staining in specific test conditions. The antibody dilution is normally expressed as the proportion of stock solution to the total volume of the desired dilution. These primary antibodies were used for immunohistochemistry and were commercially available except for MAGEA4 and SSX, which were gifted by Prof. Gulio C. Spagnoli (Department of Urology, University Hospital of Zurich, Zurich, Switzerland) and Prof. Dr. A. Geurts van Kessel (Department of Human Genetics, University Hospital, Nijmegen, The Netherlands) respectively. In summary, the details of each antibody are described in Table 2.3.

Table 2.3: A panel of antibodies included into the studies using immunohistochemistry.

Antibody	Type	Clone	Epitope	Dilution	Provider
FGFR3	Mouse [1]mAb	B9	IgG_{2a}	1:100	Santa Cruz Biotechnology Inc.
FGFR3	Rabbit [2]pAb	C-15	IgG	1:2000	Santa Cruz Biotechnology Inc.
GPR125	Rabbit pAb	Ab51705 & GB-10400	IgG	1:100-1:5000	Abcam & Genesis Biotech Inc
Ki67	Mouse mAb	MIB-1	IgG	undiluted	Dako
MAGEA4	Mouse mAb	57B	IgG	1:500	Prof. Gulio C. Spagnoli
OCT2	Mouse mAb	Oct-207	IgG_{2b}	1:100	Novocastra Laboratories Ltd
OCT3/4	Mouse mAb	C-10	IgG_{2b}	1:100	Santa Cruz Biotechnology Inc.
PLAP	Mouse mAb	8A9	IgG	1:50	Dako
Phospho-p44/42 MAPK (Erk1/2) (Thr202/Tyr204)	Rabbit mAb	20G11	IgG	1:100	Cell Signalling Technology
Phospho-Akt (Ser473)	Rabbit mAb	736E11	IgG	1:100 / 1:150	Cell Signalling Technology
PLZF	Mouse mAb	D-9	IgG	1:300	Santa Cruz Biotechnology Inc.
SAGE1	Rabbit pAb	HPA003033	IgG	1:350 / 1:3000	Sigma-Aldrich Inc.
SSX	Mouse mAb	E3AS	IgG	1:100	Prof. Dr. A. Geurts van Kessel

[1]mAb, monoclonal antibody; [2]pAb, polyclonal antibody.

2.5 DNA extraction

For DNA extraction, each tumour sample was first prepared using a biopsy punch to cut out a cylindrical piece of tissue from the paraffin-embedded block. These were then treated with Histoclear, and rehydrated with 100% ethanol before incubation for 3 days at 4 °C. DNA extraction was performed using Nucleon ® Genomic DNA Extraction Kit for hard tissue (code: SL 8509; Tepnel Life Sciences) in accordance with the manufacturer's instructions. After the final step of DNA washing, the DNA pellet was resuspended in 50 µl of TE buffer (10 mM Tris-HCl, pH 7.5; 1 mM EDTA). The concentration of fully resuspended DNA was obtained using a GE Healthcare DyNA Quant™ 200 Fluorometer,

with a fixed wavelength of 365 nm and 460 nm for excitation and emission respectively. Finally, each sample was diluted to 20 ng/µl DNA concentration for use in subsequent reactions.

2.6 DNA amplification

2.6.1 Polymerase Chain Reaction, PCR

The PCR was performed using primers designed for the amplification of exons 7, 10 and 15 of the *FGFR3* gene as well as exons 2 and 3 of the *HRAS* gene (see Table 2.2). Each reaction was conducted using 60 ng of genomic DNA in a total reaction volume of 40 µl unless otherwise specified. It consisted of a final concentration of 0.25 µM of forward and reverse oligonucleotide primers, 1x concentration of the 10x PCR Buffer with $MgCl_2$ (FastStart Taq DNA Polymerase, Roche) or 1x concentration of the 10x PCR Buffer without $MgCl_2$ (GeneAmp, Applied Biosystems) and 1.25 mM of $MgCl_2$ (Applied Biosystems; Roche), 200 µM dNTPs and 1 unit of *Taq* polymerase (AmpliTaq® Gold, Applied Biosystems; FastStart Taq DNA Polymerase, Roche). Reactions were carried out on one of the three PCR machines: two BIORAD Peltier Thermal Cyclers and a MJ Research Peltier Thermal Cycler. Programmes comprised, unless stated otherwise, an initial denaturation step at 96 °C for 8 min, followed by 36 cycles of denaturing, annealing and extension (95 °C, 30 s; annealing temperature, 30 s; 72 °C, 30 s) and ending with a final 10 min extension at 72 °C. Primers were tested across various temperature gradients and the optimal annealing temperature was 68 °C in all cases.

2.6.2 Product visualisation

PCR products were visualised by gel electrophoresis. A 3% agarose gel was run in a buffer of 1x TBE (10x TBE: 89 mM Tris-base, 89 mM boric acid, 225 mM EDTA). Ethidium bromide (1 µg/ml) was added during the gel preparation in order to enable visualisation of the DNA by trans-illumination with UV light. Samples were loaded in buffer (6x: 0.25% bromophenol blue, 15% Ficoll 400) and run simultaneously with a molecular weight marker (O'GeneRuler™ 100 bp DNA ladder, Fermentas; pBR322 DNA/BsuRI (HaeIII) Marker, 5, Fermentas; pUC19 DNA/MspI (HpaII) Marker, 23, Fermentas), selected according to fragment size.

2.7 DNA digestion

Unless otherwise stated, 10 µl of PCR products were digested in a total volume of 25 µl, containing 10 U of enzyme (New England Biolabs or Fermentas) and a final 1x concentration of the manufacturer's buffer. Incubation was performed at the recommended temperature for 3 h.

2.8 DNA purification

Products of PCR amplification and digestion were purified using QIAquick gel extraction kit (QIAGEN), according to the manufacturer's recommendations. The purified product was eluted in MiliQ water and sequenced.

2.9 DNA sequencing

Samples were prepared for DNA sequencing on the ABI PRISM 3100 DNA sequencer, with Big Dye Terminator mix (Applied Biosystems). Fragments for analysis were amplified with their respective primers, subjected to agarose gel electrophoresis, and purified with the QIAquick gel extraction kit. Sequencing reactions were subsequently performed on purified PCR products using the same forward and reverse primers employed in the initial amplification, this time independently. DNA for sequencing was mixed with 4 µl of

BigDye® 10x sequencing buffer (Applied Biosystems), 1 µl of forward or reverse primer (2.5 µM), and made up to 16 µl total volume with sterile H_2O. Samples were mixed and incubated at 96 °C for 5 min before transferring to ice for 2 min. At this stage 4 µl of Big Dye was added to each sample ready for amplification with the following procedure; 5 min denaturation at 96 °C, followed by 25 cycles of denaturing, annealing and extension (95 °C, 45 s; 55 °C, 45 s; 60 °C, 3.5 min). Following amplification, samples were prepared for electrophoresis using ethanol precipitation by the addition of 80 µl of 80% ethanol. The mixtures were vortexed and incubated at room temperature for 20 min before they were centrifuged at 16,100 x*g* for 20 min at room temperature. Supernatant was removed and the DNA pellet was allowed to dry at room temperature. Electrophoresis was conducted by Kevin Clarke (Weatherall Institute of Molecular Medicine, Oxford).

2.10 Tissue sectioning

Before sectioning, tissue blocks were pre-cooled to - 20 °C to ensure that a continuous ribbon of paraffin sections was produced. A water bath was heated up to ~45 °C whilst a new blade was placed on the microtome. Each formalin-fixed, paraffin-embedded (FFPE) block was inserted into the microtome chuck where the wax block was facing the blade and aligned in the vertical plane. The block was trimmed as necessary before cutting a thickness of 5 µm. Subsequently, the paraffin ribbon was picked up with forceps or a fine paint brush and placed on the surface of the water bath. The section was then mounted onto the surface of a clean X-Tra® adhesive slide (Surgipath Medical Industries, Inc) and air-dried overnight before storing at 4 °C for future applications.

2.11 Haematoxylin and Eosin (H&E) staining

The FFPE sections were deparaffinised in two changes of Histoclear (5 min each) and rehydrated through three changes of absolute ethanol and once in 95%, 80%, 70% and 50% ethanol (5 min each) before rinsing with running distilled water. This was followed by

staining in Mayer haematoxylin for 8 min and washing with running tap water for 5 min. Subsequently, the sections were dipped in acid alcohol (prepared with 5 ml hydrochloric acid and 495 ml 70% ethanol) 7 times, and quick-rinsed with water, before incubating in 0.1% w/v (weight/volume) of eosin for 3.5 min. Finally, the sections were dehydrated through 70% ethanol for 2 dips, 100% ethanol for 1 min and Histoclear for 5 min. All the sections were mounted with Aquatex® (MERCK). When the section was viewed under the microscope, the nuclei were stained blue and the cytoplasm appeared red/pink.

2.12 Immunohistochemical Staining

Immunohistochemistry (IHC) is the detection of specific antigens in tissues using antibodies labelled with fluorescent or pigmented materials. Sections from the FFPE blocks are first treated for antigen retrieval which involves the application of heat for varying lengths of time in an aqueous antigen retrieval solution. This method termed Heat Induced Epitope Retrieval aims to restore the immunoreactivity of antigens by uncovering the antigenic determinants which become 'masked' as a result of formalin fixation. Subsequently, the visualisation of antigen-antibody interaction is usually performed with a two-step indirect method (Figure 2.1). In this approach, an antigen is first bound with an unconjugated primary antibody and followed by an enzyme (e.g. peroxidase)-labelled secondary antibody which is directed against the primary antibody. With the addition of substrate-chromogen (e.g. 3,3' diaminobenzidine tetrahydrochloride, DAB) solutions, the enzyme catalyses a chemical reaction with the substrate resulting in the formation of a coloured precipitate at the antigenic site.

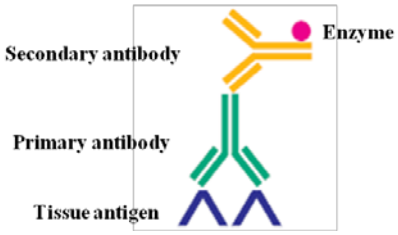

Figure 2.1: Two-step indirect method. Enzyme-tagged secondary antibody binds to primary antibody reacts with tissue antigen (Adapted from Dako Handbook for Immunochemical Staining Methods).

2.12.1 Single staining

FFPE tissue sections with a thickness of 5 µm each were incubated in the oven at 55 °C for an hour prior to immunohistochemical staining. The sections were deparaffinised twice in Histoclear and rehydrated with graded ethanol incubations (100%, 95%, 80% and 70%) for 5 min each. All incubations were performed at room temperature unless stated otherwise. For antigen retrieval, a staining rack consisting of 20 sections was immersed in a staining trough (93x75x55mm) containing citrate buffer (10 mM, pH 6) and heated with a microwave on high mode for 1 min, followed by simmer mode for 15 min. Samples were allowed to cool to room temperature before incubating with Dako REAL™ Peroxidase-Blocking Solution (code S2023, Dako) for 10 min to quench endogenous peroxidase activity. Subsequently, sections were incubated overnight at 4°C with primary antibodies at the optimal concentration (see Table 2.2).

The primary antibodies were detected using EnVision+Dual Link System, Peroxidase (DAB+) kit (code K5007, Dako), which is based on the chain polymer-conjugated technology. The principle of this technology relies on the application of a ‘spine’ molecule of dextran conjugated with an average of 10 molecules of secondary antibody (both anti-mouse and anti-rabbit) and 70 molecules of horseradish peroxidase (HRP) enzyme (Figure 2.2a). Compared to labelled streptavidin-biotin technology, which applies the conjugation of a biotinylated secondary antibody with the enzyme-labelled streptavidin (Figure 2.2b), the

Envision system reduces the number of incubation steps, increases sensitivity of the assay and eliminates non-specific background staining caused by endogenous biotin.

After binding with Dako Envision^{TM}/HRP, Rabbit/Mouse polymer, sections were incubated with 3,3'-diaminobenzidine (DAB+) substrate-chromogen for 10 min before counterstaining with haematoxylin, and mounted with Aquatex® (MERCK). During incubations, slides were placed in a humidity chamber to prevent evaporation and drying of the tissue sections. Washing steps using TBS/Tween-20 buffer were conducted between each step of antibody incubation and detection. Positive and negative control slides were included in each study. The staining was assessed independently by 2-3 investigators (myself; Dr Gareth Turner from Department of Pathology, John Radcliffe Hospital, Oxford; and / or Dr. Ewa Rajpert-De Meyts from University Department of Growth and Reproduction, Copenhagen University Hospital (Rigshospitalet), Copenhagen, Denmark) using a systematic semi-quantitative scoring system which was adapted from a previous study (Sonne, *et al.*, 2010). The staining was scored based on (i) the approximate proportion of cells stained: +++, nearly all cells stained; ++, approximately half of the cells stained; +, a low percentage of cells stained; +/-, only single cells stained; -, no positive cells detected and (ii) the staining intensity which was evaluated as strong, medium, weak, very weak or absent.

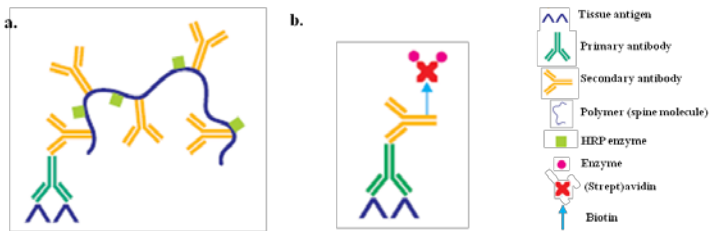

Figure 2.2: Antigen-antibody binding detection system. a. Envision technology: the primary antibody is detected by the secondary antibody which is attached to the HRP enzyme-tagged polymer. b. Labelled (strept)avidin-biotin technology: the enzyme-labelled (strept)avidin conjugates with the biotinylated secondary antibody (Adapted from Dako Handbook for Immunochemical Staining Methods).

2.12.2 Double staining

Sequential double-staining for OCT2 and SSX (PLAP or OCT3/4) was performed using the EnVision™ G|2 Doublestain System, Rabbit/Mouse (DAB+/Permanent Red) kit (code K5361, Dako), according to the manufacturer's recommendations. Following heat-induced epitope retrieval, the endogenous peroxidase, alkaline phosphatase (AP) and pseudoperoxidase activities were inhibited with Dual Endogenous Enzyme Block reagent for 10 min and sections were incubated with the OCT2 antibody overnight at 4 °C. After the detection with Polymer/HRP (horseradish peroxidase) and visualisation by DAB+ Chromogen, the sections were blocked with Doublestain Block reagent before incubating with SSX, OCT3/4 or PLAP antibody at 4 °C overnight. Sections were incubated with Rabbit/Mouse (LINK), followed by Polymer/AP and the reaction was visualised with Permanent Red Chromogen. The summary of the protocols is presented in Figure 2.3. All the specified reagents, except the primary antibodies, were provided with the kit. Double-stained sections were then counterstained with haematoxylin and mounted with Aquatex® (MERCK). Washing steps using TBS/Tween-20 buffer were conducted between each step of antibody incubation, detection and colour development.

After completing the single and double staining, sections were scanned with dotSlide-digital virtual microscope (Olympus) or NanoZoomer virtual microscopy (Hamamatsu) at 200x magnification. The digital images ("virtual slides") were analysed using the viewer software either from OlyVIA-Viewer (Olympus) or NanoZoomer Digital Pathology (NDP).view, depending on the format in which the images were saved.

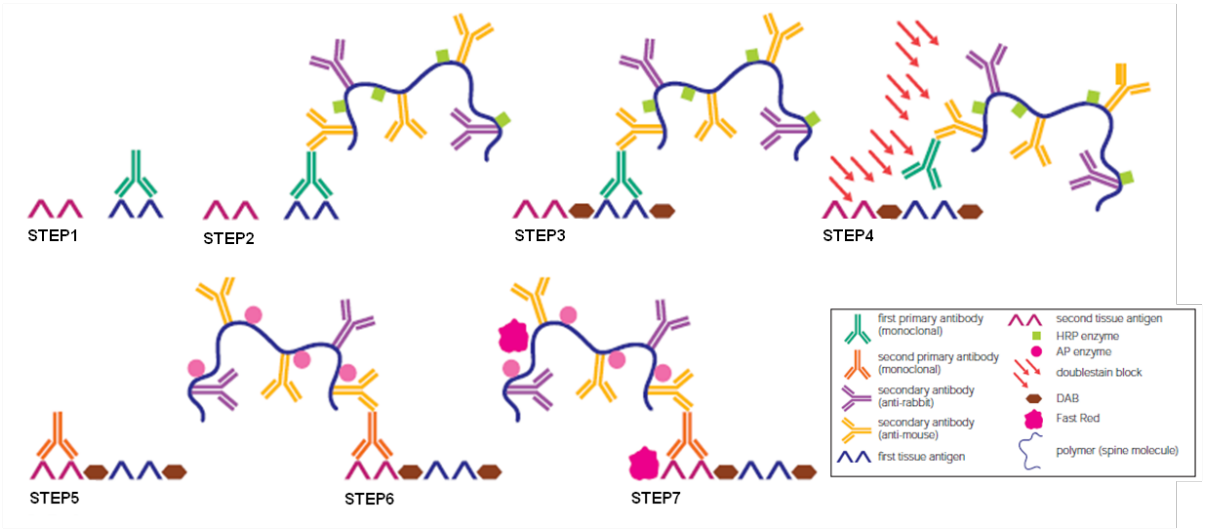

Figure 2.3: EnVision™ G|2 Doublestain System for Rabbit/Mouse primary antibodies (DAB+/Permanent Red). The first primary antibody (step1) is conjugated with the first spine molecule (step 2), followed by the use of DAB to stain the first antigen (step 3) before the incubation with the doublestain block (step 4). After binding the second tissue antigen with second primary antibody (step 5), the second spine molecule (step 6) is employed and the colour of the Fast Red chromogen is then developed (step 7). This system allows the application of a combination of mouse monoclonal and/or rabbit polyclonal antibodies, peroxidase and/or alkaline phosphatase as well as chromogens containing DAB and Fast Red (Adapted from Dako Handbook for Immunochemical Staining Methods).

2.13 Additional methods

Additional methods developed to search for putative clones in the normal adult testis are described in the relevant Results Chapter 6 sections. Please refer to Section 6.2.1 (for sample collection and preparation from first individual), Section 6.2.2 (for the methodology to screen for putative clones) and Section 6.2.5 (for the analysis of a testicular block from a second individual).

CHAPTER 3

CHOICE OF CANDIDATE MARKERS – BACKGROUND AND PRELIMINARY STUDIES IN NORMAL ADULT TESTIS

Chapter 3: Choice of candidate markers – background and preliminary studies in normal adult testis

3.1 Introduction

An extensive role of paternal age-effect mutations has been described in congenital disorders and human malignancies (Section 1.5). It has been proposed that these activating mutations confer a selective advantage to the spermatogonia in which they arise, leading to clonal expansion in the normal testis and testicular neoplasms in some cases (Sections 1.7.1, 1.8.2 and 1.8.3). The challenge for the current study was to develop an approach based on histology and /or immunohistochemistry by which evidence for such clonal events could be obtained, whilst retaining the normal tissue architecture; these were the elements that could not be fulfilled by previous DNA-based approaches (Section 1.8.2). The current strategy would provide a more general platform to the problem that could explore issues including size, frequency, heterogeneity and abnormal cellular signalling associated with these events.

To address this, the first stage was to search for potential candidate markers that could potentially identify the presence of putative clones in the normal adult testis. Several general selection criteria for the markers were considered including their specificity, the host species of the primary antibodies, the localisation and perhaps the function of the detected protein during normal human spermatogenesis, their expression in testicular tumours and their practical applicability. This chapter describes efforts to explore and identify markers that were compatible with these selection features, based on evidence from previous literature and the Human Protein Atlas database (www.proteinatalas.org).

3.2 Results

Based on the previously summarised work, I hypothesised that proteins with positive staining both in the spermatogonia of the adult testis and in spermatocytic seminoma may reveal clones formed by mutant spermatogonia. A systematic search from the literature and the online databases of the Human Protein Atlas (Berglund, et al., 2008) was conducted to select the potential candidates. Notably, the Human Protein Atlas Project is a program that is undertaken to explore the human proteome systematically using antibody-based proteomics; one of the key components to this project is to study the expression profiles of a large number of proteins in normal and cancerous tissues using immunohistochemistry.

Several promising markers were identified after reviewing the literature (presented in detail below). These comprised previously studied spermatogonial markers (MAGEA4, SSX, Ki67, FGFR3, PLZF, GPR125) as well as downstream effectors of MAPK (phospho-ERK1/2) and PI3K-AKT (phospho-AKT) pathways. In addition, two novel spermatogonial markers, OCT2 and SAGE1, were chosen based on two key selection criteria designed to identify potential candidates from the database available in the Human Protein Atlas. These requirements were strong immunopositivity preferably in spermatogonial cells within the seminiferous tubules of the normal testis, and negative expression in other testicular germ cells tumours (TGCTs) including embryonal carcinoma and classical seminoma. A preliminary study was undertaken to explore the expression of all of the selected markers on normal adult testis with immunohistochemistry. Details of the antibodies used, including their clonality, epitope, working dilution and manufacturer were summarised in Table 2.3. The next sections briefly review the known characteristics and testicular staining pattern of each of the antibody.

3.2.1 MAGEA4 (Melanoma antigen family A, 4)

The MAGEA gene family are all encoded on the X chromosome and consist of 12 members that share 64-85% homology. These proteins are expressed in multiple tumour types; however, in normal adult tissues, they are restricted to the male germ cells. The biological function of the MAGEA family proteins is obscure. It has been suggested that MAGEA proteins may function as transcriptional repressors and disrupt NOTCH1 signalling cascades by binding with transcriptional regulator SKI-interacting protein (SKIP) and recruiting histone deacetylase 1 (HDAC1) (Laduron, *et al.*, 2004). In the context of tumourigenesis, suppression of selected MAGEA proteins caused the induction of p53-dependent apoptosis and thus reduced the viability of melanoma cells *in vitro* and *in vivo* (Yang, *et al.*, 2007). The potential role of MAGEA proteins in facilitating fibronectin-mediated progression and metastasis has also been documented in thyroid carcinoma (Liu, *et al.*, 2008). Interestingly, downregulation of FGFR2 in breast cancer was associated with the re-activation of MAGEA via an epigenetic mechanism, suggesting the role of MAGEA protein as a functional integrator of diverse signals including FGFR2 in regulating cancer progression (Zhu, *et al.*, 2010).

The expression of the MAGEA family especially MAGEA4 has been widely studied in a number of malignancies and normal tissues by immunohistochemistry. The MAGEA4 mouse monoclonal antibody (clone 57B) was raised against a recombinant MAGEA protein and its immunostaining specificity was validated by previous studies (Landry, *et al.*, 2000; Aubry, et al., 2001). In the normal adult testis, strong expression of MAGEA4 protein was observed in most of the spermatogonia localised to the basement membrane of the seminiferous tubules. By comparison, primary spermatocytes showed weaker immunoreactivity, and neither spermatids nor Sertoli cells were stained (Figure 3.1) (Aubry, et al., 2001). During normal testicular development, MAGEA4 was proposed as a marker for

prespermatogonia which was the most abundant cell type in the fetal testes starting from 18th weeks of gestation (Gaskell, et al., 2004). The presence of MAGEA4 has also been reported in classical seminoma and spermatocytic seminoma; however, anaplastic seminoma and non-seminomatous tumours were negative for this protein (Aubry, et al., 2001; Rajpert-De Meyts, *et al.*, 2003).

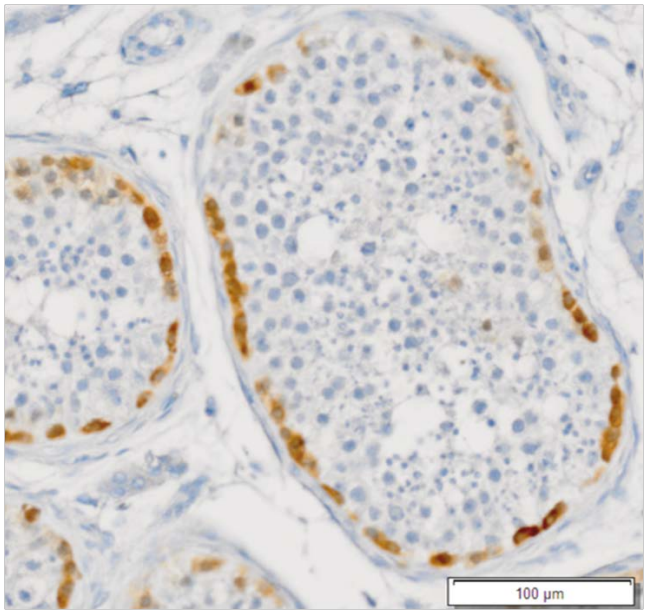

Figure 3.1: Example of immunohistochemical expression of MAGEA4 in the normal adult testis. Scale bar: 100 µm.

3.2.2 SSX (Synovial sarcoma X chromosome breakpoint)

The SSX gene family and MAGEA gene family belong to a group of proteins known as cancer testis antigens, which are encoded by genes that are normally only expressed in human germ cells, trophoblast and certain tumours (Simpson, *et al.*, 2005). There are ten highly homologous members of the SSX gene family and each encodes two main domains, a KRAB-A domain (exons 4 and 5) and a SSX repression domain (exon 9). These homologues share 73-92% and 87%-96% identity at the protein and cDNA levels, respectively. The expression of SSX mRNA in multiple myeloma as well as in bone and soft tissue tumours was associated with a more advanced stage of disease and poorer prognosis (Naka, *et al.*,

2005; Taylor, *et al.*, 2005). Moreover, colocalisation of SSX proteins with MMP2 was identified in mesenchymal stem cells and downregulation of these proteins was correlated with a marked impairment of tumour invasive abilities (Cronwright, *et al.*, 2005). Like many other cancer testis antigens, the biological function of SSX proteins remains poorly understood. It has been postulated that SSX may be involved in transcriptional regulation as the KRAB domain in the SSX proteins was found to facilitate transcriptional repressor activity in a subgroup of zinc finger proteins (Margolin, *et al.*, 1994; Witzgall, *et al.*, 1994).

A previous study generated a SSX (clone E3AS) mouse monoclonal antibody that was suitable for identification of SSX protein in paraffin-embedded tissues. The antibody specifically recognised SSX2, SSX3 and SSX4 and its epitope mapped between amino acids 25 and 80 from the NH_2-terminus (dos Santos, et al., 2000). Immunohistochemical studies performed on the human adult testis revealed that nuclear positivity against SSX (E3AS) was detected in a subset of spermatogonia with a weak reaction observed occasionally in the primary spermatocytes. The protein was totally absent in Sertoli cells and interstitial cells (Figure 3.2) (Stoop, *et al.*, 2001). Studies of SSX protein expression during testicular development revealed that it was present at least from 17^{th} weeks of gestation onwards (Stoop, *et al.*, 2001). In terms of oncogenic correlation, SSX proteins were consistently present in spermatocytic seminoma but not in other common seminomas (Stoop, *et al.*, 2001); this was corroborated by evidence from mRNA expression profiling showing that transcripts encoding *SSX1-4* were among the top 50 discriminators specifically expressed in spermatocytic seminoma (Looijenga, *et al.*, 2006).

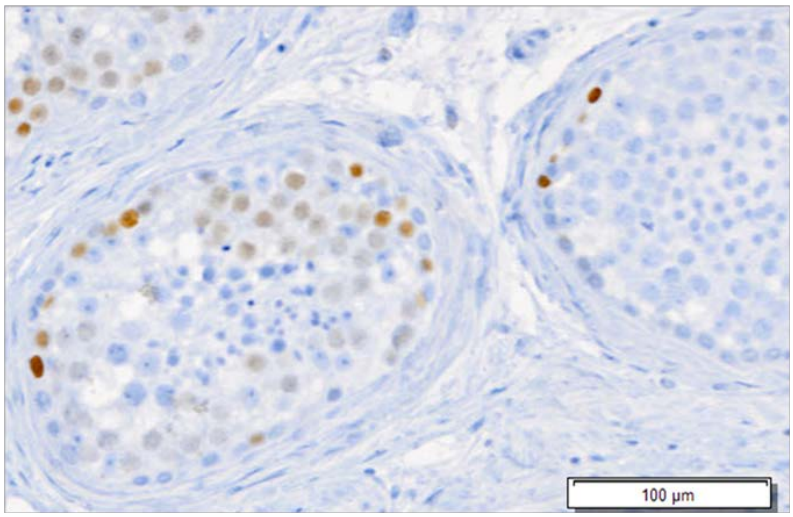

Figure 3.2: Example of immunohistochemical expression of SSX in the normal adult testis. Scale bar: 100 µm.

3.2.3 SAGE1 (Sarcoma antigen 1)

SAGE1 is another cancer testis antigen which was originally identified in a human sarcoma cell line (Martelange, *et al.*, 2000). *In vitro* studies indicate that the aberrant expression of *SAGE1* gene in different histological types of tumours including bladder, lung as well as head and neck carcinoma was triggered by demethylating agent 5-aza-2'-deoxycytidine, implying the role of demethylation in the activation of this gene in neoplasms (Martelange, et al., 2000). According to the Human Protein Atlas database, the SAGE1 rabbit polyclonal antibody (HPA003033) was raised against recombinant protein and its specificity has been validated (Berglund, et al., 2008); this protein was localised in the normal seminiferous tubules but not testicular tumours comprising embryonal carcinoma and classical seminoma. In the normal seminiferous tubules, nuclear staining of SAGE1 protein was observed in a small subset of spermatogonia (Figure 3.3) whilst other spermatogenic cells and somatic cells remained unstained. To date, the ontogenic expression of SAGE1 in the normal testis and the function of SAGE1 protein are still not fully understood.

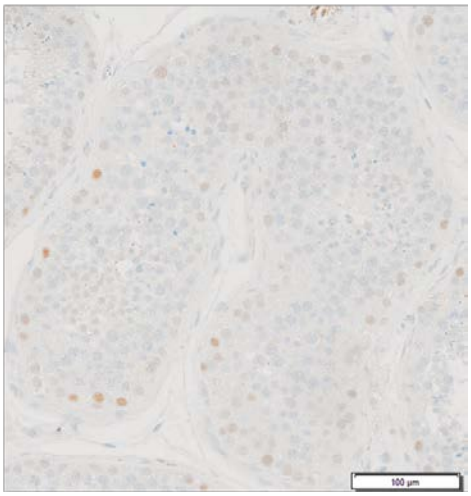

Figure 3.3: Example of immunohistochemical expression of SAGE1 in the normal adult testis. Scale bar: 100 µm.

3.2.4 OCT2 (Octamer binding protein 2; also known as POU2F2, POU class 2 homeobox 2)

OCT2 is a homeobox transcription factor encoded by gene from the POU (Pit-1, Oct1 / 2, UNC-86) family that shares a conserved 150-160 amino acid domain (Latchman, 1996). Expression of OCT2 has been described in B lymphocytes, neuronal cells, activated T cells and macrophages (Singh, et al., 1986; He, *et al.*, 1989; Kang, *et al.*, 1992; Dunn, *et al.*, 1996). The presence of OCT2 in the normal adult testis was initially identified from the Human Protein Atlas; none of the common testicular tumour cases was positive for this protein. The OCT2 antibody (clone: Oct-207) was raised against the recombinant protein corresponding to 129 amino acids of the N-terminus of human OCT2; it was validated for specificity of immunohistochemical staining on tonsillar tissue sections (Berglund, et al., 2008). Nuclear positivity was only observed in a subpopulation of spermatogonia of the normal adult testis (Figure 3.4), an issue that is explored further in the next Chapter. Unlike OCT2 which has not been investigated in the testis of any non-human species and about which much remains unknown about its functions particularly in spermatogenesis, another member of this family, OCT3/4, has been studied extensively in the human testis. The

expression of OCT3/4 has been documented during embryonic germ cell maturation (Gaskell, et al., 2004; Honecker, *et al.*, 2004; Rajpert-De Meyts, *et al.*, 2004) and in various testicular tumours (Oosterhuis and Looijenga, 2005).

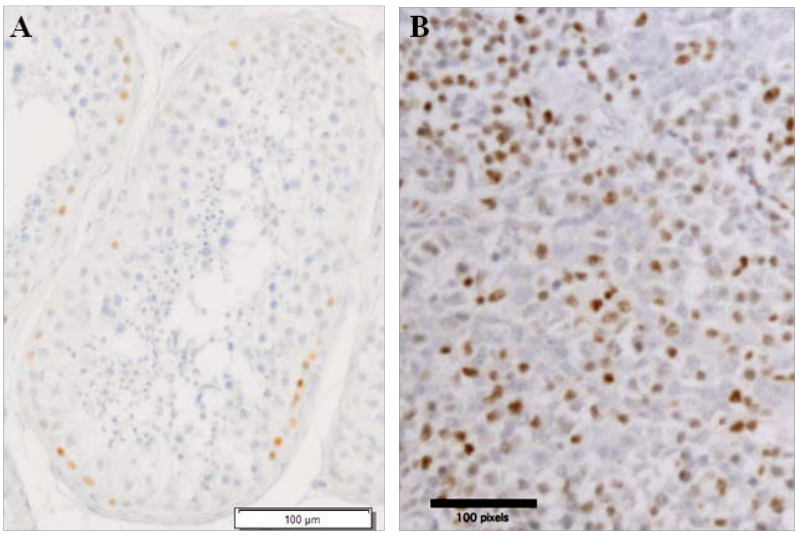

Figure 3.4: Examples of immunohistochemical expression of OCT2 in the normal adult testis (A) and tonsil (B) as the positive control. Scale bar: 100 µm for (A) and 100 pixels (B).

3.2.5 Ki67

Ki67 protein is a proliferation marker that enables estimation of the growth fraction (i.e. the number of cells in cell cycle) in normal and neoplastic tissue. The expression of this protein is detected by an IgG_1 mouse monoclonal antibody generated from a crude fraction of the Hodgkin's lymphoma cell line L428 (Gerdes, *et al.*, 1983; 1984). The Ki67 antibody recognises an antigen that is located within the cell nucleus and is consistently present in all stages of the cell cycle except G_0 and early G_1 phase (Gerdes, et al., 1984). The exact function of Ki67 remains undetermined. Recent data demonstrated its potential link with ribosomal RNA transcription in quiescent and proliferating cells (Bullwinkel, *et al.*, 2006). For instance, inactivation of Ki67 protein markedly inhibited RNA polymerase I-dependent nucleolar ribosomal RNA synthesis (Rahmanzadeh, *et al.*, 2007). Notably, Ki67 antigen is not essential for cell proliferation as the proliferation in some cell hybrids continued in the

absence of this antigen (Verheijen, *et al.*, 1989). Analysis from western blotting and competitive binding experiments demonstrated that the Ki67 monoclonal mouse antibody (clone: MIB-1) reacted with an epitope encoded by the 66 base pair repetitive element in the *MKI67* gene. In immunohistochemistry, identical nuclear staining pattern was observed consistently on serial tonsillar sections. Ki67 protein was only found in a very small subset of spermatogonia but absent in other spermatogenic cells and Sertoli cells in the normal seminiferous tubules (Figure 3.5). The immunohistochemical expression of Ki67 was described in classical seminoma (Gallegos, *et al.*, 2011); however, its presence in spermatocytic seminoma has not been previously investigated.

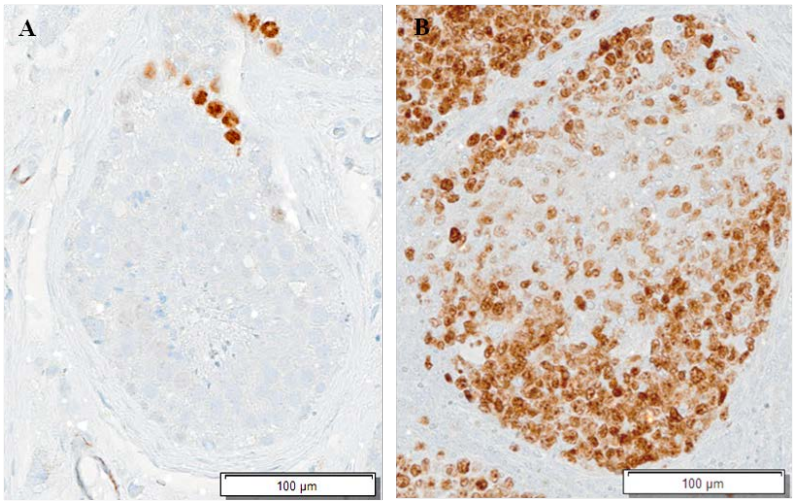

Figure 3.5: Examples of immunohistochemical expression of Ki67 in the normal adult testis (A) and tonsil (B) as the positive control. Scale bar: 100 µm.

3.2.6 FGFR3 (Fibroblast growth factor receptor 3)

As a receptor tyrosine kinase located upstream of the MAPK pathway, FGFR3 is activated by specific FGF ligands, leading to receptor dimerisation and initiation of intracellular downstream signalling cascades. Gain-of-function mutations in the *FGFR3* gene were documented in congenital malformations associated with advanced paternal age (Section 1.5.1.2). Indeed, FGFR3 has been suggested as a potential biomarker of spermatogonia within the human testis. The expression of this surface marker (mouse

monoclonal antibody; clone B9) was restricted to spermatogonial cells only and it was detected in the prespermatogonia in the fetal testis as early as 19 weeks of gestation (Juul, *et al.*, 2007; von Kopylow, *et al.*, 2010). In spermatocytic seminoma, presence of FGFR3 protein was described in 5/24 tumours including a sample bearing *FGFR3* K650E mutation and there was no simple correlation between the protein expression and the mutation status (Goriely, et al., 2009). There are two commercially available markers for FGFR3 protein, known as the mouse monoclonal (clone B9) and rabbit polyclonal (clone C-15) antibodies. The former maps to amino acids 25-125 of human FGFR3 and has been widely used in many previous immunohistochemical studies whilst, the latter was raised against a peptide mapping to amino acids 792-806 in the carboxyl terminus of human FGFR3 (Johnston, *et al.*, 1995) and has been studied in relatively few cases (Delezoide, *et al.*, 1997; Qiu, *et al.*, 2005; Maric, *et al.*, 2007; Martinez-Torrecuadrada, *et al.*, 2008). In view of the localisation of *FGFR3* genetic alterations within the activated tyrosine kinase domain in congenital disorders (including thanatophoric dysplasia and SADDAN; Section 1.5.1.2) and spermatocytic seminoma, FGFR3 rabbit polyclonal antibody was employed for the studies on normal adult testis. There is no cross reactivity between FGFR3 antibody (C-15) with other FGFRs including FGFR1, FGFR2 and FGFR4; nuclear and cytoplasmic localisation of FGFR3 (C-15) was observed on western blots of fractionated cells (Johnston, *et al.*, 1995). In the normal adult testis, the membraneous/cytoplasmic staining of FGFR3 was evident in the spermatogonia of the seminiferous tubules (Figure 3.6), indicating that the specificity of rabbit polyclonal antibody FGFR3 (C-15) is comparable to mouse monoclonal antibody FGFR3 (B-9).

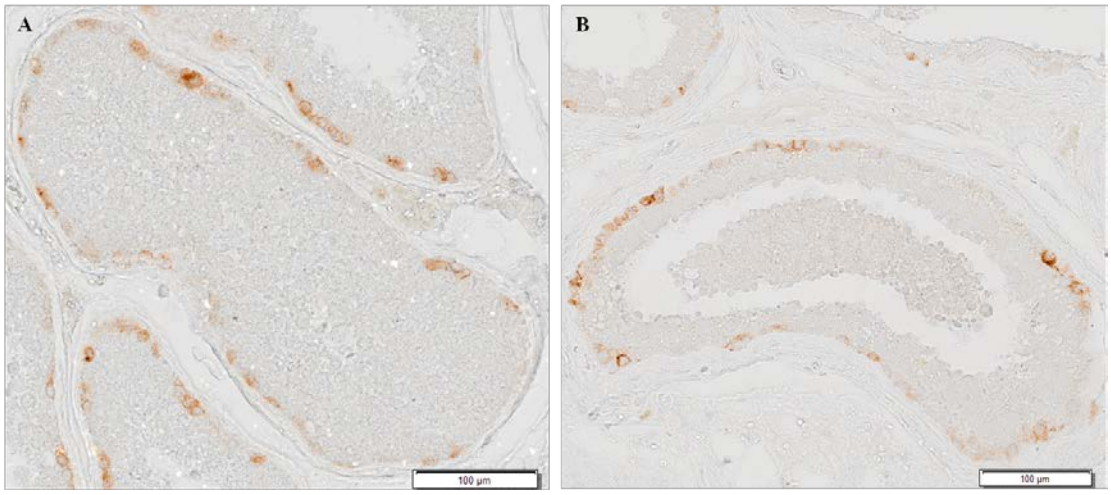

Figure 3.6: Examples of immunohistochemical expression of FGFR3 - clone B9 (A) and FGFR3 - clone C-15 (B) in the normal adult testis. Scale bar: 100 µm.

3.2.7 PLZF (Promyelocytic leukemia zinc finger protein)

The *PLZF* gene was first described as a chromosomal translocation partner with RARα (retinoic acid receptor-α) in patients with acute promyelocytic leukaemia (Chen, *et al.*, 1993). Following the identification of its role in embryonic stem cell renewal (Nichols, *et al.*, 1998; Niwa, *et al.*, 2000), PLZF was later shown to be essential for mouse spermatogenesis where disruption of this gene in male mice resulted in impaired spermatogenesis and infertility. Functional transplantation in which germ cells from the targeted *Plzf*$^{-/-}$ male mice were transplanted to recipient mice, failed to reconstitute spermatogenesis, suggesting an important intrinsic function of Plzf in spermatogonial stem cell renewal. PLZF transcription factor is present in the male gonad during mouse embryogenesis and postnatal life, where it is restricted to single cells, pairs and small chains of aligned undifferentiated spermatogonia (Buaas, *et al.*, 2004; Costoya, *et al.*, 2004). Recent work has also demonstrated that PLZF was observed in human spermatogonia in the whole mount of seminiferous tubule (Dym, et al., 2009b). The mouse monoclonal anti-PLZF antibody (clone D9) was mapped to amino acids 101-400 of human PLZF and its specificity for immunohistochemical labelling on human spermatogonia was validated (Sadri-Ardekani,

et al., 2009). The PLZF protein was confined to the nuclei of spermatogonia in normal human spermatogenesis (Figure 3.7) whilst immunohistochemical data from the Human Protein Atlas showed negative immunoreactivity with PLZF (D9) in all the testicular tumours tested.

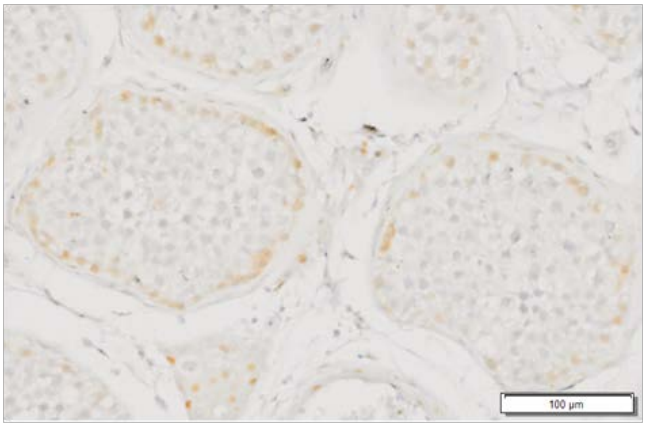

Figure 3.7: Example of immunohistochemical expression of PLZF in the normal adult testis. Scale bar: 100 µm.

3.2.8 GPR125 (G protein-coupled receptor 125)

Another spermatogonial surface marker that was initially selected is GPR125, originally described as a potential stem and progenitor cell surface marker in adult mouse testis (Valenzuela, *et al.*, 2003). Immunohistochemical examination of adult mouse testis revealed that GPR125 expression was restricted to spermatogonia and was not present in differentiated germ cells in the seminiferous tubule (Seandel, *et al.*, 2007). Murine spermatogonia expressing GPR125 were able to restore spermatogenesis in busulphan-treated mice as well as generating multipotent adult spermatogonial-derived stem cells (Seandel, et al., 2007). A recent study demonstrated a similar pattern of GPR125 protein expression in adult human testis, with positive cells being found exclusively in a subpopulation of spermatogonia adjacent to the basement membrane of the seminiferous tubule (Dym, *et al.*, 2009a). However, I did not obtain satisfactory staining (see Methods 2.5.2) on normal testicular tissues using the rabbit polyclonal anti-GPR125 (Figure 3.8)

which was commercially available from two different companies, at various antibody concentrations. Results showing membranous and cytoplasmic staining pattern of GPR125 surface marker on spermatogonia by previous studies were not reproducible (Dym, et al., 2009a; 2009b). The antigenic profile of this protein in normal adult testis was therefore not analysed in detail.

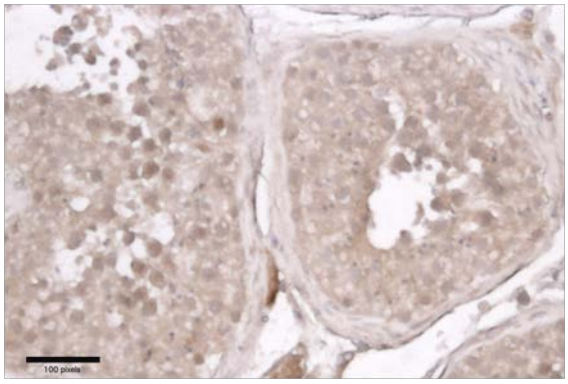

Figure 3.8: Example of non-specific staining of GPR125 antibody with the dilution of 1:5000 in the normal adult testis. Scale bar: 100 pixels.

3.2.9 Phospho-p44/42 MAPK (ERK1/2 - extracellular signal-regulated kinase 1/2)

The MAPK pathway is one of the downstream pathways transducing receptor tyrosine kinase-RAS activation, and there is evidence to support a role for this pathway in spermatogonial proliferation (Section 1.8.4). Hence, pERK1/2 was used as phosphorylation of ERK1/2 is the hallmark of activation of this effector pathway (Section 1.6). In mouse spermatogenesis, ERK1/2 phosphorylation was detected in all stages from premeiotic spermatogonia to zygotene spermatocytes, with peak activity in primitive spermatogonia and preleptotene primary spermatocytes. Phosphorylated ERK1/2 is detected in only a small subpopulation of pachytene primary spermatocytes and spermatids; suggesting that the MAPK pathway is potentially involved in the mitotic proliferation of primitive spermatogonia, the early stage of spermatogenic meiosis and in acquisition of sperm motility (Lu, *et al.*, 1999; Wong and Cheng, 2005). The pERK1/2 rabbit monoclonal antibody (clone:

20G11) used in this study was generated by immunising animals with a synthetic phosphopeptide corresponding to residues surrounding Thr202/Tyr204 of human p44 MAPK. Specific binding with phospho-p44/p42 MAPK was demonstrated in western blot analysis; there was no cross-reactivity between this antibody with the other phosphorylated MAP kinase residues of either JNK/SAPK or p38 (Cell Signalling Technology). Immunohistochemical analysis showed that pERK was immunolocalised in a small fraction of spermatogonia and occasionally in the round spermatids which were situated near the lumen of the seminiferous tubules (Figure 3.9) (Goriely, et al., 2009). pERK1/2 was identified in 14/25 (56%) of the spermatocytic seminoma cases studied and the protein expression was not correlated with the mutation status of the tumours (Goriely, et al., 2009).

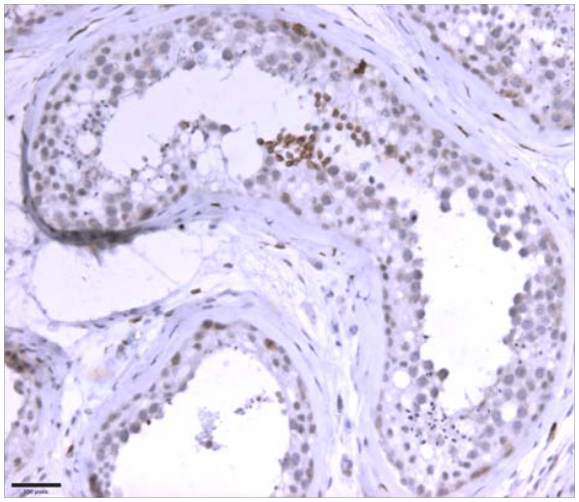

Figure 3.9: Example of immunohistochemical staining of pERK antibody in the normal adult testis. Scale bar: 100 pixels.

3.2.10 pAKT (phospho - v-AKT murine thymoma)

AKT modulates the self-renewal machinery of mouse spermatogonial stem cells via PI3K/AKT signalling cascade which may potentially be the underlying mechanism driving the clonal expansion events in the normal adult testis as proposed (Section 1.8.4.2). The serine-threonine protein kinase AKT (also recognised as protein kinase B, PKB) comprises three closely related enzymatic paralogues AKT1 (PKBα), AKT2 (PKBβ) and AKT3

(PKBγ). These paralogues share high homology both in structure as well as size, and are thought to be activated by a common pathway (Okano, *et al.*, 2000). AKT3 is more restricted in tissue distribution compared to AKT1 and AKT2, being confined predominantly to brain and testis (Konishi, *et al.*, 1995). The phosphorylated AKT rabbit monoclonal antibody (clone: 736E11) has been employed for immunohistochemistry in previous studies (Kimura, *et al.*, 2008; Al-Saad, *et al.*, 2009). It was generated against the synthetic phoshopeptide corresponding to amino acids surrounding Ser473 of mouse Akt1 which are highly conserved between mouse and human. This antibody recognised Akt1 if the phosphorylation occurs at serine 473 whilst Akt2 and Akt3 were detected only when phosphorylated at equivalent sites (Cell signalling technology). Of note, AKT1 shares a high degree of amino acid homology across that region with AKT2 and AKT3. Membranous/cytoplasmic staining pattern of pAKT was most prominent in the spermatogonia of normal seminiferous epithelium whilst other spermatogenic cells remained unstained for this antibody (Figure 3.10).

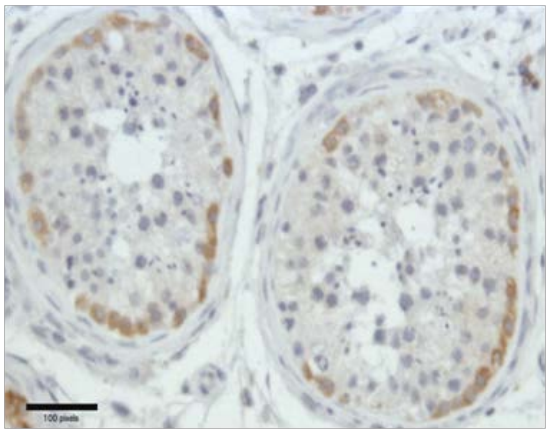

Figure 3.10: Example of immunohistochemical staining of pAKT antibody in the normal adult testis. Scale bar: 100 pixels.

3.3 Discussion

In this chapter, I have explored and chosen potential protein markers, comprising MAGEA4, SSX, SAGE1, OCT2, FGFR3, PLZF and Ki67, for identifying putative clonal events in the testis based on my preliminary immunohistochemical findings in normal human testis and supporting evidence from the literature. All steps in the immunohistochemistry assay were optimised to visualise specific signal and minimise non-specific background staining. The optimal concentration and incubation condition of each antibody were determined and validated from initial studies using control and normal testicular tissues. In each localisation attempt, the control experiment was performed simultaneously to ensure the specificity of the primary antibody labelling. The test results with GPR125 did not yield satisfactory specific staining as had been reported previously (Dym, et al., 2009a; 2009b), therefore studies with this marker were not pursued further.

The selected spermatogonial markers (as mentioned above) are localised either in the nucleus (e.g. OCT2, SAGE1 and Ki67) or at the surface (e.g. FGFR3) of spermatogonia, providing an additional advantage in defining the phenotype of cells of interest especially during double-staining. Moreover, the heterogeneous distribution of these proteins was observed in the normal seminiferous tubules. For instance, MAGEA4 (clone 57B antibody), a germ cell specific marker is present in all of the spermatogonia in the normal seminiferous tubules (Aubry, et al., 2001) whilst SSX and OCT2 are defined by their spatial distribution in spermatogonia; these intrinsic differences between the markers are explored further in the next chapter. The use of MAGEA4 in the panel proved important as an internal control for the integrity of tissue, due to its strong expression in spermatocytic seminoma and human spermatogonia. PLZF which was initially included in the panel of potential markers was, however, not studied extensively in the immunohistochemical analysis on spermatocytic seminoma owing to its inconsistent staining pattern (explained in detail in Section 5.2.2.1). It

is worth noting, in the context of searching for candidate markers, that there are both similarities and differences between the phenotypes of mouse and human spermatogonia, which have been reviewed recently (Dym, et al., 2009b). For example, expression of PLZF and GFRα1 (a co-receptor of RET receptor tyrosine kinase) was identified both in mouse and human; however, some spermatogonial markers are applicable to either human or mouse only. Expression of TSPY (testis specific protein, Y-linked 1) is preferentially confined to the adult human spermatogonia (Schnieders, *et al.*, 1996), whereas in mice it was detected in the elongated spermatids only (Kido and Lau, 2006). On the other hand, β1-integrin, which is regarded as a marker for mouse spermatogonial stem/progenitor cells, was present in human spermatogenic cells containing spermatocytes, spermatids and spermatozoa, but was not expressed in human spermatogonia (Schaller, *et al.*, 1993; Shinohara, *et al.*, 1999).

In this study, of the list of potential candidate markers, the downstream effectors of MAPK (phospho-ERK1/2) and PI3K/AKT (phospho-AKT) signalling pathways were included with the aim of establishing a possible correlation between the mutation status and antigenic profile of the putative clone. To address this, a pilot study was first conducted with urothelial carcinoma to establish whether the tumour's genotype is correlated with the expression of signalling molecules (phospho-ERK1/2 and phospho-AKT) (as discussed further in Chapter 5; Sections 5.2.1 and 5.3.1). Of note, the gene mutated in the mutation-positive tumours did not always show a simple correlation with the protein expression (Section 5.3.1). The feasibility of these activated downstream components to be incorporated into the study of searching for putative clones in the normal adult testis would also depend on the size of the localised clonal expansion events.

In summary, the observations from this preliminary study have set up the fundamental framework for the following chapters in the thesis. Specifically, the presence of subpopulations of spermatogonia represented by different spermatogonial markers was

investigated in more detail during testicular development and the normal adult testis (Chapter 4). The expression of these spermatogonial markers in spermatocytic seminoma is described in Chapter 5. My aim was to further characterise their antigenic profile during testicular oncogenic events, potentially shedding light on the cellular origins of this tumour (a subject still under debate). Collectively, evidence from these studies would provide fundamental insights and practical experience in finalising the selection of candidate markers to search for the proposed clonal event in the normal adult testis (Chapter 6).

CHAPTER 4

EXPRESSION OF OCT2, SSX AND SAGE1 IN ADULT AND DEVELOPING TESTES

Chapter 4: Expression of OCT2, SSX and SAGE1 in adult and developing testes

4.1 Introduction

As described in Section 1.8.1, by the second trimester there are three distinct populations of germ cells for which Gaskell et al (2004) demonstrated different immunohistochemical profiles. Gonocytes and intermediate cells were characterised as $OCT4^{pos}/KIT^{pos}/MAGEA4^{neg}$ and $OCT4^{neg}/KIT^{low/neg}/MAGEA4^{neg}$ respectively; prespermatogonia, usually lying in groups at the periphery of the seminiferous cords, had a $OCT4^{neg}/KIT^{neg}/MAGEA4^{pos}$ staining pattern. After puberty, prespermatogonia were no longer observed in the normal adult testis; instead, the presence of mature spermatogonia, positive for MAGEA4 (Chapter 3) were identified in distinct morphological phenotypes in the seminiferous tubules and associated with different maturation stages (Section 1.8.1).

The aims of this study were to evaluate selected immunohistochemical markers during testicular development and to determine whether different subpopulations of adult germ cells could be identified with these markers. Based on the differences in observed spatial distribution of spermatogonial staining in the normal adult testis (Chapter 3), three candidate markers were chosen for detailed study comprising OCT2, SSX and SAGE1. These markers were investigated in a series of testicular tissues representing different stages of germ cell maturation during fetal and childhood development as well as in the normal adult testis.

4.2 Results

In the normal adult testis, OCT2, SSX and SAGE1 nuclear staining were detected in distinct subpopulations of spermatogonia (Figure 4.1A-C). OCT2 was present predominantly in the A_{dark} spermatogonia recognised by the presence of the vacuole-like cavity in the nucleus (Section 1.8.1), whilst the immunoreactivity of SSX was detected mainly in A_{pale}/B spermatogonia (Section 1.8.1), with a weak reaction also observed in a subset of pre-

leptotene primary spermatocytes. Observations from earlier studies were consistent with these results, showing the expression of SSX during male germ cell developmental stages in human primarily in spermatogonia and primary spermatocytes (dos Santos, et al., 2000; Stoop, et al., 2001). SAGE1 was seen in a small subset of type A spermatogonia but was localised predominantly to more differentiated B spermatogonia (Section 1.8.1), distinguished by their larger and more circular nucleus compared to A_{dark} and A_{pale} spermatogonia (which have smaller, ovoid nuclei). The specificity of these antibodies was previously validated as described in Section 3.2. Comparative staining of OCT2, SSX and SAGE1 on adjacent sections revealed that OCT2 and SSX were restricted in two separate subpopulations of spermatogonia (Figures 4.1D-E). SAGE1-immunopositive spermatogonia showed a rather scattered distribution pattern; of which coexpression of SAGE1 and SSX was observed in a subset of spermatogonia within the same seminiferous epitheliums (Figures 4.1E-F). The mutually exclusive staining pattern of OCT2 and SSX in spermatogonia was further confirmed by dual immunohistochemistry as shown in the seminiferous tubules in Figures 4.2A-D. Spermatogonia that were negative for both OCT2 and SSX were occasionally identified in the same sections (Figure 4.2A-D, arrows).

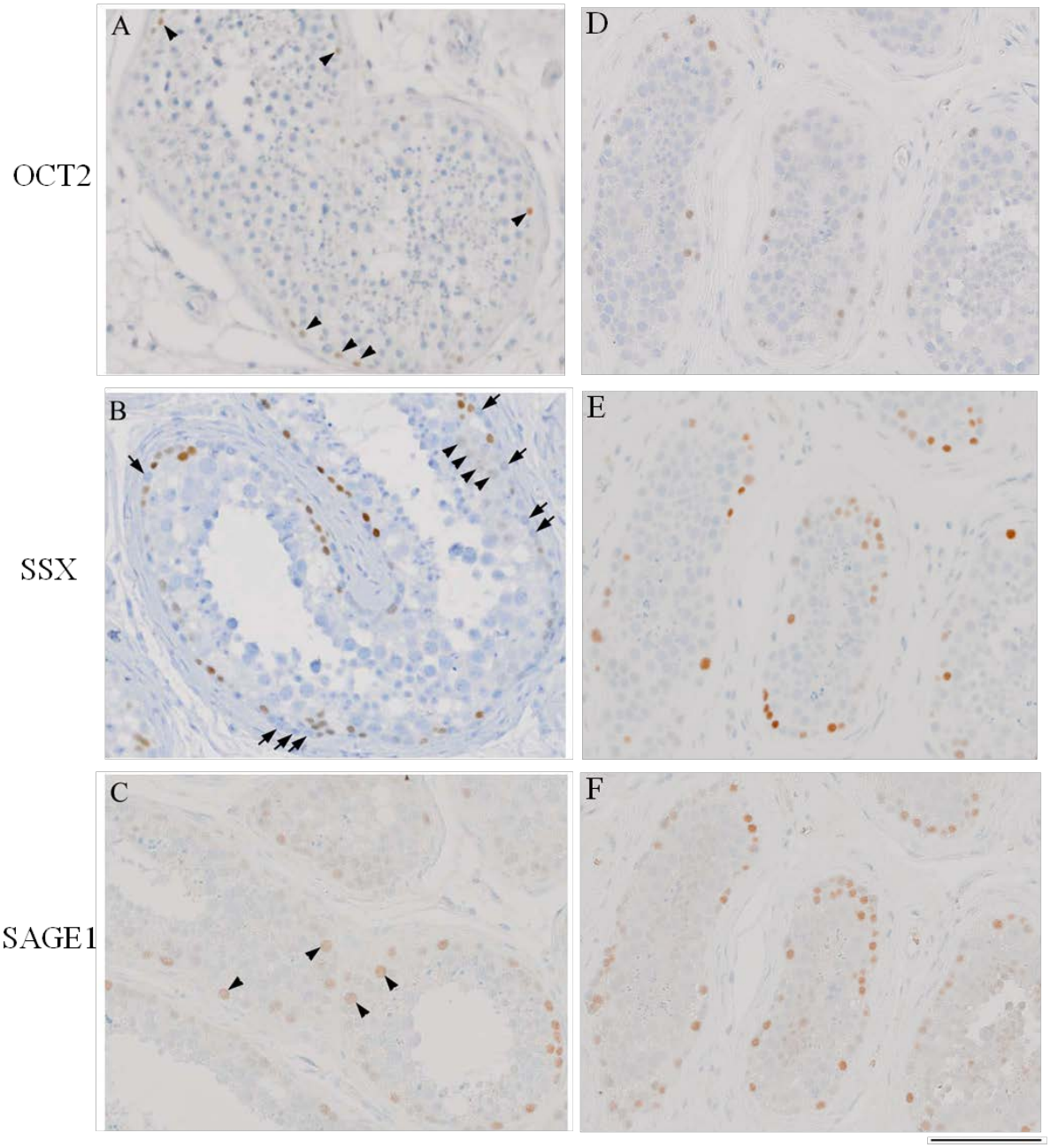

Figure 4.1: Distribution of OCT2, SSX and SAGE1 in the normal adult testis. A. OCT2: Note nuclear staining in a minority of spermatogonia located adjacent to the basement membrane of the tubules (arrowheads). B. SSX was detected mainly in A_{pale}/B spermatogonia but absent in A_{dark} (arrows) spermatogonia. Some of the primary spermatocytes (arrowheads) showed weak staining. C. SAGE1 was found predominantly in B spermatogonia, characterised by a large circular shape and more internal position in the tubule (arrow heads). D-F. These images were adjacent sections from a testis which was labelled with OCT2 (D), SSX (E) and SAGE1 (F). Scale bar: 100 µm.

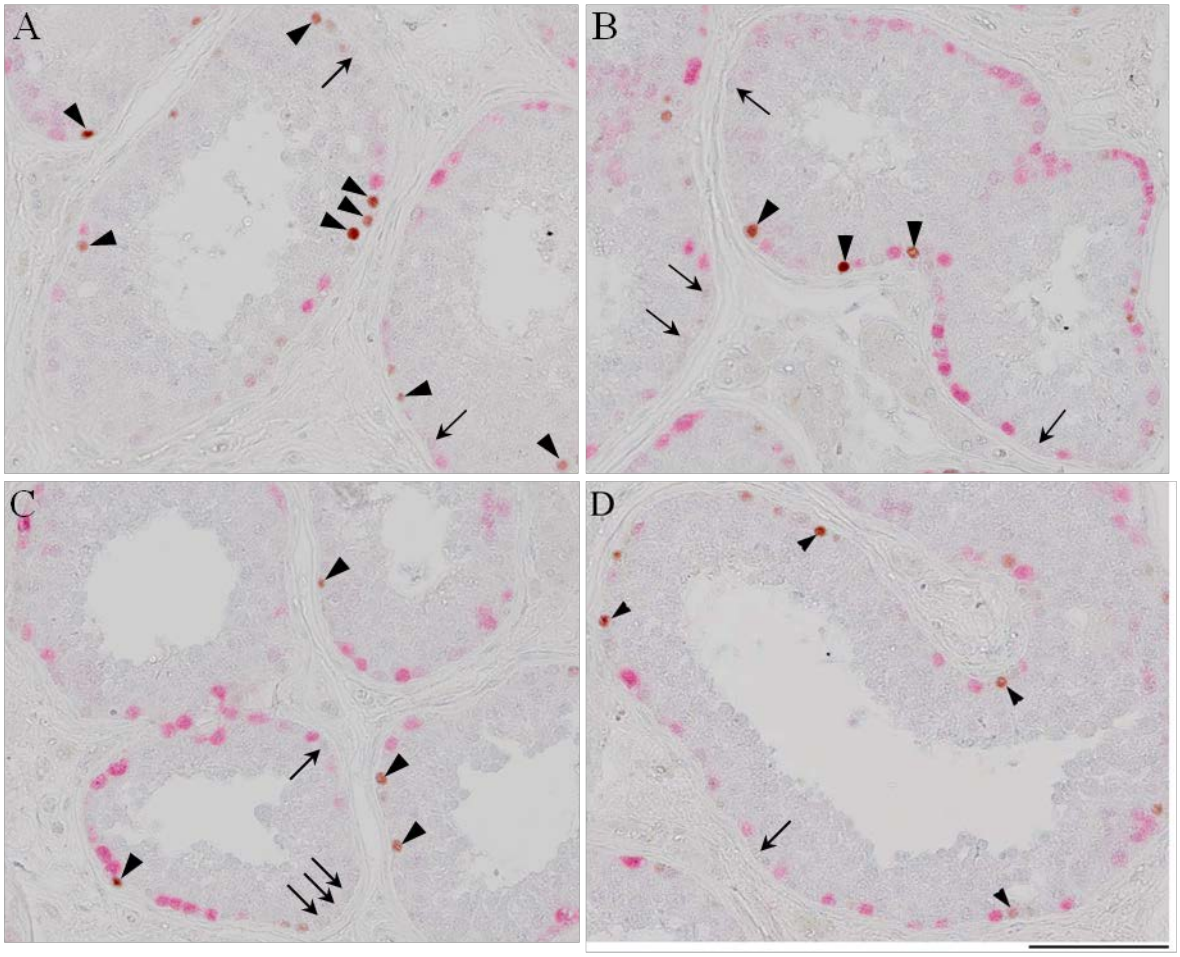

Figure 4.2: Double-staining of OCT2 and SSX in the normal adult testis. A-D. OCT2 and SSX double-staining revealed that OCT2 (brown nuclei) and SSX (red nuclei) were present in two distinct subpopulations of spermatogonia. OCT2 was mainly found in the A_{dark} spermatogonia (arrowheads). Some spermatogonial cells were $OCT2^-/SSX^-$ (arrows). Scale bar: 100 µm.

This study was extended to outline the antigenic profile of OCT2, SSX and SAGE1 during different phases of testis development, in which a series of twenty-three formalin-fixed, paraffin embedded fetal testes starting from 16^{th} to 42^{nd} wg as well as five infantile and prepubertal testicular tissues (age 2 months – 4.5 years) were recruited (Table 2.1). The immunohistochemical results illustrating the ontogeny of expression of OCT2, SSX and SAGE1 spermatogonial markers in fetal, postnatal/prepubertal and adult testes are summarised in Table 4.1. In mid-gestation, single germ cells (possibly prespermatogonia)

with strong OCT2 expression were identified only in 17th wg and 18th wg. Of note, prespermatogonia were larger and contained more cytoplasm compared to gonocytes; these prespermatogonia were usually present near the basement membrane of the seminiferous cord and lacked a prominent nucleolus (Fukuda, et al., 1975; Gaskell, et al., 2004). By 33rd wg, the intense OCT2-immunopositive cells reappeared and these cells were then consistently observed in post-natal testicular tissue. Germ cells with weak OCT2 immunoreactivity were present in most of the testicular development stages studied. Furthermore, SSX was investigated only in a number of representative cases because this antigen has been studied previously (Stoop, et al., 2001). Weak expression of SSX was first noted at 16th wg but a subset of cells showing strong immunoreactivity was found from 21st to 33rd wg and also in testicular tissue from a 3 month old child. The expression of SAGE1 protein was absent at all ages during pre-pubertal development, suggesting that upregulation of this protein occurs after puberty. By comparing adjacent serial sections (Figure 4.3A), SSX and OCT2 immunopositive staining was always observed in mutually exclusive subsets of germ cells, consistent with the results found in the normal adult testis. OCT2 was not detected in gonocytes, which were identified by double staining with OCT3/4 or PLAP (placental-like alkaline phosphatase) protein (Figure 4.3B). Notably, OCT3/4 and PLAP are also markers of CIS – the precursor of testicular germ cell tumours (Section 1.8.3) (Skakkebaek, *et al.*, 1987; Hoei-Hansen, *et al.*, 2005). As a control for tissue integrity, MAGEA4 was detected in the prespermatogonia from 20th wg onwards, but not in the gonocytes, in agreement with the previously established pattern (Gaskell, et al., 2004).

Table 4.1: The expression profiles of OCT2, SSX and SAGE1 during normal human testis development.

Antigens		OCT2		SSX		SAGE1	
Staining intensity		Weak	Strong	Weak	Strong	Weak	Strong
Age of gestation							
Weeks	16	-*	-	-	-†	-	-
	17	-	-*	n/d	n/d	-	-
	18	-	-*	-	-	-	-
	20	-*	-	n/d	n/d	-	-
	21	-*	-	-†	+	-	-
	22	-*	-	+	-†	-	-
	24	-*	-	+	-†	-	-
	25	-	-	-†	-†	-	-
	27	-	-	n/d	n/d	-	-
	31	-*	-	n/d	n/d	-	-
	33	++	-*	+	-†	-	-
	39	-	-	n/d	n/d	-	-
	41	-*	-	n/d	n/d	-	-
	42	+	-	n/d	n/d	-	-
Months	2	+	-*	n/d	n/d	-	-
	3	+	-*	-†	-†	-	-
	4	-*	-	n/d	n/d	-	-
	23	-*	-*	n/d	n/d	-	-
Years	4.5	++	-	-	-	-	-

Staining score describes the proportion of positive cells as +++, nearly all cells stained; ++, approximately half of the cells stained; +, a low percentage of cells stained; -, no positive cell detected; -* & -†, only single cells stained for OCT2 and SSX respectively, both markers represent different subsets of cells. The staining intensity was depicted as weak or strong. n/d; not done.

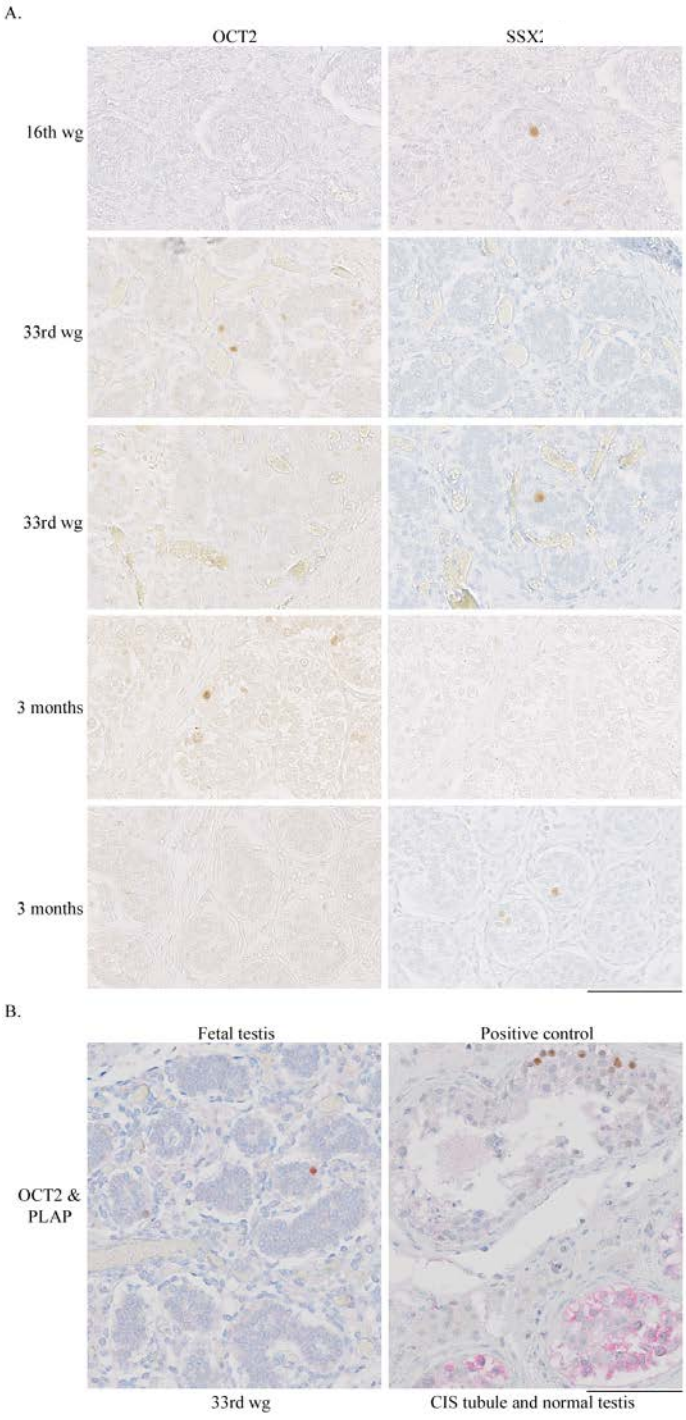

Figure 4.3: Comparative staining of OCT2, SSX and PLAP in distinct germ cell subpopulations during testis development. A. The presence of SSX was first noted at 16th wg. OCT2 and SSX are expressed distinctively in two different subsets of germ cells starting from 33rd week to adulthood including at the age of 3 months. Note that horizontally paired images, taken from adjacent sections of the same testis, allow comparison of staining of individual germ cells for each protein. B. Left, double labelling of fetal testis at 33rd wg demonstrates that PLAP (red) is not detected in germ cells expressing OCT2 (brown nuclei). Right, positive control showing membranous and cytoplasmic immunoreactivity of PLAP in CIS cells (red) and OCT2 positive spermatogonia (brown) in the adjacent tubule. Scale bars: 100 µm (all images).

4.3 Discussion

Since different subsets of human spermatogonia were first described (Clermont, 1963), many studies have been performed to identify markers which are potentially specific for these subtypes of spermatogonia (Dym, et al., 2009b). In the current study, the presence of different subpopulations of spermatogonia was distinguished in the normal adult testis using the combination of OCT2, SSX and SAGE1 markers.

OCT2 (also known as POU2F2) is a transcription factor mainly expressed in B lymphocytes and neuronal cells (Latchman, 1996). In contrast to OCT2 which has not previously been characterised in spermatogenesis, other members of this family such as OCT3/4 and OCT6 were shown to be involved during embryonic germ cell maturation and GDNF-mediated self-renewal process of spermatogonia stem cells, respectively (Section 3.2.4). The identification of OCT2 as a potential marker of A_{dark} spermatogonia, the reserve population of germ cells, is one of the most interesting findings in this study. It may have some clinical value for a more objective assessment of the recovery of spermatogenesis and fertility potential, for example in cancer survivors or young individuals with a history of cryptorchidism (a developmental defect where one or both of the testes failed to descend into the scrotum). By contrast, SSX was predominantly identified in a distinct subset of germ cells matching the morphological characteristics of A_{pale}/B spermatogonia established by Clermont (1963), whilst SAGE1 was present preferably in the more differentiated B spermatogonia. Coexpression of both proteins was seen in a subset of spermatogonia on consecutive serial sections, suggesting the involvement of both proteins in the differentiation stages of spermatogonia.

Following these observations, further investigations were performed to understand their expression patterns during early testicular development. Strong expression of OCT2 and SSX in germ cells was seen at different phases of germ cell maturation. Intriguingly,

OCT2 and SSX were present in two mutually exclusive subsets of germ cells, in line with what was observed in the normal adult testes. Most of the cells expressing OCT2 and SSX were located adjacent to the basement membrane although some cells with strong SSX immunopositivity were observed in the centre of the seminiferous cord. The mutually exclusive staining pattern of OCT2 and SSX from embryonic stages until adulthood suggests that these proteins play distinctive roles at different phases during normal testicular development; it also raises the possibility that the mutually exclusive pattern of OCT2 and SSX protein expression corresponds to cell fate switch between self-renewal and differentiation particularly in spermatogonial stem cells. Consistent with the observation in the normal adult testis, OCT2 was absent in gonocytes positive for PLAP, indicating that it is specific for more mature germ cells. SAGE1 was absent in the fetal and infantile testes, and based on its expression preferentially in the B spermatogonia of normal adult testis, I hypothesise that this protein is upregulated in differentiating spermatogonia only after puberty.

Taken together, the distinct temporal pattern of expression of OCT2, SSX and SAGE1 proteins was likely to be dependent on the maturation stages of spermatogonia (as summarised in Figure 4.4), with mutual exclusivity of OCT2 and SSX, demonstrating the existence of different populations of spermatogonia not only in the adult testis, but also before puberty. The discrepancy of ontogenic expression between OCT2 and OCT3/4 also suggest that OCT2 may have distinctive roles in regulating the transcription activity of pre- and post-pubertal spermatogonia (preferentially in A_{dark} spermatogonia), which is dissimilar from OCT3/4. Of note, OCT2 has been proposed to act as a bifunctional regulator which either stimulates neuronal differentiation or represses differentiation in precursor cells during neuronal development, depending on its isoforms resulting from alternative splicing events (Theodorou, *et al.*, 2009). The biological function of another two proteins (SSX and SAGE1)

remains largely unknown although there is evidence to suggest SSX proteins act as transcriptional repressors (Sections 3.2.2 and 3.2.3).

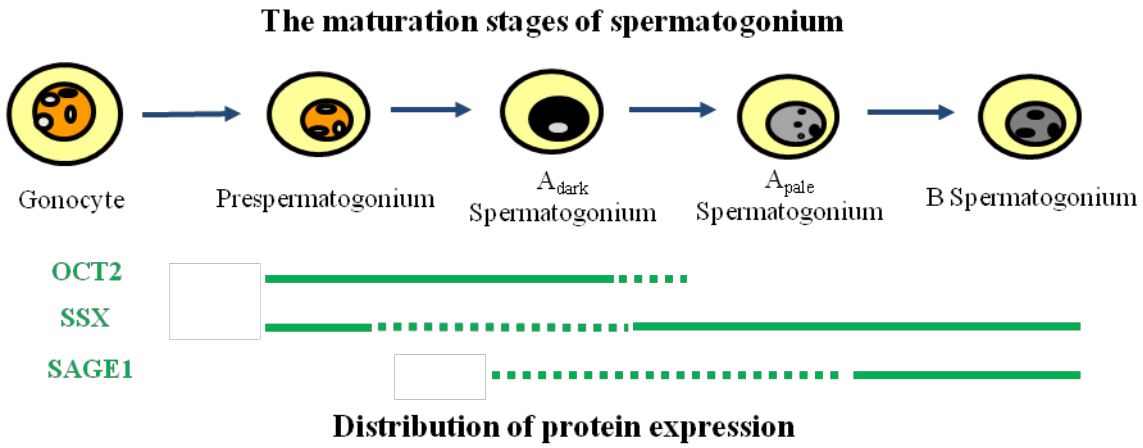

Figure 4.4: Schematic diagram illustrating the antigenic profile of OCT2, SSX and SAGE1 during the maturation of a normal spermatogonium. The different lines, each drawn in the various styles, describe the distribution of protein expression as (blank), never been observed; ····· , occasionally observed; ——, predominantly observed.

In summary, this is the first documented evidence of the expression profile of OCT2 and SAGE1 in the human testis from embryonic development to adulthood. In addition, this study has highlighted the presence of two mutually exclusive subpopulations of germ cells defined by OCT2 or SSX protein expression. Understanding the immunohistochemical properties of human spermatogonia may help in elucidating the cellular origin of spermatocytic seminoma, which has been a subject of controversy (Section 1.8.3) (discussed in detail in Chapter 5). Future studies will be necessary to confirm whether OCT2 is indeed a specific marker for human reserve spermatogonial stem cells, which could have potential clinical use, and to uncover its role in germ cell development and spermatogenesis. The experimental findings and conclusions from this chapter were recently published in *Journal of Pathology* (Lim, *et al.*, 2011).

CHAPTER 5

SPERMATOCYTIC SEMINOMA: CELLULAR ORIGIN AND IDENTIFICATION OF CANDIDATE PROTEIN MARKERS OF PUTATIVE CLONES

Chapter 5: Spermatocytic seminoma: cellular origin and identification of candidate protein markers of putative clones

5.1 Introduction

Spermatocytic seminoma (SS) is a rare, distinct testicular neoplasm and its histogenesis is discussed in detail in the Introduction (Section 1.8.3). Spermatocytic seminoma has recently emerged as a key link between the processes of somatic and germline mutation, as described in recent work by our group (Goriely, et al., 2009). Paternal age-effect mutations in the *FGFR3* and *HRAS* genes previously found to be mutated in congenital disorders were present in about 25% of SS specimens that were associated with a relatively older age of patients (Goriely, et al., 2009) (Section 1.8.3). Hence, as described in Chapter 3, spermatocytic seminoma was chosen as an ideal testicular model to develop a screen for immunohistochemical markers to identify the histological correlates of paternal age-effect mutations in the normal adult testis.

To address this, a pilot study was first set up using urothelial carcinoma (UC) (Section 1.5.1.2) to establish optimal conditions for immunohistochemical and genetic analysis, owing to the scarcity of SS material. UC originates from epithelial cells and approximately 70-80% are well-differentiated papillary tumours confined outside the epithelium basement membrane (Eble and Young, 1997; Billerey, *et al.*, 2001; Reuter, 2006). This lesion is staged Ta bladder cancer and activating *FGFR3* mutations are present in up to 75% of this tumour (Dalbagni, *et al.*, 1993; Zieger, *et al.*, 2005). In addition, *HRAS* mutations are identified in around 9% of urothelial malignancies; of which the majority were staged Ta and T1 (Jebar, *et al.*, 2005). Mutual exclusivity of *FGFR3* and *HRAS* mutations was observed in UC (Jebar, et al., 2005). Recent data (Goriely, *et al.*, 2009) demonstrated a strong correlation between the total number of reported cases of papillary non-invasive bladder carcinoma harbouring each *FGFR3* Lys650 somatic mutation and the level of these mutations in sperm of healthy men, which may lead to testicular tumour predisposition;

indicating a similar tumour biology of UC and SS. Here, I have assessed the prevalence of activating *FGFR3* and *HRAS* mutations in a series of 32 staged Ta UC as well as their immunoreactivities against FGFR3 and downstream effector molecules phospho-ERK1/2 and phospho-AKT. The possible correlations between the antigenic profile of these markers and the mutational status of these tumours were also included in the pilot study.

Following this, I instigated a screen of a panel of markers (Chapter 3) in 36 overt SS cases and normal adult testis controls using immunohistochemistry. This marker screen has gained additional insights on the origin and pathogenesis of SS as well as the selection of candidate markers of putative clones. Further analysis of OCT2, SSX and SAGE1 expression in SS tumours and four intratubular spermatocytic seminoma (ISS) cases (Section 1.8.3) revealed a heterogeneous phenotype of SS which was in parallel with the distribution of these markers in subpopulations of spermatogonia in the normal testis (Chapter 4).

5.2 Results

5.2.1 Pilot study of genotyping and immunohistochemical analysis on urothelial carcinoma (UC)

The clinicopathological data of the patients are summarised in Table 5.1. Tumours were classified according to the TNM classification and graded histologically as recommended by World Health Organization.

Table 5.1: Clinicopathologic patient data

Characteristic	Number of patients
Gender	
Female	11
Male	21
Mean age (years)	70.31 (range, 55 – 92)
Grade / Stage	
G1 / Ta	7
G2 / Ta	25

5.2.1.1 Sequence variants identified in UC samples

A total of 32 UC cases (Table 5.1) were screened for their common mutation sites in the *FGFR3* and *HRAS* genes. PCR amplification of individual exons (Table 2.2) was

performed and followed by restriction enzyme digestion (Table 5.2). Only amplification products from *FGFR3* exon 10 were subjected to direct sequencing because there are various base substitutions previously known to be present in that region and no suitable screening restriction enzymes were available for these mutations.

Table 5.2: Restriction enzymes used for DNA digestion.

Gene	Exon	Codon	Nucleotide	Restriction enzymes	Restriction site
FGFR3	7	248	CGC	*HaeII*	RGCGCY[1]
	7	249	TCC	*BbvI*	GCAGC
				BslI	$CC(N)_7GG$
	15 (IIIb)	650	AAG	*BbsI*	GAAGAC
HRAS	2	12	GGC	*MspI*	CCGG
	3	61	CAG	*BstNI*	CCWGG[2]
				EaeI	YGGCR[1]

[1]Y=C/T, R=A/G; [2]W=A/T, the restriction site covered all the possible point mutations at codon 61 except Gln61Leu which was later examined with *EaeI* restriction enzyme.

Samples showing a mutant restriction fragment pattern were sequenced for further confirmation (Figure 5.1). Four distinct *FGFR3* single nucleotide substitutions were detected in 26 of the samples, of which these mutations were located at the linker regions either between the D2 and D3 domains (Arg248Cys; R248C and Ser249Cys; S249C) or between the D3 domain and transmembrane (TM) region (Gly372Cys; G372C and Tyr375Cys; Y375C) (Section 1.5.1.2). None of the samples was found with *HRAS* mutations. The *FGFR3* somatic mutation profile as summarised in Table 5.3 is consistent with that detailed in the COSMIC database (http://www.sanger.ac.uk/genetics/CGP/cosmic/). The c.746C>G transversion mutation in *FGFR3*, leading to amino acid change S249C, was observed in 22/26 (85%) of mutated bladder tumours. The amino acid change to cysteine promotes interchain disulphide bond formation of the extracellular domains of receptor monomers, resulting in ligand-independent dimerisation and constitutive activation of downstream signalling pathways (Sections 1.5.1.2 and 1.6). The oncogenic properties of the *FGFR3* Y375C mutation, which also stabilises FGFR3 dimerisation via an intermolecular disulphide bond, were analysed in previous studies in which the transformation activity on a bladder

carcinoma cell line expressing FGFR3b-Y375C was inhibited upon treatment with FGFR kinase inhibitors and/or *FGFR3* shRNA (Bernard-Pierrot, *et al.*, 2006; Tomlinson, *et al.*, 2007b).

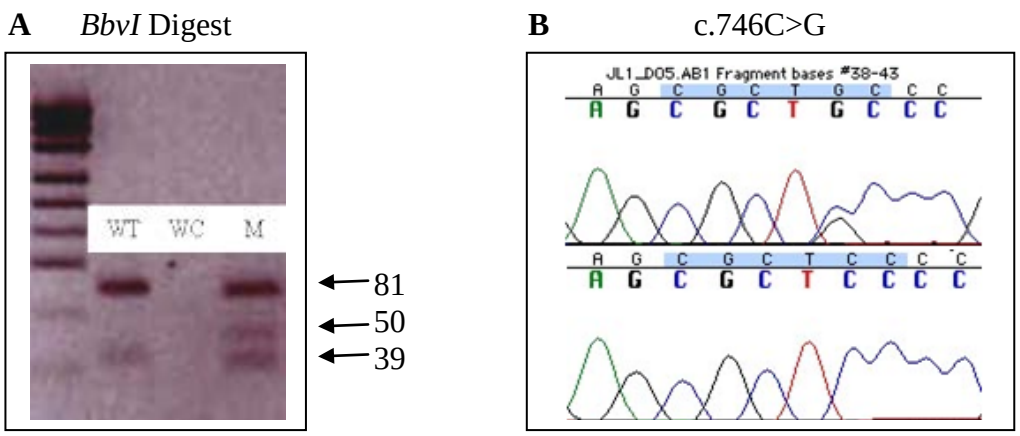

Figure 5.1: Analysis of *FGFR3* mutations in UC samples. (**A)** Pattern of *BbvI* restriction fragments for a UC with a heterozygous sequence change (*FGFR3* exon 7, c.746C>G, p.S249C). The water control and wild type fragments are shown for comparison. (WT) wild type, (WC) water control, (M) Mutant. (**B)** DNA-sequence electropherogram providing independent confirmation of this mutation with a normal control shown below for comparison.

Table 5.3: *FGFR3* mutation profile in urothelial carcinoma.

Exon	Codon (IIIb isoform)	Mutation	Amino acid change	Number of tumours
7	248	c.742C>T	Arg → Cys (R248C)	1
7	249	c.746C>G	Ser → Cys (S249C)	22
10	372	c.1114G>T	Gly → Cys (G372C)	1
10	375	c.1124A>G	Tyr → Cys (Y375C)	2
Total samples with detectable mutations				26
Total samples with no detectable mutations				6

5.2.1.2 Analysis of FGFR3, pERK and pAKT immunoexpression in selected UC samples with known mutational status

With the knowledge of the mutation status of each UC, eight samples were chosen for immunohistochemical analysis. Of the 8 UC cases selected, 3 were heterozygous p.S249C, 1 was heterozygous p.R248C, 2 were heterozygous p.Y375C, and 2 were without detectable mutation. These tumours were stained with FGFR3, phospho-ERK1/2 (pERK1/2) and phospho-AKT (pAKT) antibodies in order to establish the staining pattern of different

antibodies in each tumour (Table 2.1). In addition, I wished to investigate the correlation between expression of these proteins and mutation status of the tumours. The staining was evaluated independently by two investigators (myself and Dr. Gareth Turner).

FGFR3, pERK1/2 and pAKT immunoreactivities were present in all the tumours screened but to a markedly variable extent (Table 5.4). Expression of FGFR3, pERK1/2 and pAKT proteins is weak in normal ureteric urothelium (Hughes, 1997; Mo, *et al.*, 2007; Tomlinson, *et al.*, 2007a). Increased FGFR3 protein expression characterized by both membranous and cytoplasmic staining was observed in all of the tumours tested, with 3/8 cases showing strong FGFR3 immunoreactivity. Interestingly, strong FGFR3 positivity was found in one of the samples with no detectable mutation while some tumours harbouring FGFR3 mutations showed weaker FGFR3 immunoreactivity (Figure 5.2; Table 5.4). These findings suggest that the upregulation of FGFR3 activity is pivotal to non-invasive bladder tumourigenesis, but not solely caused by activating FGFR3 point mutations. Other gain-of-function genetic alterations of *FGFR3* including gene amplification and gene translocation may contribute to the overexpression of FGFR3 protein in UC of bladder cancer. All samples exhibited high pERK1/2 protein expression with strong nuclear and cytoplasmic staining observed, accentuated at the surface of the papillary region. These staining patterns were in parallel with the functions of pERK as a regulator of gene expression targeting both nuclear and cytoplasmic proteins. In contrast, heterogeneous pAKT protein expression with variable staining intensity was observed across the tumours (Figure 5.2; Table 5.4).

Table 5.4: Protein expression profile of FGFR3, pERK1/2 and pAKT in selected UCs.

Sample ref no.	Mutational status	FGFR3	pERK1/2	pAKT
BC19	FGFR3 R248C	+ (w)	+++ (str)	+ (w)
BC24[a]	Negative	++ (str)	+++ (str)	++ (str)
BC25	FGFR3 S249C	+ (w)	+++ (str)	++ (str)
BC26	Negative	+ (w)	+++ (str)	++ (str)
BC28	FGFR3 S249C	++ (str)	+++ (str)	+ (w)
BC30	FGFR3 Y375C	+ (w)	+++ (str)	++ (str)
BC33	FGFR3 Y375C	+++ (str)	+++ (str)	+ (w)
BC34[b]	FGFR3 S249C	+ (w)	+++ (str)	+ (w)

[a] Figure 5.2 (D, E, F); [b] Figure 5.2 (A, B, C). Staining score describes the proportion of positive cells as: +++, nearly all cells stained; ++, approximately half of the cells stained; +, a low percentage of cells stained. Staining intensity is categorised as: str, strong; or w, weak.

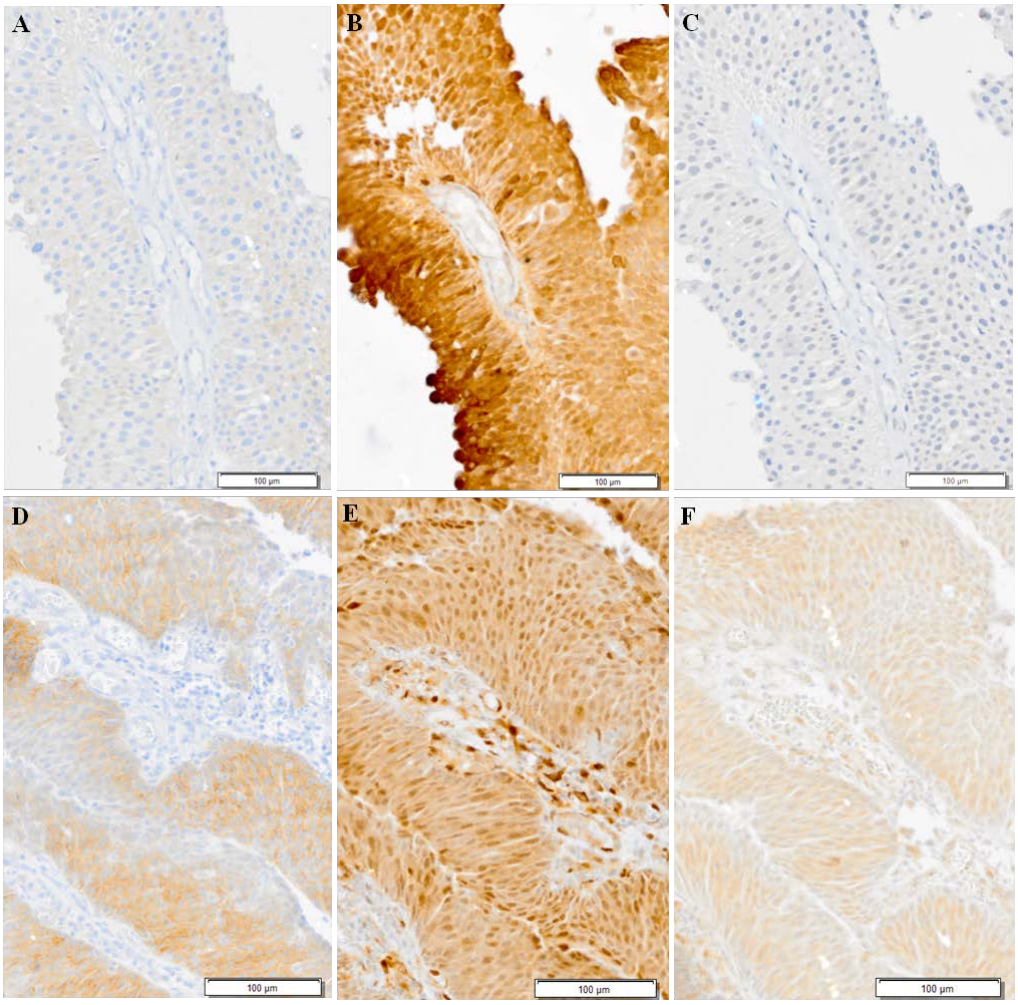

Figure 5.2. Examples of FGFR3 (A, D), pERK (B, E) and pAKT (C, F) protein expression in two UC. (A, B, C) are from sample BC34 with *FGFR3* p.S249C mutation and (D, E, F) are from sample BC24 with no detected mutation. Different staining patterns of three antibodies are demonstrated by examining a similar region within each tumour (A-B-C; D-E-F). The heterogeneous protein expression across the tumours is observed by comparing two different samples (e.g A and D). Scale bar: 100 µm.

5.2.2 Analysis of candidate markers in spermatocytic seminoma (SS) and intratubular spermatocytic seminoma (ISS)

5.2.2.1 Immunohistochemical analysis of candidate markers in SS and ISS

In this study, I first analysed the expression of seven candidate proteins MAGEA4, OCT2, SSX, SAGE1, FGFR3 and Ki67 in 36 SS cases. The staining was assessed independently by three investigators (myself, Dr. Gareth Turner and Dr. Ewa Rajpert-De Meyts) according to the approximate proportion of cells stained and the staining intensity (Section 2.12.1). For Ki67 (a cell proliferation marker), the numbers of stained cells were counted in 1-4 representative areas (in most cases two, because the core size was quite small) comprising approximately 100 cells per area by Dr Katherine A Ewen (University Department of Growth and Reproduction, Copenhagen University Hospital (Rigshospitalet), Copenhagen, Denmark); an unbiased estimate of standard deviation (SD) was calculated using Microsoft Excel when more than two counts were taken. The proportions of large, intermediate and small cells were similarly quantitated. Statistical comparisons of staining patterns, age of the subjects with SS and mutation status of the SS employed 2-tailed Fisher's exact test or Student's *t*-test as appropriate. The immunohistochemical studies with PLZF were inconsistent on SS samples; staining results were occasionally irreproducible although the same optimal staining conditions were applied, therefore no further investigations were pursued with this marker to reduce the chance of misinterpretation on any potential false-negative or false-positive results.

The immunohistochemical analysis on SS (as summarised in Table 5.5; examples shown in Figure 5.3A) revealed that these proteins were all expressed, with variable intensities, in subpopulations of tumour cells in a proportion of SSs. Strong cytoplasmic staining with some nuclear-stained MAGEA4 positive cells was detected in all of the SS tumours (36; 100%). Most tumours (32; 89%) were positive for SSX and amongst these, 14 (39%) were positive for SAGE1 whilst FGFR3 was found in 22 (61%) of the cases. All FGFR3

expressing tumours (23; 64%) exhibited a cytoplasmic staining pattern with occasional nuclear positivity observed in a subset of tumour cells in some cases (Table 5.5). OCT2 was expressed in a much smaller proportion of tumours (5; 14%), all of which were either positive for SSX and SAGE1, or negative for both markers (Figure 5.3B); there was a negative trend between OCT2 and SSX expression, although this did not achieve formal statistical significance ($P = 0.08$, Fisher's exact test) (Figure 5.4). No significant positive or negative correlation was obtained between the expression of any other pairs of antibodies. MAGEA4 was not included in the Fisher's exact test as it was present in all the tumours and thereby would not have associated with the expression of other markers. Student's *t*-test was employed to investigate the relation between the age of the patients and the expression of markers. The results showed that the average age of subjects with marker-positive SS was not statistically different from those who were negative for the marker (Figure 5.5). Age data was unavailable for one tumour (SS26; Table 5.5). In addition, the proliferation index based on Ki67 staining was very variable in all SS samples and did not correlate with the expression of any of the five markers (Table 5.5).

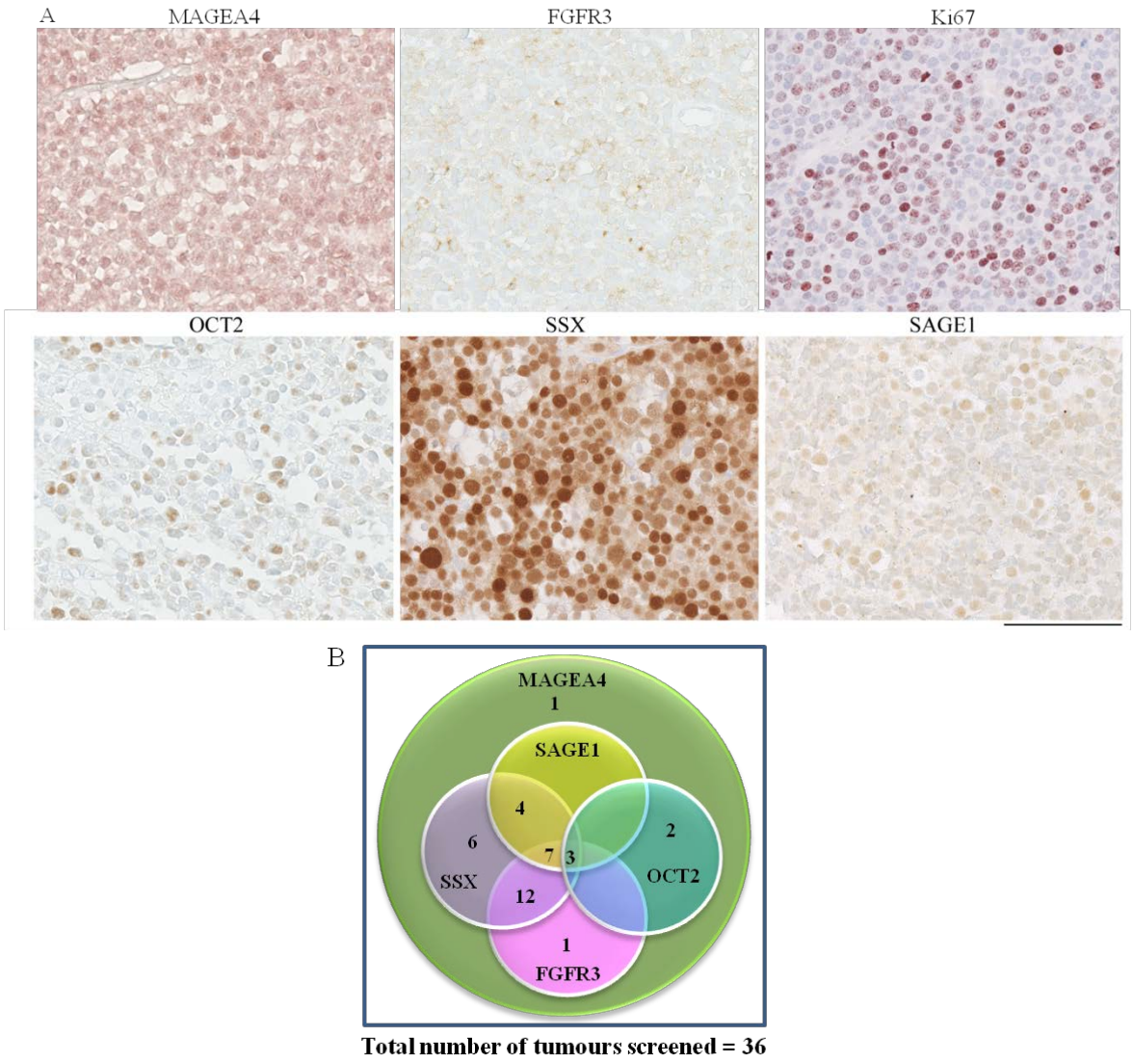

Figure 5.3: Expression of a panel of MAGEA4, FGFR3, Ki67, OCT2, SSX and SAGE1 in spermatocytic seminoma (SS). A. Examples of immunohistochemical detection of MAGEA4 (SS25), FGFR3 (SS35), Ki67 (SS22), OCT2 (SS38), SSX (SS15) and SAGE1 (SS28) in SS cases. Heterogeneous nuclear and cytoplasmic staining patterns with different intensities are seen in the tumour cells. Scale bar: 100µm. B. Venn diagram shows the relationship of MAGA4, FGFR3, OCT2, SSX and SAGE1 expression in SS.

Table 5.5: Summary of the immunohistochemical analysis in relation to the mutation status in the series of spermatocytic seminoma (SS).

Case no[1].	Age (years)	Mutation found[1]	MAGEA4	OCT2	SSX	SAGE1	FGFR3	Ki67 (% positive ± SD)
SS4†	75	-	+++ (str)	Neg	+ (w)	neg	+ǂ (w)	7.0, 11.5
SS5†	76	-	+++ (str)	Neg	+ (w)	neg	+ǂ (w)	42.2[2]
SS7†	50	-	+++ (str)	Neg	++ (str)	neg	+ (w)	n/a
SS8†	86	-	+++ (str)	Neg	+++ (str)	+ (w)	+++ (str)	0, 9.1
SS9†	87	*FGFR3* (K650E)	+++ (str)	Neg	+ (w)	neg	++ (str)	5.4, 0.9
SS10	61	-	+++ (str)	Neg	++ (str)	neg	++ (w)	6.4, 6.8
SS11†	64	-	+++ (str)	+ (w)	neg	neg	neg	24.2[2]
SS13†	34	-	+++ (str)	+ (w)	++ (str)	+++ (str)	+++ (w)	4.3, 5.4
SS14†	71	n/r	+++ (str)	Neg	+ (str)	+ (w)	++ǂ (w)	0, 0.9
SS15†	53	-	+++ (str)	+ (w)	+++ (str)	++ (str)	++ (w)	8.1, 6.1
SS16†	40	-	+ (str)	Neg	+++ (str)	neg	+ (w)	30.8, 26.1
SS17†	61	n/r	+++ (str)	Neg	neg*	neg	neg	18.5, 19.8
SS19†	44	-	++ (str)	Neg	++ (str)	+ (w)	+++ (w)	3.3, 17.2
SS20	37	-	++ (str)	Neg	++ (str)	neg* (w)	neg	15.8, 19.6
SS21	67	*HRAS* (Q61R)	+++ (str)	Neg	+++ (str)	+ (w)	++ǂ (w)	28.6, 13.7
SS22	41	-	+++ (str)	Neg	+ (w)	neg	neg	46.0, 59.5
SS23	69	*HRAS* (Q61R)	+++ (str)	Neg	++ (str)	neg	neg	44.3, 43.2
SS24	79	n/r	++ (str)	Neg	+ (w)	++ (w)	+++ (w)	13.5, 7.6
SS25	89	n/r	+++ (str)	Neg	++ (str)	neg	+ǂ (w)	0, 0[3]
SS26	n/a	-	+++ (str)	Neg	+++ (str)	++ (str)	neg	31.5, 24.4
SS27	55	-	+++ (str)	Neg	+++ (str)	+++ (str)	+++ (str)	22.8, 17.2
SS28	63	n/r	+++ (str)	Neg	+ (str)	+++ (str)	+++ (str)	n/a
SS29	75	n/r	+++ (str)	Neg	+ (str)	neg	++ (w)	2.2, 0
SS30	79	*HRAS* (Q61K)	++ (str)	Neg	+++ (str)	neg	+ǂ (w)	0, 1.1
SS31	75	*FGFR3* (K650E)	+++ (str)	Neg	+++ (str)	neg	+ǂ (w)	32.1, 44.2
SS32†	44	n/r	+++ (str)	+ (w)	++ (str)	+++ (str)	+++ (str)	9.2 ± 3.5
SS33	52	-	++ (str)	Neg	+ (w)	neg	+ (w)	2.7, 6.0
SS35	80	*HRAS* (Q61R)	+++ (str)	Neg	+++ (str)	neg	+++ (str)	22.0, 19.0
SS37	47	-	+++ (str)	Neg	+++ (str)	++ (str)	neg	46.4, 39.1
SS38	74	-	+++ (str)	++ (str)	neg	neg	neg	51.3, 62.0
SS39	43	n/r	+++ (str)	Neg	+++ (str)	++ (w)	neg	24.8, 23.5
SS40	67	*HRAS* (Q61K)	+++ (str)	Neg	++ (str)	neg	neg	6.2, 2.9
SS41	61	n/r	+++ (str)	Neg	neg	neg	+ (w)	3.8, 2.9
SS42	73	n/r	+++ (str)	Neg	++ (w)	neg	neg	15.5, 9.6
SS43†	87	n/a	++ (str)	Neg	++ (str)	+ (w)	neg	n/a
SS44	75	n/a	++ (str)	Neg	+ (w)	neg	neg	n/a

[1]Most of the tumours were investigated for candidate gene mutations in the previous study (Goriely, et al., 2009), so the original numbering is retained; -, no mutation found; n/r, no results owing to the low quality of tumour DNA; n/a, not available. † represents tumours which were included in the previous immunohistochemical study by Rajpert-De Meyts *et al* (2003). Staining score describes the proportion of positive cells as: +++, nearly all cells stained; ++, approximately half of the cells stained; +, a low percentage of cells stained; neg, no positive cell detected; or *, only single cells stained. ‡ indicates a subset of cells with nuclear positivity. Staining intensity is categorised as: str, strong; or w, weak. Ki67 results are presented as a percentage (%) of stained cells, when 1-2 separate counts were taken, or as % of stained cells ± unbiased estimate of SD, when four separate counts were taken (staining intensity was strong in all specimens). [2]Only a very small number of cells were available in the tissue core. [3]Ki67 antigen negative but some mitotic figures visible in the core.

A

	SSX (+)	SSX (-)	OCT2 (+)	OCT2 (-)	SAGE1 (+)	SAGE1 (-)
FGFR3 (+)	22	1	3	20	10	13
FGFR3 (-)	10	3	2	11	4	9
SAGE1 (+)	14	0	3	11		
SAGE1 (-)	18	4	2	20		
OCT2 (+)	3	2				
OCT2 (-)	29	2				

B

	SSX	OCT2	SAGE1
FGFR3	0.12	1.00	0.50
SAGE1	0.14	0.36	
OCT2	0.08		

Figure 5.4: Relations between antibody expression in 36 spermatocytic seminoma cases. A. The distribution of number of positive and negative tumours labelling with SSX, OCT2, SAGE1 and FGFR3 markers are depicted as (+) and (-) respectively. B. Diagram showing test for different staining distributions of pairs of antibodies indicated by *p*-values (Fisher's exact test).

	SSX (+)	SSX (-)	OCT2 (+)	OCT2 (-)	SAGE1 (+)	SAGE1 (-)	FGFR3 (+)	FGFR3 (-)
Average age of subjects (years)	63.1	65	53.8	65.5	59.5	66.4	65.0	61.5
p-values	0.67		0.18		0.24		0.54	

Figure 5.5: Relations between the patients' age and the expression of the markers in 36 spermatocytic seminoma cases. Diagram showing the association between the average age of the subjects and antibody expression (presence, +; absence, -), indicated by *p*-values (Student's *t*-test).

Having established the pattern of expression in the normal testis (Chapter 4) and SS (as described above), I examined the expression profiles of OCT2, SSX and SAGE1 in ISS to gain further insight into the cell populations expressing these markers. ISS is a pathological condition where the abnormal cells accumulate within the seminiferous tubule with or without partially preserved spermatogenesis (Section 1.8.3). The immunohistochemical analysis is based on only 4 cases (Table 5.6) owing to the apparent rarity with which this pattern is recognised. This revealed that most of the ISS cells clustering within the seminiferous tubules were either positive for SSX only, or co-expressed SSX and SAGE1 proteins (Table 5.6). A heterogeneous staining pattern suggesting tumour evolution was identified within two of the four ISS cases studied (Table 5.6, Figure 5.6A). There were some regions where ISS cells only expressed SSX but not SAGE1, while coexpression of both proteins was found in other regions. In the region closer to the overt SS, the expression of SAGE1 appeared to be gradually reduced and was totally undetectable in the cells located in close vicinity to the bulk of the tumour. However, SSX remained present even in cells close to the tumour and was found focally in the overt SS. OCT2 was found occasionally in the spermatogonia within the normal seminiferous tubule but was absent from the precursor stage of SS and the overt tumour in these 4 cases (Figure 5.6B, Table 5.6).

A.

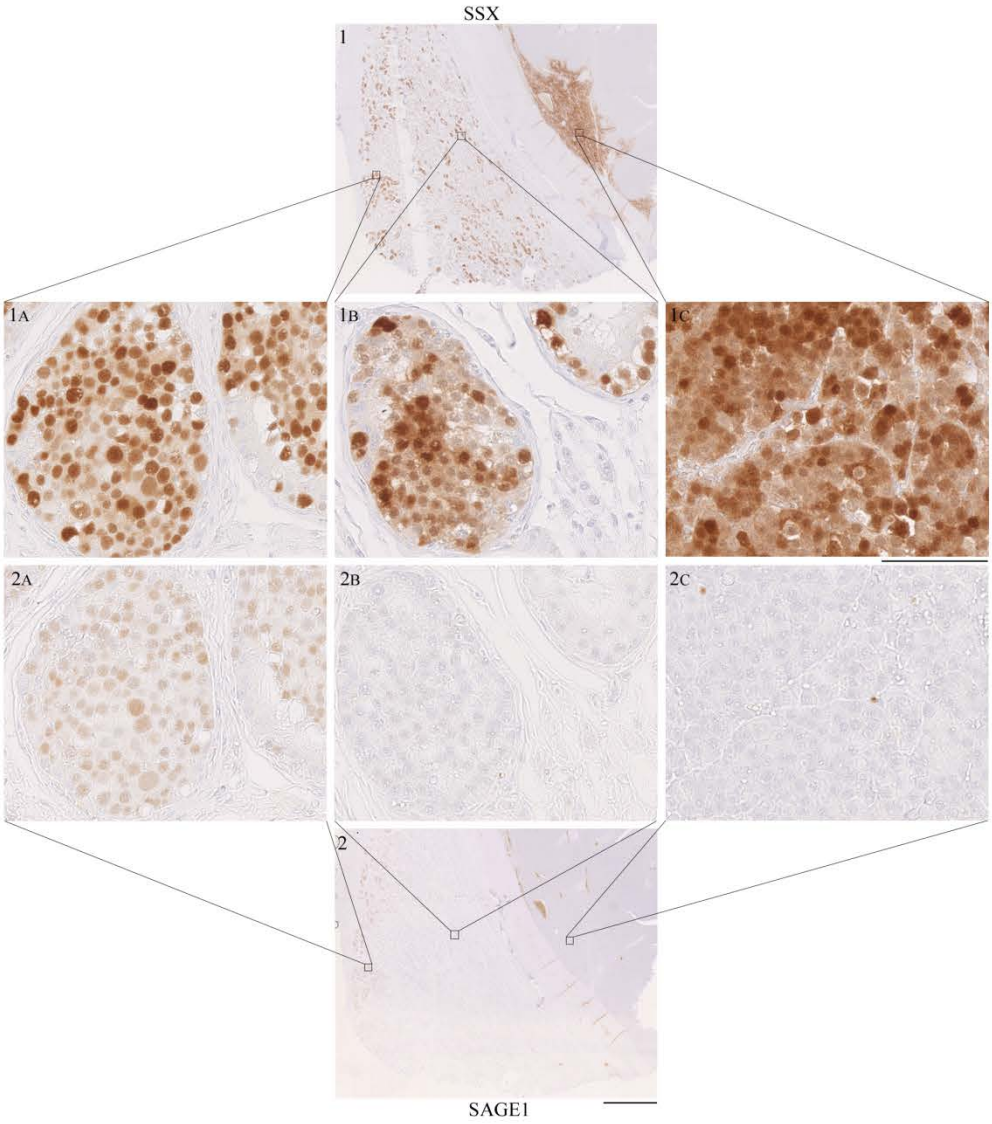

B.

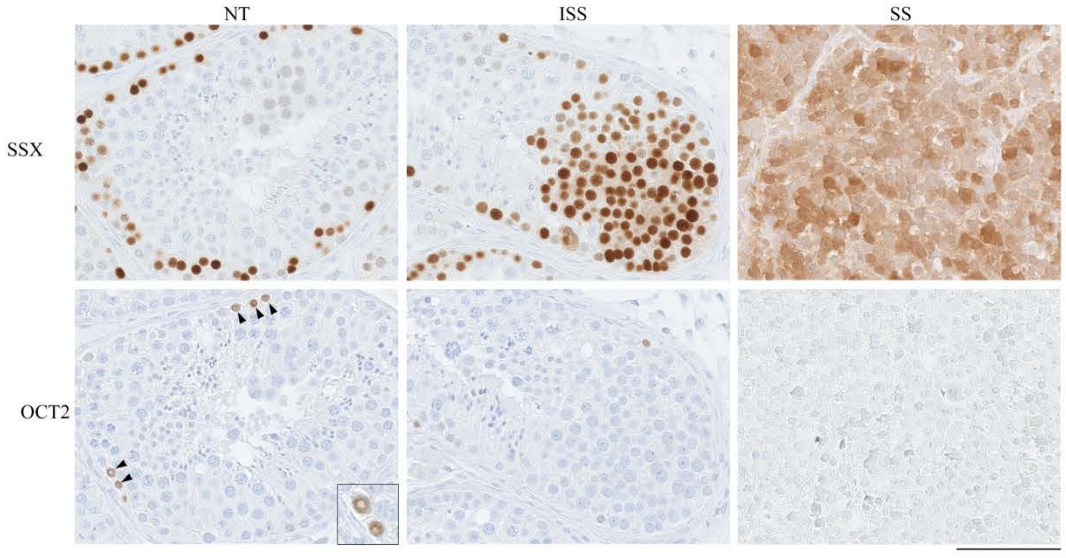

Figure 5.6: The distribution of spermatogonial markers during progression in two cases of intratubular spermatocytic seminoma (ISS).

A. ISS4. Sections labelled 1 and 2 provide low power (scale bar: 2.5 mm) overview of adjacent sections stained with SSX and SAGE1 respectively. A subpopulation of ISS tumour cells coexpressing both SSX and SAGE1 (1_A, 2_A) is mainly found in a region located away from the bulk of the tumour (starting from the edge of the sections). However, SAGE1 is absent and only SSX is observed in the ISS cells in close vicinity to tumour (1_B, 2_B). In the overt SS region, focal SSX expression is found (1_C) and no SAGE1-immunopositive cells are detected (2_C). Scale bar: 100 µm.

B. ISS2 showing the presence of normal tubules (NT), ISS and SS within a single section. Note positive staining for SSX, but negative staining for OCT2, within both SS and ISS. However, occasional cells (A_{dark} spermatogonia shown in the inset) are OCT2 positive in adjacent normal tubules (arrowheads). Scale bar: 100µm.

Table 5.6: Intratubular spermatocytic seminoma (ISS) samples included in the study. Staining score and the Ki67-based proliferation score are the same as in Table 5.5.

Case no.	Age (years)	Mutation found	Cell type	OCT2	SSX	SAGE1	Ki67 (% positive ± SD)
ISS1	75	*FGFR3* K650E	Overt SS (SS31)	-	+++	-	32.1, 44.2
			ISS	-	+++	++	36.6, 25.8
			SPG[1] (adjacent tubule)	+	+++	+	n/d
ISS2	68	-	Overt SS	-	+++	+++	39.6 ± 7.4
			ISS	-	+++	+++	19.1 ± 2.9
			SPG (adjacent tubule)	+	+	+	n/d
ISS3	31	-	Overt SS	-	+++	+++	22.9 ± 4.4
			ISS	-	+++	+++ (focal)	15.3, 18.5
			SPG (adjacent tubule)	+	+	+	n/d
ISS4	36	-	Overt SS	-	+++ (focal)	-	13.1 ± 7.1
			ISS	-	++	+++ (focal)	15.3, 5.0
			SPG (adjacent tubule)	+	+	+	n/d

[1] SPG, spermatogonia; n/d: not done.

5.2.2.2 Mutational analysis of samples with intratubular spermatocytic seminoma (ISS)

The mutation status in 24 SS samples (Table 4.1) was previously investigated for 17 different candidate genes (Goriely, et al., 2009) (Section 1.8.3). Tumours identified with *FGFR3* or *HRAS* mutations expressed SSX (7/7) and FGFR3 (5/7), whereas all OCT2-positive tumours were mutation negative (4/4); however these differences were not statistically significant. The two $OCT2^{+}/SSX^{-}/SAGE1^{-}$ samples were negative for *FGFR3* and *HRAS* mutations (Table 5.5) and exhibited a relative paucity of large cells (which in OCT2-negative samples ranged from 0.6 to 2.7% of the total cell population). One sample that included a region of ISS (ISS1) was positive for the *FGFR3* mutation 1948A>G encoding K650E. In this study, the bulk of tumour from three additional ISS cases was screened for activating mutations in exon 15 and exon 3 of *FGFR3* and *HRAS* respectively by restriction digest; these exons harbour the germline *FGFR3* mutation (1948A>G causing TDII) and two somatic *HRAS* mutations (181C>A and 182A>G encoding Q61K and Q61R respectively) that were previously identified in seven different SS cases (Goriely, et al., 2009). In addition, the initial PCR amplification covering *HRAS* exon 3 region was redesigned for ISS4 DNA sample owing to the poor DNA quality. The forward primer was replaced by HRAS IFW (Table 2.2), and the amplification process was modified in which the total cycle was increased from 36 cycles to 40 cycles with a new annealing temperature of 66 °C. No sequence variations were identified in these samples (Table 5.6, Figure 5.7), specifically excluding the presence of the TDII or previously identified *HRAS* mutations in these samples.

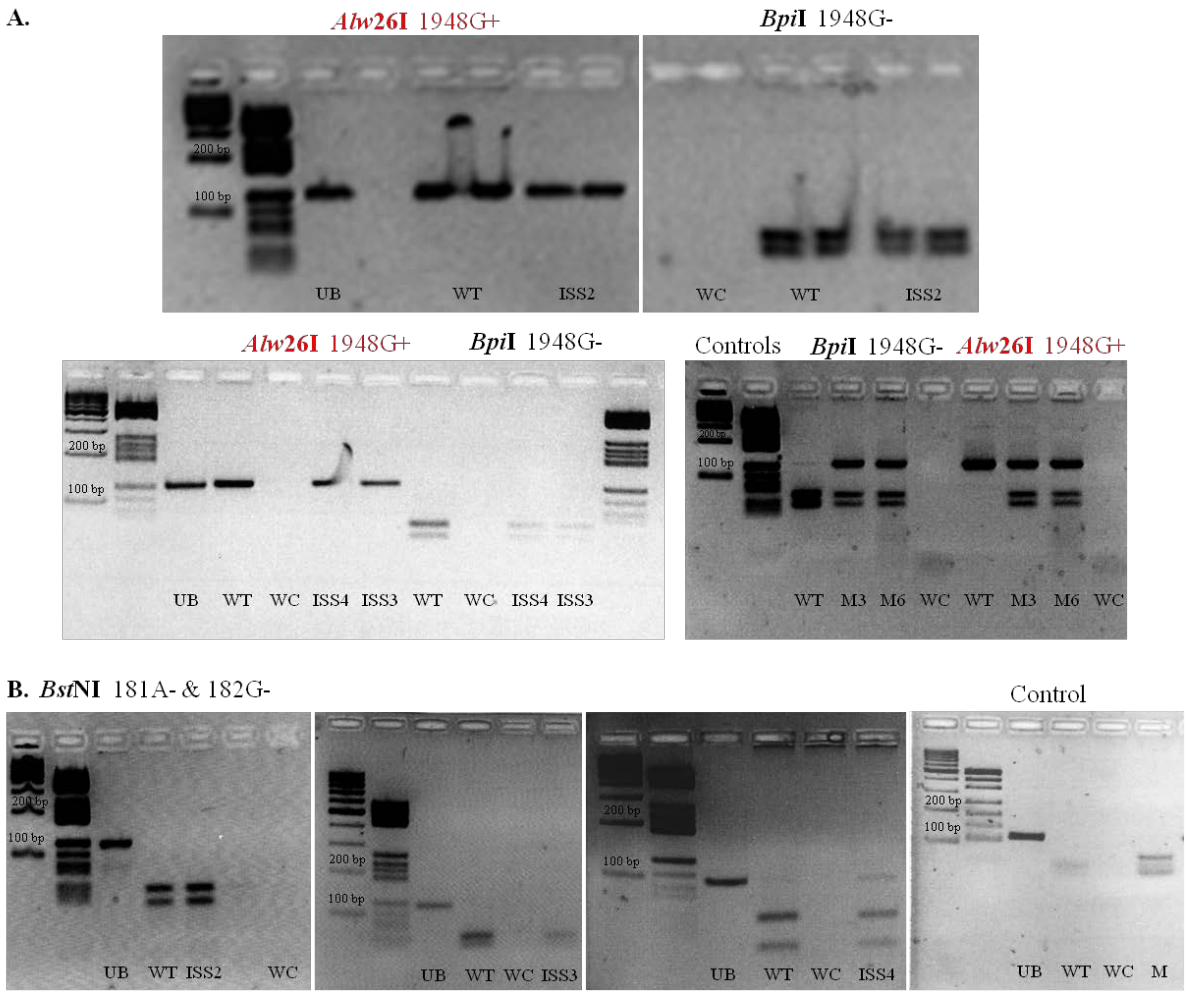

Figure 5.7: Diagnostic restriction digests on the bulk of tumour of intratubular spermatocytic seminoma (ISS) samples (ISS2-4). A. Canonical TDII mutations (*FGFR3* 1948A>G) was sought by restriction digests *Alw26I* (1948G+) or *BpiI* (1948G-) (Fermentas) for the *FGFR3* 1948A>G substitution. The normal allele is digested into two fragments (67 and 59 bp) using *BpiI* restriction enzyme as shown in WT. Alternatively, the mutation is recognised by the *Alw26I* restriction enzyme which cleave the mutant allele into two fragments (71 and 55 bp). The heterozygous digestion pattern of this mutation is shown in M3 (1948A>G heterozygote TD patient 3) and M4 (1948A>G heterozygote TD patient 6) samples from the controls (on the right). B. *BstNI* (Fermentas) restriction digest of 117 bp (for ISS2 and ISS3) or 93 bp (for ISS4) PCR product for genomic DNA samples from WT and ISS, shows that the normal allele (181A and 182G) is cut into either three fragments (57, 45 and 15 bp) for ISS2 & ISS3 or two fragments (57 and 36 bp) for ISS4. The control diagnostic pattern on the right demonstrates that sample (M) bearing the 182A>G mutation abolishes the *BstNI* restriction site (CCWGG), as shown by the mutant fragment (72 bp). No mutations were found in these specific sites of *FGFR3* and *HRAS* genes; faint resistant band evident for one sample on digestion with *BstNI* is caused by incomplete digestion. UB: undigested band; WT: wild type (normal blood control); WC: water negative control.

5.3 Discussion

5.3.1 Pilot study of genotyping and immunohistochemical analysis on urothelial carcinoma (UC)

Although the pilot study on UC was largely aimed at optimising protocols and immunohistochemical specificity, the results are of interest because they impact on the interpretation of data subsequently generated in SS. Gain-of-function point mutations in either *FGFR3* or *HRAS* are thought to be the main events initiating the tumourigenesis of papillary superficial (Ta) UC. In this study, activating *FGFR3* missense mutations encoding a cysteine amino acid change that, when present in the heterozygous state in the germline, cause severe, lethal skeletal dysplasia syndromes known as thanatophoric dysplasia I, TDI (Section 1.5.1.2) (Tavormina, *et al.*, 1995) were identified in 81% (26/32) of the UC cases; all of which showed the absence of any base substitution at codons 12 and 61 in the *HRAS* gene. Four previous studies on large panels of UC cases showed that the frequency of *HRAS* mutations at these particular codons were 7/98 (7%) (Jebar, et al., 2005), 3/92 (3%) (Platt, *et al.*, 2009), 12/257 (5%) (Kompier, *et al.*, 2010) and 6/218 (3%) (Sjodahl, *et al.*, 2011). Therefore, based on the sample size (n=32) and the average proportion of previous cases with *HRAS* mutations (4.2%), the failure to identify *HRAS* mutations in the current study was not too surprising as these genetic lesions would be expected in approximately 1-2 cases only. The mutually exclusive occurrence of *FGFR3* and *HRAS* genetic lesions was previously observed in urothelial carcinoma (Section 1.5.2), suggesting that RAS-MAPK pathway is responsible in the initiation and progression of transitional cell carcinomas as both genes are involved the same signalling pathway (Jebar, et al., 2005; Platt, et al., 2009; Kompier, et al., 2010). This is further supported by recent evidence demonstrating non-invasive clinical phenotypes including urothelial hyperplasia and low grade papillary superficial tumours in transgenic murine models bearing the constitutively active *HRAS* Gln61Leu mutation (Section 1.5.2) (Zhang, *et al.*, 2001; Mo, et al., 2007).

In order to understand the correlation between the mutation status of the tumours and the expression pattern of signalling molecules involved in RAS-MAPK and PI3K-AKT pathways which are involved in urothelial tumourigenesis (Knowles, *et al.*, 2009; Mitra and Cote, 2009), a subset of UC cases were selected to be stained for FGFR3, pERK and pAKT markers. In the small sample studied, the protein expression of FGFR3 was unrelated with the mutational status. Overexpression of pERK was observed in all the UC samples studied indicating the aberrant activation of RAS-MAPK pathway in papillary superficial (Ta) tumour development as phosphorylation of ERK1/2 is the hallmark of the activation of this cascade. However, this event has no strict correlation either with the FGFR3 protein expression or the tumour genotype; implicating that constitutive ERK activation may not be solely initiated by *FGFR3* mutation or protein upregulation. Instead, other point mutations or genetic alterations derived from various signalling molecules along the MAPK pathway including RAS or BRAF may also be responsible, as supported by recent identification of a significant minority of UC tumours (28/257; ~11%) harbouring mutations in the *HRAS*, *KRAS* or *NRAS* genes (Kompier, et al., 2010). These observations were obtained in parallel with data from other studies showing that the FGFR3 immunoreactivity was correlated neither with the mutational status nor with the pERK expression in UC (Tomlinson, et al., 2007a; Karlou, *et al.*, 2009). Likewise, study from Tomlinson *et al* (2007a) revealed that 45% of the UC with no detectable *FGFR3* mutations exhibited the upregulation of this protein activity although high level FGFR3 expression was observed in 85% of UC identified with *FGFR3* mutations (Tomlinson, et al., 2007a). Constitutive activation of RAS-MAPK signalling pathway in non invasive bladder cancer promotes proliferation, differentiation as well as senescence events via $p21^{CIP1}$ (Schulz, 2006). This may lead to the formation of a growth-arrested, self-limiting tumour which could explain the generally lower malignancy of UC.

In contrast, the expression pAKT (an activated downstream effector of the PI3K-AKT pathway) was heterogeneous amongst the chosen low grade UC tumours with different genotypes. Notably, AKT activation is often associated with cellular survival whereas ERK1/2 activation is involved in cellular proliferation (Schubbert, *et al.*, 2007). Approximately 13-27% of the low grade papillary tumours harbour missense mutations of the PI3-kinase (*PI3KCA*) gene (Lopez-Knowles, *et al.*, 2006; Platt, et al., 2009; Kompier, et al., 2010; Sjodahl, et al., 2011), which is involved in the induction of PI3K-AKT signalling pathway (Section 1.6). Interestingly, a subset of papillary non-invasive bladder carcinoma was found bearing gain-of-function point mutations in both *FGFR3* and *PIK3CA* genes and associated with early tumour progression; this co-occurrence event suggested that the *PIK3CA* alterations may exert additive oncogenic effects to *FGFR3* mutations in the initiation of UC tumourigenesis (Lopez-Knowles, *et al.*, 2006; Platt, et al., 2009; Kompier, et al., 2010; Sjodahl, et al., 2011).

Furthermore, using the immortalised normal human urothelial cells (TERT-NHUC), di Martino *et al* (2009) demonstrated that no significant increase in AKT activity was detectable in any of the TERT-NHUC expressing FGFR3 S249C, Y375C or K652E mutant; instead, ERK1/2 signalling pathway was activated by these FGFR3 mutants through the phosphorylation of FRS2α. Constitutive activation of AKT signalling cascades in squamous cell carcinoma cell lines was also found to trigger epithelial to mesenchymal transition and enhance motility which is required in tumour invasion and metastasis (Grille, *et al.*, 2003). All these fundamental key events suggest that the presence of AKT signal transduction pathway is crucial in promoting invasion in bladder tumourigenesis, in addition to the activation of RAS-MAPK pathway. Alternatively, these may also explain the relevance of the immunohistochemical analysis in this study showing the strong immunoreactivity with pERK in all the selected non-invasive, low grade UC tumours, whilst the number of pAKT-

positive cells in the tumours was variable, ranging from low to approximately half of the cells being stained (Table 5.4).

In short, these results from a pilot study on low grade UC of bladder cancer suggested that none of chosen signalling molecules markers has strict correlation with the tumour genotypes. This conclusion is consistent with more extensive analysis recently undertaken in other laboratories (Tomlinson, et al., 2007a; Karlou, et al., 2009). Superficial papillary bladder cancer (Ta) was viewed as having several features analogous to spermatocytic seminoma; recent molecular analysis on this testicular tumour also demonstrated a lack of clear relationship between the immunohistochemical status and the genetic lesions identified in the tumours (Goriely, et al., 2009). Nevertheless, this study allowed me to optimise many aspects of laboratory techniques and understand the variability of expression of proteins within or across each tumour, with either the same or different mutational backgrounds.

5.3.2 OCT2, SSX and SAGE1 reveal the phenotypic heterogeneity of spermatocytic seminoma

Analysis of the expression pattern in the normal testes (Chapter 4) showed that OCT2 was predominantly expressed in the A_{dark} spermatogonia and SSX in A_{pale}/B spermatogonia; SAGE1 was preferentially confined to B spermatogonia. Interestingly, the expression of OCT2 and SSX in the germ cells was mutually exclusive both during embryonic development and in adulthood. In accordance with these earlier observations, I report for the first time the immunohistochemical heterogeneity of SS.

Although a previous study suggested primary spermatocytes as the origin of this tumour (Looijenga, et al., 2006), the findings presented here confirmed that SS is most likely to have its origins in different spermatogonial cell populations characterised by either SSX or (in a minority) OCT2 expression. Notably, the hitherto unknown OCT2-positive SS represents a relatively rare subtype of this tumour (14%; 5/36); therefore, previous

comprehensive profiling of SS may have failed to identify this marker (Looijenga, et al., 2006). Alternatively, the expression of OCT2 may be a sign that some spermatogonia reverted to a less mature A_{dark} cell type, but this is less likely, because dark spermatogonia divide rarely and are considered a reserve population. In addition, SAGE1 was identified in a subset of SSX-expressing SS, indicating an origin from the same cell type but potentially at different stage of tumour progression.

This was further investigated in SS samples that included ISS (Section 1.8.3), where at least in some tubules the morphology of the cells suggested a transition between normal germ cells and SS tumour cells indicating that these ISS forms were indeed an early, pre-invasive stage in SS progression. In two of these rare cases, spatial differences of SSX and SAGE1 expression were identified in different subpopulations of ISS cells, with the invasive tumour expressing only SSX antigen (Figure 5.6A). The gradual loss of SAGE1- and gain of SSX-positive cells (the first expressed in spermatogonia, the latter in spermatogonia and early spermatocytes) in one ISS specimen with morphological signs of transformation may suggest that a subset of the transformed cells mature further towards pre-leptotene spermatocytes, which still express at least one of the SSX proteins. This is consistent with known plasticity of neoplastic germ cells, which may be at different stages of differentiation, and would explain the expression in SS of some genes that are also expressed in early spermatocytes (Looijenga, et al., 2006). Of note, SSX antibody recognises 3 different SSX antigens (dos Santos, et al., 2000) and there may be subtle differences in their expression pattern within germ cell maturation stages; all genes were represented in overt SS at the mRNA level (Looijenga, et al., 2006), but it is not known whether all are translated.

Taken together, the expression profile of OCT2, SSX and SAGE1 proteins in the present study provides further evidence to support the spermatogonial origin of SS. I suggest that SS is derived predominantly from the more mature spermatogonia (A_{pale} or B

spermatogonia), as proposed in previous studies (Romanenko and Persidskii Iu, 1983; Rajpert-De Meyts, et al., 2003), and a relatively small subset of this tumour type may derive from A_{dark} spermatogonia. However, the observed phenotypic heterogeneity of SS may reflect changes of gene expression occurring during tumour progression. Most of the subtypes of SS, except those with $OCT2^{+}$/ SSX^{-}/$SAGE1^{-}$ expression pattern, which seem to be locked in this phenotype, seem to retain plasticity and ability to partial maturation towards early spermatocytes, at least in a subset of tumour cells. These findings provide a new understanding of the histogenesis and progression of SS, which appears to be a more heterogeneous tumour type than previously thought. These findings have recently been published in *Journal of Pathology* (Lim, *et al.*, 2011).

5.3.3 Selection of the candidate markers to detect putative clones in the normal adult testis

The parallel screening of the panel of markers in 36 SS tumours revealed that MAGEA4 was expressed in all of the cases studied (36, 100%). MAGEA4 serves a germ cell specific marker which is present in all spermatogonia in the normal seminiferous tubules (Aubry, et al., 2001) (Chapter 3), and was consistently observed during the progression of this testicular neoplasm including ISS and the overt tumour. Hence, MAGEA4 was chosen as the first line screening marker to look for the presence of putative clones with spermatogonial origin in the normal adult testis.

Moving on, three spermatogonial markers characterised by their spatial distribution in the normal adult testis were selected and these are SSX, SAGE1 and OCT2. Looking at the number of spermatocytic seminoma cases stained by these markers, SSX which was found in 32 (89%) of the tumours, was chosen as the most crucial complementary marker after MAGEA4. Because of the coexpression of SAGE1 and SSX during testicular tumourigenesis, SAGE1 was also included in the panel of primary complementary marker to further describe the expression profile of the putative clone. Although the number of OCT2-

positive tumours (5; 14%) was low, OCT2 was chosen because of its predominant existence in A_{dark} spermatogonia (proposed as the spermatogonial stem cell with self-renewal properties) and reciprocal staining pattern with SSX. I expected that the probability of a putative clone being marked by OCT2 was likely to be relatively low compared to SSX and the coexpression of both markers would usually not be observed in a single putative clone. Furthermore, Ki67 (a universal proliferation marker) was found in 35 (97%) of the SS cases with variable proliferation index and limited number of spermatogonia in the normal seminiferous tubules. It was proposed that the clonal expansion events driven by paternal age-effect mutations may be eventually controlled by senescence before turning into overt tumours (Goriely, et al., 2009; Ota, *et al.*, 2009). The selection of this marker would provide new insight into the proliferation index of these mutational events occurring in the testis, although it was highly variable in SS and did not associate with the presence of any of the markers.

It has been proposed that pathological activation of MAPK and PI3K-AKT pathways could be responsible in promoting the proliferation of mutant spermatogonia in the normal adult testis, leading to the enrichment and formation of mutant clones over a course of time (Sections 1.8.4.1 and 1.8.4.2). Results from the pilot study on urothelial carcinomas suggests the elevated expression of signalling molecules (phospho-ERK and phospho-AKT) in tumours does not always correlate with their mutation status and the upregulation of FGFR3 protein expression as discussed previously. Earlier data has also shown that there was no correlation between the presence of phospho-ERK and the gene mutated in the mutation-positive SS tumours (Goriely, et al., 2009). Furthermore, PI3K-AKT pathway is less likely to be directly involved in the tumourigenesis of SS because the activation of this signalling cascade is usually associated with tumour invasion, metastasis and promotion of cell survival (Schubbert, et al., 2007); these are in contrast to the tumour biology of SS that usually

confined to its primary site and rarely metastasises (Section 1.8.3). Therefore, phospho-ERK and phospho-AKT were not used in the current immunohistochemical analysis of SS.

Finally, with the aim to establish possible correlations between the mutation status and expression profile of the putative clone, FGFR3 was included in the panel of complementary markers as it is both subject to paternal age-effect mutations and a potential surface biomarker of spermatogonia (von Kopylow, et al., 2010),. In short, MAGEA4 was identified as the ideal screening antibody to search for putative clones, which would be further characterised by five complementary markers including SSX, SAGE1, Ki67, OCT2 and FGFR3.

CHAPTER 6

A SEARCH FOR PUTATIVE CLONES IN THE NORMAL ADULT TESTIS

Chapter 6: A search for putative clones in the normal adult testis

6.1 Introduction

The work described in the previous chapters provided the prelude to the major goal of this study, which was to visualise and understand the proposed clonal events in the normal testis resulting from the enrichment of initial rare paternal age-effect mutations through selective proliferation of mutant spermatogonia. Previous experiments that demonstrated such events in the case of Apert mutations involved the destruction of the source testes in the process (Section 1.8.2). In the present study, I aimed to investigate the microscopic correlates of these proposed clonal events within the seminiferous tubules of structurally intact, normal adult testes. The choice of antibodies used was determined by the previous studies of their expression in normal testis and spermatocytic seminoma, as described in Chapter 3 and 5. Here, I have developed a *de novo* screening approach using these candidates and sought evidence for putative clones of cells that show altered patterns of protein expression within the normal adult testis.

6.2 Results

6.2.1 Sample collection and preparation from first individual

Paired testes were collected from one individual (33456, 71 years) who was diagnosed with prostate cancer (Section 2.2). The patient had been previously treated with deep X-ray therapy and followed by 3 months of hormone therapy with goserilin acetate (Zoladex), which stimulates the production of testosterone in a non-pulsatile (non-physiological) manner and causes the disruption of endogenous hormonal feedback systems, leading to the downregulation of testosterone production. Bilateral orchidectomy was done five years after these initial treatments were performed. Each testis was dissected into 7-8 slices by a histopathologist (Dr. Gareth Turner) in the Cellular Pathology Unit, John Radcliffe Hospital, University of Oxford. The left testis was processed into a total of 5 FFPE

blocks and 3 frozen fresh slices whilst 3 individual FFPE blocks were obtained from the right testis (Figure 6.1). The frozen fresh tissues were kept for future potential DNA analysis.

6.2.2 Methodology of screening for putative clones

To begin with, I developed a protocol which exploits immunohistochemical staining and digital microscopy technology using the left testis of sample 33456 (Figure 6.1). Of the five paraffin blocks of sample 33456, every block was trimmed and cut into ~ 200 sections of 5 µm each (Table 6.1) whilst the remaining (~ 2 mm = 2000 µm) were kept for future microdissection. Notably, the thickness of each section correlates with the diameter of spermatogonia that is approximately 5-7 µm (Paniagua, *et al.*, 1986); double-counting of the same spermatogonia for the number of cells in a clonal event could therefore be largely avoided in a quantitative analysis. Sections were stored at 4 °C for haematoxylin & eosin (H&E) and immunohistochemical staining. By evaluating the slide with H&E staining, the level of spermatogenesis of this testicular sample was scored as 9 (Dr. Gareth Turner) based on Johnsen's criteria (range 10-1; presence of spermatozoa scores 10, 9 or 8; spermatids (and no further) 7 or 6; spermatocytes (and no further) 5 or 4; only spermatogonia 3; only Sertoli cells 2 and no cells 1) (Johnsen, 1970).

Table 6.1: Summary of the number of sections for all the FFPE blocks of sample 33456 from the left testis.

Block no.	Number of sections
Block 1A	184
Block 1B	211
Block H&E	217
Block 1C	199
Block 1D	204
Total	**1015**

Based on the immunohistochemical analysis (Chapter 5), MAGEA4 was chosen as the first line screening marker together with five other complementary markers comprising SSX, SAGE1, Ki67, FGFR3 and OCT2. With the establishment of a list of candidate

markers, I decided to stain serial sections of every 50 µm (10 sections) of each FFPE block with MAGEA4. Collectively, there were 104 sections labelled with MAGEA4 antibody which were scanned and converted into digital images with the Olympus dotSlide digital virtual microscope at 200x magnification. Each testicular section consisted of approximately 2800-3000 seminiferous tubules; all of which were assessed independently using OlyVIA-Viewer software (Olympus) to provide an overview of the presence of clonal expansion events in the whole testis and develop predetermined criteria to flag up unusual clusters of cells positively stained with MAGEA4 (as described in Box 6.1).

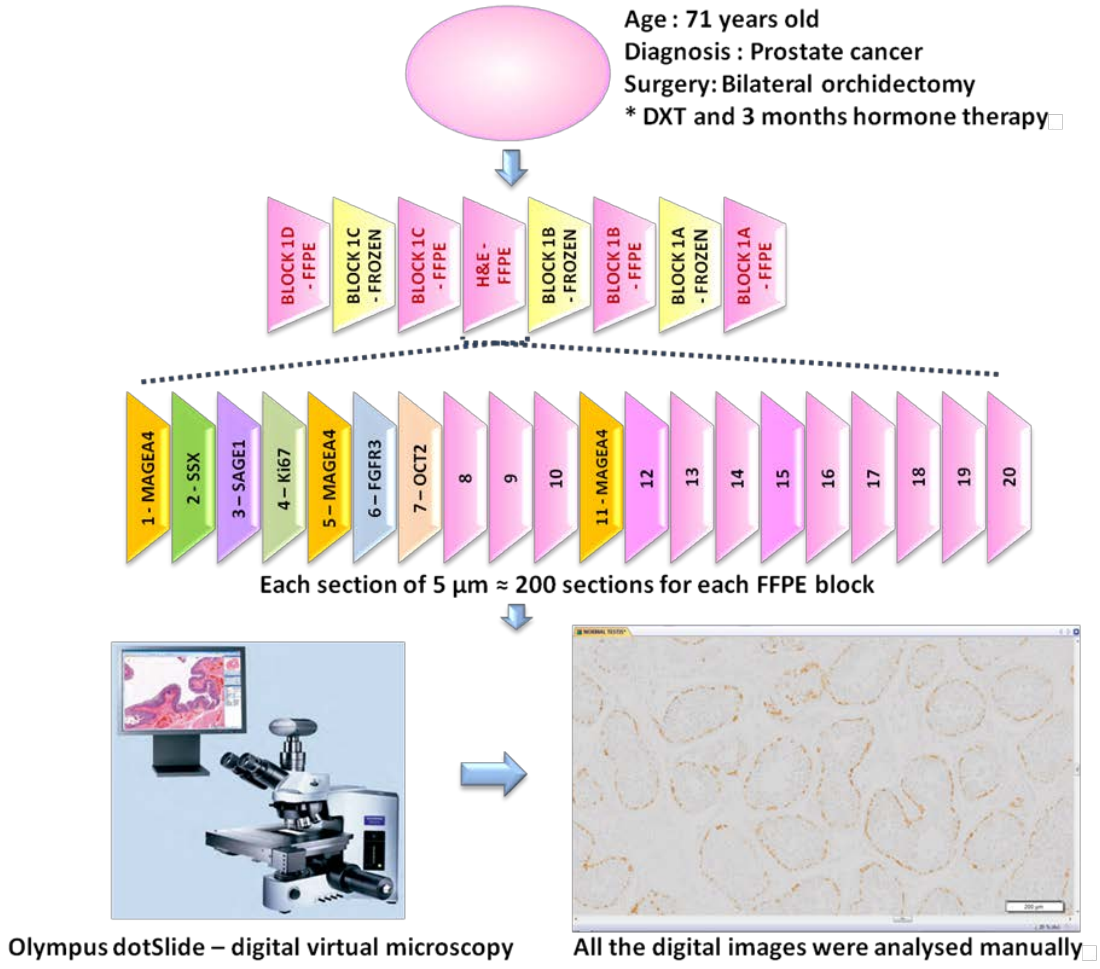

Figure 6.1 Strategy to detect the presence of putative clones in the normal adult testis. DXT: deep X-ray therapy.

Box 6.1: Summary of the criteria and scoring for unusual clusters of cells labelling with MAGEA4 and other screening antibodies.

Location	Criteria for positivity
Lumen	≥ 3 continuous positive cells, any pattern (clump or chain)
Periphery	≥ 3 positive cells in clump (preferably nuclear positivity, if applicable)

- Every cluster which met the criteria was annotated with 'red flag' using OlyVIA-Viewer software (Olympus).

Score	Examples
1 (Positive)	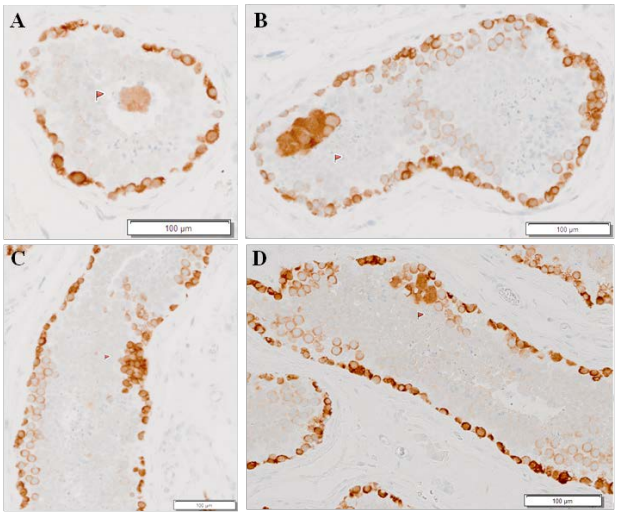 Clusters of cells were located in the lumen (A) and at the periphery (B, C & D) of the tubules. These unusual clusters of MAGEA4-positve cells met the preset criteria including number of MAGEA4-nuclear staining cells (≥ 3) and their location in the tubular structure. Scale bar: 100 µm.
0 (Negative)	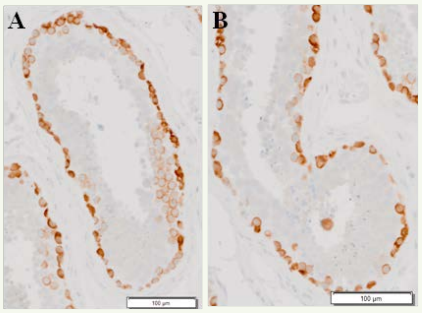 Groups of cells that did not meet the preset criteria particularly in the number of positive cells (<3), the staining pattern and the location of these cells. These were illustrated in (A) showing chain of membranous MAGEA4 staining cells located at the periphery and (B) where a single cell is situated in the lumen of the tubule. Scale bar: 100 µm.
0* (*Post hoc*)	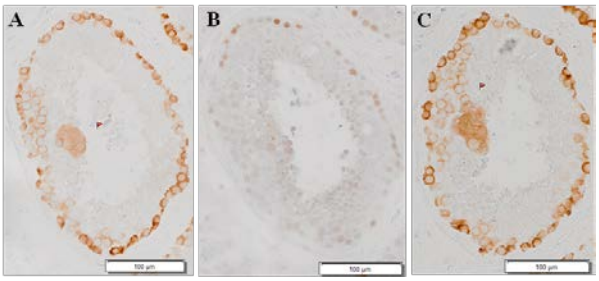 Clusters of cells that were not selected during the primary screening for several reasons including (i) the number of cells was lower than the preset criteria (<3), (ii) relatively low staining intensity or (iii) false negative error. These clusters were only scored in the *post hoc* analysis by comparing series of adjacent sections within the specified seminiferous tubule. For instance, (A), (B) and (C) were 3 serial sections in which (A) & (C) were stained with MAGEA4 and (B) was stained for SAGE1. The cluster located near the periphery of the tubule was identified independently in (A) and (C) (score = 1). However, (B) was only scored as positive (3 cells) in the post hoc analysis (score = 0*) by cross-checking with the adjacent sections (A) and (C). This was due to the relatively lower staining intensity of SAGE1 compared to MAGEA4. Scale bar: 100 µm.

Since apparent clusters of positive cells might have several trivial explanations including sectioning or staining artefacts, I wished to establish whether any of these clusters could be identified independently on different sections. However, the 50 µm separation of sections in the primary screen proved to be too great for the tubular architecture of serial sections to be matched with confidence. To address this, I selected regions from blocks 1B and 1D that yielded positive clusters in the primary screen and stained sections located every 20 µm and 30 µm alternately from the original sections with MAGEA4. These sections were scored independently using the original criteria (Box 6.1). This narrower spacing confirmed that some MAGEA4 positive clusters could be identified independently in different sections. Finally, to achieve a detailed picture of the size, shape and extent of these clusters, further MAGEA4 staining of sections at 10 µm and 15 µm intervals was undertaken, and these sections were again scored independently. Figure 6.2 shows the final pattern of MAGEA4 staining of the regions analysed in detail.

Moving on, these unusual clusters of cells expressing MAGEA4 were further analysed by intercalating complementary antibodies including SSX, Ki67, FGFR3, SAGE1 and OCT2 into the adjacent sections (Figure 6.2). The order of the complementary markers was decided based on their expression profile in spermatocytic seminoma. The nearest adjacent sections located before and after the 'original 50 µm-separated sections' were labelled with SSX and Ki67 which were positive in approximately 88% of the spermatocytic seminoma collectively (Chapter 5). This was followed by FGFR3 and SAGE1 on the subsequent adjacent sections. SAGE1 was occasionally excluded to accommodate other markers if the cellular cluster would resolve in less than two consecutive sections; nevertheless, this exclusion could be compensated by the staining with SSX due to coexpression pattern of SSX in all the SAGE1-positive spermatocytic seminoma (Chapter 5). With the least number of positive tumours (14%), OCT2 was the last candidate on the list

of complementary markers. All these neighbouring serial sections were assessed as separate entities to annotate the occurrence of the clonal events based on the characteristics designed earlier (see box 6.1). The antigenic profile of a cluster was studied by comparing between sections staining with the screening marker (MAGEA4) and nearest serial sections labelling with complementary markers (SSX, SAGE1, FGFR3, Ki67 and OCT2).

In summary, a definitive event (subsequently termed a *clone*) was established when a cluster of cells expressing the selected markers that met the predetermined criteria (see Box 6.1) was registered at least twice independently (total score ≥ 2) in the equivalent location on adjacent, or nearly adjacent sections. The requirement for independent identification should substantially decrease the number of false positive cases, which in turn increases the positive predictive value of the study. Additionally, the presence of complementary markers in the 'clone' was characterised either independently or during *post hoc* analysis which was introduced to identify false negative staining patterns resulting from a lower number of cells labelled with other screening markers and / or their reduced staining intensity compared to MAGEA4. In this analysis, a total of 84 clones fulfilling these criteria were discovered and their characteristics are presented in the following section.

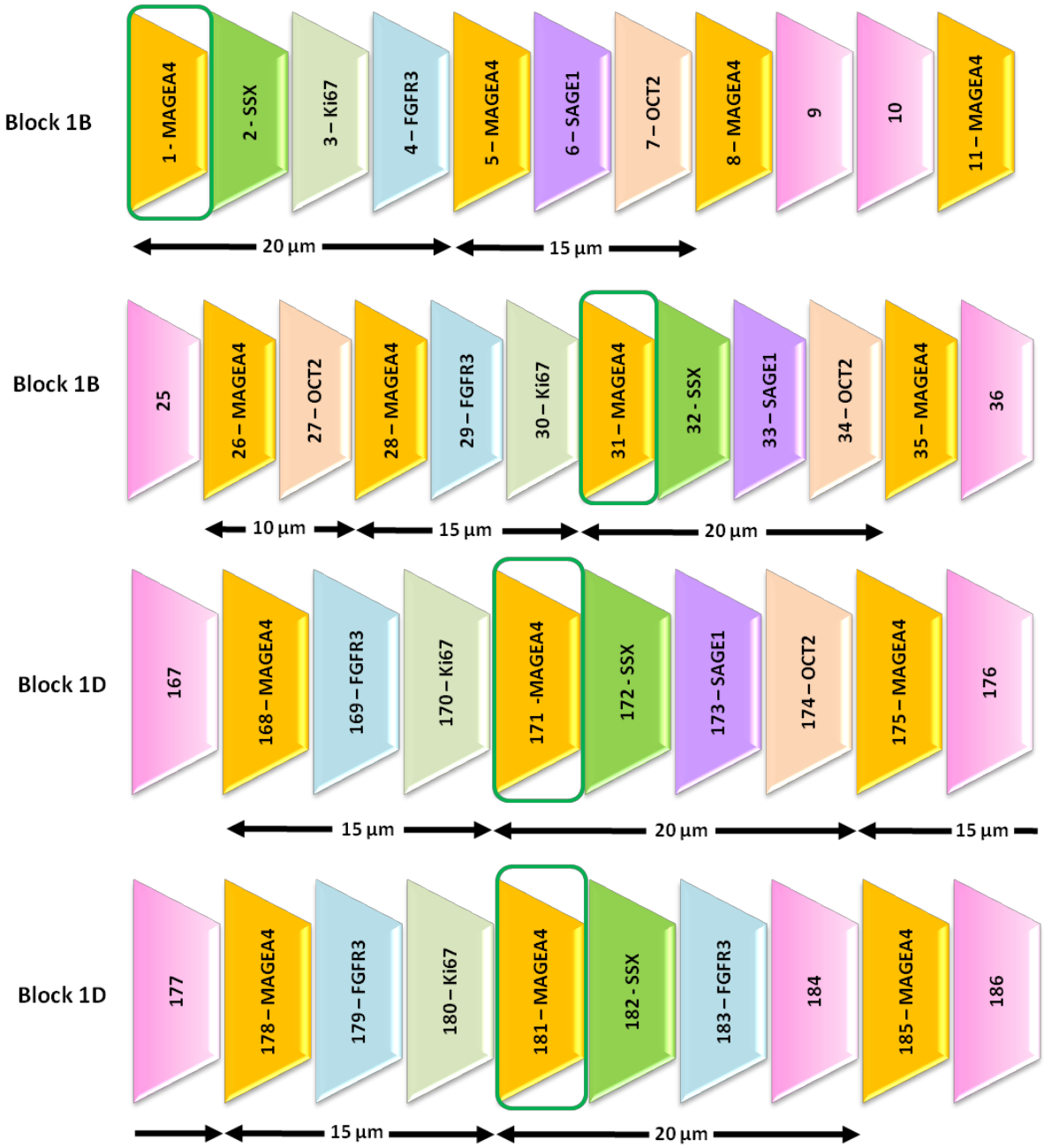

Figure 6.2 Screening method for putative clones in the normal adult testis using MAGEA4 in graded distances and further characterisation of neighbouring sections with complementary markers. Each of the serial sections was prepared at a thickness of 5 µm. The originally selected sections identified with unusual positively MAGEA4 staining cells are marked in green boxes. Using these sections as the template, bidirectional staining was applied together with additional protein markers (including SSX, SAGE1, Ki67, FGFR3 and OCT2) to investigate the size of the putative clone and the evolution of the clonal event.

6.2.3 Qualitative analysis of the putative clones

Based on the analysis of serial sections, I have sought evidence for putative clonal expansion events based on patterns of protein expression as defined in the previous section. Examples of these observations are presented below (Figures 6.3 – 6.8) in a generic format which includes a table (A; adapted from Table 6.4) demonstrating from top to bottom the antibodies used, the scoring of the clusters for each antigen (1, 0 or 0*), the number of cells in each cluster, the minimum length of each clone (highlighted in pink), the number of clusters scored in each section, the minimum number of cells in each clone and (B) a series of immunohistochemical images showing the expression of markers of interest in the putative clone. Estimation was made of the minimum length as well as the minimum number of cells of each clonal event. The minimum length was determined from the total number of 5 μm thick sections studied with the clonal events; quantitation did not extend beyond the first and last positive sections. The minimum number of cells in one clone was made up of the number of cells in each cluster expressing MAGEA4 and the amount calculated from linear interpolation between the numbers in two MAGEA4-positive slides where there was a gap, unless the section last described for the clone was stained with other markers. The calculation was made based on MAGEA4 clusters alone because other markers such as FGFR3 stained only a subset of cells of the clone (i.e. Figure 6.5 and 6.7) which did not represent its absolute total number of cells. For those clonal events negative for MAGEA4 (i.e. Figure 6.8), the minimum number of cells was estimated according to the amount of cells expressing their respective markers.

Unusual clusters of cells that were identified independently were marked with a ‘red flag’ in the images as shown in (B). Notably, the staining intensity of the selected markers was comparable in both clonal events and normal spermatogonia in the seminiferous tubules. In the course of establishing the clonal events, series of consecutive sections were examined

with *post hoc* analysis to identify clusters that were part of the clones but were missed in the primary screening. These events depicted as 0* were mainly caused by an incompatible total number of positive cells (n < 3) or false negative error which occurred when the unusual positively-staining cells meeting the preset selection criteria were not annotated.

A

Clone no	Location	Slide 168	Slide 169	Slide 170	Slide 171	Slide 172	Slide 173	Slide 174	Slide 175	Slide 176	Slide 177	Slide 178	Slide 179	Slide 180	Slide 181	Minimum number of cells
		MAGEA4	FGFR3	Ki67	MAGEA4	SSX	SAGE1	OCT2	MAGEA4	n.s	OCT2	MAGEA4	FGFR3	Ki67	MAGEA4	
1D-C1	Center	1 20 cells	0	0	1 22 cells	0	0	0	1 15 cells			0* 5 cells			0	180
		55 µm														
No of clusters identified in slide		89	33	9	61	14	3	0	97	NA	0	81	24	7	58	

B

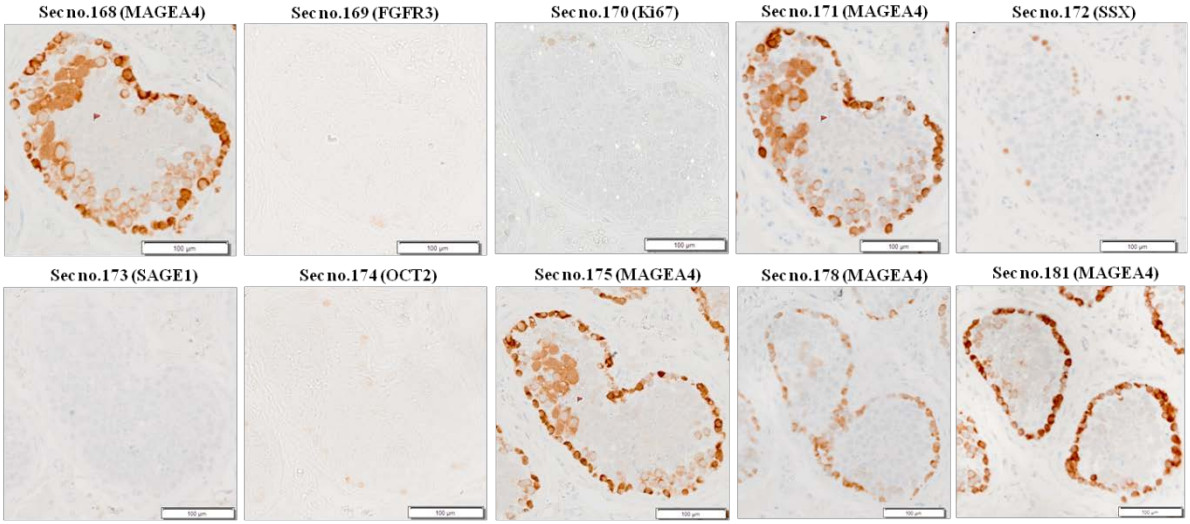

Figure 6.3: Identification of a putative clone expressing MAGEA4 only in normal adult testis (clone no: 1D-C1). The table (A) shows a series of consecutive sections from slides 168-181 which were chosen for further characterisation with a combination of complementary markers. Note the presence of a cluster of cells (tagged with red flag) located near the periphery of the seminiferous tubule (B). Immunoreactivity to MAGEA4 was identified independently in sections no.168, 171 and 175. The MAGEA4-postive cluster in section no.178 was only noted during the *post hoc* analysis (scored as 0* in panel A) owing to its low staining intensity. This cellular cluster was negative for additional markers tested including SSX, SAGE1, FGFR3, Ki67 and OCT2. The series of immunohistochemical images stained with MAGEA4 demonstrated that the structure of the seminiferous tubule changed and resolved gradually from section no.168 to section no.181. It was technically challenging to correlate a same seminiferous tubule from two sections that were ≥30 µm apart. Scale bar: 100 µm.

A

Clone no	Location	Slide 168	Slide 169	Slide 170	Slide 171	Slide 172	Slide 173	Slide 174	Slide 175	Minimum number of cells
		MAGEA4	FGFR3	Ki67	MAGEA4	SSX	SAGE1	OCT2	MAGEA4	
1D-C14	Center	0* 7 cells	0	0	1 12 cells	1 13 cells	0* 7 cells	0	NA	58
		30 µm								
No of clusters identified in slide		89	33	9	61	14	3	0	97	

B

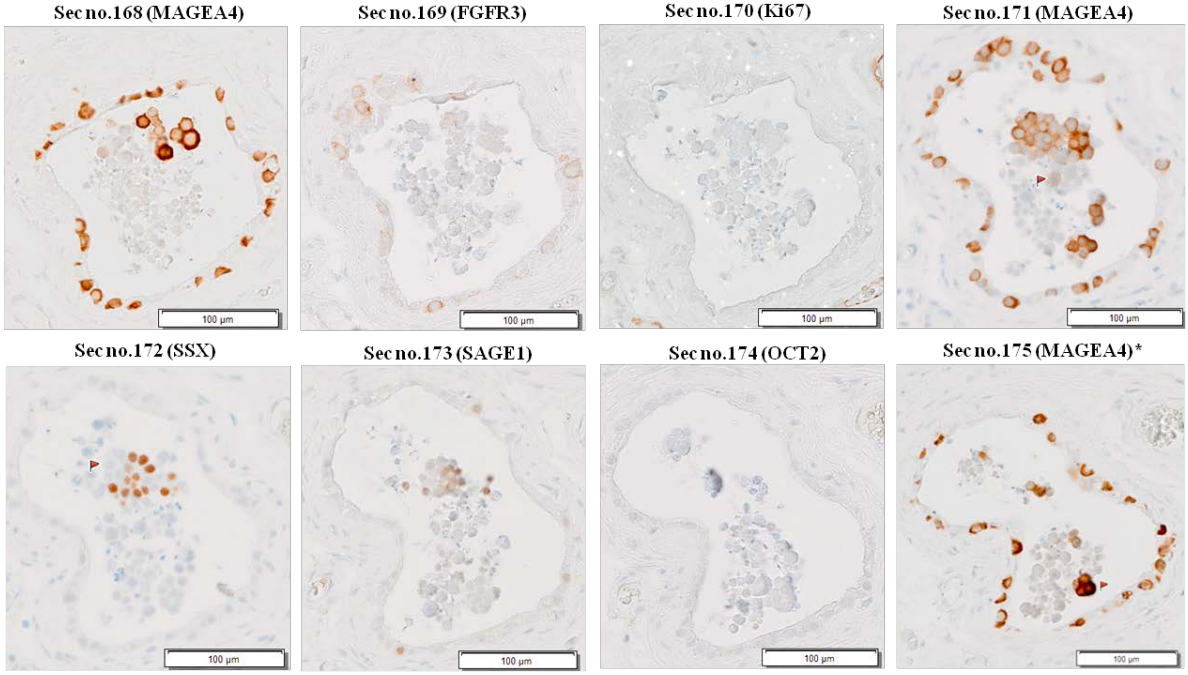

Figure 6.4: Identification of a putative clone expressing MAGEA4, SSX and SAGE1 in normal adult testis (clone no: 1D-C14). Clusters of cells expressing MAGEA4 and SSX (tagged with red flag) located in lumen of the tubule were identified independently on sections no.171 and 172. The *post hoc* analysis extended the clone to sections no. 168 and 173, which had not been flagged; it also showed that the clone is negative for FGFR3 and Ki67. Scale bar: 100 µm.

A

Clone no.	Location	Slide 1	Slide 2	Slide 3	Slide 4	Slide 5	Slide 6	Slide 7	Slide 8	Minimum number of cells
		MAGEA4	SSX	Ki67	FGFR3	MAGEA4	SAGE1	OCT2	MAGEA4	
1B-C2	Periphery	1 80 cells	0	0	1 10 cells	1 23 cells	0	0	0* 3 cells	287
		40 µm								
No of clusters identified in slide		29	22	1	7	53	13	0	55	

B

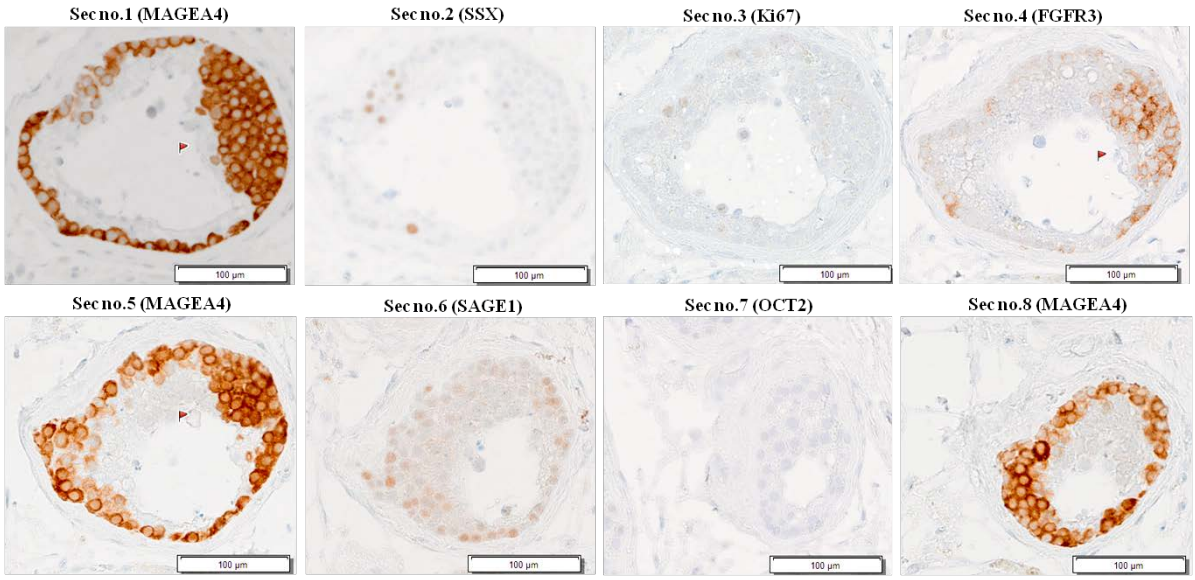

Figure 6.5: Identification of a putative clone expressing MAGEA4 and FGFR3 in normal adult testis (clone no: 1B-C2). All the spermatogonia residing adjacent to the basement membrane of the seminiferous tubule were labelled with MAGEA4, forming a ring-like pattern. Note the presence of a cluster of cells (tagged with red flag) derived from the periphery of the tubule expressing MAGEA4 and FGFR3 on adjacent serial sections but negative for SSX, Ki67, SAGE1 and OCT2. Section no.8 was screened negative but 3 cells were scored positive on *post hoc* analysis. Bidirectional screening (as described in Figure 6.2) was not applicable to clusters of cells present in section no.1 because it was the first section of the FFPE tissue block. Scale bar: 100 µm.

A

Clone no	Location	Slide 26	Slide 27	Slide 28	Slide 29	Slide 30	Slide 31	Slide 32	Slide 33	Slide 34	Slide 35	Minimum number of cells
		MAGEA4	OCT2	MAGEA4	FGFR3	Ki67	MAGEA4	SSX	SAGE1	OCT2	MAGEA4	
1B-C36	Center	0* 4 cells	0	1 7 cells	0* 1 cell	1 9 cells	1 21 cells	1 17 cells	1 15 cells	0	0	98
		40 µm										
No of clusters identified in slide		90	0	98	24	35	62	25	45	0	90	

B

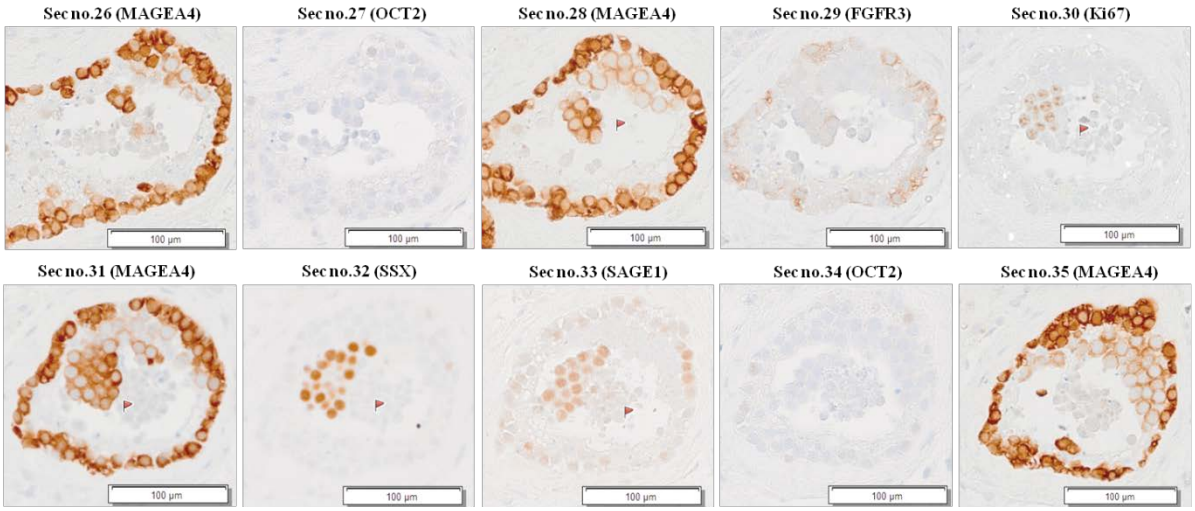

Figure 6.6: Identification of a putative clone expressing MAGEA4, SSX, SAGE1, FGFR3 and Ki67 in normal adult testis (clone no: 1B-C36). Note the presence of a clone of positively staining cells defined by its immunoreactivity to MAGEA4, SSX, SAGE1 and Ki67, observed within the tubule on 4 consecutive serial sections. This event occurred in the lumen of the tubule and its evolution was observed across the serial sections starting from section no.26 until section no.35. Section no.26 was scored as positive (4 cells) in the *post hoc* analysis. Interestingly, this event expressed a similar antigenic pattern to that observed during the progression of spermatocytic seminoma (Chapter 5). Scale bar: 100 µm.

A

Clone no	Location	Slide 26	Slide 27	Slide 28	Slide 29	Slide 30	Slide 31	Slide 32	Slide 33	Slide 34	Slide 35	Minimum number of cells
		MAGEA4	OCT2	MAGEA4	FGFR3	Ki67	MAGEA4	SSX	SAGE1	OCT2	MAGEA4	
1B-C37	Center	0	0	1 9 cells	0* 2 cells	0	1 13 cells	0	1 3 cells	0	0	55
				30 µm								
No of clusters identified in slide		90	0	98	24	35	62	25	45	0	90	

B

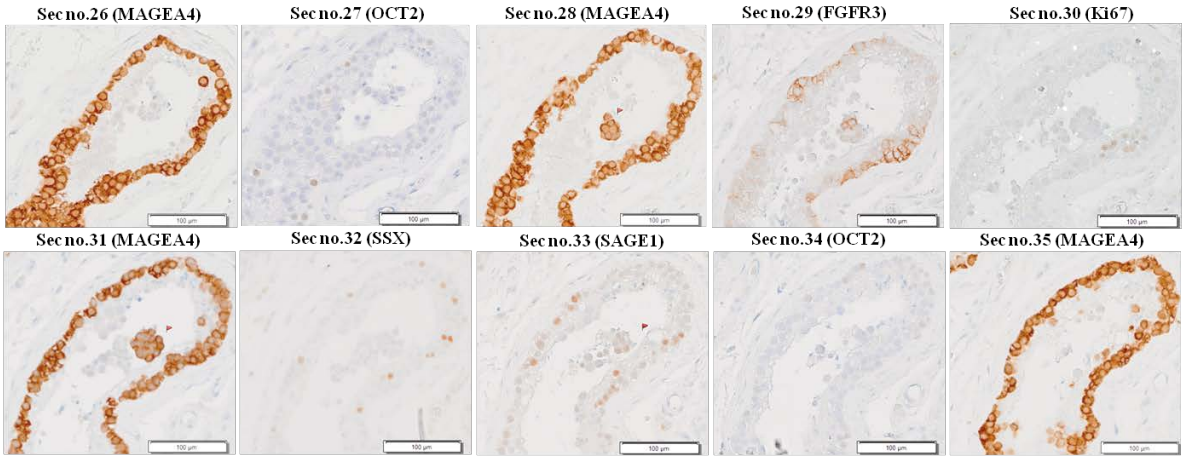

Figure 6.7: Identification of a putative clone expressing MAGEA4, SAGE1 and FGFR3 in normal adult testis (clone no: 1B-C37). As observed in consecutive serial immunohistochemical images, the cellular cluster which located in the lumen of the tubule was first found on section 28 and was last observed on section 33. It was identified independently in sections stained with MAGEA4 and SAGE1 whilst the presence of FGFR3 protein was recognised only after a *post hoc* analysis owing to the limited number of positive cells (<3). SSX, Ki67 and OCT2 were absent in this cluster of cells. Scale bar: 100 µm.

A

Clone no	Location	Slide 29	Slide 30	Slide 31	Slide 32	Slide 33	Slide 34	Minimum number of cells
		FGFR3	Ki67	MAGEA4	SSX	SAGE1	OCT2	
1B-C41	Center	0	0	0	1 10 cells	1 14 cells	0	24
					10 µm			
No of clusters identified in slide		24	35	62	25	45	0	

B

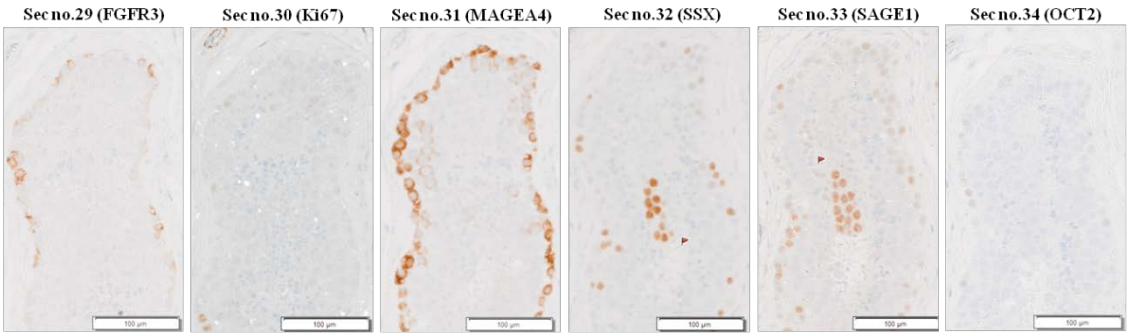

Figure 6.8: Identification of a putative clone expressing SSX and SAGE1 in normal adult testis (clone no: 1B-C41). This is one of the few examples where a putative clone was identified that was negative for MAGEA4 expression. In this case, the cluster of cells was positive for SSX and SAGE1 only. The specificity of all markers including MAGEA4 was confirmed by their expression in spermatogonia situated at the periphery of the tubule (internal positive control). Scale bar: 100 µm.

A total of 84 putative clones were identified within Block 1B and Block 1D; of which 61 (73%) were positive for MAGEA4 only (Figure 6.3), 21 (25%) showed the coexpression of MAGEA4 and other complementary markers (Figures 6.4-6.7) whilst the remaining 2 (2%) expressed SSX and SAGE1 only (Figure 6.8) without the presence of MAGEA4. The patterns of positive staining identified are summarised as Venn diagrams in Figure 6.9. By comparing the expression profile of the putative clones between the two blocks, clonal events in Block 1B demonstrated more varieties of combinations of markers whilst in Block 1D, coexpression of SSX and / or SAGE1 in MAGEA4-positive cells was only observed in five independent events. All the staining with FGFR3 and Ki67 worked equally well in both tissue blocks as assessed by the immunopositivity in normal spermatogonia. Independent analysis on slides labelled with complementary markers discovered the presence of clusters of cells expressing SSX and SAGE1 only (Figure 6.8). The absence of MAGEA4 may raise the question of the origin of these cells located in the

lumen of the tubules; however, this could be clarified by the properties of SSX and SAGE1 as markers for more differentiating spermatogonia in the normal adult testis (Chapter 4).

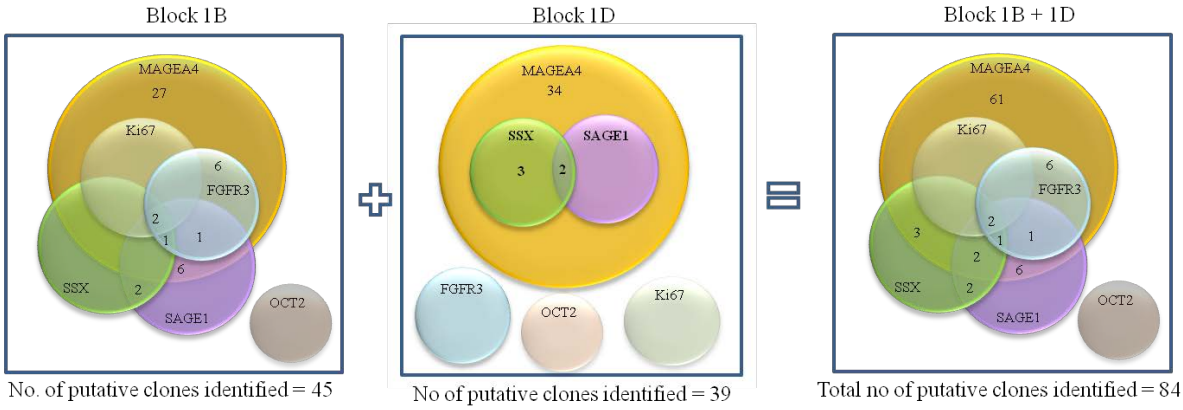

Figure 6.9: Summary of the antigenic profile of the putative clones identified in the normal adult testis. Venn diagram shows the relationship of MAGEA4, SSX, SAGE1, FGFR3, Ki67 and OCT2 expression in the putative clones studied in Block 1B and 1D of sample 33456. Most of the cellular clusters expressed MAGEA4 but there were two positively-staining clusters with SSX and SAGE1 only.

6.2.4 Quantitative analysis of the putative clones

Two selected series of consecutive sections representing ~ 9% of the total sections of block 1B and 1D were screened for the presence of clonal events of interest (as described in 6.2.2 and Figure 6.2). Every section contained ~ 2900 seminiferous tubules and clusters matching the predetermined selection features (score = 1; see Box 6.1) were identified and the overall numbers are summarised in Table 6.2. For instance, 979 clusters were noted independently in 14 sections stained with MAGEA4, on average 69.9 clusters per section; of which 20% were involved in the identification of 82 putative clonal events as defined in Section 6.2.2. The proportion of clones detected by MAGEA4 was approximately 13.71 per section which is the highest compared to other markers including SSX (2.25), SAGE1 (3.33), FGFR3 (1.0) and Ki67 (0.25). In addition, two putative clones were established by independent events labelled with SSX and SAGE1 markers only.

Table 6.2: Summary of the number of independent clusters identified in relation to the antibodies used and their participation in forming putative clones within the selected serial sections of sample 33456/08.

Antibody	No of sections stained	No of clusters identified	Clusters per section	No of clusters involved in forming putative clones	Clones per section	No of putative clones
MAGEA4	14	979	69.9	192 (20%)	13.71	84
SSX	4	74	18.5	9 (12%)	2.25	
Ki67	4	22	5.5	1 (5%)	0.25	
FGFR3	5	95	19	5 (5%)	1.0	
SAGE1	3	61	20.3	10 (16%)	3.33	
OCT2	5	0	0	0 (0%)	0	

False negative errors (i.e. *post hoc* observations scored as 0*) were seen in clusters expressing MAGEA4, SSX, SAGE1, FGFR3 and Ki67 markers as summarised in Table 6.3. The false negative error rate of SSX was the lowest (1/10 = 10%), followed by MAGEA4 (52/244 = 21.3%), SAGE1 (4/14 = 28.6%) and lastly FGFR3 and Ki67 which both demonstrated a false negative error rate as high as 50%. Together, these data further support the choice of selecting MAGEA4 as the first line screening marker after comparing its high average proportion of clones identified per section (13.71) and the relatively low rate of false negative results (21.3%) with other markers. The list of clones is summarised in Table 6.4 which employs the same format as already described in Figures 6.3-6.8. The staining patterns of all 84 clones are provided on the CD-ROM accompanying this thesis.

Table 6.3: Summary of the false negative error rate of each antibody.

Antibody	True positive observations	False negative observations	False negative error rate
MAGEA4	192	52	21.3% (52/244)
SSX	9	1	10% (1/10)
Ki67	1	1	50% (1/2)
FGFR3	5	5	50% (5/10)
SAGE1	10	4	28.6% (4/14)

Following these, study was conducted to illustrate the relationship between the minimum number of cells in each clone (calculated as described in Section 6.2.3) and the expression of markers (Figure 6.10). The majority of the clonal events (73/84; 87%) consisted of ≤100 cells; 47 (56% of total) were made up of ≤50 cells. There were 11% (9/84) of the putative clones containing between 100 and 200 cells; of which 6/9 were positive for MAGEA4 only and 3/9 combined MAGEA4 with combinations of SAGE1, SSX, and FGFR3. Interestingly, two clonal events were much larger than the others, comprising 287 (clone 1B-C2; Table 6.4; Figure 6.5) and 356 cells (clone 1B-C1; Table 6.4; Figure 6.11) and located at the periphery and the centre of the seminiferous tubules respectively.

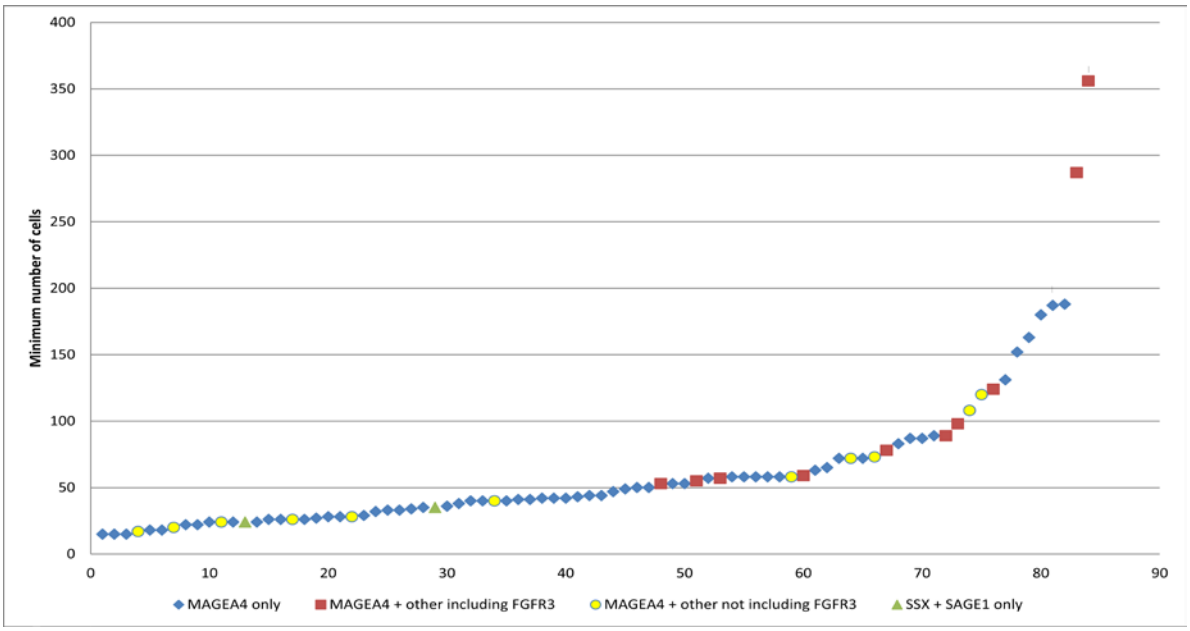

Figure 6.10: Distribution of the minimum number of cells of each clone in relation to the expression of markers. Asterisk (*) indicates clone where slide at the edge of region analysed was positive for ≥10 cells. Totals include markers scored positive on the *post hoc* analysis.

These clones, which were both truncated on one side of the consecutive serial sections, were positive for MAGEA4 and FGFR3; in addition to the presence of SAGE1 in clone 1B-C1. The sizes of these clones, together with others (labelled with * in Figure 6.10 where ≥100 cells were positive at the border of the region analysed), may have been significantly

underestimated owing to a boundary effect. Interestingly, amongst the 23 putative clones expressing more than one marker, all 10 of the FGFR3-labelled clones contained at least 50 cells compared to those that were negative for FGFR3 consisting of ≤50 cells in the majority of cases (8/13 = 62%). These FGFR3 positive clones potentially reflect gain-of-function *FGFR3* paternal age-effect mutations which drive the clonal growth.

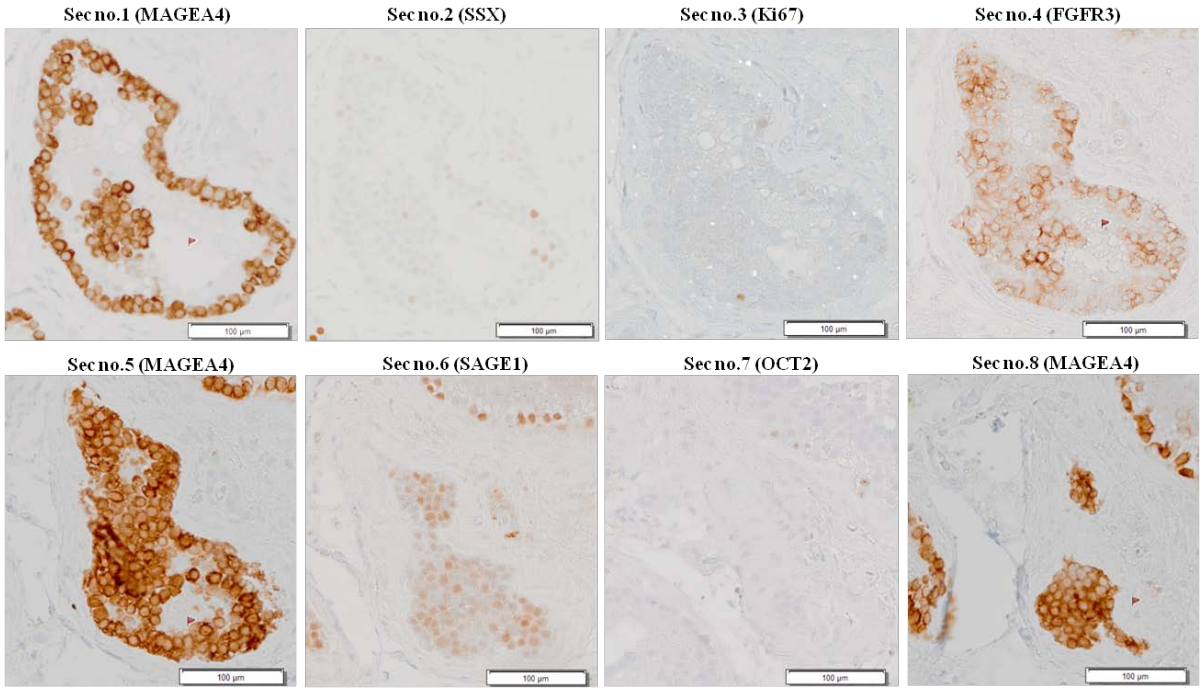

Figure 6.11: Identification of a putative clone expressing MAGEA4, FGFR3 and SAGE1 in a seminiferous tubule (clone no: 1B-C1). It was present in the center of the semiferous tubule which evolved across the consecutive sections from section no.1 until section no.8. This clone consisted of the highest number cells amongst all the list of clonal events described in this study. Scale bar: 100 µm.

Further statistical analysis demonstrated that the minimum number of cells in clones positive for both MAGEA4 and other markers was significantly larger than clones expressing MAGEA4 only (Mann-Whitney U test, p = 0.029); suggesting that the heterogeneity of marker expression may be associated with the clone genotype or some artefactual explanation. For instance, the homogenous expression profile of smaller clonal events comprising a limited number of cells (≤50 cells) may result from technical limitations as these microclones tend to resolve within the distance of few sections (e.g. 10 µm ≡ the

distance between three 5 µm sections) making the complete immunohistochemical characterisation of microclones impossible.

6.2.5 Analysis of a testicular block from second individual

To demonstrate that the occurrence of putative clones within the testis was not peculiar to the particular individual studied, a FFPE testicular block for a different 75 year old man (sample no: H10/24188) was retrieved from the archive of the Cellular Pathology Unit, John Radcliffe Hospital, Oxford according to the application procedures outlined by the Oxford Centre for Histopathology Research (OCHRe). The testicular tissue was removed due to an incarcerated left inguinal hernia. Its spermatogenesis level was graded as 8 (Dr. Gareth Turner) based on Johnsen's criteria (Johnsen, 1970).

The strategy applied on sample 33456 (as described in Section 6.2.2) was slightly modified and is summarised in Figure 6.12. The testicular block was first sectioned for a total of twenty one slides at a thickness of 5 µm whilst the remaining was reserved for future

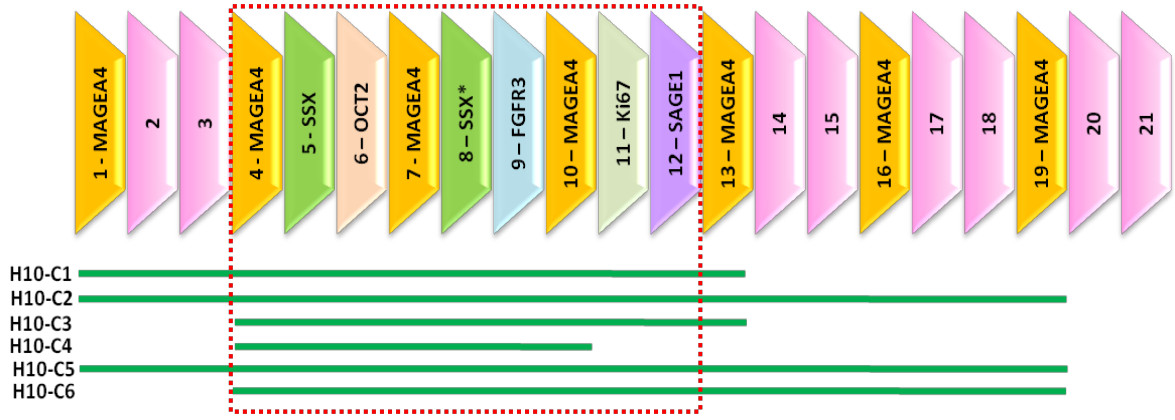

Figure 6.12: Modified screening approach for a normal testicular sample (H10/24188). A total of seven sections were labelled with MAGEA4, consisting of slides every 15 µm. The adjacent sections of MAGEA4-stained slide were characterised independently with complementary markers including SSX, FGFR3, Ki67, SAGE1 and OCT2. Six clonal events were discovered; all of which were labelled accordingly on the left whilst, the green line after each clone represents the number of slides identified with the event. The red box highlights the consecutive section comprising most of the clonal events studied. Staining with SSX antibody was repeated on section no.5 owing to the inconsistent results on section no.8 (*). 1 section ≡ 5 µm.

microdissection. Consecutive sections of every 15 µm were stained with MAGEA4 and analysed to annotate unusual positively-stained clusters of cells using the same criteria as before (Section 6.2.2; Box 6.1). By comparing the MAGEA4-labelled slides across the whole series, six putative clonal events satisfying the preset criteria were identified. For each event, the number of positive cells in every MAGEA4-staining section was counted and its length was determined with reference to the number of slides identified with the particular cluster. The adjacent sections were further investigated independently with a combination of complementary markers including SSX, FGFR3, Ki67, SAGE1 and OCT2 to establish the antigenic profile of the putative clones.

Using the standard method as described in Section 6.2.3 and 6.2.4, systematic analysis of ~ 1842 seminiferous tubules on each serial section revealed the presence of six putative clones which localised either in the lumen or at the periphery of the tubule (as summarised in Table 6.5; Figure 6.13A). Unusual cell clusters of each marker which satisfied the criteria were studied independently and are summarised in Table 6.6.

Table 6.6: Summary of the number of independent clusters which identified in relation to the antibodies used and their participations in forming putative clones within the selected serial sections of sample H10/24188.

Antibody	No of sections stained	No of clusters identified	Clusters per section	No of clusters involved in forming putative clones	Clones per section	No of putative clones
MAGEA4	7	181	25.8	6 (3%)	0.86	6
SSX	1*	5	5	0 (0%)	0	
Ki67	1	0	0	0 (0%)	0	
FGFR3	1	7	7	0 (0%)	0	
SAGE1	1	0	0	0 (0%)	0	
OCT2	1	8	8	0 (0%)	0	

*****unsatisfactory results on original section

Consistent with the previous observations in testicular sample 33456, MAGEA4 remained an important screening marker as most of clonal events (5/6) were positive for MAGEA4 only (Figures 6.14 and 6.15) whilst coexpression of FGFR3 and OCT2 (both identified *post hoc*) was present in one MAGEA4-positive putative clone (Figure 6.16). The minimum number of cells in most of the clonal events (5/6; 83%) was 44-79 but the remaining clone (positive for MAGEA4 only) contained at least 350 cells (Figure 6.15). The number of clones identified was too small to draw any conclusions about the relationship between clone size and antibody staining pattern exhibited by the clonal event (Figure 6.13B).

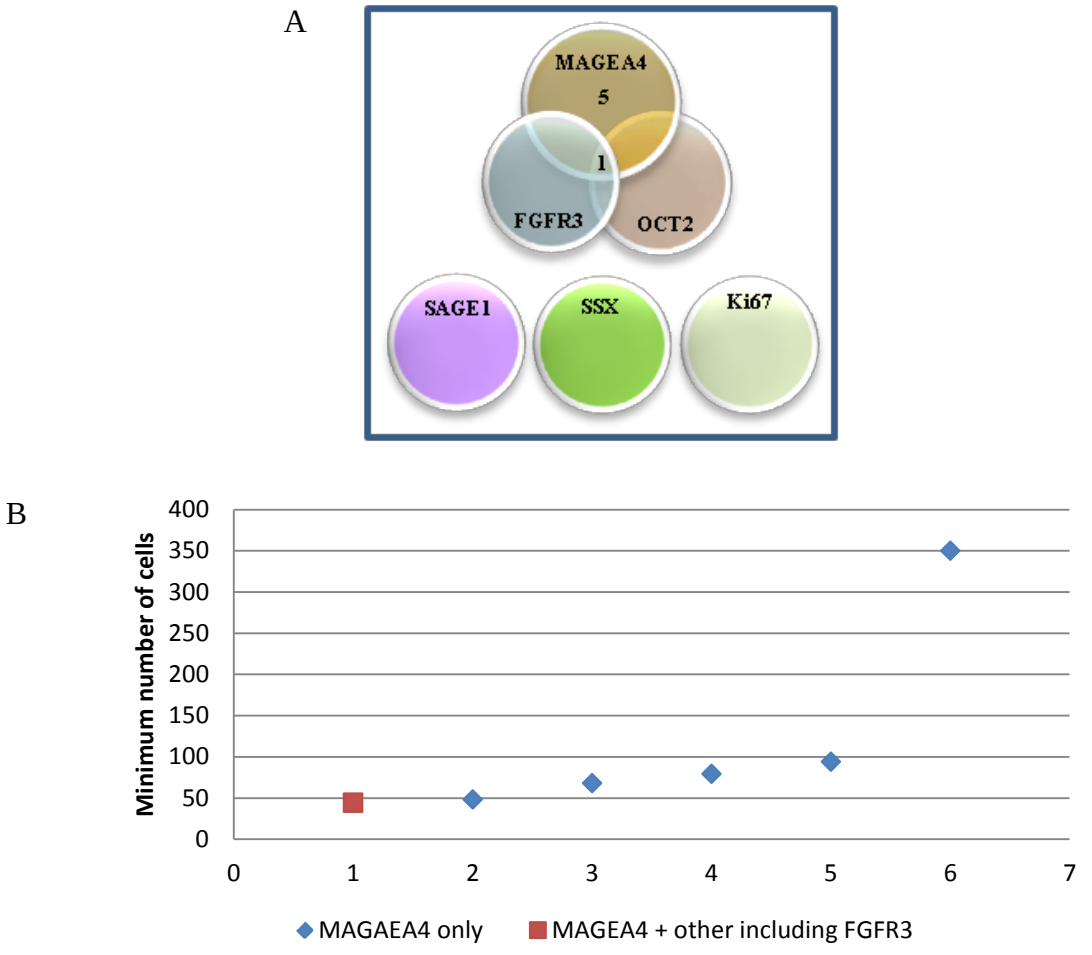

Figure 6.13: Summary of the immunohistochemical properties of the putative clones identified in the testicular sample H10/24188. A Venn diagram demonstrates the association of MAGEA4, SSX, SAGE1, FGFR3, Ki67 and OCT2 expression in the clonal events. B. Graph illustrates the minimum number of cells corresponding with the antigenic profile of the clones.

A

Clone no	Location	Slide 1	Slide 2	Slide 3	Slide 4	Slide 5	Slide 6	Slide 7	Slide 8	Slide 9	Slide 10	Slide 11	Slide 12	Slide 13	Minimum number of cells
		MAGEA4	unstained	unstained	MAGEA4	SSX	OCT2	MAGEA4	SSX*	FGFR3	MAGEA4	Ki67	SAGE1	MAGEA4	
H10-C3	Center	0			1 5 cells	0	0	1 9 cells		0	1 9 cells	0	0	0* 2 cell	68
					50 µm										
No of clusters identified in slide		21	NA	NA	22	0	0	20	NA	0	17	0	0	36	

B

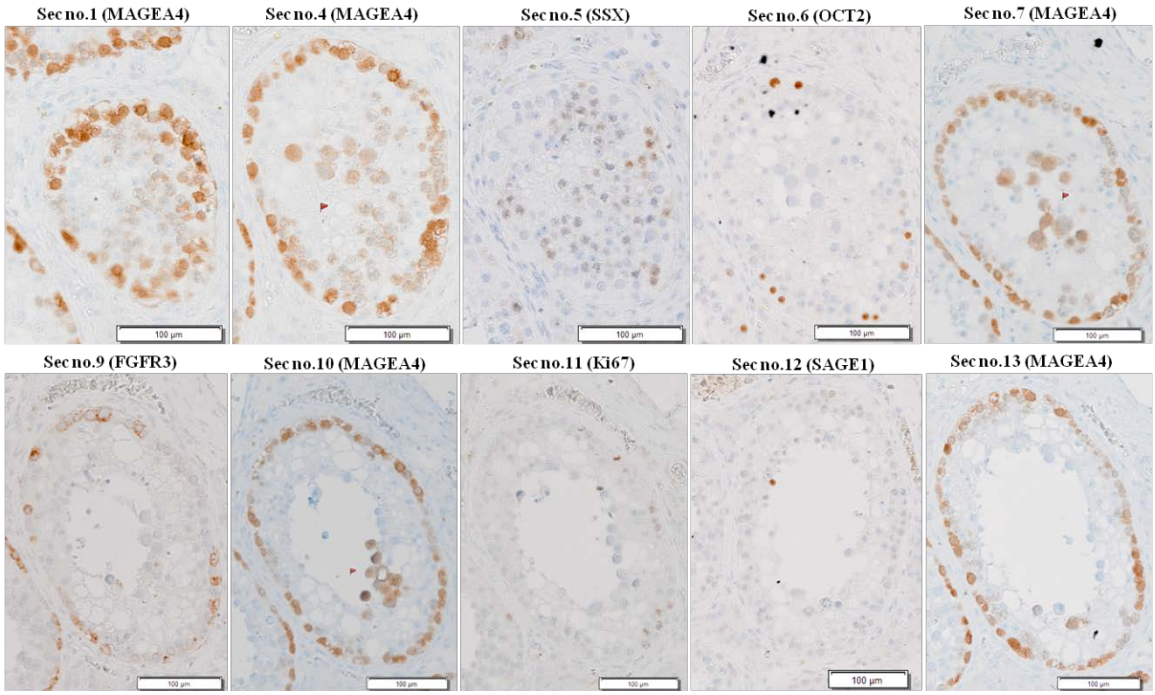

Figure 6.14: Identification of a putative clone expressing MAGEA4 only in sample H10/24188 (clone no: H10-C3). These MAGEA4 positively staining cells were independently identified in sections no.4, 7 and 10 (marked by a red flag). *Post hoc* analysis revealed 2 cells staining in sections no.13. The cell cluster was negative for all other antibodies (SSX, OCT2, FGFR3 and Ki67). The specificity of the expression of other markers in this clone was supported by their immunopositivities in spermatogonia located at the periphery of the tubule (internal positive control). Scale bar: 100 µm.

A

Clone no	Location	Slide 1	Slide 2	Slide 3	Slide 4	Slide 5	Slide 6	Slide 7	Slide 8	Slide 9	Slide 10	Slide 11	Slide 12	Slide 13	Slide 14	Slide 15	Slide 16	Slide 17	Slide 18	Slide 19	Minimum number of cells
		MAGEA4	unstained	unstained	MAGEA4	SSX	OCT2	MAGEA4	SSX*	FGFR3	MAGEA4	Ki67	SAGE1	MAGEA4	unstained	unstained	MAGEA4	unstained	unstained	MAGEA4	
H10-C2	Periphery	1 10 cells			0* 19 cells	0	0	1 17 cells		0	1 16 cells	0	0	1 24 cells			1 22 cells			1 18 cells	350
		95 µm																			
No of clusters identified in slide		21	NA	NA	22	0	0	20	NA	0	17	0	0	36	NA	NA	35	NA	NA	30	

B

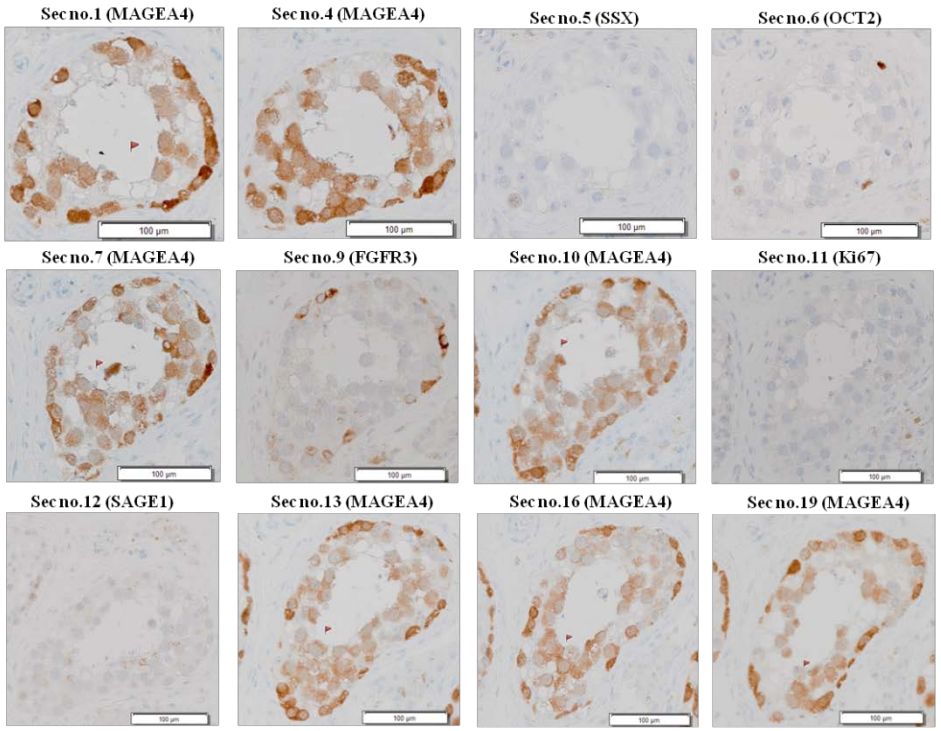

Figure 6.15: Identification of a putative clone expressing MAGEA4 only which located near the periphery of a seminiferous tubule in sample H10/24188 (clone no: H10-C2). This clone consisted of an estimated minimum number of 350 cells and incomplete spermatogenesis with the absence of spermatids was observed in the tubule. Note that this cellular cluster was negative for other markers including SSX, OCT2, FGFR3, Ki67 and SAGE1. Scale bar: 100 µm.

A

Clone no	Location	Slide 1	Slide 2	Slide 3	Slide 4	Slide 5	Slide 6	Slide 7	Slide 8	Slide 9	Slide 10	Slide 11	Slide 12	Slide 13	Minimum number of cells
		MAGEA4	unstained	unstained	MAGEA4	SSX	OCT2	MAGEA4	SSX*	FGFR3	MAGEA4	Ki67	SAGE1	MAGEA4	
H10-C4	Center	NA			1 7 cells	NA	0* 5 cells	0* 7 cells		0* 5 cells	1 8 cells			0	44
					35 µm										
No of clusters identified in slide		21	NA	NA	22	0	0	20	NA	0	17	0	0	36	

B

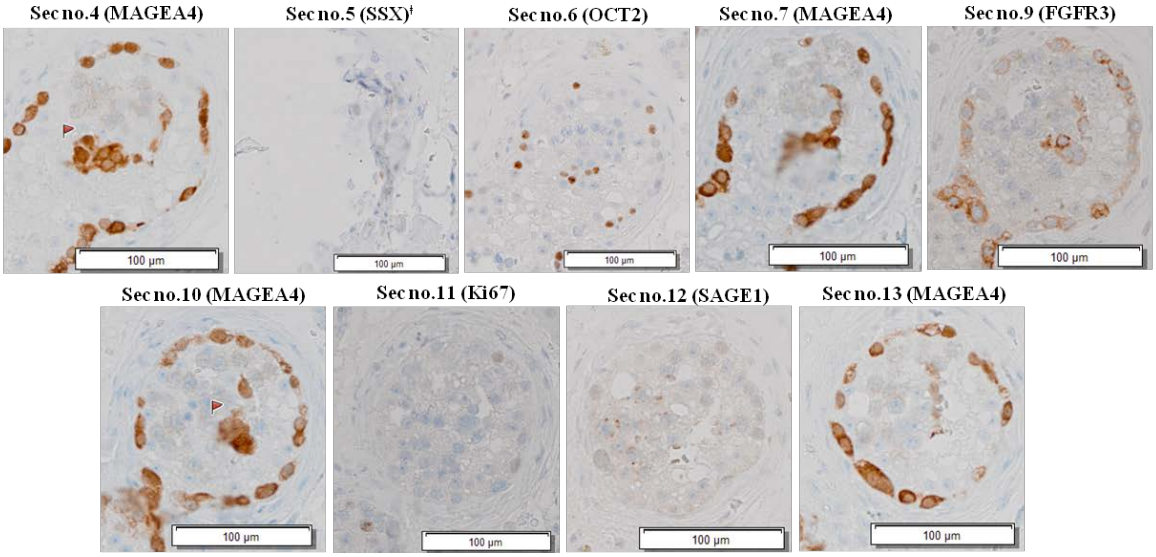

Figure 6.16: Identification of a putative clone expressing MAGEA4, FGFR3 and OCT2 in the sample H10/24188 (clone no: H10-C4). Whilst the MAGEA4-positive spermatogonia forming a ring-like pattern at the periphery of the tubule, a cluster of cells showing aberrant expression pattern was observed independently in sections 4 and 10 (denoted with the red flag). Post-hoc analysis revealed the positivity of FGFR3 and OCT2 within the cellular cluster as well as MAGEA4 in section no.7, which had not been flagged in the primary screen owing to its structure which was thought to represent artefact. Similar tubular structure was missing in section 5 (*). Scale bar: 100 µm.

6.3 Discussion

In the present study, attempts to visualise putative clones in structurally intact normal adult testes have been successfully undertaken using immunohistochemistry on a panel of spermatogonial markers. In the first testis, 84 putative clonal events were identified, and in the second testis a more limited survey identified 6 such events; histological structure of the testes from both individuals was equally well preserved as formalin-fixed paraffin embedded tissue. Assuming the testicular volume of a healthy European man aged 50-90 years is 18 ml (= 18 cm^3) per testis on average (normal range: 12-30 ml; Behre, *et al.*, 2000) (Johnson, *et*

al., 1986), the total of 84 clonal events which identified in two particular serial sections of 5 µm each constituted 0.37% (0.067/18 cm^3) or ~1/269 of the total testis screened from the first individual. The volume of the testis analysed in the first individual was made up of the total proportions of Block 1B and 1D screened; of which the volume of each block was determined by multiplying the area measurements (using milimeter graph paper) by the total thickness of the serial sections studied. By extrapolation, there would be an estimated 22596 putative clones present in the whole testis. Notably, each clonal event was made up of at least two cellular clusters which were compatible with the predetermined characteristics and scored in separate entities within the same seminiferous tubule on consecutive (or at least contiguous) sections; suggesting that these unusual positively staining cells are not randomly present (false positive) in the normal testis. Instead, these events could evolve across serial sections within a seminiferous tubule.

Furthermore, the antigenic profile of the putative clones was described with a panel of markers comprising proteins that were spatially distributed in spermatogonia (including SSX, SAGE1, OCT2, FGFR3 and Ki67) and candidates expressed in most of the spermatogonial cells (including MAGEA4). Collectively, these clonal events which localised in the seminiferous tubules exhibited distinctive staining patterns with the majority (73%; 66/90) positive for MAGEA4 only. The presence of combinations of different markers was noted in the minority (27%; 24/90) of the clonal events; of which most (21/24) expressed one or both FGFR3 and SAGE1 proteins, in addition to immunopositivity with MAGEA4 (for 22/24 cases). Interestingly, different cellular appearances were noted between clonal events expressing MAGEA4 only and clones with a heterogeneous antigenic profile. The cells in most of the putative clones expressing MAGEA4 only (70%; 43/61) was relatively larger than the size of the spermatogonia residing at the periphery of the seminiferous tubules, exhibiting a diffuse nuclear staining pattern (eg Figures 6.3 and 6.17).

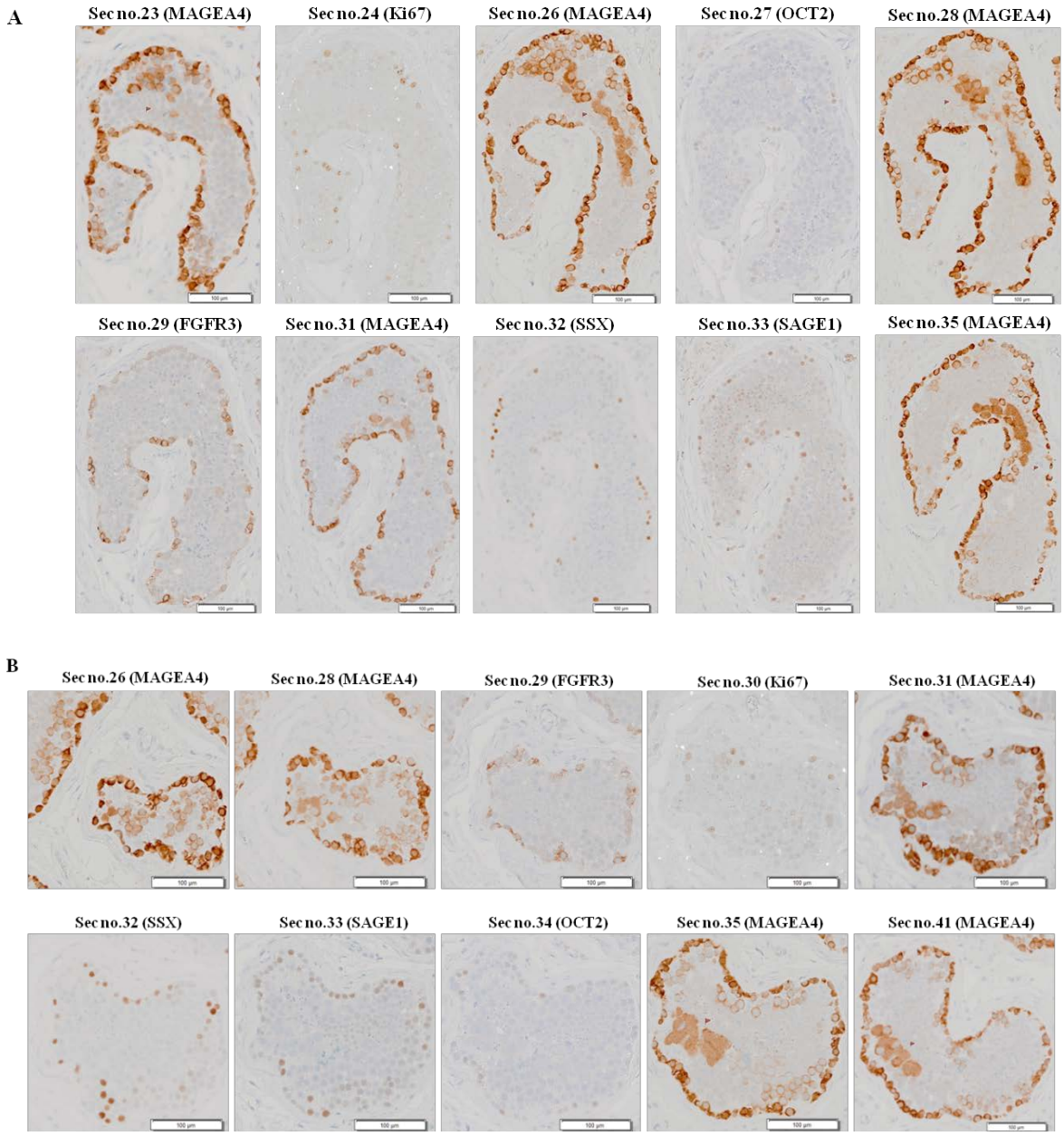

Figure 6.17: Examples of clones expressing MAGEA4 only which consist of large, spermatocyte-like cells (A – clone no: 1B-C27; B – C44). Note strong diffuse staining in the nuclei of the cellular cluster that was distinguishable from the spermatogonia residing at the periphery of the somniferous tubule. Scale bar: 100 µm.

In contrast, the cell size of 91% (21/23) of the clones labelled with combinations of markers was consistently indistinguishable from the spermatogonial cells (eg Figures 6.6, 6.7 and 6.8); suggesting that those large, spermatocyte-like cells which were positive for MAGEA4 only were often derived from a more differentiated cellular phenotype. The putative clonal

events with different antigenic profiles may also represent their distinct genetic backgrounds, an issue that remains to be addressed (see below). In relation to the clonal size (quantified by minimum cell number), approximately 21% (5/24) of the clones that expressed more than one marker comprised >100 cells, compared to 11% (7/66) of $MAGEA4^{+}$/other $markers^{-}$ clones. Interestingly, five $MAGEA4^{+}$ clones which either expressed or coexpressed FGFR3 and SAGE1 proteins contained at least 111 cells whilst $SSX^{+}/SAGE1^{+}/MAGEA4^{-}$ and $SSX^{+}/SAGE1^{-}/MAGEA4^{+}$ clonal events were distributed among clones with less than 50 cells, suggesting the presence of certain markers (such as FGFR3 and SAGE1) may be associated with biological differences in the behaviour of the putative clones. Overall in the first individual, staining for markers additional to MAGEA4 was positively correlated with the clone size (Figure 6.10).

With the identification of these cellular clusters showing unusual staining pattern in the normal adult testis, the next key question would be whether these represent the genuine putative microclones I have been looking for or are there some other explanations? Some cases involving small clusters of cells or unusual patterns may well still be artefactual; for example I suspect that the cellular clusters identified in Figure 6.16 might be artefactual both on the grounds of morphology (ring-like pattern) and antibody positivity (OCT2, not present in any other putative clone). Some of the MAGEA4 only 'clones' consisting large, spermatocyte-like cells may also represent just unusual groups or sectioning artefacts of normal cells (e.g. Figures 6.3 and 6.15). Nevertheless, this is harder to argue when cellular clumps are large, identified in multiple independent sections and stained with multiple independent antibodies. Examples of convincing clones include those shown in Figures 6.4, 6.5, 6.6, 6.7, 6.8 and 6.11 as well as others (eg clones 1B-C1, 1B-C4, 1B-C6, 1D-C18 and 1D-C35) that were documented on the supplementary CD. This would represent an important advance because, to my knowledge, such features have not previously been

described in the normal testis. The presence of several markers with unknown biological functions in human spermatogenesis might not have a direct correlation with the genotypes of the clones. Nevertheless, the correlation of FGFR3 positively with large clone size is intriguing, suggesting that these events at least may be driven by a selective advantage mechanism mediated by activating paternal age-effect mutations.

CHAPTER 7

SUMMARY AND CONCLUDING DISCUSSION

Chapter 7: Summary and concluding discussion

Paternal age-effect mutations (as defined in Section 1.4) that account for the incidence of autosomal dominant congenital disorders involving skull and limb malformations are implicated in testicular oncogenesis. The pathological basis of these events could be explained in the context of spermatogenesis in which the spermatogonia with stem cell properties generally undergo asymmetrical divisions resulting in the formation of a daughter spermatogonial cell and another cell committed to differentiating into sperm. These pathogenic *de novo* base substitutions encode overeactive proteins that confer a selective advantage to the spermatogonia in which they arise, leading to progressive clonal expansion over a course time within the normal testis (Section 1.7.1) and spermatocytic seminoma in some cases (Section 1.8.3). This thesis has examined, and provides evidence to support, the phenomenon of this abnormal clonal growth within the normal adult testis, which may be attributable to paternal age-effect mutations or allied processes. Following the search for candidate markers for the *de novo* screening approach using spermatocytic seminoma and normal adult testis, this work has also provided new data on the heterogeneity of this testicular neoplasm and highlighted the presence of two mutually exclusive subpopulations of germ cells defined by OCT2 or SSX expression.

7.1 The characterisation of OCT2, SSX and SAGE1during testicular development

In the course of searching for markers for the putative clones, OCT2, SSX and SAGE1 were chosen for detailed morphological study on normal testis due to their spatial distribution in human spermatogonia. Evidence from this study further supports the heterogeneous population of spermatogonial cells in the normal adult testis, defined by OCT2, SSX and SAGE1 (Chapter 4). Immunostaining for these markers unveiled that the expression of each protein may represent spermatogonia at different maturation stages. Intriguingly, OCT2 and SSX were identified in two mutually exclusive subpopulations of

spermatogonia in which OCT2 was predominantly present in A_{dark} spermatogonia whilst SSX was preferentially expressed in A_{pale}/B spermatogonia and leptotene primary spermatocytes. The mutually exclusive pattern was also consistently observed in more mature germ cells (possibly prespermatogonia) present in testicular tissues from early fetal to prepubertal life, suggesting the biological significance of these proteins during testicular development. Analysis of the ontogeny of expression of OCT2 from embryonic development to adulthood supports the hypothesis that this transcription factor may be involved in maintaining the reserve spermatogonial stem cell population. In future work, it will be interesting to characterise the function of this gene via *in vitro* studies on spermatogonial cell lines and spermatogonial stem cell transplantation assay in mice to understand its role in regulating spermatogenesis. Notably, the functional transplantation assay is a method where the recipient testes are microinjected with a donor or experimental testis cell population. Reestablishment of spermatogenesis from injected cells provides a direct means to quantify the stem cell number and its biological activity; it is worth noting that the phenotypic characteristic of Oct2 in mouse spermatogenesis could be varied from human as previously reviewed in other human spermatogonial markers such as TSPY (Dym, et al., 2009b). In short, OCT2 is demonstrated for the first time as a novel marker of human A_{dark} spermatogonia, considered as spermatogonial stem cells; the identification of this marker opens the possibility of monitoring of the spermatogonial reserve in patients with different forms of infertility and suppressed spermatogenesis (for example cryptorchidism and recovery after cytotoxic treatment).

7.2 The phenotypic heterogeneity of spermatocytic seminoma (SS)

SS has emerged as a key link between mutational events occurring in the soma and germline, as described recently (Section 1.8.3) (Goriely, et al., 2009). This benign, rare testicular neoplasm, which predominantly occurs in older men and has a distinctively

different origin from other common testicular tumours, has here been employed as a testicular model to study the pathological correlates of paternal age-effect mutations. Systematic analysis of candidate protein expression on thirty-six SS has supported its spermatogonial origin as proposed earlier (Rajpert-De Meyts, et al., 2003) and has demonstrated new evidence for the heterogeneity of this tumour as well as its mechanisms of progression (Chapter 5). Specifically, my data support the existence of two types of SS, the majority being derived from A_{pale}/B spermatogonia characterised by SSX expression, but with a small subset attributed to a hitherto unknown OCT2-positive variant likely to arise from A_{dark} spermatogonia. Although the differences in expression of SSX and OCT2 in SS did not reach statistical significance, the biological distribution is in accordance with the expression patterns of OCT2 and SSX in normal adult testis, which highlight the presence of two mutually exclusive subpopulations of spermatogonia as observed in my earlier study (Chapter 4). In addition, investigation of SAGE1 (mainly expressed in B spermatogonia) and SSX in intratubular spermatocytic seminoma (ISS) (the preinvasive lesion of SS) showed spatial differences suggesting ongoing maturation of germ cells during progression of SS tumourigenesis. Collectively, evidence from the present study suggest that the neoplastic germ cells still retain some developmental plasticity which could explain the immunopositivity of proteins involved during maturation towards early primary spermatocytes in some of the SS samples; for instance, SS expressing DMRT1 (a male-specific transcriptional regulator), which is expressed in spermatogonia and primary spermatocytes, seems to fit into this phenotype (Looijenga, et al., 2006).

Together, this study provides further understanding of the histogenesis of SS and confirms SS as the ideal pathological correlate of paternal age-effect mutations. Of note, canine seminoma shares strong similarities with human SS in terms of its morphology, clinical behaviour and immunohistological profile; this animal counterpart could serve as a

useful model to shed light on some of the unanswered histological questions about this tumour (such as the cellular origin of three different sizes of tumour cells in SS) as well as to investigate the mutation spectrum particularly in paternal age-effect mutations and its occurrence in comparison with the events occurring in human (Scully, 1961; Bush, *et al.*, 2011).

7.3 A search for putative clones in the normal adult testis

The primary goal of this thesis was to search for the existence of putative clones in the fully structurally intact seminiferous tubules. With the *de novo* screening approach using a combination of immunohistochemistry and digital microscopy technology, I have successfully visualised these clonal events characterised by panel of markers (including MAGEA4, SSX, SAGE1, OCT2, FGFR3 and Ki67) in the normal adult testis (Chapter 6). A number of antigenic profiles were observed in these putative clones in which heterogeneous staining pattern was significantly associated with clones containing higher number of minimum cells. Although there might be some other reasons which explain some of these clonal events, I believe that the existence of such putative clone in the normal testis represents a phenomenon with parallels to that described in paternal age-effect mutations (Section 1.8.2).

It has been proposed that spermatogonia bearing paternal age-effect mutations would expand clonally and lead to the enrichment of mutant sperm over time during normal spermatogenesis. In the disease context, this is essential for the occurrence of congenital anomalies in newborns with paternal age-effect syndromes. Hence, if such clones are present in the normal testis, one would expect to identify this event in the seminiferous tubules with virtually normal testicular architecture. Results from the present study involving two testicular tissues of ~70 year old men demonstrated that most of the putative clones identified were located either in the centre or the periphery of the seminiferous epithelium

with normal lamina propria where intact spermatogenesis showing maturation from spermatogonia to spermatids was observed. These clones which could possibly produce sperm were evident in clonal events such as clones 1D-C7 (Figure 7.1A), 1D-C22 (Figure 7.1B) and 1D-C1 (Figure 6.3), in line with the testicular characteristic as proposed.

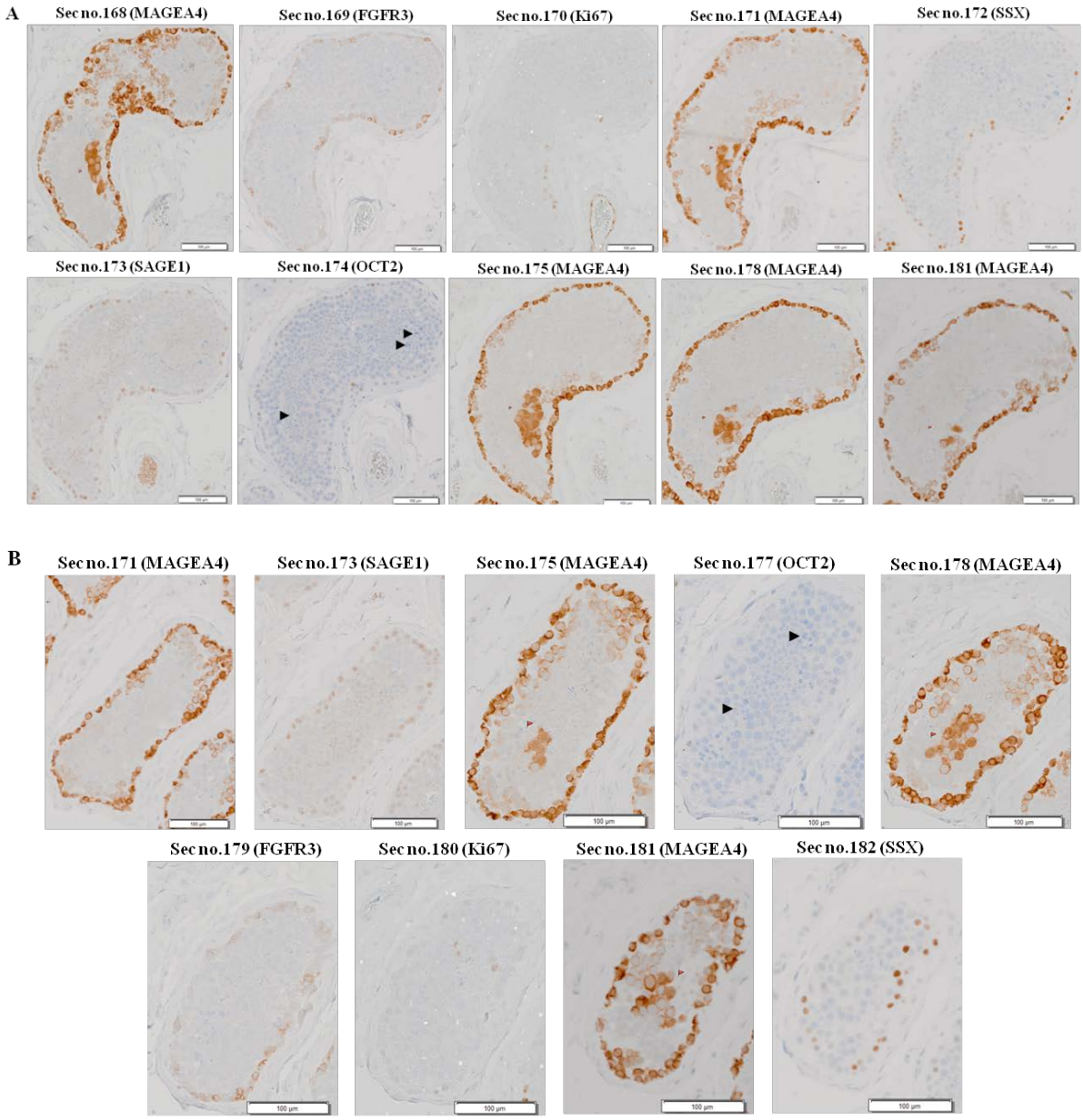

Figure 7.1: Identification of putative clones expressing MAGEA4 only in the seminiferous tubules showing normal spermatogenesis (A - clone no: 1D-C7; B – clone no: 1D-C22). Note the presence of early spermatids which appeared as small spherical cells with round darkly stained nuclei and mature spermatids characterised by the mature shaped heads (arrowhead). Scale bar: 100 µm.

Nevertheless, there are some clones which look as though they are ‘dead ends’ that would never evolve into lesions producing sperm with paternal age-effect mutations. These events were studied mainly in seminiferous tubules characterised by a thickened tunica propria and incomplete spermatogenesis with the absence of spermatids (e.g. clones 1B-C2, Figure 6.5; 1B-C8, Figure 7.2 and 1D-C14, Figure 6.4). Notably, the presence of germ cell loss showing maturation arrest at spermatogonial or spermatocyte level is associated with morphological alterations of tunica propria; these age-related phenomena which have been studied in the testes of elderly men were associated with a reduction in the length of the seminifeorus tubules (Johnson, *et al.*, 1986). In some cases, these may progress to a sclerotic lesion where only an intensely collagenised tunica propria with myoid cells are found in the tubules (Paniagua, *et al.*, 1991).

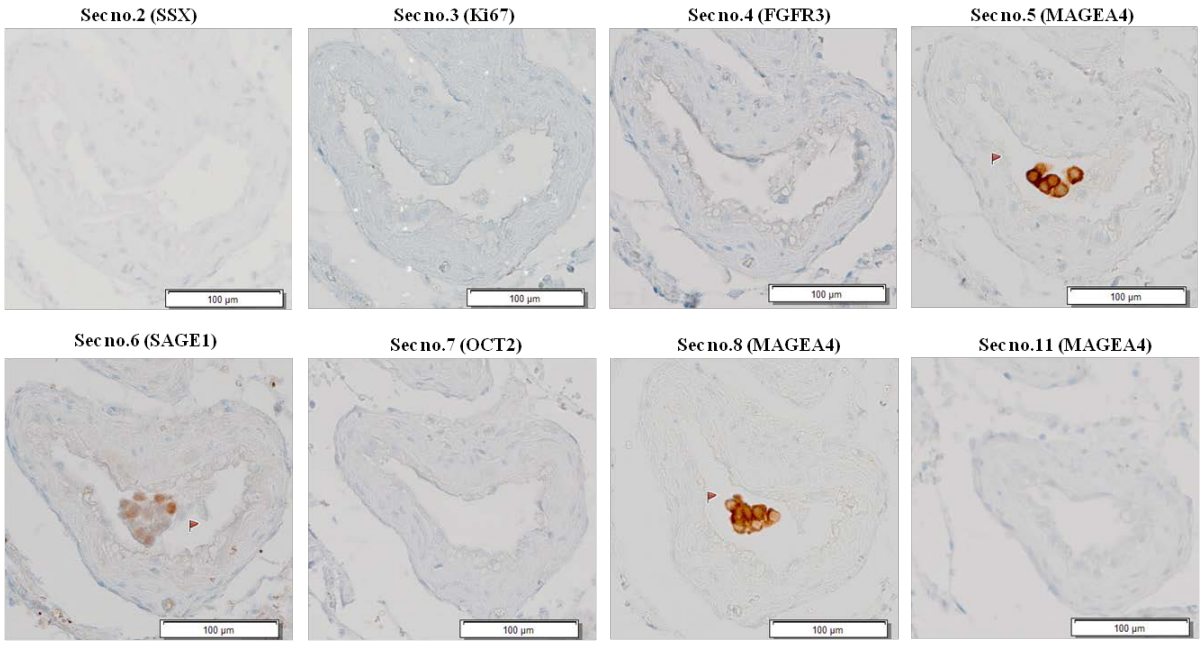

Figure 7.2: Identification of a putative clone expressing MAGEA4 and SAGE1 in a seminiferous tubule with thickened tunica propria, showing the absence of normal spermatogenesis (clone no: 1B-C8). Scale bar: 100 µm.

Besides these, the ‘dead end-looking’ clones were occasionally seen in the lumen of the structurally intact tubules (e.g. clones 1B-C21, Figure 7.3 and 1B-C37, Figure 6.7),

suggesting these were cross sections of groups of spermatogonial cells which arise potentially from the tip of the tubule and progressively grow into its lumen. Although this type of clone may have lost its ability to produce sperm, the proliferation of the cells continues and potentially forms a neoplastic lesion that may transform into a tumour over a course of time. This growth of these cells might not be supported by the canonical testicular niche environment (Section 1.8.1); instead, this phenomenon is potentially mediated by the oncogenic mutation-induced niche-independent self renewal process, which was previously proposed as an alternative pathway adopted by the mouse spermatogonial progenitor cells that were insensitive to niche-derived signals and yet continue to self renew and develop into cancer (Hobbs, *et al.*, 2010).

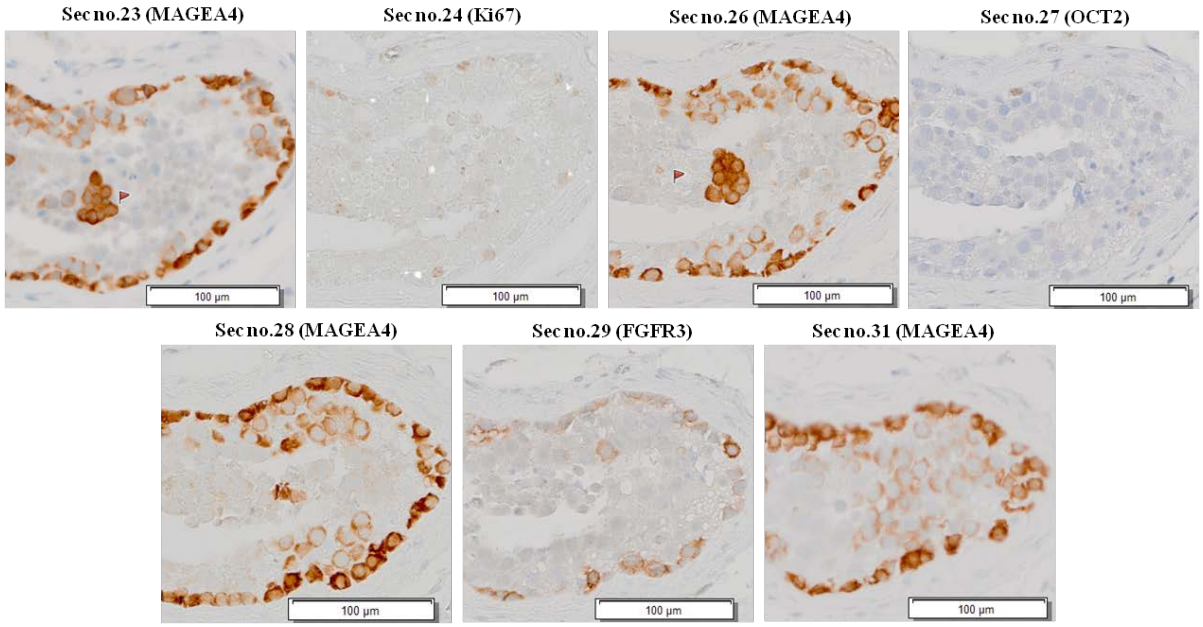

Figure 7.3: Identification of a putative clone expressing MAGEA4 only in the lumen of a seminiferous tubule where normal spermatogenesis was identified (clone no: 1B-C21). Scale bar: 100 µm.

Earlier studies (Qin, *et al.*, 2007; Choi, *et al.*, 2008) analysed the *FGFR2* Apert mutations at codons 252 and 253 in normal testes dissected into ~192 pieces; results showed that 95% of the mutations were confined to no more than 6% of the whole testis in which the

two mutation events arose independently of one another (Section 1.8.2). Based on the original data from the Arnheim studies, further analysis was undertaken in the current study to estimate the clonal size of these two specific mutations in the normal testis (Box 7.1).

Box 7.1: Estimation of the size of putative clones bearing *FGFR2* Apert mutations in the normal adult testis (Source: Qin, *et al.*, 2007; Choi, *et al.*, 2008).

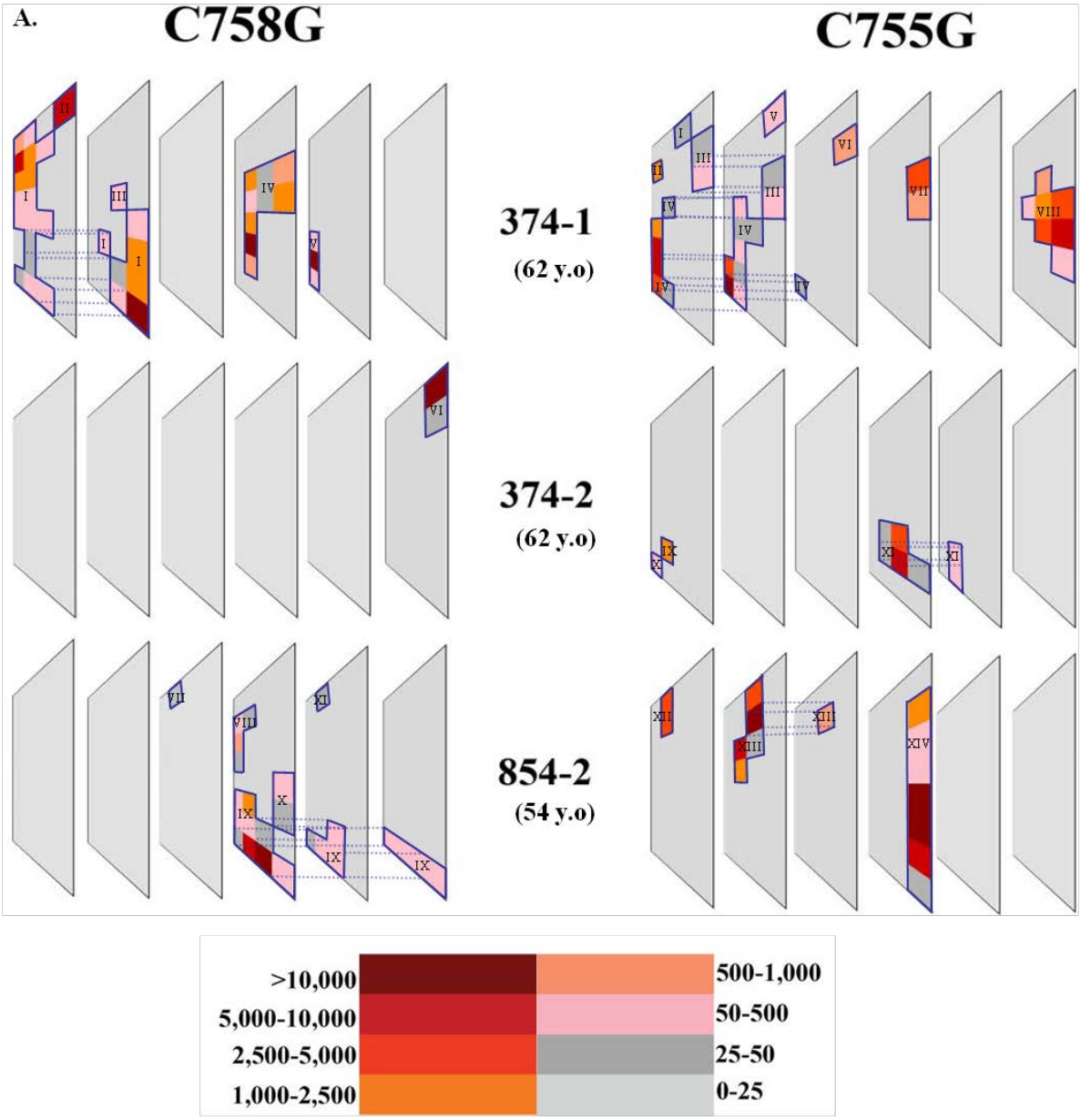

The localised distribution of *FGFR2* C758G and C755G mutations in the normal testis was shown in (A) and the colour code represented the number of mutant molecules per million genomes. Both 374-1 and 374-2 testes were from a 62 year old (y.o) donor whilst the 854-2 sample was obtained from a 54 y.o man. The details of the experimental approach were illustrated in Chapter 1; Section 1.8.2 and Figure 1.15.

Each clone was encircled with blue line and contiguous event which occasionally found on the next adjacent piece was shown by the blue dotted line.

To estimate the size of a clone, the minimum number of cells in each clone is calculated based on the formula

Clonal size = Proportion of cells positive for mutation x No. of cells in each block in a clone

Where the proportion of cells positive for the mutation in each block (expressed as mutants/million genomes) and the number of cells for each block (assumed to be half the number of genomes per testis piece) are available from Table S1 of Qin, *et al.* (2007) and Choi, *et al.* (2008) studies.

The size of each clone harbouring the specific point mutation causing Apert syndrome (a paternal age-effect syndrome) is summarised in (B).

B.

	***FGFR2* C758G mutation**		***FGFR2* C755G mutation**	
Sample no.	**Clone no.**	**Clonal size (number of cells)**	**Clone no.**	**Clonal size (number of cells)**
374-1	I	1030304	I	266
	II	103640	II	22565
	III	836	III	3533
	IV	563461	IV	727227
	V	279005	V	1541
			VI	10693
			VII	90230
			VIII	174383
374-2	VI	282361	IX	31555
			X	5671
			XI	144226
854-2	VII	167	XII	28790
	VIII	6210	XIII	437406
	IX	183723	XIV	600600
	X	779		
	XI	526		

The putative clones were defined by the presence of dissected pieces with high mutation levels lying in adjacent blocks, either in a single slice or between slices. A total of 25 clonal events bearing either *FGFR2* 755C>G or 758C>G base substitutions were identified in three testicular samples, ranging in size from 167 to 103034 cells. The number of events was independent and varied amongst different persons or even within the pairs of testes from the same individual. For instance, testis 374-1 had a higher number of putative clones harbouring either of these mutations than testes 374-2 (another paired testis of 374-1) and 854-2 (testis from the second individual). Notably, it has been proposed that the enrichment of initial rare paternal age-effect mutations leading to clonal expansion is likely to occur in

all men (Goriely and Wilkie, 2010). Compared to the data from my own work (Table 7.1), the occurrence of the clonal events in the Arnheim studies was less common (N=25) but with much bigger clones; the extent of clonal size found in the present study barely overlapped with those of Arnheim and the Arnheim studies were in any case not sensitive for the detection of small clones. These observations do reflect the challenge of the current approach in defining 'large clones' in the structurally intact seminiferous tubules (demonstrated in Arnheim studies at DNA level) as the total clonal size range in the present study appeared to be between 15 to 356 cells only which was relatively much smaller.

Table 7.1: Summary of the number of putative clones identified in the current study and Arnheim studies as well as their clonal sizes.

	Current study			Arnheim studies (Qin, *et al.*, 2007; Choi, *et al.*, 2008)		
	Number of clones per testis					
	Sample ID	MAGEA4 only	≥2 markers	Sample ID	*FGFR2* C758G mutation	*FGFR2* C755G mutation
1st testis	33456*	61	23	374-1	5	8
Clonal size range (minimum no. of cells)		15-188	17-356		836-1030304	266-727227
2nd testis	H10/2488*	5	1	374-2	1	3
Clonal size range (minimum no. of cells)		48-350	44		282361	5671-144226
3rd testis				854-2	5	3
Clonal size range (minimum no. of cells)					167-183723	28790-600600
Total no. of clones		22596#			25	
Total clonal size range		15-356*			167-1030304	

*The analysis was done based on 35 and 12 sections screened for samples 33456 and H10/2488 respectively. #The total no. of clone in the whole testis of the first individual is extrapolated from the proportion of the testis screened in this study (see Section 6.3).

Could these differences be attributed to sampling error, or are the appearances of the tubules in large clones? The presence of the 'large clones' might have been missed in the normal testis (from the first individual) of this study since only 2 regions were analysed and these represented only 1/269 of the whole testis. Alternatively, reconstruction of histological serial

sections from this normal testis (in future studies) may render a 3-dimensional image of the long, convoluted seminiferous tubules which are more informative than the 2-dimensional cross sections; such that some of the putative clones identified in this study (especially those extending beyond the margins of the analysis) might be contiguous within the same seminiferous tubules and their sizes could be considerably bigger than earlier estimated. The results would be more conclusive if the immunohistochemical study on the whole testis along with the reconstruction of the histological sections are completed in future studies using the screening approach which I have established. In term of the tubular architecture, findings from this study suggest that most of tubular structure and normal spermatogenesis were retained in seminiferous tubules containing putative clones; clonal events could be identified in structurally altered seminiferous tubules with incomplete spermatogenesis in some cases. Parallel histological findings were also documented in previous study in which the normal spermatogenesis was indicated in the Hras G12V–mutated germline stem cells recipient mouse testis despite the occurrence of seminomatous tumours in the structurally intact seminiferous tubules (Section 1.8.4) (Lee, *et al.*, 2009).

Following the findings described to date, it would be interesting to undertake further analysis of the downstream pathways involved in the putative clonal events with HRAS, phospho-ERK (activated downstream effector of MAPK pathway) and phospho-AKT (activated downstream effector of PI3K-AKT pathway) markers. These proteins are components of RAS signalling cascades (consisting MAPK and PI3K-AKT pathways) which have been previously suggested to be involved in the proliferation and / or differential survival of spermatogonia (Section 1.8.5). The proposed clonal expansion in the normal adult testis might be eventually restricted by growth arrest or senescence and never progress into overt tumours (Goriely, et al., 2009; Ota, et al., 2009). This potential correlation of senescence with the activating levels of mutant proteins opens the opportunity of using

senescence markers (including p16INK4a, p21 and ARF) (Collado and Serrano, 2006) to further characterise the biological significance of putative clonal events and explore their underlying mechanisms. However, since the number of sections available for immunohistochemistry is highly dependent on the clonal size (the minimum number of cells), spermatogonial markers selected based on the immunohistochemical analysis on spermatocytic seminoma (Chapter 5) were given a higher priority than the signalling molecules in characterising the clonal events. In future work, the graded distance between each MAGEA4-labelled section and the order of other spermatogonial markers characterising the adjacent sections, which were established in the current study, may be modified as necessary to accommodate the signalling molecules of interest in the panel of markers.

This work also forms a prelude to coupling the immunohistochemical study with mutation analysis on the microdissected cells from the region of interest. The isolation of these clonal events using laser-capture microdissection (LCM) for downstream DNA genetic analysis would directly address the question whether some of these putative clones contain paternal age-effect mutations. LCM provides a method for the reliable procurement of pure cellular clusters of interest from the heterogeneous spermatogenic populations within the seminiferous epithelium under direct microscopic visualisation. There are two main groups of LCM: infrared (IR) capture systems (Emmert-Buck, *et al.*, 1996; Bonner, *et al.*, 1997) and ultraviolet (UV) cutting systems (Schutze, *et al.*, 1998; Kolble, 2000; Micke, *et al.*, 2005). The fundamentals of LCM technology comprise (i) visualisation of the cells of interest via microscopy, (ii) transfer of focused laser energy to photo volatize cells surrounding a selected area (UV system) or to a thermolabile polymer with formation of a polymer-cell composite (IR system) and (iii) isolation of the cells of interest from the heterogeneous tissue section. Successful application of LCM on both frozen and fixed tissues, which relies on

three key factors (tissue morphology, capture success and maintenance of molecular integrity), enables the recovered cell to be used for subsequent DNA, RNA and protein analysis. In the context of this study, immuno-LCM which allows tissue to be stained immunohistochemically before LCM, would be essential to identify clonal events of interest. The microdissection of the clonal events with distinct staining pattern chosen from the earlier screening approach is crucial to study the potential genetic alterations harboured by these unusual positively staining cells.

The major concern of this prospective LCM work is the recovery of DNA from the microdissected cells. The use of formalin as tissue fixative may result in highly degraded DNA as it causes the formation of cross-links between nucleic acid strands. Hence, to minimise further degradation of DNA during the staining process, optimal immune-LCM methods capitalise on short overall staining times with the use of high-affinity antibodies at high concentrations. Several factors have to be taken into consideration during DNA extraction of laser microdissected samples including the efficiency in removing PCR inhibitors, optimal DNA recovery and the yield of DNA extract. To obtain a relatively pure DNA extract from cells after LCM work, spin columns containing a silica membrane that binds nucleic acids have been used to remove proteins and other contaminant that can potentially serve as PCR inhibitors via a series of washing and elution protocols (Di Martino, *et al.*, 2004; Sanders, *et al.*, 2006). Alternatively, a single tube Proteinase K DNA extraction method, in which the sample is extracted directly in the cap of the collection tube, has resulted in maximal recovery of DNA from microdissected tissues (Elliott, *et al.*, 2003; Vandewoestyne, *et al.*, 2009; McAlister, 2011). A newly invented technology known as AmpliGrid slide (Advalytix AG, Germany) has recently been applied and satisfactory results can be acquired from as few as one cell, by collecting the laser-microdissected cells directly onto the AmpliGrid slide (Novotný J, 2008). AmpliGrid slide is a standard microscope slide

sized amplification platform for ultra low volume applications in the 1 µl range, based on a chemically structured microscope slide (Schmidt, *et al.*, 2006). DNA extraction and PCR can be conducted directly on these reaction sites after placing the laser microdissected (single) cells into one of the hydrophilic reaction sites on the slide.

For downstream analysis, large amounts of DNA would be required to profile the mutation spectrum of paternal age-effect lesions in these putative clonal events at the whole genome level. Based on the quantification of minimum number of cells (Chapter 6), it would be difficult to obtain sufficient DNA from at least 87% of the clonal events (containing less than 100 cells) as the DNA is estimated at 3 pg in the mammalian haploid genome (de Gruyter, 1996). To address this, the multiple displacement amplification (MDA) method could be used to generate sufficient DNA from low number of cells with minute DNA content. MDA is a technique to amplify DNA using random hexamers which target the whole DNA template and is catalysed by the ϕ29 DNA polymerase (Blanco, *et al.*, 1989; Dean, *et al.*, 2001; 2002). The random hexamers are first bound to the denatured DNA and followed by strand-displacement synthesis at a constant temperature, leading to the accumulation of DNA products with high molecular weight (up to 12 kb). As DNA is synthesised by strand displacement, the number of concurrent priming events gradually increases, forming a network of hyperbranched DNA structures. The utility of MDA has been reported on single sperm cells (Jiang, *et al.*, 2005) and genomic DNA from just a few cells in forensic genetic investigation (Ballantyne, *et al.*, 2006). Of note, MDA produces the least amplification bias compared with other whole genome amplification methods documented to date (Hosono, *et al.*, 2003). In a test of human DNA, 10 ng of DNA template (around 3000 haploid genome copies) was synthesised to an average of ~40 µg DNA yield, resulting in a 4000-fold amplification (Lasken, 2009). It is worth noting that the amplification bias will be accentuated if less template is used which thereby produces greater

fold of amplification, owing to local sequence effects on the efficiency of the random hexamers (Binga*, et al.,* 2008). The amplified DNA from MDA is suitable for multiple downstream applications including genotyping and sequencing.

Taken together, in this thesis I have demonstrated for the first time the presence of putative clones in the normal adult testis with immunohistochemistry. Subsequent mutation screening coupled to microdissected cells (as suggested above) would provide an avenue to understand the impact of selective clonal expansion drive by the activating paternal age-effect mutations on normal testes. As the mutation spectrum may vary among individuals, it would be of interest to analyse testes from other individuals with a similar screening approach especially if a LCM mutation analysis assay can be incorporated.

PUBLICATIONS

Publications

Lim J, Goriely A, Turner GD, Ewen KA, Jacobsen GK, Graem N, Wilkie AO, Rajpert-De Meyts E. 2011. OCT2, SSX and SAGE1 reveal the phenotypic heterogeneity of spermatocytic seminoma reflecting distinct subpopulations of spermatogonia. *J Pathol* 224: 473-83

Goriely A, Lord H, Lim J, Johnson D, Lester T, Firth HV, Wilkie AO. 2010. Germline and somatic mosaicism for FGFR2 mutation in the mother of a child with Crouzon syndrome: Implications for genetic testing in "paternal age-effect" syndromes. *Am J Med Genet A.* 152A(8): 2067-73.

REFERENCES

References

1. Adar R, Monsonego-Ornan E, David P, Yayon A. 2002. Differential activation of cysteine-substitution mutants of fibroblast growth factor receptor 3 is determined by cysteine localization. *J Bone Miner Res* 17: 860-8
2. Agapova LS, Volodina JL, Chumakov PM, Kopnin BP. 2004. Activation of Ras-Ral pathway attenuates p53-independent DNA damage G2 checkpoint. *J Biol Chem* 279: 36382-9
3. Al-Saad S, Donnem T, Al-Shibli K, Persson M, Bremnes RM, Busund LT. 2009. Diverse prognostic roles of Akt isoforms, PTEN and PI3K in tumor epithelial cells and stromal compartment in non-small cell lung cancer. *Anticancer Res* 29: 4175-83
4. Andersen JN, Mortensen OH, Peters GH, Drake PG, Iversen LF, Olsen OH, Jansen PG, Andersen HS, Tonks NK, Moller NP. 2001. Structural and evolutionary relationships among protein tyrosine phosphatase domains. *Mol Cell Biol* 21: 7117-36
5. Anderson J, Burns HD, Enriquez-Harris P, Wilkie AO, Heath JK. 1998. Apert syndrome mutations in fibroblast growth factor receptor 2 exhibit increased affinity for FGF ligand. *Hum Mol Genet* 7: 1475-83
6. Aoki Y, Niihori T, Kawame H, Kurosawa K, Ohashi H, Tanaka Y, Filocamo M, Kato K, Suzuki Y, Kure S, Matsubara Y. 2005. Germline mutations in HRAS proto-oncogene cause Costello syndrome. *Nat Genet* 37: 1038-40
7. Aubry F, Satie AP, Rioux-Leclercq N, Rajpert-De Meyts E, Spagnoli GC, Chomez P, De Backer O, Jegou B, Samson M. 2001. MAGE-A4, a germ cell specific marker, is expressed differentially in testicular tumors. *Cancer* 92: 2778-85
8. Bader AG, Kang S, Zhao L, Vogt PK. 2005. Oncogenic PI3K deregulates transcription and translation. *Nat Rev Cancer* 5: 921-9
9. Balakireva M, Rosse C, Langevin J, Chien YC, Gho M, Gonzy-Treboul G, Voegeling-Lemaire S, Aresta S, Lepesant JA, Bellaiche Y, White M, Camonis J. 2006. The Ral/exocyst effector complex counters c-Jun N-terminal kinase-dependent apoptosis in Drosophila melanogaster. *Mol Cell Biol* 26: 8953-63
10. Ballantyne KN, van Oorschot RA, Mitchell RJ, Koukoulas I. 2006. Molecular crowding increases the amplification success of multiple displacement amplification and short tandem repeat genotyping. *Anal Biochem* 355: 298-303
11. Behre HM, Yeung CH, Holstein AF, Weinbauer, Gassner P, Nieschlag E. 2000. Diagnosis of male infertility and hypogadism In *Andrology: male reproductive health and dysfunction, 2nd ed.* Nieschlag E, Behre HM (eds). Heidelbergh: Springer; 90-124.
12. Bellus GA, Bamshad MJ, Przylepa KA, Dorst J, Lee RR, Hurko O, Jabs EW, Curry CJ, Wilcox WR, Lachman RS, Rimoin DL, Francomano CA. 1999. Severe achondroplasia with developmental delay and acanthosis nigricans (SADDAN): phenotypic analysis of a new skeletal dysplasia caused by a Lys650Met mutation in fibroblast growth factor receptor 3. *Am J Med Genet* 85: 53-65
13. Bellus GA, Hefferon TW, Ortiz de Luna RI, Hecht JT, Horton WA, Machado M, Kaitila I, McIntosh I, Francomano CA. 1995a. Achondroplasia is defined by recurrent G380R mutations of FGFR3. *Am J Hum Genet* 56: 368-73
14. Bellus GA, McIntosh I, Smith EA, Aylsworth AS, Kaitila I, Horton WA, Greenhaw GA, Hecht JT, Francomano CA. 1995b. A recurrent mutation in the tyrosine kinase

domain of fibroblast growth factor receptor 3 causes hypochondroplasia. *Nat Genet* 10: 357-9

15. Bellus GA, Spector EB, Speiser PW, Weaver CA, Garber AT, Bryke CR, Israel J, Rosengren SS, Webster MK, Donoghue DJ, Francomano CA. 2000. Distinct missense mutations of the FGFR3 lys650 codon modulate receptor kinase activation and the severity of the skeletal dysplasia phenotype. *Am J Hum Genet* 67: 1411-21
16. Berglund L, Bjorling E, Oksvold P, Fagerberg L, Asplund A, Szigyarto CA, Persson A, Ottosson J, Wernerus H, Nilsson P, Lundberg E, Sivertsson A, Navani S, Wester K, Kampf C, Hober S, Ponten F, Uhlen M. 2008. A genecentric Human Protein Atlas for expression profiles based on antibodies. *Mol Cell Proteomics* 7: 2019-27
17. Bernard-Pierrot I, Brams A, Dunois-Larde C, Caillault A, Diez de Medina SG, Cappellen D, Graff G, Thiery JP, Chopin D, Ricol D, Radvanyi F. 2006. Oncogenic properties of the mutated forms of fibroblast growth factor receptor 3b. *Carcinogenesis* 27: 740-7
18. Bignell G, Smith R, Hunter C, Stephens P, Davies H, Greenman C, Teague J, Butler A, Edkins S, Stevens C, O'Meara S, Parker A, Avis T, Barthorpe S, Brackenbury L, Buck G, Clements J, Cole J, Dicks E, Edwards K, Forbes S, Gorton M, Gray K, Halliday K, Harrison R, Hills K, Hinton J, Jones D, Kosmidou V, Laman R, Lugg R, Menzies A, Perry J, Petty R, Raine K, Shepherd R, Small A, Solomon H, Stephens Y, Tofts C, Varian J, Webb A, West S, Widaa S, Yates A, Gillis AJ, Stoop HJ, van Gurp RJ, Oosterhuis JW, Looijenga LH, Futreal PA, Wooster R, Stratton MR. 2006. Sequence analysis of the protein kinase gene family in human testicular germ-cell tumors of adolescents and adults. *Genes Chromosomes Cancer* 45: 42-6
19. Billerey C, Chopin D, Aubriot-Lorton MH, Ricol D, Gil Diez de Medina S, Van Rhijn B, Bralet MP, Lefrere-Belda MA, Lahaye JB, Abbou CC, Bonaventure J, Zafrani ES, van der Kwast T, Thiery JP, Radvanyi F. 2001. Frequent FGFR3 mutations in papillary non-invasive bladder (pTa) tumors. *Am J Pathol* 158: 1955-9
20. Binga EK, Lasken RS, Neufeld JD. 2008. Something from (almost) nothing: the impact of multiple displacement amplification on microbial ecology. *ISME J* 2: 233-41
21. Blanco L, Bernad A, Lazaro JM, Martin G, Garmendia C, Salas M. 1989. Highly efficient DNA synthesis by the phage phi 29 DNA polymerase. Symmetrical mode of DNA replication. *J Biol Chem* 264: 8935-40
22. Bochukova EG, Roscioli T, Hedges DJ, Taylor IB, Johnson D, David DJ, Deininger PL, Wilkie AO. 2009. Rare mutations of FGFR2 causing apert syndrome: identification of the first partial gene deletion, and an Alu element insertion from a new subfamily. *Hum Mutat* 30: 204-11
23. Boguski MS, McCormick F. 1993. Proteins regulating Ras and its relatives. *Nature* 366: 643-54
24. Bohm J, Munk-Schulenburg S, Felscher S, Kohlhase J. 2006. SALL1 mutations in sporadic Townes-Brocks syndrome are of predominantly paternal origin without obvious paternal age-effect. *Am J Med Genet A* 140: 1904-8
25. Bonner RF, Emmert-Buck M, Cole K, Pohida T, Chuaqui R, Goldstein S, Liotta LA. 1997. Laser capture microdissection: molecular analysis of tissue. *Science* 278: 1481,3
26. Boriack-Sjodin PA, Margarit SM, Bar-Sagi D, Kuriyan J. 1998. The structural basis of the activation of Ras by Sos. *Nature* 394: 337-43
27. Braydich-Stolle L, Kostereva N, Dym M, Hofmann MC. 2007. Role of Src family kinases and N-Myc in spermatogonial stem cell proliferation. *Dev Biol* 304: 34-45

28. Buaas FW, Kirsh AL, Sharma M, McLean DJ, Morris JL, Griswold MD, de Rooij DG, Braun RE. 2004. Plzf is required in adult male germ cells for stem cell self-renewal. *Nat Genet* 36: 647-52
29. Bullwinkel J, Baron-Luhr B, Ludemann A, Wohlenberg C, Gerdes J, Scholzen T. 2006. Ki-67 protein is associated with ribosomal RNA transcription in quiescent and proliferating cells. *J Cell Physiol* 206: 624-35
30. Bush JM, Gardiner DW, Palmer JS, Rajpert-De Meyts E, Veeramachaneni DN. 2011. Testicular germ cell tumours in dogs are predominantly of spermatocytic seminoma type and are frequently associated with somatic cell tumours. *Int J Androl*
31. Cancilla B, Risbridger GP. 1998. Differential localization of fibroblast growth factor receptor-1, -2, -3, and -4 in fetal, immature, and adult rat testes. *Biol Reprod* 58: 1138-45
32. Carlson KM, Bracamontes J, Jackson CE, Clark R, Lacroix A, Wells SA, Jr., Goodfellow PJ. 1994. Parent-of-origin effects in multiple endocrine neoplasia type 2B. *Am J Hum Genet* 55: 1076-82
33. Carriere P, Baade P, Fritschi L. 2007. Population based incidence and age distribution of spermatocytic seminoma. *J Urol* 178: 125-8
34. Chang EH, Gonda MA, Ellis RW, Scolnick EM, Lowy DR. 1982. Human genome contains four genes homologous to transforming genes of Harvey and Kirsten murine sarcoma viruses. *Proc Natl Acad Sci U S A* 79(16): 4848-52
35. Chellaiah AT, McEwen DG, Werner S, Xu J, Ornitz DM. 1994. Fibroblast growth factor receptor (FGFR) 3. Alternative splicing in immunoglobulin-like domain III creates a receptor highly specific for acidic FGF/FGF-1. *J Biol Chem* 269: 11620-7
36. Chen H, Ma J, Li W, Eliseenkova AV, Xu C, Neubert TA, Miller WT, Mohammadi M. 2007. A molecular brake in the kinase hinge region regulates the activity of receptor tyrosine kinases. *Mol Cell* 27: 717-30
37. Chen Z, Brand NJ, Chen A, Chen SJ, Tong JH, Wang ZY, Waxman S, Zelent A. 1993. Fusion between a novel Kruppel-like zinc finger gene and the retinoic acid receptor-alpha locus due to a variant t(11;17) translocation associated with acute promyelocytic leukaemia. *EMBO J* 12: 1161-7
38. Chesi M, Brents LA, Ely SA, Bais C, Robbiani DF, Mesri EA, Kuehl WM, Bergsagel PL. 2001. Activated fibroblast growth factor receptor 3 is an oncogene that contributes to tumor progression in multiple myeloma. *Blood* 97: 729-36
39. Chesi M, Nardini E, Brents LA, Schrock E, Ried T, Kuehl WM, Bergsagel PL. 1997. Frequent translocation t(4;14)(p16.3;q32.3) in multiple myeloma is associated with increased expression and activating mutations of fibroblast growth factor receptor 3. *Nat Genet* 16: 260-4
40. Chien Y, White MA. 2003. RAL GTPases are linchpin modulators of human tumour-cell proliferation and survival. *EMBO Rep* 4: 800-6
41. Cho JY, Guo C, Torello M, Lunstrum GP, Iwata T, Deng C, Horton WA. 2004. Defective lysosomal targeting of activated fibroblast growth factor receptor 3 in achondroplasia. *Proc Natl Acad Sci U S A* 101: 609-14
42. Choi SK, Yoon SR, Calabrese P, Arnheim N. 2008. A germ-line-selective advantage rather than an increased mutation rate can explain some unexpectedly common human disease mutations. *Proc Natl Acad Sci U S A* 105: 10143-8
43. Clermont Y. 1963. The cycle of the seminiferous epithelium in man. *Am J Anat* 112: 35-51
44. Clermont Y. 1966a. Renewal of spermatogonia in man. *Am J Anat* 118: 509-24
45. Clermont Y. 1966b. Spermatogenesis in man. A study of the spermatogonial population. *Fertil Steril* 17: 705-21

46. Collado M, Serrano M. 2006. The power and the promise of oncogene-induced senescence markers. *Nat Rev Cancer* 6: 472-6
47. Conrad DF, Keebler JE, Depristo MA, Lindsay SJ, Zhang Y, Casals F, Idaghdour Y, Hartl CL, Torroja C, Garimella KV, Zilversmit M, Cartwright R, Rouleau GA, Daly M, Stone EA, Hurles ME, Awadalla P. 2011. Variation in genome-wide mutation rates within and between human families. *Nat Genet* 43: 712-4
48. Cooper DN, Krawczak M. 1993. *Human gene mutation*. Oxford: BIOS Scientific. xiv, 402 p. pp.
49. Costoya JA, Hobbs RM, Barna M, Cattoretti G, Manova K, Sukhwani M, Orwig KE, Wolgemuth DJ, Pandolfi PP. 2004. Essential role of Plzf in maintenance of spermatogonial stem cells. *Nat Genet* 36: 653-9
50. Cronwright G, Le Blanc K, Gotherstrom C, Darcy P, Ehnman M, Brodin B. 2005. Cancer/testis antigen expression in human mesenchymal stem cells: down-regulation of SSX impairs cell migration and matrix metalloproteinase 2 expression. *Cancer Res* 65: 2207-15
51. Crow JF. 2006. Age and sex effects on human mutation rates: an old problem with new complexities. *J Radiat Res (Tokyo)* 47 Suppl B: B75-82
52. Crow JF, Denniston C. 1985. Mutation in human populations. *Adv Hum Genet* 14: 59-123
53. Dakouane Giudicelli M, Serazin V, Le Sciellour CR, Albert M, Selva J, Giudicelli Y. 2008. Increased achondroplasia mutation frequency with advanced age and evidence for G1138A mosaicism in human testis biopsies. *Fertil Steril* 89: 1651-6
54. Dalbagni G, Presti J, Reuter V, Fair WR, Cordon-Cardo C. 1993. Genetic alterations in bladder cancer. *Lancet* 342: 469-71
55. Datta SR, Brunet A, Greenberg ME. 1999. Cellular survival: a play in three Akts. *Genes Dev* 13: 2905-27
56. Datta SR, Dudek H, Tao X, Masters S, Fu H, Gotoh Y, Greenberg ME. 1997. Akt phosphorylation of BAD couples survival signals to the cell-intrinsic death machinery. *Cell* 91: 231-41
57. Davies H, Hunter C, Smith R, Stephens P, Greenman C, Bignell G, Teague J, Butler A, Edkins S, Stevens C, Parker A, O'Meara S, Avis T, Barthorpe S, Brackenbury L, Buck G, Clements J, Cole J, Dicks E, Edwards K, Forbes S, Gorton M, Gray K, Halliday K, Harrison R, Hills K, Hinton J, Jones D, Kosmidou V, Laman R, Lugg R, Menzies A, Perry J, Petty R, Raine K, Shepherd R, Small A, Solomon H, Stephens Y, Tofts C, Varian J, Webb A, West S, Widaa S, Yates A, Brasseur F, Cooper CS, Flanagan AM, Green A, Knowles M, Leung SY, Looijenga LH, Malkowicz B, Pierotti MA, Teh BT, Yuen ST, Lakhani SR, Easton DF, Weber BL, Goldstraw P, Nicholson AG, Wooster R, Stratton MR, Futreal PA. 2005. Somatic mutations of the protein kinase gene family in human lung cancer. *Cancer Res* 65: 7591-5
58. de Gruyter. 1996. *Concise Encyclopedia Biology*: Walter de Gruyter. 1287 pp.
59. De Moerlooze L, Spencer-Dene B, Revest JM, Hajihosseini M, Rosewell I, Dickson C. 2000. An important role for the IIIb isoform of fibroblast growth factor receptor 2 (FGFR2) in mesenchymal-epithelial signalling during mouse organogenesis. *Development* 127: 483-92
60. de Rooij DG. 2009. The spermatogonial stem cell niche. *Microsc Res Tech* 72: 580-5
61. de Rooij DG, Russell LD. 2000. All you wanted to know about spermatogonia but were afraid to ask. *J Androl* 21: 776-98
62. De Ruiter ND, Burgering BM, Bos JL. 2001. Regulation of the Forkhead transcription factor AFX by Ral-dependent phosphorylation of threonines 447 and 451. *Mol Cell Biol* 21: 8225-35

63. Dean FB, Hosono S, Fang L, Wu X, Faruqi AF, Bray-Ward P, Sun Z, Zong Q, Du Y, Du J, Driscoll M, Song W, Kingsmore SF, Egholm M, Lasken RS. 2002. Comprehensive human genome amplification using multiple displacement amplification. *Proc Natl Acad Sci U S A* 99: 5261-6
64. Dean FB, Nelson JR, Giesler TL, Lasken RS. 2001. Rapid amplification of plasmid and phage DNA using Phi 29 DNA polymerase and multiply-primed rolling circle amplification. *Genome Res* 11: 1095-9
65. del Peso L, Gonzalez-Garcia M, Page C, Herrera R, Nunez G. 1997. Interleukin-3-induced phosphorylation of BAD through the protein kinase Akt. *Science* 278: 687-9
66. Delezoide AL, Lasselin-Benoist C, Legeai-Mallet L, Brice P, Senee V, Yayon A, Munnich A, Vekemans M, Bonaventure J. 1997. Abnormal FGFR 3 expression in cartilage of thanatophoric dysplasia fetuses. *Hum Mol Genet* 6: 1899-906
67. Deng C, Wynshaw-Boris A, Zhou F, Kuo A, Leder P. 1996. Fibroblast Growth Factor Receptor 3 Is a Negative Regulator of Bone Growth. *Cell* 84: 911-21
68. Der CJ, Finkel T, Cooper GM. 1986. Biological and biochemical properties of human rasH genes mutated at codon 61. *Cell* 44: 167-76
69. Di Martino D, Giuffre G, Staiti N, Simone A, Le Donne M, Saravo L. 2004. Single sperm cell isolation by laser microdissection. *Forensic Sci Int* 146 Suppl: S151-3
70. di Martino E, L'Hote CG, Kennedy W, Tomlinson DC, Knowles MA. 2009. Mutant fibroblast growth factor receptor 3 induces intracellular signaling and cellular transformation in a cell type- and mutation-specific manner. *Oncogene* 28: 4306-16
71. Donovan S, Shannon KM, Bollag G. 2002. GTPase activating proteins: critical regulators of intracellular signaling. *Biochim Biophys Acta* 1602: 23-45
72. dos Santos NR, Torensma R, de Vries TJ, Schreurs MW, de Bruijn DR, Kater-Baats E, Ruiter DJ, Adema GJ, van Muijen GN, van Kessel AG. 2000. Heterogeneous expression of the SSX cancer/testis antigens in human melanoma lesions and cell lines. *Cancer Res* 60: 1654-62
73. Downward J. 2006. Signal transduction. Prelude to an anniversary for the RAS oncogene. *Science* 314: 433-4
74. Drost JB, Lee WR. 1995. Biological basis of germline mutation: comparisons of spontaneous germline mutation rates among drosophila, mouse, and human. *Environ Mol Mutagen* 25 Suppl 26: 48-64
75. Drosten M, Putzer BM. 2006. Mechanisms of Disease: cancer targeting and the impact of oncogenic RET for medullary thyroid carcinoma therapy. *Nat Clin Pract Oncol* 3: 564-74
76. Dryja TP, Morrow JF, Rapaport JM. 1997. Quantification of the paternal allele bias for new germline mutations in the retinoblastoma gene. *Hum Genet* 100: 446-9
77. Dryja TP, Mukai S, Petersen R, Rapaport JM, Walton D, Yandell DW. 1989. Parental origin of mutations of the retinoblastoma gene. *Nature* 339: 556-8
78. Dunn TL, Ross IL, Hume DA. 1996. Transcription factor Oct-2 is expressed in primary murine macrophages. *Blood* 88: 4072
79. Dutt A, Salvesen HB, Chen TH, Ramos AH, Onofrio RC, Hatton C, Nicoletti R, Winckler W, Grewal R, Hanna M, Wyhs N, Ziaugra L, Richter DJ, Trovik J, Engelsen IB, Stefansson IM, Fennell T, Cibulskis K, Zody MC, Akslen LA, Gabriel S, Wong KK, Sellers WR, Meyerson M, Greulich H. 2008. Drug-sensitive FGFR2 mutations in endometrial carcinoma. *Proc Natl Acad Sci U S A* 105: 8713-7
80. Dym M, He Z, Jiang J, Pant D, Kokkinaki M. 2009a. Spermatogonial stem cells: unlimited potential. *Reprod Fertil Dev* 21: 15-21
81. Dym M, Kokkinaki M, He Z. 2009b. Spermatogonial stem cells: mouse and human comparisons. *Birth Defects Res C Embryo Today* 87: 27-34

82. Eble JN. 1994. Spermatocytic seminoma. *Hum Pathol* 25: 1035-42
83. Eble JN, Young RH. 1997. Carcinoma of the urinary bladder: a review of its diverse morphology. *Semin Diagn Pathol* 14: 98-108
84. Edghill EL, Gloyn AL, Goriely A, Harries LW, Flanagan SE, Rankin J, Hattersley AT, Ellard S. 2007. Origin of de novo KCNJ11 mutations and risk of neonatal diabetes for subsequent siblings. *J Clin Endocrinol Metab* 92: 1773-7
85. Ellegren H, Fridolfsson AK. 1997. Male-driven evolution of DNA sequences in birds. *Nat Genet* 17: 182-4
86. Elliott K, Hill DS, Lambert C, Burroughes TR, Gill P. 2003. Use of laser microdissection greatly improves the recovery of DNA from sperm on microscope slides. *Forensic Sci Int* 137: 28-36
87. Emmert-Buck MR, Bonner RF, Smith PD, Chuaqui RF, Zhuang Z, Goldstein SR, Weiss RA, Liotta LA. 1996. Laser capture microdissection. *Science* 274: 998-1001
88. Essers MA, Weijzen S, de Vries-Smits AM, Saarloos I, de Ruiter ND, Bos JL, Burgering BM. 2004. FOXO transcription factor activation by oxidative stress mediated by the small GTPase Ral and JNK. *EMBO J* 23: 4802-12
89. Eswarakumar VP, Lax I, Schlessinger J. 2005. Cellular signaling by fibroblast growth factor receptors. *Cytokine Growth Factor Rev* 16: 139-49
90. Evans DG, Huson SM, Donnai D, Neary W, Blair V, Teare D, Newton V, Strachan T, Ramsden R, Harris R. 1992. A genetic study of type 2 neurofibromatosis in the United Kingdom. I. Prevalence, mutation rate, fitness, and confirmation of maternal transmission effect on severity. *J Med Genet* 29: 841-6
91. Feng GS. 1999. Shp-2 tyrosine phosphatase: signaling one cell or many. *Exp Cell Res* 253: 47-54
92. Fragale A, Tartaglia M, Wu J, Gelb BD. 2004. Noonan syndrome-associated SHP2/PTPN11 mutants cause EGF-dependent prolonged GAB1 binding and sustained ERK2/MAPK1 activation. *Hum Mutat* 23: 267-77
93. Fresno Vara JA, Casado E, de Castro J, Cejas P, Belda-Iniesta C, Gonzalez-Baron M. 2004. PI3K/Akt signalling pathway and cancer. *Cancer Treat Rev* 30: 193-204
94. Fukuda T, Hedinger C, Groscurth P. 1975. Ultrastructure of developing germ cells in the fetal human testis. *Cell Tissue Res* 161: 55-70
95. Gallegos I, Valdevenito JP, Miranda R, Fernandez C. 2011. Immunohistochemistry expression of P53, Ki67, CD30, and CD117 and presence of clinical metastasis at diagnosis of testicular seminoma. *Appl Immunohistochem Mol Morphol* 19: 147-52
96. Gaskell TL, Esnal A, Robinson LL, Anderson RA, Saunders PT. 2004. Immunohistochemical profiling of germ cells within the human fetal testis: identification of three subpopulations. *Biol Reprod* 71: 2012-21
97. Gerdes J, Lemke H, Baisch H, Wacker HH, Schwab U, Stein H. 1984. Cell cycle analysis of a cell proliferation-associated human nuclear antigen defined by the monoclonal antibody Ki-67. *J Immunol* 133: 1710-5
98. Gerdes J, Schwab U, Lemke H, Stein H. 1983. Production of a mouse monoclonal antibody reactive with a human nuclear antigen associated with cell proliferation. *Int J Cancer* 31: 13-20
99. Gibbs JB, Sigal IS, Poe M, Scolnick EM. 1984. Intrinsic GTPase activity distinguishes normal and oncogenic ras p21 molecules. *Proc Natl Acad Sci U S A* 81: 5704-8
100. Glaser RL, Broman KW, Schulman RL, Eskenazi B, Wyrobek AJ, Jabs EW. 2003. The paternal-age-effect in Apert syndrome is due, in part, to the increased frequency of mutations in sperm. *Am J Hum Genet* 73: 939-47

101. Glaser RL, Jiang W, Boyadjiev SA, Tran AK, Zachary AA, Van Maldergem L, Johnson D, Walsh S, Oldridge M, Wall SA, Wilkie AO, Jabs EW. 2000. Paternal origin of FGFR2 mutations in sporadic cases of Crouzon syndrome and Pfeiffer syndrome. *Am J Hum Genet* 66: 768-77
102. Goi T, Shipitsin M, Lu Z, Foster DA, Klinz SG, Feig LA. 2000. An EGF receptor/Ral-GTPase signaling cascade regulates c-Src activity and substrate specificity. *EMBO J* 19: 623-30
103. Goriely A, Hansen RM, Taylor IB, Olesen IA, Jacobsen GK, McGowan SJ, Pfeifer SP, McVean GA, Meyts ER, Wilkie AO. 2009. Activating mutations in FGFR3 and HRAS reveal a shared genetic origin for congenital disorders and testicular tumors. *Nat Genet* 41: 1247-52
104. Goriely A, Lord H, Lim J, Johnson D, Lester T, Firth HV, Wilkie AO. 2010. Germline and somatic mosaicism for FGFR2 mutation in the mother of a child with Crouzon syndrome: Implications for genetic testing in "paternal age-effect" syndromes. *Am J Med Genet A* 152A: 2067-73
105. Goriely A, McVean GA, Rojmyr M, Ingemarsson B, Wilkie AO. 2003. Evidence for selective advantage of pathogenic FGFR2 mutations in the male germ line. *Science* 301: 643-6
106. Goriely A, McVean GA, van Pelt AM, O'Rourke AW, Wall SA, de Rooij DG, Wilkie AO. 2005. Gain-of-function amino acid substitutions drive positive selection of FGFR2 mutations in human spermatogonia. *Proc Natl Acad Sci U S A* 102: 6051-6
107. Goriely A, Wilkie AO. 2010. Missing heritability: paternal age-effect mutations and selfish spermatogonia. *Nat Rev Genet* 11: 589
108. Grille SJ, Bellacosa A, Upson J, Klein-Szanto AJ, van Roy F, Lee-Kwon W, Donowitz M, Tsichlis PN, Larue L. 2003. The protein kinase Akt induces epithelial mesenchymal transition and promotes enhanced motility and invasiveness of squamous cell carcinoma lines. *Cancer Res* 63: 2172-8
109. Grosso AR, Martins S, Carmo-Fonseca M. 2008. The emerging role of splicing factors in cancer. *EMBO Rep* 9: 1087-93
110. Gujral TS, Singh VK, Jia Z, Mulligan LM. 2006. Molecular mechanisms of RET receptor-mediated oncogenesis in multiple endocrine neoplasia 2B. *Cancer Res* 66: 10741-9
111. Guo C, Degnin CR, Laederich MB, Lunstrum GP, Holden P, Bihlmaier J, Krakow D, Cho YJ, Horton WA. 2008. Sprouty 2 disturbs FGFR3 degradation in thanatophoric dysplasia type II: a severe form of human achondroplasia. *Cell Signal* 20: 1471-7
112. Hafner C, Hartmann A, van Oers JM, Stoehr R, Zwarthoff EC, Hofstaedter F, Landthaler M, Vogt T. 2007a. FGFR3 mutations in seborrheic keratoses are already present in flat lesions and associated with age and localization. *Mod Pathol* 20: 895-903
113. Hafner C, Lopez-Knowles E, Luis NM, Toll A, Baselga E, Fernandez-Casado A, Hernandez S, Ribe A, Mentzel T, Stoehr R, Hofstaedter F, Landthaler M, Vogt T, Pujol RM, Hartmann A, Real FX. 2007b. Oncogenic PIK3CA mutations occur in epidermal nevi and seborrheic keratoses with a characteristic mutation pattern. *Proc Natl Acad Sci U S A* 104: 13450-4
114. Hafner C, van Oers JM, Hartmann A, Landthaler M, Stoehr R, Blaszyk H, Hofstaedter F, Zwarthoff EC, Vogt T. 2006. High frequency of FGFR3 mutations in adenoid seborrheic keratoses. *J Invest Dermatol* 126: 2404-7
115. Hafner C, Vogt T, Landthaler M, Musebeck J. 2008. Somatic FGFR3 and PIK3CA mutations are present in familial seborrhoeic keratoses. *Br J Dermatol* 159: 214-7

116. Haldane JB. 1947. The mutation rate of the gene for haemophilia, and its segregation ratios in males and females. *Ann Eugen* 13: 262-71
117. Han IS, Sylvester SR, Kim KH, Schelling ME, Venkateswaran S, Blanckaert VD, McGuinness MP, Griswold MD. 1993. Basic fibroblast growth factor is a testicular germ cell product which may regulate Sertoli cell function. *Mol Endocrinol* 7: 889-97
118. Hansen R. 2006. *Fibroblast growth factor receptor 2 mutations in human sperm: Biological implications.* DPhil thesis. University of Oxford
119. Hansen RM, Goriely A, Wall SA, Roberts IS, Wilkie AO. 2005. Fibroblast growth factor receptor 2, gain-of-function mutations, and tumourigenesis: investigating a potential link. *J Pathol* 207: 27-31
120. He L, Horton W, Hristova K. 2010. Physical basis behind achondroplasia, the most common form of human dwarfism. *J Biol Chem* 285: 30103-14
121. He X, Treacy MN, Simmons DM, Ingraham HA, Swanson LW, Rosenfeld MG. 1989. Expression of a large family of POU-domain regulatory genes in mammalian brain development. *Nature* 340: 35-41
122. He Z, Jiang J, Kokkinaki M, Golestaneh N, Hofmann MC, Dym M. 2008. Gdnf upregulates c-Fos transcription via the Ras/Erk1/2 pathway to promote mouse spermatogonial stem cell proliferation. *Stem Cells* 26: 266-78
123. Hennekam RC. 2003. Costello syndrome: an overview. *Am J Med Genet C Semin Med Genet* 117C: 42-8
124. Henry DO, Moskalenko SA, Kaur KJ, Fu M, Pestell RG, Camonis JH, White MA. 2000. Ral GTPases contribute to regulation of cyclin D1 through activation of NF-kappaB. *Mol Cell Biol* 20: 8084-92
125. Heron SE, Scheffer IE, Iona X, Zuberi SM, Birch R, McMahon JM, Bruce CM, Berkovic SF, Mulley JC. 2010. De novo SCN1A mutations in Dravet syndrome and related epileptic encephalopathies are largely of paternal origin. *J Med Genet* 47: 137-41
126. Hobbs RM, Seandel M, Falciatori I, Rafii S, Pandolfi PP. 2010. Plzf regulates germline progenitor self-renewal by opposing mTORC1. *Cell* 142(3):468-79
127. Hoei-Hansen CE, Rajpert-De Meyts E, Daugaard G, Skakkebaek NE. 2005. Carcinoma in situ testis, the progenitor of testicular germ cell tumours: a clinical review. *Ann Oncol* 16: 863-8
128. Honecker F, Stoop H, de Krijger RR, Chris Lau YF, Bokemeyer C, Looijenga LH. 2004. Pathobiological implications of the expression of markers of testicular carcinoma in situ by fetal germ cells. *J Pathol* 203: 849-57
129. Hosono S, Faruqi AF, Dean FB, Du Y, Sun Z, Wu X, Du J, Kingsmore SF, Egholm M, Lasken RS. 2003. Unbiased whole-genome amplification directly from clinical samples. *Genome Res* 13: 954-64
130. Huckins C. 1971. The spermatogonial stem cell population in adult rats. I. Their morphology, proliferation and maturation. *Anat Rec* 169: 533-57
131. Hughes SE. 1997. Differential expression of the fibroblast growth factor receptor (FGFR) multigene family in normal human adult tissues. *J Histochem Cytochem* 45: 1005-19
132. Hurst LD, Ellegren H. 1998. Sex biases in the mutation rate. *Trends Genet* 14: 446-52
133. Ibrahimi OA, Eliseenkova AV, Plotnikov AN, Yu K, Ornitz DM, Mohammadi M. 2001. Structural basis for fibroblast growth factor receptor 2 activation in Apert syndrome. *Proc Natl Acad Sci U S A* 98: 7182-7

134. Ibrahimi OA, Zhang F, Eliseenkova AV, Itoh N, Linhardt RJ, Mohammadi M. 2004. Biochemical analysis of pathogenic ligand-dependent FGFR2 mutations suggests distinct pathophysiological mechanisms for craniofacial and limb abnormalities. *Hum Mol Genet* 13: 2313-24
135. Iwashita T, Asai N, Murakami H, Matsuyama M, Takahashi M. 1996. Identification of tyrosine residues that are essential for transforming activity of the ret proto-oncogene with MEN2A or MEN2B mutation. *Oncogene* 12: 481-7
136. Iwashita T, Kato M, Murakami H, Asai N, Ishiguro Y, Ito S, Iwata Y, Kawai K, Asai M, Kurokawa K, Kajita H, Takahashi M. 1999. Biological and biochemical properties of Ret with kinase domain mutations identified in multiple endocrine neoplasia type 2B and familial medullary thyroid carcinoma. *Oncogene* 18: 3919-22
137. Jadayel D, Fain P, Upadhyaya M, Ponder MA, Huson SM, Carey J, Fryer A, Mathew CG, Barker DF, Ponder BA. 1990. Paternal origin of new mutations in von Recklinghausen neurofibromatosis. *Nature* 343: 558-9
138. Jain S, Naughton CK, Yang M, Strickland A, Vij K, Encinas M, Golden J, Gupta A, Heuckeroth R, Johnson EM, Jr., Milbrandt J. 2004. Mice expressing a dominant-negative Ret mutation phenocopy human Hirschsprung disease and delineate a direct role of Ret in spermatogenesis. *Development* 131: 5503-13
139. Jang JH, Shin KH, Park JG. 2001. Mutations in fibroblast growth factor receptor 2 and fibroblast growth factor receptor 3 genes associated with human gastric and colorectal cancers. *Cancer Res* 61: 3541-3
140. Jasim S, Ying AK, Waguespack SG, Rich TA, Grubbs EG, Jimenez C, Hu MI, Cote G, Habra MA. 2011. Multiple endocrine neoplasia type 2B with a RET proto-oncogene A883F mutation displays a more indolent form of medullary thyroid carcinoma compared with a RET M918T mutation. *Thyroid* 21: 189-92
141. Jebar AH, Hurst CD, Tomlinson DC, Johnston C, Taylor CF, Knowles MA. 2005. FGFR3 and Ras gene mutations are mutually exclusive genetic events in urothelial cell carcinoma. *Oncogene* 24: 5218-25
142. Jiang Z, Zhang X, Deka R, Jin L. 2005. Genome amplification of single sperm using multiple displacement amplification. *Nucleic Acids Res* 33: e91
143. John J, Frech M, Wittinghofer A. 1988. Biochemical properties of Ha-ras encoded p21 mutants and mechanism of the autophosphorylation reaction. *J Biol Chem* 263: 11792-9
144. Johnsen SG. 1970. Testicular biopsy score count--a method for registration of spermatogenesis in human testes: normal values and results in 335 hypogonadal males. *Hormones* 1: 2-25
145. Johnson DE, Williams LT. 1993. Structural and functional diversity in the FGF receptor multigene family. *Adv Cancer Res* 60: 1-41
146. Johnston CL, Cox HC, Gomm JJ, Coombes RC. 1995. Fibroblast growth factor receptors (FGFRs) localize in different cellular compartments. A splice variant of FGFR-3 localizes to the nucleus. *J Biol Chem* 270: 30643-50
147. Johnson L, Petty CS, Neaves WB. 1986. Age-related variation in seminiferous tubules in men. A stereologic evaluation. *J Androl* 7:316-22.
148. Jorgensen N, Rajpert-De Meyts E, Graem N, Muller J, Giwercman A, Skakkebaek NE. 1995. Expression of immunohistochemical markers for testicular carcinoma in situ by normal human fetal germ cells. *Lab Invest* 72: 223-31
149. Juul A, Aksglaede L, Lund AM, Duno M, Skakkebaek NE, Rajpert-De Meyts E. 2007. Preserved fertility in a non-mosaic Klinefelter patient with a mutation in the fibroblast growth factor receptor 3 gene: case report. *Hum Reprod* 22: 1907-11

150. Kan SH, Kan SH, Elanko N, Johnson D, Cornejo-Roldan L, Cook J, Reich EW, Tomkins S, Verloes A, Twigg SR, Rannan-Eliya S, McDonald-McGinn DM, Zackai EH, Wall SA, Muenke M, Wilkie AO. Genomic screening of fibroblast growth-factor receptor 2 reveals a wide spectrum of mutations in patients with syndromic craniosynostosis. *Am J Hum Genet* 70(2): 472-86.
151. Kang SM, Tsang W, Doll S, Scherle P, Ko HS, Tran AC, Lenardo MJ, Staudt LM. 1992. Induction of the POU domain transcription factor Oct-2 during T-cell activation by cognate antigen. *Mol Cell Biol* 12: 3149-54
152. Karlou M, Saetta AA, Korkolopoulou P, Levidou G, Papanastasiou P, Boltetsou E, Isaiadis D, Pavlopoulos P, Thymara I, Thomas-Tsagli E, Patsouris E. 2009. Activation of extracellular regulated kinases (ERK1/2) predicts poor prognosis in urothelial bladder carcinoma and is not associated with B-Raf gene mutations. *Pathology* 41: 327-34
153. Kato MV, Ishizaki K, Shimizu T, Ejima Y, Tanooka H, Takayama J, Kaneko A, Toguchida J, Sasaki MS. 1994. Parental origin of germ-line and somatic mutations in the retinoblastoma gene. *Hum Genet* 94: 31-8
154. Keilhack H, David FS, McGregor M, Cantley LC, Neel BG. 2005. Diverse biochemical properties of Shp2 mutants. Implications for disease phenotypes. *J Biol Chem* 280: 30984-93
155. Kelley GG, Reks SE, Ondrako JM, Smrcka AV. 2001. Phospholipase C(epsilon): a novel Ras effector. *EMBO J* 20: 743-54
156. Khokhlatchev AV, Canagarajah B, Wilsbacher J, Robinson M, Atkinson M, Goldsmith E, Cobb MH. 1998. Phosphorylation of the MAP kinase ERK2 promotes its homodimerization and nuclear translocation. *Cell* 93: 605-15
157. Kido T, Lau YF. 2006. The rat Tspy is preferentially expressed in elongated spermatids and interacts with the core histones. *Biochem Biophys Res Commun* 350: 56-67
158. Kimelman D, Kirschner M. 1987. Synergistic Induction of Mesoderm by Fgf and Tgf-Beta and the Identification of an Messenger-Rna Coding for Fgf in the Early Xenopus Embryo. *Cell* 51: 869-77
159. Kimura M. 1968. Evolutionary rate at the molecular level. *Nature* 217: 624-6
160. Kimura T, Tomooka M, Yamano N, Murayama K, Matoba S, Umehara H, Kanai Y, Nakano T. 2008. AKT signaling promotes derivation of embryonic germ cells from primordial germ cells. *Development* 135: 869-79
161. Kitamura Y, Scavarda N, Wells SA, Jr., Jackson CE, Goodfellow PJ. 1995. Two maternally derived missense mutations in the tyrosine kinase domain of the RET protooncogene in a patient with de novo MEN 2B. *Hum Mol Genet* 4: 1987-8
162. Klein AM, Nakagawa T, Ichikawa R, Yoshida S, Simons BD. 2010. Mouse germ line stem cells undergo rapid and stochastic turnover. *Cell Stem Cell* 7: 214-24
163. Kluwe L, Mautner V, Parry DM, Jacoby LB, Baser M, Gusella J, Davis K, Stavrou D, MacCollin M. 2000. The parental origin of new mutations in neurofibromatosis 2. *Neurogenetics* 3: 17-24
164. Knowles MA, Platt FM, Ross RL, Hurst CD. 2009. Phosphatidylinositol 3-kinase (PI3K) pathway activation in bladder cancer. *Cancer Metastasis Rev* 28: 305-16
165. Koike S, Noumura T. 1995. Immunohistochemical detection of the expression of the alpha subunit of inhibin, TGF-beta, basic-FGF and IGF-II in fetal ovarian grafts grown with fetal testes beneath the kidney capsule of adult castrated male rats. *J Exp Zool* 272: 319-28
166. Kolble K. 2000. The LEICA microdissection system: design and applications. *J Mol Med* 78: B24-5

167. Kompier LC, Lurkin I, van der Aa MN, van Rhijn BW, van der Kwast TH, Zwarthoff EC. 2010. FGFR3, HRAS, KRAS, NRAS and PIK3CA mutations in bladder cancer and their potential as biomarkers for surveillance and therapy. *PLoS One* 5: e13821
168. Kondrashov AS. 2003. Direct estimates of human per nucleotide mutation rates at 20 loci causing Mendelian diseases. *Hum Mutat* 21: 12-27
169. Kondrashov FA, Kondrashov AS. 2010. Measurements of spontaneous rates of mutations in the recent past and the near future. *Philos Trans R Soc Lond B Biol Sci* 365: 1169-76
170. Konishi H, Kuroda S, Tanaka M, Matsuzaki H, Ono Y, Kameyama K, Haga T, Kikkawa U. 1995. Molecular cloning and characterization of a new member of the RAC protein kinase family: association of the pleckstrin homology domain of three types of RAC protein kinase with protein kinase C subspecies and beta gamma subunits of G proteins. *Biochem Biophys Res Commun* 216: 526-34
171. Kops GJ, de Ruiter ND, De Vries-Smits AM, Powell DR, Bos JL, Burgering BM. 1999. Direct control of the Forkhead transcription factor AFX by protein kinase B. *Nature* 398: 630-4
172. Krenz M, Gulick J, Osinska HE, Colbert MC, Molkentin JD, Robbins J. 2008. Role of ERK1/2 signaling in congenital valve malformations in Noonan syndrome. *Proc Natl Acad Sci U S A* 105: 18930-5
173. Kubota H, Avarbock MR, Brinster RL. 2004. Growth factors essential for self-renewal and expansion of mouse spermatogonial stem cells. *Proc Natl Acad Sci U S A* 101: 16489-94
174. Kuniba H, Pooh RK, Sasaki K, Shimokawa O, Harada N, Kondoh T, Egashira M, Moriuchi H, Yoshiura K, Niikawa N. 2009. Prenatal diagnosis of Costello syndrome using 3D ultrasonography amniocentesis confirmation of the rare HRAS mutation G12D. *Am J Med Genet A* 149A: 785-7
175. Laduron S, Deplus R, Zhou S, Kholmanskikh O, Godelaine D, De Smet C, Hayward SD, Fuks F, Boon T, De Plaen E. 2004. MAGE-A1 interacts with adaptor SKIP and the deacetylase HDAC1 to repress transcription. *Nucleic Acids Res* 32: 4340-50
176. Lajeunie E, Cameron R, El Ghouzzi V, de Parseval N, Journeau P, Gonzales M, Delezoide AL, Bonaventure J, Le Merrer M, Renier D. 1999. Clinical variability in patients with Apert's syndrome. *J Neurosurg* 90: 443-7
177. Lambert JM, Lambert QT, Reuther GW, Malliri A, Siderovski DP, Sondek J, Collard JG, Der CJ. 2002. Tiam1 mediates Ras activation of Rac by a PI(3)K-independent mechanism. *Nat Cell Biol* 4: 621-5
178. Landry C, Brasseur F, Spagnoli GC, Marbaix E, Boon T, Coulie P, Godelaine D. 2000. Monoclonal antibody 57B stains tumor tissues that express gene MAGE-A4. *Int J Cancer* 86: 835-41
179. Lasken RS. 2009. Genomic DNA amplification by the multiple displacement amplification (MDA) method. *Biochem Soc Trans* 37: 450-3
180. Latchman DS. 1996. The Oct-2 transcription factor. *Int J Biochem Cell Biol* 28: 1081-3
181. Lee J, Kanatsu-Shinohara M, Inoue K, Ogonuki N, Miki H, Toyokuni S, Kimura T, Nakano T, Ogura A, Shinohara T. 2007. Akt mediates self-renewal division of mouse spermatogonial stem cells. *Development* 134: 1853-9
182. Lee J, Kanatsu-Shinohara M, Morimoto H, Kazuki Y, Takashima S, Oshimura M, Toyokuni S, Shinohara T. 2009. Genetic reconstruction of mouse spermatogonial stem cell self-renewal in vitro by Ras-cyclin D2 activation. *Cell Stem Cell* 5: 76-86

183. Li R, Johnson AB, Salomons GS, van der Knaap MS, Rodriguez D, Boespflug-Tanguy O, Gorospe JR, Goldman JE, Messing A, Brenner M. 2006. Propensity for paternal inheritance of de novo mutations in Alexander disease. *Hum Genet* 119: 137-44
184. Li W, Zhu T, Guan KL. 2004. Transformation potential of Ras isoforms correlates with activation of phosphatidylinositol 3-kinase but not ERK. *J Biol Chem* 279: 37398-406
185. Li WH, Yi S, Makova K. 2002. Male-driven evolution. *Curr Opin Genet Dev* 12: 650-6
186. Lievens PM, Liboi E. 2003. The thanatophoric dysplasia type II mutation hampers complete maturation of fibroblast growth factor receptor 3 (FGFR3), which activates signal transducer and activator of transcription 1 (STAT1) from the endoplasmic reticulum. *J Biol Chem* 278: 17344-9
187. Lievens PM, Mutinelli C, Baynes D, Liboi E. 2004. The kinase activity of fibroblast growth factor receptor 3 with activation loop mutations affects receptor trafficking and signaling. *J Biol Chem* 279: 43254-60
188. Lievens PM, Roncador A, Liboi E. 2006. K644E/M FGFR3 mutants activate Erk1/2 from the endoplasmic reticulum through FRS2 alpha and PLC gamma-independent pathways. *Journal of Molecular Biology* 357: 783-92
189. Lievens PM, Zanolli E, Garofalo S, Liboi E. 2009. Cell adaptation to activated FGFR3 includes Sprouty4 up regulation to inhibit the receptor-mediated ERKs activation from the endoplasmic reticulum. *Febs Letters* 583: 3254-8
190. Lim J, Goriely A, Turner GD, Ewen KA, Jacobsen GK, Graem N, Wilkie AO, Rajpert-De Meyts E. 2011. OCT2, SSX and SAGE1 reveal the phenotypic heterogeneity of spermatocytic seminoma reflecting distinct subpopulations of spermatogonia. *J Pathol* 224: 473-83
191. Liu W, Cheng S, Asa SL, Ezzat S. 2008. The melanoma-associated antigen A3 mediates fibronectin-controlled cancer progression and metastasis. *Cancer Res* 68: 8104-12
192. Lo IF, Brewer C, Shannon N, Shorto J, Tang B, Black G, Soo MT, Ng DK, Lam ST, Kerr B. 2008. Severe neonatal manifestations of Costello syndrome. *J Med Genet* 45: 167-71
193. Looijenga LH, Hersmus R, Gillis AJ, Pfundt R, Stoop HJ, van Gurp RJ, Veltman J, Beverloo HB, van Drunen E, van Kessel AG, Pera RR, Schneider DT, Summersgill B, Shipley J, McIntyre A, van der Spek P, Schoenmakers E, Oosterhuis JW. 2006. Genomic and expression profiling of human spermatocytic seminomas: primary spermatocyte as tumorigenic precursor and DMRT1 as candidate chromosome 9 gene. *Cancer Res* 66: 290-302
194. Lopez-Knowles E, Hernandez S, Malats N, Kogevinas M, Lloreta J, Carrato A, Tardon A, Serra C, Real FX. 2006. PIK3CA mutations are an early genetic alteration associated with FGFR3 mutations in superficial papillary bladder tumors. *Cancer Res* 66: 7401-4
195. Lu Q, Sun QY, Breitbart H, Chen DY. 1999. Expression and phosphorylation of mitogen-activated protein kinases during spermatogenesis and epididymal sperm maturation in mice. *Arch Androl* 43: 55-66
196. Makova KD, Li WH. 2002. Strong male-driven evolution of DNA sequences in humans and apes. *Nature* 416: 624-6
197. Malliri A, van der Kammen RA, Clark K, van der Valk M, Michiels F, Collard JG. 2002. Mice deficient in the Rac activator Tiam1 are resistant to Ras-induced skin tumours. *Nature* 417: 867-71

198. Malumbres M, Barbacid M. 2003. RAS oncogenes: the first 30 years. *Nat Rev Cancer* 3: 459-65
199. Manivel JC, Jessurun J, Wick MR, Dehner LP. 1987. Placental alkaline phosphatase immunoreactivity in testicular germ-cell neoplasms. *Am J Surg Pathol* 11: 21-9
200. Margarit SM, Sondermann H, Hall BE, Nagar B, Hoelz A, Pirruccello M, Bar-Sagi D, Kuriyan J. 2003. Structural evidence for feedback activation by Ras.GTP of the Ras-specific nucleotide exchange factor SOS. *Cell* 112: 685-95
201. Margolin JF, Friedman JR, Meyer WK, Vissing H, Thiesen HJ, Rauscher FJ, 3rd. 1994. Kruppel-associated boxes are potent transcriptional repression domains. *Proc Natl Acad Sci U S A* 91: 4509-13
202. Maric D, Fiorio Pla A, Chang YH, Barker JL. 2007. Self-renewing and differentiating properties of cortical neural stem cells are selectively regulated by basic fibroblast growth factor (FGF) signaling via specific FGF receptors. *J Neurosci* 27: 1836-52
203. Markert CL, Amet TM, Goldberg E. 1998. Human testis-specific lactate dehydrogenase-C promoter drives overexpression of mouse lactate dehydrogenase-1 cDNA in testes of transgenic mice. *J Exp Zool* 282: 171-8
204. Martelange V, De Smet C, De Plaen E, Lurquin C, Boon T. 2000. Identification on a human sarcoma of two new genes with tumor-specific expression. *Cancer Res* 60: 3848-55
205. Martinez-Torrecuadrada JL, Cheung LH, Lopez-Serra P, Barderas R, Canamero M, Ferreiro S, Rosenblum MG, Casal JI. 2008. Antitumor activity of fibroblast growth factor receptor 3-specific immunotoxins in a xenograft mouse model of bladder carcinoma is mediated by apoptosis. *Mol Cancer Ther* 7: 862-73
206. Masson P. 1946. Études sur le séminome. *Revue Canadienne de Biologie* 5: 361-87
207. McAlister C. 2011. The use of fluorescence in situ hybridisation and laser microdissection to identify and isolate male cells in an azoospermic sexual assault case. *Forensic Sci Int Genet* 5: 69-73
208. McVean GT, Hurst LD. 1997. Evidence for a selectively favourable reduction in the mutation rate of the X chromosome. *Nature* 386: 388-92
209. Meng X, Lindahl M, Hyvonen ME, Parvinen M, de Rooij DG, Hess MW, Raatikainen-Ahokas A, Sainio K, Rauvala H, Lakso M, Pichel JG, Westphal H, Saarma M, Sariola H. 2000. Regulation of cell fate decision of undifferentiated spermatogonia by GDNF. *Science* 287: 1489-93
210. Micke P, Ostman A, Lundeberg J, Ponten F. 2005. Laser-assisted cell microdissection using the PALM system. *Methods Mol Biol* 293: 151-66
211. Miki T, Bottaro DP, Fleming TP, Smith CL, Burgess WH, Chan AM, Aaronson SA. 1992. Determination of ligand-binding specificity by alternative splicing: two distinct growth factor receptors encoded by a single gene. *Proc Natl Acad Sci U S A* 89: 246-50
212. Mitin N, Rossman KL, Der CJ. 2005. Signaling interplay in Ras superfamily function. *Curr Biol* 15: R563-74
213. Mitra AP, Cote RJ. 2009. Molecular pathogenesis and diagnostics of bladder cancer. *Annu Rev Pathol* 4: 251-85
214. Mo L, Zheng X, Huang HY, Shapiro E, Lepor H, Cordon-Cardo C, Sun TT, Wu XR. 2007. Hyperactivation of Ha-ras oncogene, but not Ink4a/Arf deficiency, triggers bladder tumorigenesis. *J Clin Invest* 117: 314-25
215. Moloney DM, Slaney SF, Oldridge M, Wall SA, Sahlin P, Stenman G, Wilkie AO. 1996. Exclusive paternal origin of new mutations in Apert syndrome. *Nat Genet* 13: 48-53

216. Muenke M, Gripp KW, McDonald-McGinn DM, Gaudenz K, Whitaker LA, Bartlett SP, Markowitz RI, Robin NH, Nwokoro N, Mulvihill JJ, Losken HW, Mulliken JB, Guttmacher AE, Wilroy RS, Clarke LA, Hollway G, Ades LC, Haan EA, Mulley JC, Cohen MM, Jr., Bellus GA, Francomano CA, Moloney DM, Wall SA, Wilkie AO, et al. 1997. A unique point mutation in the fibroblast growth factor receptor 3 gene (FGFR3) defines a new craniosynostosis syndrome. *Am J Hum Genet* 60: 555-64
217. Mullaney BP, Skinner MK. 1992. Basic fibroblast growth factor (bFGF) gene expression and protein production during pubertal development of the seminiferous tubule: follicle-stimulating hormone-induced Sertoli cell bFGF expression. *Endocrinology* 131: 2928-34
218. Muller J, Skakkebaek NE, Parkinson MC. 1987. The spermatocytic seminoma: views on pathogenesis. *Int J Androl* 10: 147-56
219. Mulligan LM, Eng C, Healey CS, Clayton D, Kwok JB, Gardner E, Ponder MA, Frilling A, Jackson CE, Lehnert H, et al. 1994. Specific mutations of the RET proto-oncogene are related to disease phenotype in MEN 2A and FMTC. *Nat Genet* 6: 70-4
220. Myers SM, Eng C, Ponder BA, Mulligan LM. 1995. Characterization of RET proto-oncogene 3' splicing variants and polyadenylation sites: a novel C-terminus for RET. *Oncogene* 11: 2039-45
221. Nachman MW, Crowell SL. 2000. Estimate of the mutation rate per nucleotide in humans. *Genetics* 156: 297-304
222. Naka N, Joyama S, Tsukamoto Y, Yoshioka K, Hashimoto N, Ujiiye T, Hayashi T, Kawase M, Mano M, Ishiguro S, Myoui A, Ueda T, Yoshikawa H, Araki N, Itoh K. 2005. Quantification of SSX mRNA expression in human bone and soft tissue tumors using nucleic acid sequence-based amplification. *J Mol Diagn* 7: 187-97
223. Nakagawa T, Nabeshima Y, Yoshida S. 2007. Functional identification of the actual and potential stem cell compartments in mouse spermatogenesis. *Dev Cell* 12: 195-206
224. Naski MC, Ornitz DM. 1998. FGF signaling in skeletal development. *Front Biosci* 3: d781-94
225. Naski MC, Wang Q, Xu J, Ornitz DM. 1996. Graded activation of fibroblast growth factor receptor 3 by mutations causing achondroplasia and thanatophoric dysplasia. *Nat Genet* 13: 233-7
226. Naughton CK, Jain S, Strickland AM, Gupta A, Milbrandt J. 2006. Glial cell-line derived neurotrophic factor-mediated RET signaling regulates spermatogonial stem cell fate. *Biol Reprod* 74: 314-21
227. Neal SE, Eccleston JF, Hall A, Webb MR. 1988. Kinetic analysis of the hydrolysis of GTP by p21N-ras. The basal GTPase mechanism. *J Biol Chem* 263: 19718-22
228. Neel BG, Gu H, Pao L. 2003. The 'Shp'ing news: SH2 domain-containing tyrosine phosphatases in cell signaling. *Trends Biochem Sci* 28: 284-93
229. Neilson KM, Friesel R. 1996. Ligand-independent activation of fibroblast growth factor receptors by point mutations in the extracellular, transmembrane, and kinase domains. *J Biol Chem* 271: 25049-57
230. Neilson KM, Friesel RE. 1995. Constitutive activation of fibroblast growth factor receptor-2 by a point mutation associated with Crouzon syndrome. *J Biol Chem* 270: 26037-40
231. Nichols J, Zevnik B, Anastassiadis K, Niwa H, Klewe-Nebenius D, Chambers I, Scholer H, Smith A. 1998. Formation of pluripotent stem cells in the mammalian embryo depends on the POU transcription factor Oct4. *Cell* 95: 379-91
232. Nicholson KM, Anderson NG. 2002. The protein kinase B/Akt signalling pathway in human malignancy. *Cell Signal* 14: 381-95

233. Nishimura G, Fukushima Y, Ohashi H, Ikegawa S. 1995. Atypical radiological findings in achondroplasia with uncommon mutation of the fibroblast growth factor receptor-3 (FGFR-3) gene (Gly to Cys transition at codon 375). *Am J Med Genet* 59: 393-5
234. Niwa H, Miyazaki J, Smith AG. 2000. Quantitative expression of Oct-3/4 defines differentiation, dedifferentiation or self-renewal of ES cells. *Nat Genet* 24: 372-6
235. Novotný J HT. 2008. Bringing laser microdissection and on-chip PCR together. *Profiles in DNA*: 6-7
236. Oakberg EF. 1971. Spermatogonial stem-cell renewal in the mouse. *Anat Rec* 169: 515-31
237. Oatley JM, Brinster RL. 2008. Regulation of spermatogonial stem cell self-renewal in mammals. *Annu Rev Cell Dev Biol* 24: 263-86
238. Okano J, Gaslightwala I, Birnbaum MJ, Rustgi AK, Nakagawa H. 2000. Akt/protein kinase B isoforms are differentially regulated by epidermal growth factor stimulation. *J Biol Chem* 275: 30934-42
239. Oldridge M, Lunt PW, Zackai EH, McDonald-McGinn DM, Muenke M, Moloney DM, Twigg SR, Heath JK, Howard TD, Hoganson G, Gagnon DM, Jabs EW, Wilkie AO. 1997. Genotype-phenotype correlation for nucleotide substitutions in the IgII-IgIII linker of FGFR2. *Hum Mol Genet* 6: 137-43
240. Oldridge M, Zackai EH, McDonald-McGinn DM, Iseki S, Morriss-Kay GM, Twigg SR, Johnson D, Wall SA, Jiang W, Theda C, Jabs EW, Wilkie AO. 1999. De novo alu-element insertions in FGFR2 identify a distinct pathological basis for Apert syndrome. *Am J Hum Genet* 64: 446-61
241. Olson JM, Breslow NE, Beckwith JB. 1993. Wilms' tumour and parental age: a report from the National Wilms' Tumour Study. *Br J Cancer* 67: 813-8
242. Oosterhuis JW, Looijenga LH. 2005. Testicular germ-cell tumours in a broader perspective. *Nat Rev Cancer* 5: 210-22
243. Ornitz DM. 2005. FGF signaling in the developing endochondral skeleton. *Cytokine Growth Factor Rev* 16: 205-13
244. Ornitz DM, Xu J, Colvin JS, McEwen DG, MacArthur CA, Coulier F, Gao G, Goldfarb M. 1996. Receptor specificity of the fibroblast growth factor family. *J Biol Chem* 271: 15292-7
245. Orr-Urtreger A, Bedford MT, Burakova T, Arman E, Zimmer Y, Yayon A, Givol D, Lonai P. 1993. Developmental localization of the splicing alternatives of fibroblast growth factor receptor-2 (FGFR2). *Dev Biol* 158: 475-86
246. Ostman A, Hellberg C, Bohmer FD. 2006. Protein-tyrosine phosphatases and cancer. *Nat Rev Cancer* 6: 307-20
247. Ota S, Zhou ZQ, Link JM, Hurlin PJ. 2009. The role of senescence and prosurvival signaling in controlling the oncogenic activity of FGFR2 mutants associated with cancer and birth defects. *Hum Mol Genet* 18: 2609-21
248. Pacold ME, Suire S, Perisic O, Lara-Gonzalez S, Davis CT, Walker EH, Hawkins PT, Stephens L, Eccleston JF, Williams RL. 2000. Crystal structure and functional analysis of Ras binding to its effector phosphoinositide 3-kinase gamma. *Cell* 103: 931-43
249. Paniagua R, Nistal M, Amat P, Rodriguez MC, Alonso JR. 1986. Quantitative differences between variants of A spermatogonia in man. *J Reprod Fertil* 77: 669-73
250. Paniagua R, Nistal M, Saez FJ, Fraile B. 1991. Ultrastructure of the aging human testis. *J Electron Microsc Tech* 19: 241-60
251. Penrose LS. 1955. Parental age and mutation. *Lancet* 269: 312-3

252. Phay JE, Shah MH. 2010. Targeting RET receptor tyrosine kinase activation in cancer. *Clin Cancer Res* 16: 5936-41
253. Platt FM, Hurst CD, Taylor CF, Gregory WM, Harnden P, Knowles MA. 2009. Spectrum of phosphatidylinositol 3-kinase pathway gene alterations in bladder cancer. *Clin Cancer Res* 15: 6008-17
254. Pollock PM, Gartside MG, Dejeza LC, Powell MA, Mallon MA, Davies H, Mohammadi M, Futreal PA, Stratton MR, Trent JM, Goodfellow PJ. 2007. Frequent activating FGFR2 mutations in endometrial carcinomas parallel germline mutations associated with craniosynostosis and skeletal dysplasia syndromes. *Oncogene* 26: 7158-62
255. Potten CS, Loeffler M. 1990. Stem cells: attributes, cycles, spirals, pitfalls and uncertainties. Lessons for and from the crypt. *Development* 110: 1001-20
256. Qin J, Calabrese P, Tiemann-Boege I, Shinde DN, Yoon SR, Gelfand D, Bauer K, Arnheim N. 2007. The molecular anatomy of spontaneous germline mutations in human testes. *PLoS Biol* 5: e224
257. Qiu WH, Zhou BS, Chu PG, Chen WG, Chung C, Shih J, Hwu P, Yeh C, Lopez R, Yen Y. 2005. Over-expression of fibroblast growth factor receptor 3 in human hepatocellular carcinoma. *World J Gastroenterol* 11: 5266-72
258. Rahmanzadeh R, Huttmann G, Gerdes J, Scholzen T. 2007. Chromophore-assisted light inactivation of pKi-67 leads to inhibition of ribosomal RNA synthesis. *Cell Prolif* 40: 422-30
259. Rajpert-De Meyts E, Hanstein R, Jorgensen N, Graem N, Vogt PH, Skakkebaek NE. 2004. Developmental expression of POU5F1 (OCT-3/4) in normal and dysgenetic human gonads. *Hum Reprod* 19: 1338-44
260. Rajpert-de Meyts E, Hoei-Hansen CE. 2007. From gonocytes to testicular cancer: the role of impaired gonadal development. *Ann N Y Acad Sci* 1120: 168-80
261. Rajpert-De Meyts E, Jacobsen GK, Bartkova J, Aubry F, Samson M, Bartek J, Skakkebaek NE. 2003. The immunohistochemical expression pattern of Chk2, p53, p19INK4d, MAGE-A4 and other selected antigens provides new evidence for the premeiotic origin of spermatocytic seminoma. *Histopathology* 42: 217-26
262. Rannan-Eliya SV, Taylor IB, De Heer IM, Van Den Ouweland AM, Wall SA, Wilkie AO. 2004. Paternal origin of FGFR3 mutations in Muenke-type craniosynostosis. *Hum Genet* 115: 200-7
263. Reardon W, Winter RM, Rutland P, Pulleyn LJ, Jones BM, Malcolm S. 1994. Mutations in the fibroblast growth factor receptor 2 gene cause Crouzon syndrome. *Nat Genet* 8: 98-103
264. Repasky GA, Chenette EJ, Der CJ. 2004. Renewing the conspiracy theory debate: does Raf function alone to mediate Ras oncogenesis? *Trends Cell Biol* 14: 639-47
265. Reuter VE. 2006. The pathology of bladder cancer. *Urology* 67: 11-7; discussion 7-8
266. Richards FM, Payne SJ, Zbar B, Affara NA, Ferguson-Smith MA, Maher ER. 1995. Molecular analysis of de novo germline mutations in the von Hippel-Lindau disease gene. *Hum Mol Genet* 4: 2139-43
267. Risch N, Reich EW, Wishnick MM, McCarthy JG. 1987. Spontaneous mutation and parental age in humans. *Am J Hum Genet* 41: 218-48
268. Roach JC, Glusman G, Smit AF, Huff CD, Hubley R, Shannon PT, Rowen L, Pant KP, Goodman N, Bamshad M, Shendure J, Drmanac R, Jorde LB, Hood L, Galas DJ. 2010. Analysis of genetic inheritance in a family quartet by whole-genome sequencing. *Science* 328: 636-9
269. Robertson SC, Meyer AN, Hart KC, Galvin BD, Webster MK, Donoghue DJ. 1998. Activating mutations in the extracellular domain of the fibroblast growth factor

receptor 2 function by disruption of the disulfide bond in the third immunoglobulin-like domain. *Proc Natl Acad Sci U S A* 95: 4567-72
270. Rodriguez-Viciana P, Warne PH, Dhand R, Vanhaesebroeck B, Gout I, Fry MJ, Waterfield MD, Downward J. 1994. Phosphatidylinositol-3-OH kinase as a direct target of Ras. *Nature* 370: 527-32
271. Romanenko AM, Persidskii Iu V. 1983. Ultrastructure and histogenesis of spermatocytic seminoma. *Vopr Onkol* 29: 60-6
272. Roovers K, Assoian RK. 2000. Integrating the MAP kinase signal into the G1 phase cell cycle machinery. *Bioessays* 22: 818-26
273. Rousseau F, Bonaventure J, Legeai-Mallet L, Pelet A, Rozet JM, Maroteaux P, Le Merrer M, Munnich A. 1994. Mutations in the gene encoding fibroblast growth factor receptor-3 in achondroplasia. *Nature* 371: 252-4
274. Rousseau F, Saugier P, Le Merrer M, Munnich A, Delezoide AL, Maroteaux P, Bonaventure J, Narcy F, Sanak M. 1995. Stop codon FGFR3 mutations in thanatophoric dwarfism type 1. *Nat Genet* 10: 11-2
275. Ryu BY, Orwig KE, Oatley JM, Avarbock MR, Brinster RL. 2006. Effects of aging and niche microenvironment on spermatogonial stem cell self-renewal. *Stem Cells* 24: 1505-11
276. Sadri-Ardekani H, Mizrak SC, van Daalen SK, Korver CM, Roepers-Gajadien HL, Koruji M, Hovingh S, de Reijke TM, de la Rosette JJ, van der Veen F, de Rooij DG, Repping S, van Pelt AM. 2009. Propagation of human spermatogonial stem cells in vitro. *JAMA* 302: 2127-34
277. Sanders CT, Sanchez N, Ballantyne J, Peterson DA. 2006. Laser microdissection separation of pure spermatozoa from epithelial cells for short tandem repeat analysis. *J Forensic Sci* 51: 748-57
278. Santoro M, Carlomagno F, Romano A, Bottaro DP, Dathan NA, Grieco M, Fusco A, Vecchio G, Matoskova B, Kraus MH, et al. 1995. Activation of RET as a dominant transforming gene by germline mutations of MEN2A and MEN2B. *Science* 267: 381-3
279. Scadden DT. 2006. The stem-cell niche as an entity of action. *Nature* 441: 1075-9
280. Schaller J, Glander HJ, Dethloff J. 1993. Evidence of beta 1 integrins and fibronectin on spermatogenic cells in human testis. *Hum Reprod* 8: 1873-8
281. Scheffzek K, Ahmadian MR, Kabsch W, Wiesmuller L, Lautwein A, Schmitz F, Wittinghofer A. 1997. The Ras-RasGAP complex: structural basis for GTPase activation and its loss in oncogenic Ras mutants. *Science* 277: 333-8
282. Schell U, Hehr A, Feldman GJ, Robin NH, Zackai EH, de Die-Smulders C, Viskochil DH, Stewart JM, Wolff G, Ohashi H, et al. 1995. Mutations in FGFR1 and FGFR2 cause familial and sporadic Pfeiffer syndrome. *Hum Mol Genet* 4: 323-8
283. Schlessinger J, Plotnikov AN, Ibrahimi OA, Eliseenkova AV, Yeh BK, Yayon A, Linhardt RJ, Mohammadi M. 2000. Crystal structure of a ternary FGF-FGFR-heparin complex reveals a dual role for heparin in FGFR binding and dimerization. *Molecular Cell* 6: 743-50
284. Schmidt U, Lutz-Bonengel S, Weisser HJ, Sanger T, Pollak S, Schon U, Zacher T, Mann W. 2006. Low-volume amplification on chemically structured chips using the PowerPlex16 DNA amplification kit. *Int J Legal Med* 120: 42-8
285. Schnieders F, Dork T, Arnemann J, Vogel T, Werner M, Schmidtke J. 1996. Testis-specific protein, Y-encoded (TSPY) expression in testicular tissues. *Hum Mol Genet* 5: 1801-7

286. Schollen E, Matthijs G, Gewillig M, Fryns JP, Legius E. 2003. PTPN11 mutation in a large family with Noonan syndrome and dizygous twinning. *Eur J Hum Genet* 11: 85-8
287. Schubbert S, Shannon K, Bollag G. 2007. Hyperactive Ras in developmental disorders and cancer. *Nat Rev Cancer* 7: 295-308
288. Schuffenecker I, Ginet N, Goldgar D, Eng C, Chambe B, Boneu A, Houdent C, Pallo D, Schlumberger M, Thivolet C, Lenoir GM. 1997. Prevalence and parental origin of de novo RET mutations in multiple endocrine neoplasia type 2A and familial medullary thyroid carcinoma. Le Groupe d'Etude des Tumeurs a Calcitonine. *Am J Hum Genet* 60: 233-7
289. Schulz AL, Albrecht B, Arici C, van der Burgt I, Buske A, Gillessen-Kaesbach G, Heller R, Horn D, Hubner CA, Korenke GC, Konig R, Kress W, Kruger G, Meinecke P, Mucke J, Plecko B, Rossier E, Schinzel A, Schulze A, Seemanova E, Seidel H, Spranger S, Tuysuz B, Uhrig S, Wieczorek D, Kutsche K, Zenker M. 2008. Mutation and phenotypic spectrum in patients with cardio-facio-cutaneous and Costello syndrome. *Clin Genet* 73: 62-70
290. Schulz WA. 2006. Understanding urothelial carcinoma through cancer pathways. *Int J Cancer* 119: 1513-8
291. Schutze K, Posl H, Lahr G. 1998. Laser micromanipulation systems as universal tools in cellular and molecular biology and in medicine. *Cell Mol Biol (Noisy-le-grand)* 44: 735-46
292. Schweitzer DN, Graham JM, Jr., Lachman RS, Jabs EW, Okajima K, Przylepa KA, Shanske A, Chen K, Neidich JA, Wilcox WR. 2001. Subtle radiographic findings of achondroplasia in patients with Crouzon syndrome with acanthosis nigricans due to an Ala391Glu substitution in FGFR3. *Am J Med Genet* 98: 75-91
293. Scully RE. 1961. Spermatocytic seminoma of the testis. A report of 3 cases and review of the literature. *Cancer* 14: 788-94
294. Seandel M, James D, Shmelkov SV, Falciatori I, Kim J, Chavala S, Scherr DS, Zhang F, Torres R, Gale NW, Yancopoulos GD, Murphy A, Valenzuela DM, Hobbs RM, Pandolfi PP, Rafii S. 2007. Generation of functional multipotent adult stem cells from GPR125+ germline progenitors. *Nature* 449: 346-50
295. Seeburg PH, Colby WW, Capon DJ, Goeddel DV, Levinson AD. 1984. Biological properties of human c-Ha-ras1 genes mutated at codon 12. *Nature* 312: 71-5
296. Shiang R, Thompson LM, Zhu YZ, Church DM, Fielder TJ, Bocian M, Winokur ST, Wasmuth JJ. 1994. Mutations in the transmembrane domain of FGFR3 cause the most common genetic form of dwarfism, achondroplasia. *Cell* 78: 335-42
297. Shibatohge M, Kariya K, Liao Y, Hu CD, Watari Y, Goshima M, Shima F, Kataoka T. 1998. Identification of PLC210, a Caenorhabditis elegans phospholipase C, as a putative effector of Ras. *J Biol Chem* 273: 6218-22
298. Shinohara T, Avarbock MR, Brinster RL. 1999. beta1- and alpha6-integrin are surface markers on mouse spermatogonial stem cells. *Proc Natl Acad Sci U S A* 96: 5504-9
299. Shukla V, Coumoul X, Wang RH, Kim HS, Deng CX. 2007. RNA interference and inhibition of MEK-ERK signaling prevent abnormal skeletal phenotypes in a mouse model of craniosynostosis. *Nat Genet* 39: 1145-50
300. Sibley K, Fenton JA, Dring AM, Ashcroft AJ, Rawstron AC, Morgan GJ. 2002. A molecular study of the t(4;14) in multiple myeloma. *Br J Haematol* 118: 514-20
301. Siep M, Sleddens-Linkels E, Mulders S, van Eenennaam H, Wassenaar E, Van Cappellen WA, Hoogerbrugge J, Grootegoed JA, Baarends WM. 2004. Basic helix-

loop-helix transcription factor Tcfl5 interacts with the Calmegin gene promoter in mouse spermatogenesis. *Nucleic Acids Res* 32: 6425-36

302. Simpson AJ, Caballero OL, Jungbluth A, Chen YT, Old LJ. 2005. Cancer/testis antigens, gametogenesis and cancer. *Nat Rev Cancer* 5: 615-25
303. Singh H, Sen R, Baltimore D, Sharp PA. 1986. A nuclear factor that binds to a conserved sequence motif in transcriptional control elements of immunoglobulin genes. *Nature* 319: 154-8
304. Sjodahl G, Lauss M, Gudjonsson S, Liedberg F, Hallden C, Chebil G, Mansson W, Hoglund M, Lindgren D. 2011. A Systematic Study of Gene Mutations in Urothelial Carcinoma; Inactivating Mutations in TSC2 and PIK3R1. *PLoS One* 6: e18583
305. Skakkebaek NE, Berthelsen JG, Giwercman A, Muller J. 1987. Carcinoma-in-situ of the testis: possible origin from gonocytes and precursor of all types of germ cell tumours except spermatocytoma. *Int J Androl* 10: 19-28
306. Sol-Church K, Stabley DL, Nicholson L, Gonzalez IL, Gripp KW. 2006. Paternal bias in parental origin of HRAS mutations in Costello syndrome. *Hum Mutat* 27: 736-41
307. Song C, Hu CD, Masago M, Kariyai K, Yamawaki-Kataoka Y, Shibatohge M, Wu D, Satoh T, Kataoka T. 2001. Regulation of a novel human phospholipase C, PLCepsilon, through membrane targeting by Ras. *J Biol Chem* 276: 2752-7
308. Sonne SB, Almstrup K, Dalgaard M, Juncker AS, Edsgard D, Ruban L, Harrison NJ, Schwager C, Abdollahi A, Huber PE, Brunak S, Gjerdrum LM, Moore HD, Andrews PW, Skakkebaek NE, Rajpert-De Meyts E, Leffers H. 2009. Analysis of gene expression profiles of microdissected cell populations indicates that testicular carcinoma in situ is an arrested gonocyte. *Cancer Res* 69: 5241-50
309. Sonne SB, Perrett RM, Nielsen JE, Baxter MA, Kristensen DM, Leffers H, Hanley NA, Rajpert-De-Meyts E. 2010. Analysis of SOX2 expression in developing human testis and germ cell neoplasia. *Int J Dev Biol* 54: 755-60
310. Soverini S, Terragna C, Testoni N, Ruggeri D, Tosi P, Zamagni E, Cellini C, Cavo M, Baccarani M, Tura S, Martinelli G. 2002. Novel mutation and RNA splice variant of fibroblast growth factor receptor 3 in multiple myeloma patients at diagnosis. *Haematologica* 87: 1036-40
311. Sovik O, Schubbert S, Houge G, Steine SJ, Norgard G, Engelsen B, Njolstad PR, Shannon K, Molven A. 2007. De novo HRAS and KRAS mutations in two siblings with short stature and neuro-cardio-facio-cutaneous features. *J Med Genet* 44: e84
312. Spradling A, Drummond-Barbosa D, Kai T. 2001. Stem cells find their niche. *Nature* 414: 98-104
313. Stanescu R, Stanescu V, Maroteaux P. 1990. Homozygous achondroplasia: morphologic and biochemical study of cartilage. *Am J Med Genet* 37: 412-21
314. Stephens K, Kayes L, Riccardi VM, Rising M, Sybert VP, Pagon RA. 1992. Preferential mutation of the neurofibromatosis type 1 gene in paternally derived chromosomes. *Hum Genet* 88: 279-82
315. Stoop H, van Gurp R, de Krijger R, Geurts van Kessel A, Koberle B, Oosterhuis W, Looijenga L. 2001. Reactivity of germ cell maturation stage-specific markers in spermatocytic seminoma: diagnostic and etiological implications. *Lab Invest* 81: 919-28
316. Superti-Furga A, Eich G, Bucher HU, Wisser J, Giedion A, Gitzelmann R, Steinmann B. 1995. A glycine 375-to-cysteine substitution in the transmembrane domain of the fibroblast growth factor receptor-3 in a newborn with achondroplasia. *Eur J Pediatr* 154: 215-9

317. Tartaglia M, Cordeddu V, Chang H, Shaw A, Kalidas K, Crosby A, Patton MA, Sorcini M, van der Burgt I, Jeffery S, Gelb BD. 2004. Paternal germline origin and sex-ratio distortion in transmission of PTPN11 mutations in Noonan syndrome. *Am J Hum Genet* 75: 492-7
318. Tartaglia M, Gelb BD. 2005. Germ-line and somatic PTPN11 mutations in human disease. *Eur J Med Genet* 48: 81-96
319. Tartaglia M, Kalidas K, Shaw A, Song X, Musat DL, van der Burgt I, Brunner HG, Bertola DR, Crosby A, Ion A, Kucherlapati RS, Jeffery S, Patton MA, Gelb BD. 2002. PTPN11 mutations in Noonan syndrome: molecular spectrum, genotype-phenotype correlation, and phenotypic heterogeneity. *Am J Hum Genet* 70: 1555-63
320. Tartaglia M, Mehler EL, Goldberg R, Zampino G, Brunner HG, Kremer H, van der Burgt I, Crosby AH, Ion A, Jeffery S, Kalidas K, Patton MA, Kucherlapati RS, Gelb BD. 2001. Mutations in PTPN11, encoding the protein tyrosine phosphatase SHP-2, cause Noonan syndrome. *Nat Genet* 29: 465-8
321. Tartaglia M, Niemeyer CM, Fragale A, Song X, Buechner J, Jung A, Hahlen K, Hasle H, Licht JD, Gelb BD. 2003. Somatic mutations in PTPN11 in juvenile myelomonocytic leukemia, myelodysplastic syndromes and acute myeloid leukemia. *Nat Genet* 34: 148-50
322. Tavormina PL, Bellus GA, Webster MK, Bamshad MJ, Fraley AE, McIntosh I, Szabo J, Jiang W, Jabs EW, Wilcox WR, Wasmuth JJ, Donoghue DJ, Thompson LM, Francomano CA. 1999. A novel skeletal dysplasia with developmental delay and acanthosis nigricans is caused by a Lys650Met mutation in the fibroblast growth factor receptor 3 gene. *Am J Hum Genet* 64: 722-31
323. Tavormina PL, Shiang R, Thompson LM, Zhu YZ, Wilkin DJ, Lachman RS, Wilcox WR, Rimoin DL, Cohn DH, Wasmuth JJ. 1995. Thanatophoric dysplasia (types I and II) caused by distinct mutations in fibroblast growth factor receptor 3. *Nat Genet* 9: 321-8
324. Taylor BJ, Reiman T, Pittman JA, Keats JJ, de Bruijn DR, Mant MJ, Belch AR, Pilarski LM. 2005. SSX cancer testis antigens are expressed in most multiple myeloma patients: co-expression of SSX1, 2, 4, and 5 correlates with adverse prognosis and high frequencies of SSX-positive PCs. *J Immunother* 28: 564-75
325. Theodorou E, Dalembert G, Heffelfinger C, White E, Weissman S, Corcoran L, Snyder M. 2009. A high throughput embryonic stem cell screen identifies Oct-2 as a bifunctional regulator of neuronal differentiation. *Genes Dev* 23: 575-88
326. Tiemann-Boege I, Navidi W, Grewal R, Cohn D, Eskenazi B, Wyrobek AJ, Arnheim N. 2002. The observed human sperm mutation frequency cannot explain the achondroplasia paternal age-effect. *Proc Natl Acad Sci U S A* 99: 14952-7
327. Tomlinson DC, Baldo O, Harnden P, Knowles MA. 2007a. FGFR3 protein expression and its relationship to mutation status and prognostic variables in bladder cancer. *J Pathol* 213: 91-8
328. Tomlinson DC, Hurst CD, Knowles MA. 2007b. Knockdown by shRNA identifies S249C mutant FGFR3 as a potential therapeutic target in bladder cancer. *Oncogene* 26: 5889-99
329. Tomlinson IP, Novelli MR, Bodmer WF. 1996. The mutation rate and cancer. *Proc Natl Acad Sci U S A* 93: 14800-3
330. Trahey M, McCormick F. 1987. A cytoplasmic protein stimulates normal N-ras p21 GTPase, but does not affect oncogenic mutants. *Science* 238: 542-5
331. Tres LL, Kierszenbaum AL. 2005. The ADAM-integrin-tetraspanin complex in fetal and postnatal testicular cords. *Birth Defects Res C Embryo Today* 75: 130-41

332. Valenzuela DM, Murphy AJ, Frendewey D, Gale NW, Economides AN, Auerbach W, Poueymirou WT, Adams NC, Rojas J, Yasenchak J, Chernomorsky R, Boucher M, Elsasser AL, Esau L, Zheng J, Griffiths JA, Wang X, Su H, Xue Y, Dominguez MG, Noguera I, Torres R, Macdonald LE, Stewart AF, DeChiara TM, Yancopoulos GD. 2003. High-throughput engineering of the mouse genome coupled with high-resolution expression analysis. *Nat Biotechnol* 21: 652-9
333. Van Dissel-Emiliani FM, De Boer-Brouwer M, De Rooij DG. 1996. Effect of fibroblast growth factor-2 on Sertoli cells and gonocytes in coculture during the perinatal period. *Endocrinology* 137: 647-54
334. Vandewoestyne M, Van Hoofstat D, Van Nieuwerburgh F, Deforce D. 2009. Automatic detection of spermatozoa for laser capture microdissection. *Int J Legal Med* 123: 169-75
335. Verheijen R, Kuijpers HJ, van Driel R, Beck JL, van Dierendonck JH, Brakenhoff GJ, Ramaekers FC. 1989. Ki-67 detects a nuclear matrix-associated proliferation-related antigen. II. Localization in mitotic cells and association with chromosomes. *J Cell Sci* 92 (Pt 4): 531-40
336. Vogel F, Rathenberg R. 1975. Spontaneous mutation in man. *Adv Hum Genet* 5: 223-318
337. von Kopylow K, Kirchhoff C, Jezek D, Schulze W, Feig C, Primig M, Steinkraus V, Spiess AN. 2010. Screening for biomarkers of spermatogonia within the human testis: a whole genome approach. *Hum Reprod* 25: 1104-12
338. Wartenberg H. 1981. Differentiation and development of the testes. In *The testis, 2nd*. Burger H, de Kretser D (eds).New York: Raven Press; 39-81
339. Wilkie AO. 2005. Bad bones, absent smell, selfish testes: the pleiotropic consequences of human FGF receptor mutations. *Cytokine Growth Factor Rev* 16: 187-203
340. Wilkie AO, Patey SJ, Kan SH, van den Ouweland AM, Hamel BC. 2002. FGFs, their receptors, and human limb malformations: clinical and molecular correlations. *Am J Med Genet* 112: 266-78
341. Wilkie AO, Slaney SF, Oldridge M, Poole MD, Ashworth GJ, Hockley AD, Hayward RD, David DJ, Pulleyn LJ, Rutland P, et al. 1995. Apert syndrome results from localized mutations of FGFR2 and is allelic with Crouzon syndrome. *Nat Genet* 9: 165-72
342. Wilkin DJ, Szabo JK, Cameron R, Henderson S, Bellus GA, Mack ML, Kaitila I, Loughlin J, Munnich A, Sykes B, Bonaventure J, Francomano CA. 1998. Mutations in fibroblast growth-factor receptor 3 in sporadic cases of achondroplasia occur exclusively on the paternally derived chromosome. *Am J Hum Genet* 63: 711-6
343. Witzgall R, O'Leary E, Leaf A, Onaldi D, Bonventre JV. 1994. The Kruppel-associated box-A (KRAB-A) domain of zinc finger proteins mediates transcriptional repression. *Proc Natl Acad Sci U S A* 91: 4514-8
344. Wohllk N, Cote GJ, Bugalho MM, Ordonez N, Evans DB, Goepfert H, Khorana S, Schultz P, Richards CS, Gagel RF. 1996. Relevance of RET proto-oncogene mutations in sporadic medullary thyroid carcinoma. *J Clin Endocrinol Metab* 81: 3740-5
345. Wolthuis RM, Bos JL. 1999. Ras caught in another affair: the exchange factors for Ral. *Curr Opin Genet Dev* 9: 112-7
346. Wong CH, Cheng CY. 2005. Mitogen-activated protein kinases, adherens junction dynamics, and spermatogenesis: a review of recent data. *Dev Biol* 286: 1-15
347. Woodward PJ, Heidenrich A, Looijenga LHJ, et al. 2004. Testicular germ cell tumours. In *WHO Classification of Tumours. Pathology and Genetics of the Urinary*

System and Male Genital Organs. Eble SG, Epstein JI, Sesterhenn IA (eds). Lyon: IARC Press; 217–278.

348. Xu X, Weinstein M, Li C, Naski M, Cohen RI, Ornitz DM, Leder P, Deng C. 1998. Fibroblast growth factor receptor 2 (FGFR2)-mediated reciprocal regulation loop between FGF8 and FGF10 is essential for limb induction. *Development* 125: 753-65
349. Yan J, Roy S, Apolloni A, Lane A, Hancock JF. 1998. Ras isoforms vary in their ability to activate Raf-1 and phosphoinositide 3-kinase. *J Biol Chem* 273: 24052-6
350. Yang B, O'Herrin SM, Wu J, Reagan-Shaw S, Ma Y, Bhat KM, Gravekamp C, Setaluri V, Peters N, Hoffmann FM, Peng H, Ivanov AV, Simpson AJ, Longley BJ. 2007. MAGE-A, mMage-b, and MAGE-C proteins form complexes with KAP1 and suppress p53-dependent apoptosis in MAGE-positive cell lines. *Cancer Res* 67: 9954-62
351. Yoon SR, Qin J, Glaser RL, Jabs EW, Wexler NS, Sokol R, Arnheim N, Calabrese P. 2009. The ups and downs of mutation frequencies during aging can account for the Apert syndrome paternal age-effect. *PLoS Genet* 5: e1000558
352. Yoshida S. 2010. Stem cells in mammalian spermatogenesis. *Dev Growth Differ* 52: 311-7
353. Yoshida S, Sukeno M, Nabeshima Y. 2007. A vasculature-associated niche for undifferentiated spermatogonia in the mouse testis. *Science* 317: 1722-6
354. Yoshida S, Sukeno M, Nakagawa T, Ohbo K, Nagamatsu G, Suda T, Nabeshima Y. 2006. The first round of mouse spermatogenesis is a distinctive program that lacks the self-renewing spermatogonia stage. *Development* 133: 1495-505
355. Yoshida S, Takakura A, Ohbo K, Abe K, Wakabayashi J, Yamamoto M, Suda T, Nabeshima Y. 2004. Neurogenin3 delineates the earliest stages of spermatogenesis in the mouse testis. *Dev Biol* 269: 447-58
356. Yu K, Herr AB, Waksman G, Ornitz DM. 2000. Loss of fibroblast growth factor receptor 2 ligand-binding specificity in Apert syndrome. *Proc Natl Acad Sci U S A* 97: 14536-41
357. Yu K, Xu J, Liu Z, Sosic D, Shao J, Olson EN, Towler DA, Ornitz DM. 2003. Conditional inactivation of FGF receptor 2 reveals an essential role for FGF signaling in the regulation of osteoblast function and bone growth. *Development* 130: 3063-74
358. Zampino G, Pantaleoni F, Carta C, Cobellis G, Vasta I, Neri C, Pogna EA, De Feo E, Delogu A, Sarkozy A, Atzeri F, Selicorni A, Rauen KA, Cytrynbaum CS, Weksberg R, Dallapiccola B, Ballabio A, Gelb BD, Neri G, Tartaglia M. 2007. Diversity, parental germline origin, and phenotypic spectrum of de novo HRAS missense changes in Costello syndrome. *Hum Mutat* 28: 265-72
359. Zhang X, Ebata KT, Robaire B, Nagano MC. 2006. Aging of male germ line stem cells in mice. *Biol Reprod* 74: 119-24
360. Zhang ZT, Pak J, Huang HY, Shapiro E, Sun TT, Pellicer A, Wu XR. 2001. Role of Ha-ras activation in superficial papillary pathway of urothelial tumor formation. *Oncogene* 20: 1973-80
361. Zhu X, Asa SL, Ezzat S. 2010. Genetic and epigenetic mechanisms down-regulate FGF receptor 2 to induce melanoma-associated antigen A in breast cancer. *Am J Pathol* 176: 2333-43
362. Zieger K, Dyrskjot L, Wiuf C, Jensen JL, Andersen CL, Jensen KM, Orntoft TF. 2005. Role of activating fibroblast growth factor receptor 3 mutations in the development of bladder tumors. *Clin Cancer Res* 11: 7709-19

SUPPLEMENTARY CD